



University of HUDDERSFIELD

University of Huddersfield Repository

Ahmaida, Anwar M.

Condition Monitoring and Fault Diagnosis of a Multi-Stage Gear Transmission Using Vibro-acoustic Signals

Original Citation

Ahmaida, Anwar M. (2018) Condition Monitoring and Fault Diagnosis of a Multi-Stage Gear Transmission Using Vibro-acoustic Signals. Doctoral thesis, University of Huddersfield.

This version is available at <http://eprints.hud.ac.uk/id/eprint/34755/>

The University Repository is a digital collection of the research output of the University, available on Open Access. Copyright and Moral Rights for the items on this site are retained by the individual author and/or other copyright owners. Users may access full items free of charge; copies of full text items generally can be reproduced, displayed or performed and given to third parties in any format or medium for personal research or study, educational or not-for-profit purposes without prior permission or charge, provided:

- The authors, title and full bibliographic details is credited in any copy;
- A hyperlink and/or URL is included for the original metadata page; and
- The content is not changed in any way.

For more information, including our policy and submission procedure, please contact the Repository Team at: E.mailbox@hud.ac.uk.

<http://eprints.hud.ac.uk/>

**Condition Monitoring and Fault Diagnosis of a
Multi-Stage Gear Transmission Using
Vibro-acoustic Signals**

A THESIS SUBMITTED IN PARTIAL FULFILMENT OF THE REQUIREMENT FOR
THE DEGREE OF DOCTOR OF PHILOSOPHY AT THE UNIVERSITY OF
HUDDERSFIELD

By

ANWAR MASOUD AHMAIDA

School of Computing and Engineering
University of Huddersfield
UK

June 2018

ABSTRACT

Gearbox condition monitoring (CM) plays a vital role in ensuring the reliability and operational efficiency of a wide range of industrial facilities such as wind turbines and helicopters. Many technologies have been investigated intensively for more accurate CM of rotating machines with using vibro-acoustic signature analysis. However, a comparison of CM performances between surface vibrations and airborne acoustics has not been carried out with the use of emerging signal processing techniques.

This research has focussed on a symmetric evaluation of CM performances using vibrations obtained from the surface of a multi stage gearbox housing and the airborne sound obtained remotely but close to the gearbox, in conjunction with state of the art signal processing techniques, in order to provide efficient and effective CM for gear transmissions subject to gradual and progressive deteriorations. By completing the comparative studies, this research has resulted in a number of new findings that show significant contributions to knowledge which are detailed as follows.

In general, through a comprehensive review of the advancement in the subject, the research has been carried out by integrating an improved dynamic modelling, more realistic experiment verification and more advanced signal processing approaches. The improved modelling has led to an in-depth understanding of the nonlinear modulation in vibro-acoustic signals due to wear effects. Thereafter, Time Synchronous Average (TSA) and Modulation Signal Bispectrum (MSB) are identified to be the most promising signal processing methods to fulfil the evaluation because of their unique properties of simultaneous noise reduction and modulation enhancement. The more realistic tests have demonstrated that a run-to-failure test is necessary to develop effective diagnostic tools as it produces datasets from gear transmissions where deterioration naturally progresses over a long operation, rather than faults created artificially to gear systems, as is common in the majority of studies and the results unreliable.

Particularly, the evaluation studies have clarified a number of key issues in the realisation of gearbox diagnostics based on TSA and MSB analysis of the vibrations from two accelerometers and acoustics from two microphones in monitoring the run-to-failure process, which showed slight gear wear of two back-to-back multiple stage helical gearboxes under variable load and speed operations.

TSA analysis of vibration signals and acoustic signals allows for accurate monitoring and diagnosis results of the gradual deterioration in the lower speed transmission of both the tested gearboxes. However, it cannot give the correct indication of the higher speed stages in the second gearbox as the reference angle signal is too erroneous due to the distortion of long transmission trains. In addition, acoustic signals can indicate that there is a small deterioration in the higher speed transmission of the first gearbox.

The MSB analysis of vibration signals and sound signals allows for the gathering of more corrective monitoring and diagnostic results of the deterioration in the four stages of transmissions of the two tested gearboxes. MSB magnitudes of both the two lower speed transmissions show monotonic increases with operational time and the increments over a longer period are in excess of three times higher than the baselines, the deteriorations are therefore regarded as severe. For the two higher speed transmissions, the MSB of vibrations and acoustics illustrates small deteriorations in the latter operating hours.

Comparatively, acoustic signal based diagnostics can out-perform vibration as it can provide an early indication of deteriorations and correct diagnosis of the faults as microphones perceive a large area of dynamic responses from gearbox housing whereas accelerometers collect a very localised response which can be distorted by transmission paths. In addition, MSB analysis can out-perform conventional TSA as it maintains all diagnostic information regarding the rotating systems and can be implemented without any additional reference channels.

DECLARATION

No portion of the work presented in this thesis has been submitted in support of an application for another degree or qualification of this or any other university or other institute of learning.

LIST OF CONTENTS

ABSTRACT	2
DECLARATION	4
LIST OF CONTENTS	5
LIST OF FIGURES	13
LIST OF TABLES	18
LIST OF ABBREVIATIONS	19
LIST OF NOTATIONS	21
ACKNOWLEDGEMENTS	25
Chapter 1 INTRODUCTION	27
1.1 CM and Maintenance Strategies	28
1.1.1 Pre-Emptive Detection and Elimination	28
1.1.2 Quality Control and Assurance	28
1.1.3 Preventative Maintenance	29
1.1.4 Predictive Maintenance.....	29
1.1.5 Reactive or Breakdown Maintenance	30
1.2 Gear Transmissions	30
1.2.1 Spur, Helical, Bevel and Worm Gears.....	31
1.2.2 Gearbox Regional Market.....	35
1.2.3 Industrial Gears Application	36
1.3 Gear Failure Modes.....	36

1.3.1	Types of Gear Failures	42
1.3.2	Causes of Gearbox Failures	43
1.4	The Demand for CM	44
1.5	Conventional CM Techniques.....	44
1.5.1	Trend Monitoring.....	45
1.5.2	Thermal Monitoring.....	46
1.5.3	Visual Inspection CM	46
1.5.4	Corrosion Monitoring	47
1.5.5	Oil Analysis and Monitoring of Wear Debris.....	47
1.5.6	Acoustic Airborne Monitoring.....	48
1.5.7	Acoustic Emission (AE) Monitoring	49
1.5.8	Vibration Monitoring	50
1.6	Research Motivation	51
1.7	Research Aim and Objectives	53
1.8	Organisation of Thesis	53
1.9	Summary	55
Chapter 2 LITERATURE REVIEW OF GEAR FAULT DETECTION AND DIAGNOSIS USING VIBRO-ACOUSTIC BASED TECHNIQUES		57
2.1	Background to Signal Processing.....	58
2.2	Time Domain Analysis.....	59
2.2.1	RMS (Root Mean Square)	60
2.2.2	The Crest Factor (CF)	60

2.2.3	Kurtosis	61
2.3	Frequency Domain Analysis	61
2.3.1	Power Spectrum Analysis	62
2.3.2	Diagnostic Features in the Frequency Domain	62
2.4	Envelope Analysis	63
2.5	Time-Frequency Domain Analysis	64
2.5.1	Spectrograms	65
2.5.2	Wavelets	66
2.6	Time Synchronous Averaging (TSA)	67
2.6.1	Order Spectrum by Applying Fourier to TSA Signals	69
2.7	Empirical Mode Decomposition (EMD)	69
2.8	Key Findings	70
Chapter 3 FUNDAMENTALS OF VIBRO-ACOUSTICS FROM A TWO STAGE HELICAL GEARBOX WITH TOOTH WEAR		72
3.1	Introduction	73
3.2	Key Advancement in Modelling Gear Dynamics	73
3.3	Modelling Overview	75
3.4	Mathematical Model of a Multi-Stage Gearbox	76
3.5	Determination of Model Parameters	81
3.6	Wear Induced Changes in Tooth Stiffness	84
3.6.1	Changes in Tooth Profile	84
3.6.2	Influences of Gear Errors	86

3.7	Implementation of Numerical Studies of Gear Vibrations.....	86
3.7.1	Rotational Responses in the Time Domain.....	87
3.7.2	Translational Response in the Time Domain.....	88
3.8	Spectral Characteristics	89
3.8.1	Spectra of Rotational Responses.....	89
3.8.2	Spectra of Translational Responses	92
3.9	Acoustic Signals from Vibrating Structures.....	93
3.9.1	Mechanisms of Sound Radiation by Vibrating Surfaces	93
3.9.2	Modelling of Sound Radiation.....	95
3.9.3	Source Addition	95
3.9.4	Sound Wave Propagation in Rooms	97
3.9.5	Background Acoustics	98
3.10	Key Findings.....	99
Chapter 4	BISPECTRUM OF GEAR VIBRO-ACOUSTIC SIGNALS.....	100
4.1	Introduction	101
4.2	Bispectrum Background.....	102
4.3	Quadratic Phase Coupling (QPC)	104
4.4	Review of Gearbox Fault Condition	104
4.5	Conventional Bispectrum Calculation	105
4.6	Difference between Bispectrum and Power Spectrum.....	107
4.7	Modulation Signal Bispectrum Calculation (MSB)	107

4.7.1	Sideband Detection Using MSB	108
4.7.2	Bispectrum Performance.....	110
4.8	Key Findings	110
Chapter 5	EXPERIMENTAL FACILITY FOR GEAR FATIGUE MONITORING TESTS	112
5.1	Test System	113
5.2	Test Rig Construction.....	113
5.2.1	Electrical Controls	117
5.2.2	Sensors for Acquiring Vibration and Acoustics Signal	117
5.2.3	Data Acquisition Hardware.....	122
5.2.4	Data Acquisition Software System	123
5.3	Calculation of Gear Characteristic Frequencies.....	125
5.4	Test Procedure and Resulting Gear Faults	127
5.5	Key Findings	130
Chapter 6	MONITORING AND DIAGNOSIS OF GEARBOX DETERIORATION BASED ON THE TSA ANALYSIS OF THE SURFACE VIBRATION SIGNAL.....	132
6.1	Introduction	133
6.2	Baseline Vibrations by Spectrum Analysis.....	135
6.3	Implementation of TSA.....	136
6.4	Monitoring and Diagnosis of Gear Deteriorations	142
6.4.1	Monitoring of the Higher Speed Stage in Gearbox 1 based on Mesh Components and Sidebands	144

6.4.2	Monitoring of the Lower Speed Stage in Gearbox 1 based on Mesh Components and Sidebands	144
6.4.3	Monitoring of the Lower Speed Stage in GB2 based on Mesh Components and Sidebands	147
6.4.4	Monitoring of the Higher Speed Stage in GB2 based on Mesh Components and Sidebands	148
6.5	Key Findings from TSA Analysis of Vibrations.....	149
Chapter 7 MONITORING AND DIAGNOSIS OF GEARBOX DETERIORATION BASED ON THE TSA OF ACOUSTIC SIGNALS		
		151
7.1	Introduction	152
7.2	Characteristics of Acoustic Signals.....	152
7.3	TSA-fr2 Acoustic Signals	154
7.4	Monitoring and Diagnosing Gear Deteriorations.....	160
7.4.1	Monitoring of the Higher Speed Stage in GB1.....	160
7.4.2	Monitoring of the Lower Speed Stage in GB1	161
7.4.3	Monitoring of the Lower Speed Stage in GB2	162
7.4.4	Monitoring of the Higher Speed Stage in GB2.....	164
7.5	Key Findings from TSA Analysis of Acoustic Signals.....	165
Chapter 8 MONITORING AND DIAGNOSIS OF GEARBOX DETERIORATION BASED ON MSB ANALYSIS OF SURFACE VIBRATION SIGNALS		
		166
8.1	Introduction	167
8.2	Implementation of MSB for Vibration.....	167
8.3	MSB Characteristics of the Baseline Vibrations.....	168

8.4	Monitoring and Diagnosing Gear Deteriorations Based on MSB Vibration Signals Analysis.....	174
8.4.1	Monitoring of the Higher Speed Stage of GB1	174
8.4.2	Monitoring of the Lower Speed Stage of GB1	176
8.4.3	Monitoring of the Lower Speed Stage of GB2	177
8.4.4	Monitoring of the Higher Speed Stage of GB2	178
8.5	Key Findings from MSB Analysis of Vibration Signals.....	180
Chapter 9 MONITORING AND DIAGNOSIS OF GEARBOX DETERIORATION BASED ON THE MSB ANALYSIS OF ACOUSTIC SIGNALS.....		
		181
9.1	Introduction	182
9.2	MSB Implementation for Acoustic Signals	182
9.3	MSB Characteristics of Acoustic Signals	183
9.4	Monitoring and Diagnosis of Gearbox Deteriorations Based on MSB Analysis of Acoustics Signals	188
9.4.1	Monitoring of the Higher Speed Stage of GB1	189
9.4.2	Monitoring of the Lower Speed Stage of GB1	190
9.4.3	Monitoring of the Lower Speed Transmission Stage of GB2.....	191
9.4.4	Monitoring of the Higher Speed Stage of GB2	191
9.5	Key Findings from MSB Analysis of Acoustics Signals	193
Chapter 10 CONCLUSION AND FUTURE WORK		
		195
10.1	Review of the Objectives and Achievements	196
10.2	Conclusions Using Vibro-acoustics on the Gear Transmission CM.....	198
10.2.1	Experimental System	198

10.2.2	Conclusions on CM Using TSA	199
10.2.3	Conclusions on CM Using MSB.....	199
10.2.4	Conclusions on Modelling for Gearbox Vibro-acoustic Analysis.....	199
10.3	Contribution to Knowledge and Novel Feature Summary	200
10.4	The Contributions to Knowledge	200
10.5	Future Work Recommendations on the Gearboxes CM Using Vibro-acoustics:	201
REFERENCES		203
Appendix A: Publications		i
Appendix B: Gear Tooth Wear Photos		xx
Appendix C: The Diagnosis of the Asymmetric Rotor in the Induction Motor		xxi

LIST OF FIGURES

Figure 1-1 Spur gear [14].....	31
Figure 1-2 Helical gears [17]	32
Figure 1-3 Bevel gear [19].....	33
Figure 1-4 Worm gear [16].....	34
Figure 1-5 Gear pitch line[21]	36
Figure 1-6 Gear terminology[22].....	37
Figure 1-7 Classification of different gear failure modes [15]	42
Figure 1-8 General usage of various monitoring techniques [15]	45
Figure 1-9 Trend monitoring record [39].....	45
Figure 2-1 Simple example of carrier wave modulation in producing a modulated wave with the signals having an amplitude [84]	64
Figure 3-1 The dynamic model of motor-gearbox and load system.....	77
Figure 3-2 Main procedure for the analysis of gearbox dynamic responses	82
Figure 3-3 Models of tooth stiffness and the effects of tooth wear	84
Figure 3-4 Tooth stiffness function superimposed by multiple tooth pair and the effect of gear wear.....	85
Figure 3-5 Angular speed of the first pinion and gear	87
Figure 3-6 Vibration responses in the time domain of the first pinion and gear	88
Figure 3-7 Spectral peaks of combined rotational responses of the first pinion and gear	89
Figure 3-8 Increases of spectral amplitudes from rotational responses with wear severity. ...	90
Figure 3-9 Spectral peaks of combined translational responses of the first pinion and gear...	91

Figure 3-10 Average of spectral amplitudes for both transmission stages of the gearbox.	92
Figure 3-11 The additional effects from two point sound sources	95
Figure 3-12 Diagram of the reverberation in an close space	96
Figure 3-13 Diagram of the reverberation in a closed space	98
Figure 4-1 Classification of higher order spectra	103
Figure 5-1 Mechanical/electromechanical test rig components.....	113
Figure 5-2 Illustration of two stage helical gearbox under test	114
Figure 5-3 Test rig schematic diagram and placement of vibro-acoustic sensors	116
Figure 5-4 Vibration accelerometer CA-YD-1182A	118
Figure 5-5 BAST's microphone system	120
Figure 5-6 Encoder mounted on the non-driving end of the AC motor.....	121
Figure 5-7 Global sensor technology YE6232B DAQ system for monitoring vibro-acoustic signals	122
Figure 5-8 Set-up screen for data acquisition	124
Figure 5-9 Screenshot of measured signals	124
Figure 5-10 Screenshot of operating status and dynamic trend graphs.	125
Figure 5-11 Schematic of the two gearbox transmission systems with key symbols used throughout the thesis	126
Figure 5-12 Test operation cycles.....	128
Figure 5-13 Illustrative photos of the location and severity of tooth wear and pitting on the surface of the gears at the lower speed stage of Gearbox 2	130
Figure 6-1 Power spectrum of vibration signal for the two stages of the helical gearbox at full load at 324 hours continuous running.....	135

Figure 6-2 Implementation of TSA vibration signals based on the angular position of the middle shaft rotating at the speed of f_{r2}	138
Figure 6-3 TSA-fr2 signals synchronised to Gear Zr2 or Gear Zi2 with respect to f_{r2}	139
Figure 6-4 TSA-fr2 signal spectrum based on Order f_{r2}	141
Figure 6-5 The correlation of mesh components with loads.....	143
Figure 6-6 Mesh frequency components and sidebands of GB1 at f_{m1} and their harmonics as a function of operating time (f_{r1} cannot be seen as the TSA is based on f_{r2}).....	145
Figure 6-7 Mesh frequency components and sidebands of GB1 at f_{m2} and their harmonics as a function of operating time.....	146
Figure 6-8 Mesh frequency components and sidebands of GB2 at f_{m3} and their harmonics as a function of operating time.....	147
Figure 6-9 Mesh frequency components and sidebands of GB2 at f_{m4} and their harmonics as a function of operating time (f_{r5} cannot be seen as the TSA is based on $f_{r2} = f_{r4}$).....	149
Figure 7-1 Raw acoustic signal of Mic.1-GB1 tested at full load and full speed	152
Figure 7-2 Acoustic power spectra of Mic.1-GB1 and Mic.2-GB2 at 324 hours.....	154
Figure 7-3 Implementation of TSA of acoustic signals based on the middle shaft angular position rotating at the speed of f_{r2}	155
Figure 7-4 TSA-fr2 acoustic signals for Mic1 and Mic 2 plotted as a function of shaft angle	156
Figure 7-5 TSA-fr2 spectra of Mic.1-GB1 and Mic.2-GB2 at 324 hours	157
Figure 7-6 Comparison of spectra between acoustic signals and vibration signals.....	158
Figure 7-7 The dependency of mesh components upon loads.....	159

Figure 7-8 Acoustic amplitudes at meshing frequency f_{m1} harmonics and their sidebands for GB1 as a function of operating time	161
Figure 7-9 Acoustic amplitudes at meshing frequency f_{m2} harmonics and their sidebands for GB1 as a function of operating time	162
Figure 7-10 Acoustic amplitudes at meshing frequency f_{m3} harmonics and their sidebands for GB2 as a function of operating time	163
Figure 7-11 Acoustic amplitudes at meshing frequency f_{m4} harmonics and their sidebands for GB2 as an operating time function	164
Figure 8-1 The stability of MSB estimation with averaging	168
Figure 8-2 MSB results of Acc.1-GB1 vibration at 324 hours	170
Figure 8-3 MSB slices at f_{m1} harmonics of Acc.1-GB1	171
Figure 8-4 MSB slices at f_{m2} harmonics of Acc.1-GB1	172
Figure 8-5 MSB results of Acc.2-GB2 at the operating time of 324 hours	173
Figure 8-6 The evolution of MSB vibration peaks at rotational frequency of f_{r1}, f_{r2} and f_{r3} from f_{m1} slices for GB1	175
Figure 8-7 The evolution of MSB vibration peaks at rotational frequency of f_{r1}, f_{r2} and f_{r3} from f_{m2} slices for GB1	176
Figure 8-8 The evolution of vibration MSB peaks at rotational frequencies of f_{r3}, f_{r4} and f_{r5} from the f_{m3} slices for GB2.....	177
Figure 8-9 The evolution of vibration MSB peaks at f_{r3}, f_{r4} and f_{r5} from the f_{m4} slices for GB2.....	179
Figure 9-1 The stability of MSB estimation for acoustic and vibration signals	183

Figure 9-2 MSB magnitude and coherence results for acoustic signal from Mic.1-GB1 after an operating time of 324 hours	184
Figure 9-3 MSB results of acoustic signal from Mic.2-GB2 at the operating time of 324 hours	186
Figure 9-4 MSB slices at f_{m1} harmonics	187
Figure 9-5 MSB slices at f_{m2} harmonics.....	188
Figure 9-6 The evolution of acoustic MSB peaks at rotational frequencies of f_{r1}, f_{r2} and f_{r3} from f_{m1} slices for GB1.	189
Figure 9-7 The evolution of acoustics MSB peaks at rotational frequencies of f_{r1}, f_{r2} and f_{r3} from f_{m2} slices for GB1	190
Figure 9-8 The evolution of acoustics MSB peaks at rotational frequencies of f_{r3}, f_{r4} and f_{r5} from the f_{m3} slices for GB2.....	192
Figure 9-9 The evolution of acoustics MSB peaks at rotational frequencies of f_{r3}, f_{r4} and f_{r5} from the f_{m4} slices for GB2.....	193

LIST OF TABLES

Table 1-1 lists properties of the most common types of gears: spur and helical.....	35
Table 1-2 Gear wear processes and mechanisms [13; 19].....	38
Table 3-1 Key baseline parameters and specification for the test gearbox.....	83
Table 5-1 Specification of AC induction motor	114
Table 5-2 Key specification of speed reduction two stage helical gearbox (GB1)	115
Table 5-3 Key specification of two stage speed increase helical gearbox (GB2)	115
Table 5-4 Specification of the DC generator	116
Table 5-5 Technical specifications of the accelerometer sensor	118
Table 5-6 Specification of microphone CHZ-211	120
Table 5-7 Specification of preamplifier	120
Table 5-8 Technical specifications of the DAQ system	123
Table 5-9 Test operation cycle and data acquisition.....	129

LIST OF ABBREVIATIONS

A	Ampere
AC	Alternating Current
ADC	Analogue to Digital Conversion
AI	Artificial Intelligence
CBM	Condition Based Maintenance
CM	Condition Monitoring
CWT	Continuous Wavelet Transforms
DAS	Data Acquisition System
DFT	Discrete Fourier Transform
DOF	Degree of Freedom
DWT	Discrete Wavelet Transform
EEMD	Ensemble Empirical Mode Decomposition
EMD	Empirical Mode Decomposition
FDD	Fault Detection and Diagnosis
FFT	Fast Fourier Transforms
FM	Frequency Modulation
FE	Finite Element
HOS	Higher Order Spectra
Hz	Hertz
I/O	Input/output
IAS	Instantaneous Angular Speed
MSB	Modulating Signal Bispectrum
MTBF	Mean Time Between Failures
MTTF	Mean Time to Failure
PM	Preventative Maintenance

QPC	Quadratic Phase Coupling
Rad/s	Radians per Second
RF	Rotational Frequency
RMS	Root Mean Square
SNR	Signal to Noise Ratio
STFT	Short Time Fourier Transform
TSA	Time Synchronous Averaging
WT	Wavelet Transforms

LIST OF NOTATIONS

$B(f_1, f_2)$	Conventional Bispectrum
$B_{ms}(f_1, f_2)$	Modulated Signal Bispectrum
c_p	First Stage Pinion Shaft Damping
c_g	First Stage Gear Shaft Damping
c_1	Shaft One Damping
c_2	Shaft Two Damping
c_3	Shaft Three Damping
c_{z1}	First Stage Gearing Damping
c_{z2}	Second Stage Gearing Damping
c_{c1}	Upper Casing Support Damping
c_{c2}	Lower Casing Support Damping
E_w	Errors in The Instantaneous Contact Forces
$E[.]$	Statistical Expectation
e	Displacement of Mass Centre
F_1	Gearing Stiffness Force at First Stage
F_2	Gearing Stiffness Force at Second Stage
F_{1t}	Gearing Damping Force at First Stage
F_{2t}	Gearing Damping Force at Second Stage
f_r	Rotor Frequency
f_{main}	Main Supply Frequency
f_{r1}	Input Shaft Frequency
f_{r2}	Middle Shaft Frequency
f_{r3}	Output Shaft Frequency
f_0	Supply Frequency
f_{m1}	Mesh Frequency at First Stage
f_{m2}	Mesh Frequency at Second Stage

f_{m3}	Mesh Frequency at 1 st Stage of Gearbox 2
f_{m4}	Mesh Frequency at 2 nd Stage of Gearbox 2
G	Gear Ratio
I_{p1}	Moment of Inertia of Z_1
I_{g1}	Moment of Inertia of Z_2
I_{p2}	Moment of Inertia of Z_3
I_{g2}	Moment of Inertia of Z_4
I_m	Moment of Inertia for Electric Motor
I_l	Moment of Inertia for the Load System
I_m	Moment of Motor
I_l	Moment of Load System
k_p	First Stage Pinion Shaft Stiffness
k_g	First Stage Gear Shaft Stiffness
k_1	Rotational Stiffness for the Input Shaft
k_2	Rotational Stiffness for the Middle Shaft
k_3	Rotational Stiffness for the Output Shaft
k_{z1}	Meshing Stiffness for the First Stage
k_{z2}	Meshing Stiffness for the Second Stage
k_{c1}	Upper Casing Support Stiffness
k_{c2}	Lower Gearing Support Stiffness
$k(t)$	Mesh Stiffness
M_1	Moment of Inertia of Input Shaft
M_2	Moment of Inertia of Middle Shaft
M_3	Moment of Inertia of Output Shaft
M_m	Input Motor Torque
M_{1t}	Coupling Damping in First Shaft
M_2	Internal Moment in Second Shaft

M_{2t}	Coupling Damping in Second Shaft
M_3	Internal Moment in Third Shaft
M_{3t}	Coupling Damping in Third Shaft
m_{c1}	Mass of Upper Casing
m_{c2}	Mass of Lower Casing
m_{s1}	Mass of the Input Shaft
m_{s2}	Mass of the Middle Shaft
m_{s3}	Mass of the Output Shaft
m_{p1}	Mass of the Drive Gear (Z_1)
m_{g1}	Mass of the Driven Gear (Z_2)
m_{p2}	Mass of the Drive Gear (Z_3)
m_{g2}	Mass of the Driven Gear (Z_4)
N_s	Synchronous Speed (RPM)
N_r	Rotor Speed
n_p	Number of Pinion Teeth
n_g	Number of Gear Teeth
P	Number of Poles
r_{s1}	Base Radius of Input Shaft
r_{s2}	Base Radius of Middle Shaft
r_{s3}	Base Radius of Output Shaft
r_{p1}	Base Radius of Drive Gear (Z_1) at First Stage
r_{g1}	Base Radius of Driven Gear Z_2
r_{p2}	Base Radius of Drive Z_3
r_{g2}	Base Radius of Z_4

$X(f)$	Fourier Transform
$X^*(f)$	Conjugate of Fourier Transform
$x[n]$	Discrete Time Current Signal
y_p	Vertical Displacement of Z_1
y_g	Vertical Displacement of Z_2
y_{c1}	Vertical Displacement of Upper Casing
y_{c2}	Vertical Displacement of Lower Casing
ρ_{w1}	Wear Error of Z_1
ρ_{w2}	Wear Error of Drive Gear Z_2
ε_c	Contact Ratio
ε_a	Overlap Ratio
μ_2	Gearing Damping Coefficient for the Second Stage
μ_1	First Stage Gearing Damping
φ_1	Angular Displacement of Motor
φ_2	Angular Displacement of (Z_1)
φ_3	Angular Displacement of (Z_2)
φ_4	Angular Displacement of (Z_3)
φ_5	Angular Displacement of (Z_4)
Z_1	Drive Gear at First Stage
Z_2	Driven Gear at First Stage
Z_3	Drive Gear at Second Stage
Z_4	Driven Gear at Second Stage

ACKNOWLEDGEMENTS

Firstly, the most important acknowledgement goes to God for being my main support, providing both guidance and light during my university career. Without Him, I could never successfully achieve any of the opportunities I have been given in my life. All my achieved goals are thanks to Him.

Secondly, my thanks are also extended to my first supervisor, **Dr. Fengshou Gu**, whose expertise, encouragement and direction were vital in completing my research project and writing this thesis. His persistence, understanding and kindness enabled me to develop a robust theoretical framework in a logical and consistent manner and guided me to perform experimental work to the highest standards. These words fail to fully convey my appreciation and deepest gratitude and I will always be in his debt.

I would like also to express my sincere gratitude to **Prof. Andrew Ball** for his continued support, assistance and his immense knowledge provided during the course of my research. I appreciate his patience, motivation and skills that have greatly enriched my graduate experience. I would also like to thank him for the guidance and opportunity to write, publish and participate in international conferences.

I would like also to convey my thanks to all colleagues at the Centre for Efficiency and Performance Engineering and research fellows and staff members who have over the years made my time such a great experience on a professional and personal level. I would like to thank my government (the government of Libya) for their financial support.

I would like to personally give thanks to the fantastic technical support staff at the University of Huddersfield in particular Steven Goldstein, Philip Holdsworth, Richard Bailey and Dennis Town, I would like to personally thank each of them for their continued support, innovation and expertise during this project.

Last but not least, I would especially like to dedicate this thesis to my wonderful family; my wife **Maha**, daughters **Mayre** and **Meral** and I thank them for their continued support, encouragement and love. Special and grateful thanks to my mother **Adila**, my father **Masoud** and all my brothers and sisters for their belief in me.

VITA

June 2001..... Bachelor of Mechanical (BSc) Engineering

Benghazi University

Libya

October 2010..... Master of Mechanical (MSc)Engineering and Design

University of Huddersfield

United Kingdom

FIELDS OF STUDY

Major Field: Mechanical Engineering.

Focus on Condition Monitoring (CM).

Chapter 1 INTRODUCTION

This chapter would explain the motivation for undertaking this research programme and choosing to concentrate on this specific area of study. Information is presented about gearbox use and engineering demand, as well as the functions of gears. In addition, a summary explanation of the causes of gear failure and modes of failure is given and a brief review of traditional monitoring techniques is presented. Finally, the aims and objectives of this research are presented and the thesis structure summarised.

1.1 CM and Maintenance Strategies

The main focus and goal of most industrial operations is to increase the maximum attainable profit from the production line whilst reducing the costs related to machine maintenance and unexpected machine shutdown due to unforeseen failures. In the start-up of a production plant, the investors are fully aware of the fact that maintaining machinery is a costly task which can form a large part of the operational expenditures. An essential key to profit maximisation is a well-structured CM programme, which in the past has received rare attention [1, 2]. However, in more recent times, most companies, if not all, are aware of the consequences of machine failure and many of them have an effective maintenance plan in place to avoid unscheduled and costly machine stoppages. Consequently, an increase in per-unit profit of production has been apparent for those companies who have adopted a maintenance plan.

A machine is well-known to fail as a result of the failure of one or more of their integral parts. There are generally combinations of reasons that cause a single part of a machine to fail. These causes can be briefly categorised as: physical attack, over-stressed components, lack of maintenance, unforeseen incidents and knock-on effects, errors or mistakes and poor design choices or poor manufacturing/assembly quality and care. [3, 4]. In the following subsections, the main three groups of maintenance plans will be discussed [5, 6].

1.1.1 Pre-Emptive Detection and Elimination

The cheapest way to reduce maintenance costs is through pre-emptive approaches. In other words, by starting with an appropriate design and selection of plant machinery and equipment, it is possible to minimise the necessity for regular maintenance. A simple means of achieving this is to begin by providing answers to a series of enquiries for each and every part of the plant. Depending on the results, one may insert appropriate design characteristics to minimise the impact of failure [7, 8]. This method benefits from having a comprehensive plan for the machine's entire operating life. The consequences of applying a pre-emptive diagnosis and exclusion maintenance strategy should begin by observing that the predicted failures of such machines are not occurring [5, 9].

1.1.2 Quality Control and Assurance

This approach required precise quality control in manufacture and assembly, so that a machine is made and assembled to the same accuracy it was designed. Good quality control will reduce

manufacturing and installation errors, and hence reduce the likelihood of faults. This means following an exact set of pre-written rules and steps on how the job should be carried out. A working machine that is precisely and correctly assembled has a longer mean time between failures (MTBF). Thus quality control can be considered a form of preventive maintenance [5, 9].

1.1.3 Preventative Maintenance

A preventative maintenance (PM) scheme is often employed to identify the maintenance tasks needed to be carried out at prescribed intervals in order to avoid equipment failure. In effect carrying out a maintenance procedure prior to the occurrence of a predicted machine malfunction. A scheduled maintenance scheme is a respectable approach which can offer significant savings in plant maintenance expenditure [5, 9].

The PM strategy can be described in two ways. The first description is defined as the “examination and observation” method, which includes regular inspection and evaluation of the condition of equipment parts for unusual signs of ageing and/or wear. Upon the detection of such failure, the damaged part should be replaced either immediately or at the earliest possible time, before the damaged part fails and causes full failure [3]. Nevertheless, this is not an effective approach, as the inspections are undertaken at scheduled intervals irrespective of the actual condition of the equipment [8, 9].

The second PM description is known as “shut-off repair” maintenance, which requires intervention and component replacement after a pre-defined period of operation. The length of operation is based on experience of component deterioration and is shorter than the MTBF. Typically, such maintenance is conducted as part of a refurbishment, where the equipment is removed from the process line during the scheduled shut-off period and moved to a workshop to undergo a full strip down. Thereafter, the component(s) are replaced and the equipment is reassembled as new [3].

1.1.4 Predictive Maintenance

Predictive maintenance is an effective approach which is based on monitoring the machine’s health during normal operations, to identify signs of changed conditions within the machinery. Usually, a set of machine parameters are measured online and compared against a reference set, which then decide whether a maintenance intervention is necessary or not. By being able

to detect the start of a fault at an early stage, it is possible to manage the machine carefully (e.g. by avoiding overloading) until it can be conveniently taken offline and maintenance arranged accordingly. By adopting this strategy, substantial financial advantages can be gained by decreasing the equipment maintenance operation costs [10]. The predictive maintenance method may include oil debris analysis, vibration monitoring, ultrasonic analysis or thermography, to identify any changes in the machine parameters and the rate-of-changes associated with them, in order to be able to predict the equipment's remaining working life [3].

1.1.5 Reactive or Breakdown Maintenance

In this approach, also known as the run-to-failure method, maintenance is only implemented when the machine is unable to operate as a result of component failures and no prescribed action is taken to avoid unwanted machine stoppage. After machine breakdown, corrective actions are taken to either replace or repair the failed component(s) [10]. The financial consequences of such maintenance approaches are usually large when applied to critical industrial machinery [11]. Generally, run-to-failure maintenance is suitable when the following cases exist [3]:

- 1) The machine or equipment is redundant;
- 2) Low price spares exist and are available immediately;
- 3) The production process is interruptible or there is a stockpile of products;
- 4) All known failure modes are safe;
- 5) There is a known long mean-time-to-failure (MTTF);
- 6) There is a low cost associated with secondary damage and
- 7) Quick repair or replacement is possible.

1.2 Gear Transmissions

Gears are used widely for power transmission from one mechanical system to another, and where a change in rotational speed is required. In basic form, a gearbox is comprised of two or more gears mounted on rotational shafts, which are supported by bearings. The entire structure is bounded within a housing, filled with adequate lubrication oil. For electrical machinery, a drive system such as an induction motor rotates the input shaft of the gearbox at a high speed. Based on the gearing ratio within the gearbox, the gears act as a speed reducer that causes the output shaft to rotate at a lower speed relative to the input shaft, to provide a high-torque output for driving the load [12]. Usually, gearboxes are equipped with one or two set of gear types.

For example, a particular gearbox can consist of one set of gear teeth meshing with different gear teeth to allow for power transfer with no slippage. Upon the engagement of the two gears, rotating one causes the other to rotate in the reverse direction. Depending on the number of teeth that is on both gears, the speed of rotation of each gear will be different. The smaller gear that has the fewer teeth is called a pinion, whereas the larger one with more teeth is called the gear. In case of the pinion driving the gear, the output rotational speed will decrease and when the pinion is driven by the gear, the opposite effect is true. For the former case, the reduction in output rotational speed can be obtained by dividing the number of pinion teeth by the number of gear teeth [13]. Ultimately, the speed reduction ratio R_s is given by,

$$R_s = \frac{Z_1}{Z_2} \quad (1.1)$$

where Z_1 is the number of pinion teeth and Z_2 is the number of gear teeth.

1.2.1 Spur, Helical, Bevel and Worm Gears

Depending on the application requirements, gear products come in a variety of sizes and shapes. As a significant example, Figure 1-1 shows a spur gear, which comes with straight-cut teeth that are parallel to the driving shaft. These gears are only suitable when the two (i.e. the input and output) shafts run in a parallel formation. Spur gears are generally favoured for moderate speed conditions as they reduce wear on the gear teeth caused by a rolling and slipping motion that occurs during engagement and disengagement. Spur gears produce no axial thrust and are relatively cheap; thus, they can be found in most mechanical applications. However, these gears are known to produce more acoustic noise, which can be more problematic at high speeds [12, 14].



Figure 1-1 Spur gear [15]

In contrast to spur gears, the helical gears, as shown in Figure 1-2, have their teeth at an angle to the gear shaft axis. Helical gears can be manufactured in both right-handed or left-handed configurations to transmit power and motion. Helical gear boxes provide reduction ratios within the range of 3:500; higher ratios can be achieved by using multiple gearing stages [16]. The helix angle can be up to 45° ; although higher angles tend to reduce the bearing's load capacity. Compared to spur gears, the teeth of helical gears mesh smoothly with each other resulting in less noise and vibration. In such gears, the contact line between the teeth during engagement runs diagonally across the face of bearing, from the side at one end to the root at the other end [14]. Moreover, the helix angle allows for the extension of the length of the contact line which can lead to a higher tooth contact ratio therefore, the load can be spread over a larger surface area. Owing to its greater tooth strength and higher contact ratio (i.e. more teeth being engaged), the helical gear is often used to transmit power and motion in high-torque applications. These attributes enable helical gears to carry larger loads, as compared with spur gears of the same size [12, 16]. Furthermore, helical gears transfer loads by a sliding, rather than a chopping action, this offers a quieter operation while carrying heavy loads with a lower wear rate. Moreover, these gears are capable of transferring power from one shaft to another that are at an angle (up to 90°) to each other. Although gear and pinion have different rotational speeds with respect to each other, when meshing two helical gears of differing diameters, a variation in speed and torque between the two rotational shafts occurs, which can disturb the meshing frequency of the gears [17]. In addition, as the teeth mesh together in a helical gear a thrust load is generated along the gear shaft, this is caused by the angular cut of the teeth. As the helix angle increases, so does the thrust load created. This effect has to be taken into consideration when selecting the correct supporting bearings for a particular shaft. Moreover, it is important to use thrust bearings to carry the thrust load generated and maintain a proper gear alignment during operation. In helical gears, since the contact surface is longer, the efficiency of power transmission is lower than that of a comparable spur gear [14].



Figure 1-2 Helical gears [18]

Figure 1-3 depicts a bevel gear. This type of gear is used in transferring power between shafts. The teeth in bevel gears are formed on a conical surface so that the shafts are perpendicular (90°) to one other and ‘intersect’ at the apex of the cone. The bevel gear teeth are straight-cut and are parallel to the line that extends to the apex of the conical surface on which the teeth are formed. These gears can be noisy at high rotational speeds. Moreover, due to their teeth arrangement, the application of bevel gears in parallel shafts is not possible [19].



Figure 1-3 Bevel gear [20]

Alternatively, worm gears, as shown in Figure 1-4, can be also used in driving helical or spur gears and allow two perpendicular and non-intersecting shafts to properly mesh. Irreversibility is an important facet of meshes in worm gear. This means that, turning the worm gear will cause the meshing spur to turn also, however, turning the spur will not rotate the worm gear. The result is a mechanism that is ‘self-locking’ that is useful in ricketing [19]. Such gears usually have a high tolerance for large loads and can be used in the conversion of rotational motion into translational motion. Additionally, worm gears can have quite a large pitch diameter [19] [21].



Figure 1-4 Worm gear [17]

“Gears are of three types depending on the shafts relative geometry which can be intersecting, parallel, non-intersecting and non-parallel”.

- 1- Helical, spur and herringbone gears are gears that mesh on the same plane and then transmits rotary motion power between the parallel shafts.
- 2- Intersecting shafts which are mutually perpendicular to one another, and are very suitable gears including the spiral, bevel and worm gears. These type of gears are used widely in locomotives, hand drills, marines, automobiles applications and in all rotorcraft drive systems, with several as planetary gearboxes. However, it should be noted here that some are non-reversible because whenever a worm gear is turned on, the meshing spur is turn on also. Attempting in rotating the spur will not cause the turning of the worm gear [22].
- 3- Gears that are suitable for non-intersecting and non-parallel shafts which include the worm, hybrid and crossed helical gears [23].

However, the most common types of gears used in the industry can be summarised in Table 1-1, which are categorised primarily as the spur gear and helical gear.

Table 1-1 lists properties of the most common types of gears: spur and helical [24].

Gear type	Sub-type	Comments
Spur gears	Normal Spur Gears	<ul style="list-style-type: none"> ➤ Most common gear in terms of their ease to design and manufacture. ➤ Allows for shafts that are parallel. ➤ High efficiencies of up to 99 percent per train. ➤ No side thrust. ➤ Capable of back drive, ➤ Single ratios of up to 1:10. ➤ Low noise and vibration owing to its precise design. ➤ Lubrication is required by the steel pinions while plastics do not.
	Internal Spur Gears	<ul style="list-style-type: none"> ➤ Have similar performance to that of the normal spur gears. ➤ Results in a drive geometry that is compact. ➤ Used commonly in manufacturing of planetary/epicyclical gears.
Helical gears	Single-Helical Gears	<ul style="list-style-type: none"> ➤ Similar properties to that of the spur gear, but the drive results in an axial thrust. ➤ Compared to spurs, helical gears are quieter and smoother for the same specification/ size. ➤ For up to huge diameters, the gears can run at a very high speed ➤ Higher life/torque capabilities can be achieved for the same spur gears size.

1.2.2 Gearbox Regional Market

In order to satisfy the current market demands, gearbox manufacturers offer a wide range of designs, with loads from 2-3 Nm up to 500,000 Nm [16]. The increase in energy costs over recent year has led to the exploration of alternative energy sources, such as wind, tidal, hydro, etc., which has led to a significant increase in demand for application-specific gearboxes with new, pre-defined requirements. Furthermore, the uptake of automated and mechanical handling machinery by product suppliers such as Amazon is expected to rise in the near future, increasing the European and UK demand for gearboxes and geared drive systems. For more details on the overall market situation, the reader is referred to reference [16]. Due to their high

reliability and efficiency, the helical gearboxes form a major proportion of the total European gearbox market and are expected to have the maximum growth, when compared to other gearbox designs [16].

1.2.3 Industrial Gears Application

Gears play a defining role in almost all industries. This is due to their structural design which allows for matching of speed and torque between a prime mover and a load. Gears are put in place to increase or decrease rotational speed and torque [16]. To achieve a specific output speed and torque, a combination of two or more gears, meshed together with specific gear ratios, can be used [24]. The type of gears employed by different industries very much depends on the intended usage and required gear properties. In some industries, including agriculture, construction, automotive, military, railways, processing equipment, machine tools, wind energy, and aerospace are wide ranges of gear applications [16].

1.3 Gear Failure Modes

The gears incorporated into the gearboxes are usually robust components with high reliabilities. Nevertheless, gear failure might occur as a result of unexpected system interactions such as an overload or lubrication deficiency, failure rarely occurs due to defects in the gear itself. A number of factors can cause gear failure. These include poor gear design, selection of the wrong gear for a given application and/or manufacturing error (e.g. improper gear geometry). Gears are designed to always rotate at the pitch line during operation (see Figure 1-5). Gear teeth engaging below or above the pitch line of action can lead to excessive wear, which, may cause a gear failure [25].

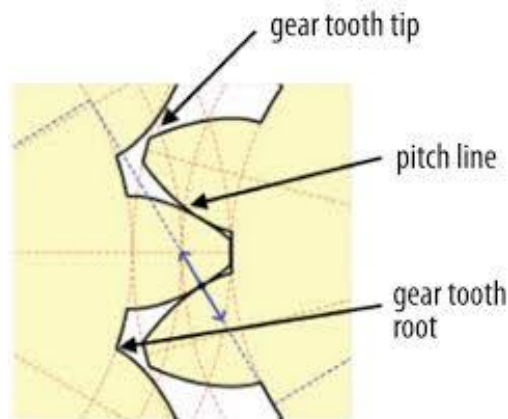


Figure 1-5 Gear pitch line [26]

Some of the on-site causes of gear failures include, most frequently, lack of adequate lubrication, misalignment of drive shafts, lack of adequate cooling, improper mounting and excessive vibration, lack of proper maintenance or even use of the wrong components in the design [16]. The physical failure modes for a particular gear can be summarised as [16] [27]:

- Overload
- Bending fatigue
- Hertzian fatigue
- Cracking
- Scuffing and Wear

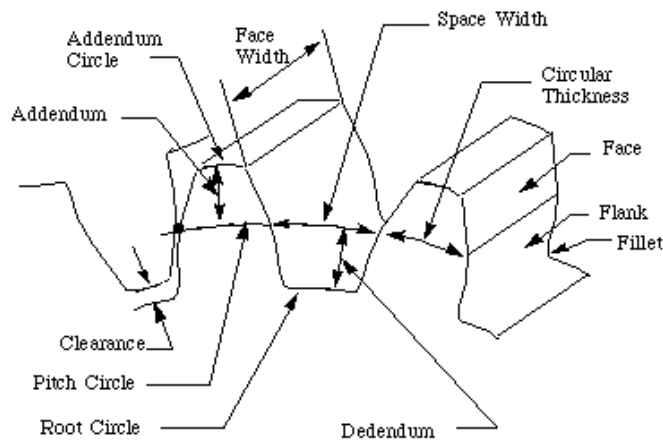
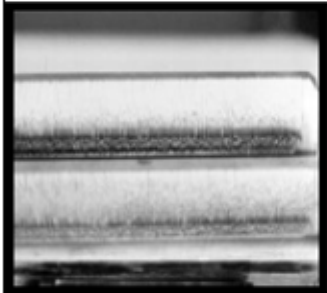
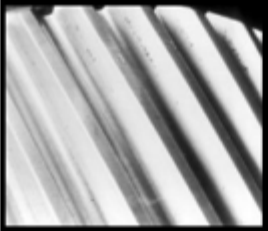
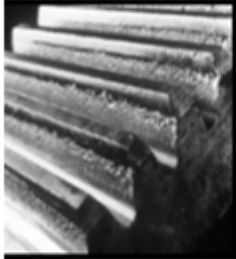
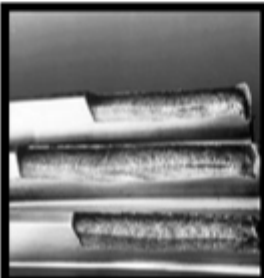


Figure 1-6 Gear terminology [28]

However, the wear probably is inevitable and yet the fundamental causes of others. Table 1-2 depicts common wear modes of gears along with processes and mechanisms that lead to their corresponding wear faults.

Table 1-2 Gear wear processes and mechanisms [13; 19]

Wear modes	Wear failure
<p>Polishing wear</p>	<p>Process – slow process of wear. Mechanism/causes – in absence of adequate lubrication, direct metal-to-metal contact creates a polished surface on the gear teeth.</p>
<p>Moderate wear</p>	<p>Process – wear process occurs when metal has been removed from the addendum of the tooth surface, while maintaining a continuous operating pitch line. Mechanism/causes – lubricant contamination and/or gear operation near boundary lubrication conditions.</p>
<p>Extreme wear</p>	<p>Process – uniform removal of relatively large amounts of material from the gear tooth surfaces, combined with the effect of pitting presence at the pitch line. Mechanism/causes – Insufficient lubrication for the given tooth load and presence of fine abrasive particles or contamination in the lubrication system.</p>
<p>Abrasive wear</p> 	<p>Process – appears as a combination of a lapped surface, radial scratches and grooves on the tooth contact points. Mechanism/causes – contaminant in the lubricating system consisting of metal particles that originate from the gears and bearings, weld spatter, scale or rust, sand, dirt or any other environmental contaminants.</p>
<p>Corrosive wear</p> 	<p>Process – appears as surface deterioration, a chemical action of active ingredients in the lubricant. Mechanism/causes – wear process caused by oil breakdown and intrusion of corrosive elements in the lubricant that ‘attack’ the gear contact surfaces. This process affects the grain boundaries, which lead to the formation of a fine and evenly distributed pitting.</p>
<p>Surface fatigue failure</p>	
<p>Pitting</p>	<p>Process – pitting tends to redistribute the load by gradually levelling ‘high contact’ spots and terminates the process</p>

	<p>once the load has been redistributed. The process eventually causes burnishing to the pitted surface and improves its appearance. Mechanism/causes – occurs at gear teeth that are over stressed.</p>
<p>Destructive pitting</p> 	<p>Process – appears as much bigger pits than the initial pitting. Mechanism/causes – severe overload conditions that cannot be contained by the formation of initial pitting. This occurs as a result of continuous stress cycles building up, which initially support the pitting wear process, but continue and eventually destroy the tooth profile.</p>
<p>Spalling</p> 	<p>Process – similar to destructive pitting, with the exception that the pits are larger, relatively shallower and irregularly shaped. Large and irregular voids will be created due to rapid breakages of the pit edges, which will eventually join to create even bigger pits. Mechanism/causes – excessively high contact stress levels.</p>
<p>Case crushing</p> 	<p>Process – longitudinal cracks on the surface of a single tooth or two teeth, which later lead to the breakaway of a long piece of the tooth surface. Mechanism/causes - when the case is significantly harder than the core, subsurface fatigue failure will occur. This wear process can also happen as the surface contact-stress at high cycle levels surpasses the material's endurance limit.</p>

Most gear defects arise when gears are operated under extreme stress conditions such as in an overload or at extreme speeds for a long period of operation [16]. Neale Consulting Engineers Ltd. (NCEL) has found that gearbox defects often start in the bearings rather than in the gears themselves [29]. This is due to the vulnerability of the gears to the impact of tiny residues of debris in the lubricant. In fact, in most cases of gear failure, lack of lubricant, lubricant contamination, oil film collapse, use of improper lubricant for the intended application and additive depletion have been identified as the causing factors as seen in Table 1-2 [14].

In general, gear failures can be placed into two categories: distributed faults and localised faults. The distributed faults are those which take place over a large area of the gear teeth surface and tend to be uniformly distributed such as gear eccentricity, uniform tooth wear and

shaft misalignment; and then produce modulation that is continuous at a particular frequency that corresponds to the gear rotational speed. (It should be noted that tooth fatigue and shaft misalignment are the main focus of this research work). On the other hand, the localised faults only affect a small area of the gear tooth surface and usually have an impact on the gear's power transmission capability. Typical examples of localised faults include cracked tooth and tooth breakage, or local wear on one more teeth (e.g. pitting). These defects usually produce a short impulse whose duration reflects on the period of tooth-mesh interval, and with a periodicity that is equal to the gear. [16]

Generally, there are two primary gear wear types [30, 31]. These are listed below, together with a brief description of each type;

1. **Adhesive wear** – this involves the particles transfer from surface to surface, when there is a relative motion. Other names in describing adhesive wear are galling, seizing, scuffing and scoring. During adhesive wear, the removed particles are either temporarily or permanently adhered to other surfaces, due to the process of cold welding. Two vital points from a forensic point of view can be made here; a) when two materials that are similar or identical, over time, slide over each other, both surfaces then become coarsened or roughened. The severities for each of the surface score and gouge the other surface until they both worsen or deteriorate which then leads to a condition of rapid wear; and b) if two dissimilar metals slide over one another, the asperities at the junction will have, between the two, an intermediate strength. Therefore, when there is sliding between two surfaces, shear dominates, leaving the harder one having small fragments from the softer material attached. As a result, damages will mainly be to the softer material surface [32].
 2. **Abrasive wear** – this involves the process of material displacement or removal from any surface by the hard particles sliding along the surface. If the surface of one is harder than the other surface and adhesion is not dominant, the hard surface asperities can cause removal of material from the softer one in two ways; a) if there are asperities of appropriate dimension and size, they behave as minute tools for cutting, removing material in the fine chips form from the surface; and b) particles that are hard sharp such as fine debris or dust from another machine part can become entrenched in the sliding surface of the softer material and then abrade the harder surface[33] [32].
- **Delamination** – if the sliding surface lubrication is poor, a different kind of fatigue failure occurs. Though the adhesion may not be sturdy enough to tear out the surface fragments,

very large forces can be produced, which in turn, can result in the surface layers becoming severely work-hardened while developing tensile stresses below the surface. Cracks are formed parallel to the surface and they will start to emerge at some point on the surface, releasing metal flakes. This process can be regarded as delamination wear and readily occurs if there is a multiphase material containing hard particles. This process of delamination is an influential factor in dying of rolling thread, bearing failure, universal joints, etc.[34].

- Fretting [35] – this type of wear manifests itself as a small vibrations or amplitude between two surfaces being mated. For instance, in a steel ball bearing, where relatively little rubbing occur between the race and the, there is a continuous unloading and loading within the race at every point, as balls approach and then recede from those points. The cumulative effects for millions of stress cycles though small, can lead to fatigue. Below the free surface is where the maximum shear stress can occur, where fatigue crack is first most likely to occur, especially if within the steel, there is some inhomogeneity including inclusion that is small and hard. The generated crack will then grow near to the surface to become a surface crack. This can be further exacerbated by the sub-surface crack growth, which will eventually spread to the surface and leads to flakes detachment. Alternatively, a flaw in the race surface may be the initiating fatigue crack cause. The crack then traverses into the race and then interacts with the maximum shear stress region, producing fragments of wear and leaving behind fatigue pit on the rolling-contact. The mechanism of this wear is accompanied often by corrosion which can be found commonly in orthopaedic implants, bearings, bolted and riveted joints, splines, oscillating couplings, etc. [36].
- Corrosive or chemical wear – this wear type is caused by chemical effects. One of most common metal corrosive wear example is the repeating formation cycle, reformation and removal of oxides (known simply as rusting). The resultant fragments are typically small and may appear as flakes that are well compacted that consists of metal particles and fine oxide mixture. A similar process of wear may also occur with films being formed by the lubricating agent on the surface of the metal bearing [34].
- Erosive wear – this involves material loss due to a relative motion-taking place in a fluid medium between the solid particles and material suspended. When there is near parallelism in the relative motion, it is termed erosion, whereas, the mechanism where the relative motion is nearly normal to that of the material is termed impingement. Erosive wear causes damages to pipe bends and joints, centrifugal pumps, valve components, turbines and compressors [37].

1.3.1 Types of Gear Failures

“Gears are said to have failed when they no longer do their job efficiently for the purpose of which they designed to. The failure causes excessive wear all the way to catastrophic breakage. Damage in the gear tooth is caused by different factors which include inappropriate specification or operating conditions, inadequate lubrication, manufacturing or installation problems and material insufficiencies. Gear systems effective lubrication is very important as it prevents tooth from direct contact [38] [25]. Figure 1-7 below shows the summary many different failure mode classifications in gear” [39].

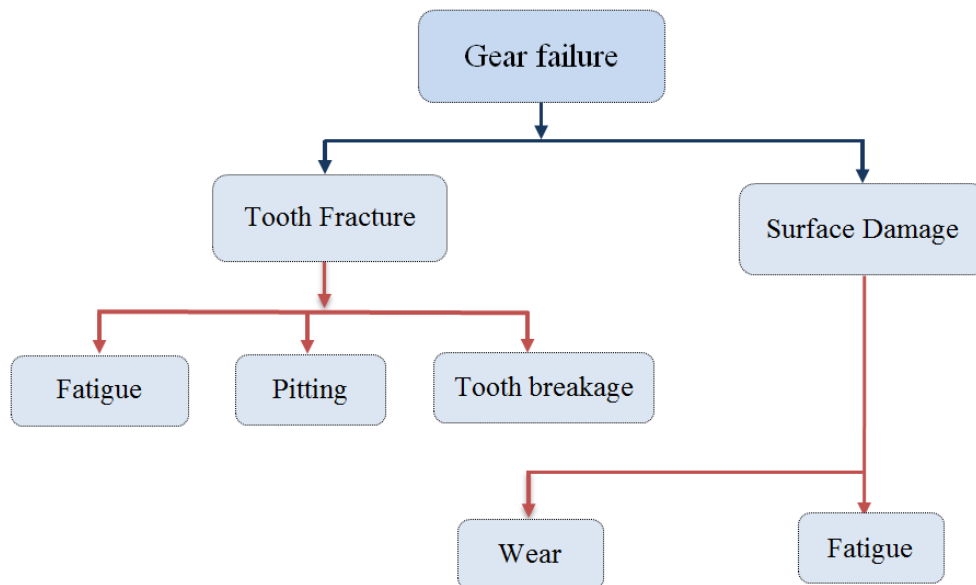


Figure 1-7 Classification of different gear failure modes [16]

Gear fatigue usually results in a catastrophic failure of the gearbox. Examples of fatigue failure include tooth bending fatigue, contact fatigue and thermal fatigue. Tooth bending often starts with a small stress which, if increased, can form a cavity at the tooth root. Over time, the cavity can extend from the initial defect location as a crack, until partial/complete failure of the tooth occurs [16, 40]. For brevity, the process of tooth fatigue failure can be explained in three stages:

- 1) Start of primary crack,
- 2) Crack progression across a cross-section,
- 3) Final unexpected fracture of the residual cross-section.

Tooth fracture failure can occur due to overload or impact. Gear tooth surface or contact damage can also cause tooth fracture, which generally occurs on the operational surfaces of the gear tooth and can be placed in one of the following categories; wear damage, scoring/scuffing,

plastic flow and pitting. Refer to Table 1-1 for more details. Ultimately, tooth surface damage can lead to localised change in the amplitude of the tooth meshing vibration which can serve as a useful tool to anticipate for breakage [40].

Wear damage is a gradual process, which is imminent due to the lack of lubrication between two surfaces in contact with each other (e.g. gear teeth meshing). Moreover, wear is the damage caused to an outer hard surface by the mechanical action of contact between two or more solid surfaces. Gear wear usually occurs on the working surface of the teeth, which is accompanied with the generation of an audible noise and reduced transmission ability of the gear [16]. Other common causes of gear tooth wear include the presence of abrasive elements in the lubricant and corrosion of internal elements within the gearbox. Thus, adhesive and abrasive wear can be thought as the most common modes of gear failure [16].

Pitting is another mode of failure that involves damage to the gear teeth surfaces under load conditions, due to direct contact between two meshing gear teeth, and may appear at various severity levels, from micro-pitting expanding to large-scale spalling. Despite the exhibition of similar microscopic characteristics, micro-pitting and pitting are usually distinguished from spalling by the shallower pits created in the affected area [41, 42]. During pitting, the contact between the meshing gear teeth can be either along a line, at a local point or small circular/elliptical area. In general, extreme load conditions can lead to tooth breakage. Often, the process starts with a small crack in the tooth root, which extends over time to breakage point. If a faulty gear in such condition continues to operate, damage can spread and cause breakage to several consecutive teeth [43]. In this work, fault progression and run-to-failure in a single pinion and gear tooth are both examined.

1.3.2 Causes of Gearbox Failures

A gear can fail due to a number of reasons. The list below provides some of the most common fundamental causes of gear failure [16, 44]:

- 1) High tooth loading for long process times.
- 2) Non-uniform distribution of load over the teeth.
- 3) Incorrect design or inadequate processing.
- 4) Inherent material defect from manufacturing error.
- 5) Careless or incorrect usage of gears.
- 6) Incorrect or bad use of lubrication.

- 7) Influence of other parts such as gearbox bearings.
- 8) Misalignment effects leading to teeth being gradually damaged.
- 9) Extreme heat due to high-temperature operating conditions.
- 10) Contamination in the lubricant e.g. moisture and abrasive particles.
- 11) Errors due to miss-installation [45] .

1.4 The Demand for CM

In today's industrial society, mechanical machines play an integral part in the design of more complex systems, intended to deliver better flexibility and functionality. This development and the parallel requirements for increased equipment life-cycle, improved production quality, greater human safety and reduced adverse environmental impacts, have set out an increasing desire for new maintenance techniques. As explained in Section 1.2, planned maintenance using on-line testing is a very cost effective measure, compared to either waiting for equipment to totally break-down before a problem is addressed or where machines are routinely taken out of production at set times regardless of their actual condition [16]. Modern CM techniques employ new technologies to evaluate the machine's health and predict when the machine is likely to fail and thus, maximise the machine profitability [16]. For example, predictive monitoring is an effective maintenance technique which is based on close monitoring of certain physical characteristics of the machine's actual condition[46].

1.5 Conventional CM Techniques

Between March and May 2002, the Plant Maintenance Resource Centre conducted a survey of CM and non-destructive testing (NDT) technologies, which revealed that the human senses were the most commonly used methods, followed by vibration characteristics and analysis of the lubricating oil [16]. Figure 1-8 shows the results of the survey for the relative frequency of different CM techniques used [16]. Some of these techniques which are used more in gearbox will be further outlined explained in detail [16, 47].

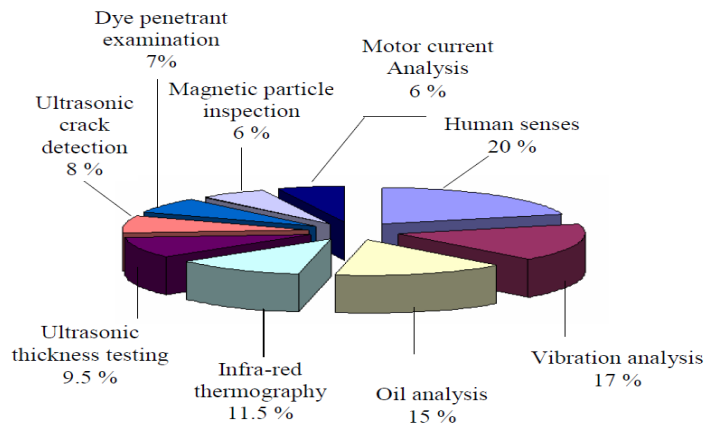


Figure 1-8 General usage of various monitoring techniques [16]

1.5.1 Trend Monitoring

This monitoring technique finds its usefulness on the repeated metrics measurement such as temperature, pressure, noise, torque, electrical current, etc., which are plotted in real time. If the plots fall within predefined operating thresholds, the machine is deemed to be healthy [48]. Otherwise, changes in the readings are compared against a set of initial/reference parameters in identifying changes in machine condition and detect any system abnormalities, see Figure 1-9 for an example. Consequently, if the readings exceed beyond the pre-specified limits, necessary corrective actions are taken [49, 50].

Figure 1-9 presents the variation of a particular machine parameter throughout its life cycle. Once the machine enters its so-called ‘final life’ state, the system becomes significantly prone to failure and faults can arise at any time. Therefore, maintenance schemes are put in place to extend the machine’s working life, which require for gathering of accurate datasets [16, 48].

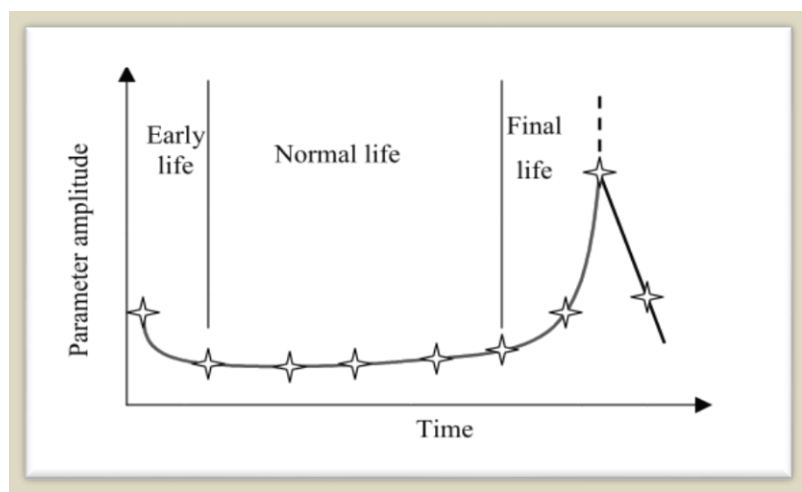


Figure 1-9 Trend monitoring record [51]

1.5.2 Thermal Monitoring

Thermal monitoring, also known as thermography, is a well-established CM technique in which the temperatures around various parts of the machine are recorded using infra-red cameras, in an effort to identify recurring thermal patterns within machine [16, 50]. Thermal monitoring can increase the capability of predicting component failure in a machine, before personnel injury, equipment damage or a costly breakdown occurs. In such technique, the thermal signature of the machine is used as an indication of the machine's health and any deviation from the machine's normal thermal signature is considered as a fault case (e.g. hot spots) [16]. Rather than finding the cause of a particular fault, thermal monitoring is used to provide the location of the fault, though, the excess heat generated must first reach the machine surface before the faults detection can occur; thus, thermal faults such as hot spots may cover a significant area of the machine.

Thermography benefits from ease of application to a wide machine variety including pumps, motors, conveyors, pulleys, drives, fans, bearings, etc. However, changes in ambient temperature must be accounted for, as it directly influences the accuracy of the measurements [48-49].

1.5.3 Visual Inspection CM

Visual inspection is a simple, yet powerful CM technique. It is usually complemented by other human senses such as hearing (listening for a change in machines noise), touch (check for changes in machine surface temperature or an increase in vibration levels) and even smell (check for smell of burning which is significant in electrical faults). The human senses allow for an instant evaluation of the machine's condition and in case of an skilled/experienced operator, faults such as corrosion, cracks, leakage and subsurface defects can be detected [52].

The technique can be further improved by using a range of tools such as a stethoscope, magnifying glass, endoscope, etc. [53]. However, a major drawback of this CM technique is that it involves the human bias and the level of skills and experience of the operator having direct effect on the final conclusion which can give rise to similar symptoms being given a different diagnoses [53]. Human senses may give an accurate evaluation of the imminent failure. For example, the smell sense could provide a satisfactory evaluation for a near-to-failure electrical component. However, advanced CM methods available in literature will not

only provide a more accurate prediction of the time to failure, but will also generate a much earlier warning in case of a fault presence.

1.5.4 Corrosion Monitoring

Corrosion is a major cause of failure in rotating machinery as it arises when a machine component is exposed to a corrosive environment, which can lead to the failure of the machine's infrastructure [54, 55]. Weight loss analysis is a common corrosion monitoring technique, where a component or sample is taken out from the machine and weighted before and after all the corrosion products have been removed. The weight loss is then deemed as an indication of average corrosion rate.

This method allows for an early corrosion damage detection and fault location, enabling corrective actions to be quickly, in extending the machine's lifetime, prevent breakdown and prevent any extra costs. Moreover, any internal corrosion can potentially lead to costly cross-contamination of other components and process streams, while external corrosion (e.g. leaks) can contaminate the plant environment, raising concerns for safety hazards [54, 55]. It should be noted that, this form of corrosion monitoring approach demands for scheduled shutdowns of the equipment to be checked, incurring costs due to loss of production, restarting energy and replacement materials.

1.5.5 Oil Analysis and Monitoring of Wear Debris

Oil analysis and monitoring of wear debris method are commonly used CM techniques, from which the machine's condition can be assessed by investigating a sample of the lubricant and looking for wear elements contained within [56]. This method also allows for the determination of the lubricant's quality based on the three main components of a lubrication oil; the base oil; lubricant additives; and contaminants. The latter is used as a measure for the rate of continuous wear, which reflects on the machine's performance. The oil CM method is capable of providing an early notice about the machine's health condition, even earlier than vibration methods. However, a disadvantage of this technique is that it is fairly insensitive to the physical size of the component which has been subjected to an abnormal wear and rather focuses on determining when the oil must be changed [54, 57].

1.5.6 Acoustic Airborne Monitoring

Acoustic-based methods for machine CM have been widely applied in maintenance of rotating machinery for many years. It is a well-known fact that, while the machine is operating, vibration and noise will be generated. The acoustic signals are then picked up by special microphones and analysed by the use of appropriate techniques for signal processing to provide information on the health of the machine. Acoustic-based techniques are non-intrusive and use inexpensive microphones which are easily mountable. This technique is considered as an ideal choice for CM of bearings, gearboxes and engines [58]. Acoustic monitoring can provide a direct indication of noise sources in a machine [59]. However, a major problem with this method is background noise contamination, especially the noise coming from connected sound sources, for example, the cooling fan, drive motor and/or from similar nearby machinery [58].

Over the past few years, acoustic-based CM of machines has been a popular subject of study amongst researchers. Of particular interest, is an acoustic monitoring method developed by Li *et al.* [60] to detect tappet clicks, misfiring and injection timing faults in diesel engines. In the proposed technique by Li *et al.*, the authors have used signal processing method which is quite advanced which include the DWF (discrete wavelet transform). As a follow-on from this pioneering work, Gu and Li [61] researched on the possibility of using monitoring technique via acoustics for fault detection in electrical motors (which has fewer noise source that can be non-stationary when compared to the diesel engine). By using the DWT and averaging techniques, Gu and Li showed how possible it is in extracting fault information that are distinctive, even in industrial environments where background noise levels are usually high. Later, Ball and Gu proceeded in investigating ways to enhance the acoustic spectra being monitored by the use of fuzzy logic and filtering techniques by Kalman [62, 63]. Other advanced techniques for signal processing developed by Gu, Li and Ball, including the CWT (Continuous Wavelet Transform) and ICA (Independent Component Analysis), were applied also to the engines acoustical signals from engines [64-66]. In [66], Li investigated CM using acoustic techniques for a diesel engine with different conditions of operation with the results showing the possibility of identifying the differences that occurs between the faulty and normal condition of an engine's, based on the features being extracted from the test generated engines acoustic signals.

In [67], Albarbar *et al.* used technique called adaptive filtering in enhancing the diesel fuel needle impact excitations injector which are contained within the airborne acoustic signals to

realise an enhanced CM information extraction method. Similarly, Jiang *et al.* [68] proposed a CM effective method for engines with diesel combustion which is based on acoustic theory of one-port and measurements of exhaust acoustic. The authors managed to provide a more engine combustion representation that is accurate, by minimising, in the exhaust system, the effects of reflection.

However, since airborne noise is pressure waves in sequence propagated via a medium that is compressible (e.g. air). During this propagation, there is either reflection or refraction of sound waves by other bodies within the medium, which can cause an attenuation of the incoming signals. If the sources of the sound are located in spaces that are enclosed, any reflections from the boundaries can affect the sound source characteristics, which makes fault diagnosis by acoustic noise analysis a difficult task. For a detailed description of machines' CM using airborne acoustics and advanced signal processing techniques, the reader is referred to references [48, 49].

1.5.7 Acoustic Emission (AE) Monitoring

AE is defined as the generation of transient elastic waves due to strain energy rapid release that have been caused by a damage or deformation on the surface or within a material. This energy is then propagated through as structure-borne or fluid borne (liquid, gas) waves [69]. In rotating machinery, AE can stem from impacts, friction, turbulence, material losses, cavitation and leakage. Traditionally, the common most measured parameters of AE for diagnosis are root-mean-square energy, kurtosis, amplitude and crest factor [70]. Due to its microscopic nature, the AE has properties akin to a broadband signal, which makes it a sensitive tool in detecting incipient damage.

The AE often has 100 kHz to 1 MHz frequency range, which makes less likely for the structural resonances and background structure borne noise to influence the captured signatures, which occur below 1 kHz. In comparison to the vibration technique analysis, the AE approach for machine CM offers earlier detection of failure advantage as increased sensitivity is offered by the AE. There are however, limitations to applying AE technique successful to monitor the wide range performance of rotating machinery, some of which include overcoming difficulties in interpreting, processing and classifying the signatures gathered during data acquisition. Another disadvantage of this CM technique is that, due to the rapid attenuation of the AE signal, the sensor must be placed very close to the AE source [71].

While it is advisable in placing the AE sensor on components that are non-rotating on the machine (e.g. on gear or bearing casing), the signal being observed that originates from the component being studied will still experience severe loss (signal-to-noise ratio) and reflections, before being picked up by the sensor. To overcome this challenge, Nakra and Tandon [72] have established the effectiveness of certain parameters of AE including peak amplitude and count for the defects detection in a ball bearings that is loaded, operating at moderate and low speeds. Tan [73] further expanded on this work and applied AE to detect different bearing failures. In his work, Tan also suggests that the area measurement under the time-amplitude curve can be utilised as a very effective tool in detecting defects in bearings with rolling-element. Later on, Yan *et al.* [74] used AE in detecting breakage in tool in a milling machine, by analysing the spectral and statistical characteristics of various AE generated signals during the processes of cutting. In their work, measuring the AE Root Mean Square (RMS) intensity values was used also in the detection of failures during the cutting processes. The work presented by Yan *et al.* helped in providing a better understanding of the relationship that exists between the different processes of cutting and the received AE signals.

Due to the short data collection and processing times, it is advantageous to use AE to achieve a fast and continuous monitoring of the performance of the machine, by placing a several (or single) sensor(s) within the structure and collecting the data over a long period. In [75], Dorge undertook a study on AE monitoring for detection of failures in glass-reinforced piping. Also, in [76], Adams developed successfully, an AE monitoring system for in detecting fiberglass tank/vessel failures. Later, Lee *et al.* [77] suggested a two-step scheme for fault detection in a lathe machine. The proposed technique is based on using a sensor-fusion concept and consists of a force sensor attached to the cutter, which measures the AE generated signal as a result of the cutting process.

1.5.8 Vibration Monitoring

All machines generate vibration in some form or another. Researchers have used this property to develop CM techniques for early fault diagnosis and trouble-shooting in rotating machinery, including gears. Vibration monitoring is generally considered as one of the most authoritative CM techniques, which forms the basis of a number of predictive maintenance programs [16, 78]. Techniques based on machine vibration analysis are thought as the most effective means of failure prevention and are commonly applied to online monitoring of a wide range of rotating machineries [79, 80]. Such statements are given because each fault in a rotating machine

produces a unique vibration signal at a specific frequency, which can be mapped exactly to machine fault conditions [81]. For example, in a gearbox, the vibration signals carry the constituent gears' fault signatures and the detection of the fault is realised via the analysis of the acquired signals by using different signal processing methods.

In rotating machines or equipment, the measured response (signal) of the system is monitored by using vibration analysis techniques. The response is then processed in obtaining a better machine's health understanding [78]. In practice, accelerometers with a wide operating range of frequency and temperature are used in collecting the data due to vibration. The gathered data is then conditioned by the use various methods of signal processing including RMS, Crest Factor, frequency content, Cepstrum, Higher Order Spectral (HOS) and Peak Values analyses [82].

Generally, signal being produced by a machine as a result of vibration is a summation of the signals coming from the components integral to the machine and the structures to which the sensors are coupled. Not only the resulting vibration signal might be a sum of both non-linear and non-stationary sources, the signal from each source could be affected by its transmission medium. Furthermore, certain machine defects may not be able to cause a substantial change in the signature of the vibration signal, as compared to a predetermined baseline signal; thus, vibration monitoring might not be an adequate technique for all CM applications [59]. Considering the aforementioned drawbacks, it is clear that the vibration monitoring technique will not always provide a desirable solution to CM problems [59].

1.6 Research Motivation

In several cases today, it is still not practical in measuring the vibration of a machine and/or acoustics directly at source. The signals are usually measured at a remote location. Signals being measured remotely inevitably suffer significant distortion and attenuation along their transmission paths, as well as being subjected to inferences from other vibration and/or acoustic sources. In situations where the measurement point is not carefully selected, the measured signals will be distorted so much so that it becomes impossible to extract certain performance characteristics from them. Hence, distortion suppression is vital for online CM purposes. Moreover, since there are usually more than one source of vibration/acoustic energy in a machine, the sources will interfere with each other, making it more difficult in accurately extracting a specific source characteristics [83, 84].

In this work, the characteristics of the measured acoustic and vibration signals from helical gearbox with two-stage will be analysed, in order to realise a CM and diagnosis for different gearbox fault conditions. The work focuses on investigating the effect of interactions between various acoustic sources on the measured acoustic signals. The experimental setup used here consists of two microphones coupled at different locations around the gearbox. The measured signals are then conditioned using array signal processing analysis, in order to better understand the features associated with different acoustic sources surrounding the gearbox. The vibration signals generated by the test rig are also measured and analysed. These signals are then combined with the acoustic signals from the gearbox to diagnose faults, CM and vibration/acoustic source identification.

This study requires an in-depth gearbox knowledge for CM methods that use acoustic and vibration analysis techniques. Thus, the first step is to review the latest CM techniques, beginning with an introduction to the fundamentals of acoustics and its applications to CM and fault diagnosis. The second step is to become familiar with the test rig that will be used in this study and perform the required measurements experimentally. Lastly, the gathered experimental data will be analysed using various algorithms for signal processing, in both the frequency and time domains, in order to extract fault features from the signals obtained from the test gearbox.

Overall, the motivations for this research work can be summarised as follow:

- 1) The vibration monitoring method is effective however it produces localised information which is not efficient in terms of the needs for more hardware and redundant analysis
- 2) Acoustic monitoring more globally captures the dynamic responses of the housing, but requires more effective methods to reduce stronger background noises
- 3) TSA is an effective method for reducing the background noise, but needs additional angular signals, which increases the cost of its implementation
- 4) MSB is another effective approach to reducing noise effects, but has not been fully evaluated for monitoring gearboxes with acoustic signals

- 5) Previous studies were carried out based on manual faults and signatures could have significant errors or deviations due to the refitting of gear sets and the accelerated test methods adopted.

1.7 Research Aim and Objectives

The research aim is to investigate more efficient fault detection and diagnosis for monitoring a multistage gearbox using both vibration and acoustics signals. This involves overcoming the deficiency of current methods available and in achieving the research aim, the research work will be implemented according to the following priority milestones:

Objective 1: To gain an in-depth understanding of gearbox CM using traditional detection and diagnostic techniques such as vibro-acoustic based spectrum analysis methods.

Objective 2: To further detail the deficiency of the traditional signal processing and methods of analysis in the frequency, time, time-frequency domains, order domains to identify the most potential techniques for analysing the noisy signals from gearboxes.

Objective 3: To investigate the vibro-acoustic generation mechanisms and their characteristics of a multistage gearbox under the most common fault conditions.

Objective 4: To develop a realistic test scheme along with an adequate test system to evaluate the vibro-acoustic based gear diagnostics.

Objective 5: To investigate the monitoring performances of using vibro-acoustics signals with conventional TSA analysis.

Objective 6: To investigate the monitoring performances of using vibro-acoustics signals with the state of art efficient analysis such as modulation signal bispectrum (MSB).

Objective 7: To propose and then recommended a guideline, in this field, that will be used for further research.

1.8 Organisation of Thesis

This thesis has been structured into ten chapters which will describe in details the research work that has been carried out for the set aims and objectives to be achieve. This thesis id given as follows:

Chapter 2

This chapter discusses literature on techniques in signal processing used in monitoring geared transmission condition systems based on vibro-acoustic signals. Significant techniques have been discussed briefly in assisting to understand the results that will be presented in subsequent chapters.

Chapter 3

Mathematical model and simulation to better understand vibro-acoustic signals have been presented in this chapter. The model characterises a gear system with one stage using an appropriate stiffness function in representing the forces that acts between each gear pair. Rotational damping and stiffness have been used in simulating the shaft and gear angular motion.

Chapter 4

This chapter surveys the literature on techniques for signal processing used in monitoring geared transmission systems condition on the basis of vibro-acoustic signals. Based on the progress, TSA and Modulation Bispectrum are explained to be the most effective tools for analysing gear vibro-acoustic signals.

Chapter 5

This chapter describes the fault simulation and the test rig facility. It describes the components of the control and test rig systems and giving summary of the main gear specification in testing. It explains also the acoustics and vibration instrumentation measurement by describing all the component involved.

Acoustic and vibration data was also evaluated in this chapter, under different operating condition, have been evaluated using frequency and time analysis (using TSA and MSB), and then referenced for comparison using methods that are more advanced.

Chapter 6

In investigating the TSA (Time Synchronous Averaging) influence on vibration signals, the results from applying traditional techniques for signal processing that has been described in chapter four are compared with results when applying TSA.

The order spectrum, the order-frequency presentation and the angular domain signal have been obtained to characterise the vibration of the gearbox further in these new domains.

Chapter 7

In order to investigate the TSA influence on the acoustic signals, results obtained from applying the traditional signal techniques for processing that have been described in the fourth chapter are compared to the obtained results by using power spectrum.

Chapter 8

This chapter evaluates the performance of MSB in conditioning vibration signals so that the amplitudes in the residual spectrum can be used for the detection and diagnoses of wear in gear tooth. It is concluded that a MSB deterioration based approach is capable of diagnosing.

Chapter 9

This chapter evaluates the performance of MSB analysis of acoustic signals from a gearbox in detecting and diagnosing gear tooth wear, it is concluded that an MSB based approach is able to diagnose real fatigue faults.

Chapter 10

A review of the achievements and objectives has been presented in this chapter. The achievements have been described one after the other and comparing them with the set objectives presented in the first chapter. In addition, novel features and knowledge contribution have been provided in details where the novel features is highlighted and the knowledge contributions regarding this research has been described. Lastly, the author proposes recommendations for future work.

1.9 Summary

The reasons for carrying this research and choosing to specific area of study have been presented in this chapter. Information is presented about the use of the gearbox in industry and the functions of gears. A summary explanation of the causes of gear failure and modes of failure is given, and the need for CM explained. After that a brief review of traditional CM techniques is presented. Finally, the aims of this research, objectives and methods are presented and the thesis structure summarised; the use of a new and advanced signal processing method (MSB)

will be combined with the TSA technique to provide a system that can be used for the diagnosis of the onset of faults in working gearbox transmission systems.

Chapter 2 LITERATURE REVIEW OF GEAR FAULT DETECTION AND DIAGNOSIS USING VIBRO-ACOUSTIC BASED TECHNIQUES

Literature overview of techniques based on vibration signals, used for signal processing in monitoring the conditions in geared transmission systems have been presented in this chapter presents a. Some significant techniques are discussed in assisting in the result understanding that are presented susequent chapters of this thesis.

2.1 Background to Signal Processing

In CM systems, signal processing involves data analysis and transformation that has been retrieved from the monitored machines. In this chapter, relevant techniques used for signal processing are discussed in providing a much better understanding for the interpretation of data collected for CM and diagnosis of faults. Techniques used in signal processing techniques are used in extracting key and useful information from the signal that has been measured, to accurately assess the conditions of the machine being monitored [85].

TSA is the simplest form of signal processing in measuring and recording the incoming raw signal magnitude as a time function. This analysis type is the basis for all techniques that uses visual inspection and trend analysis. Furthermore, time domain analysis shows the comparison between the previous values against the current measurement and a predetermined threshold. The changes in signal magnitude with time contain information on the changing condition of the machinery. When many inputs in their hundreds are being monitored, this process can still be easy to implement [17].

In time domain, signal variation can be expressed more effectively in frequency domain as spectrum and more so, analysis in frequency domain has become a more common and useful technique for signal processing in CM. For CM in machinery, several factors, not just faults but also environmental changes can lead to the measured signal changes. Nevertheless, spectral analysis is particularly effective when applied to periodic signals at steady-state where the fault on the machine gradually develops [86].

It is a known fact that signal is generated when faults occur on machinery with components that are non-stationary. Non-stationary simply means the statistical parameters that defines the changes in the signal with time. Unfortunately, though spectral analysis method is very well recognised and used widely for CM signal processing in machinery, it is somewhat unsuitable to reveal information found in non-stationary signal [87]. In general, components that are non-stationary comprise of vital information that are related to the machines' faults [87], hence it is, very critical in processing and analysing these signals that are non-stationary to determine and diagnose faults.

The processing of both stationary and non-stationary signals for CM of machines have been discussed in this chapter. More so, signal processing methods that are currently available are reviewed based on three main data analysis categories which are frequency, time and time-frequency domains.

2.2 Time Domain Analysis

This type of domain analysis is realised by plotting the amplitude of the signal against time which can then be used in determining statistical features such as Peak to Peak, Peak Crest Factor, Kurtosis, Standard Deviation Skewness and RMS (Root Mean Square) of the amplitude in describing the signal characteristics.

A widely used technique for data collection is the TSA (Time Synchronous Average) [83]. The main purpose of the TSA is using the raw signal ensemble averages to either reduce or remove effects of non-synchronous and noise from all other sources, in enhancing the signal interest components.

The key advantage of analysis in time-domain analysis is that it provides a measure of the machine condition and information when faults are present based on one or more changes in the above listed statistical parameters. Analysis in time-domain as an online CM system is easy to implement because of the fact that all of the statistical parameters above are based on a representation of a single value. Time-domain analysis can also avoid some of the limitations of analysing in frequency-domain including aliasing, spectral leakage, aliasing, the picket-fence effect and sampling determination that may be generated whilst making use of the Fourier Transform (FT). If the recorded signal sampling frequency is higher than two times the recorded highest signal frequency component, all of the signal components can be identified by the FT, though there will still be existence of picket-fence effect [88, 89], see Section (2.3).

As the fault increases, the condition index should also increase which indicates that the condition of the gearbox is deteriorating. Occasionally, this type of analysis can be performed simply by observing visually the vibration waveform of the time-domain. It is very likely that the time-domain signal will be processed in providing a statistical parameter feature that allows a known relation to the severity of the vibration [89].

2.2.1 RMS (Root Mean Square)

RMS is a normalised the signal SD (standard deviation) second central moment. The vibration signal RMS provides the overall energy measure of the signal while taking into account, the vibration time history. RMS amplitude value for a given signal is given as [90]:

$$RMS_x = \sqrt{\frac{1}{N} \sum_{n=1}^N (x(n) - \bar{x})^2} \quad (2.1)$$

$$\bar{x} = \frac{1}{N} \sum_{n=1}^N x(n)$$

Here:

N is the number of samples taken for the signal, $x(n)$ is the signal amplitude for the n th sample, and \bar{x} is the N amplitudes mean value.

RMS is the most common and simplest measure that is used in acoustic/vibration monitoring in order to measure wide-band signal overall intensity, and to also provide an averaging effect that reduces the incidental impulses influence.

2.2.2 The Crest Factor (CF)

Crest factor is the ratio of a signal crest value (maximum positive peak) to that of the overall measurement RMS, and is also useful to help detect changes that are due to impulsive force of vibration. In theory, if the gear develops an isolated fault, an impulsive signal will be generated during meshing. When the damage increases, the vibration peak level will also increase, while the RMS level of the overall acceleration will change only a little as the duration of an impulse signal is very short [91]. Crest factor analysis is normally used on the raw signal of the vibration. For an operation that is normal, the crest factor may reach a value between 2 and 6, values greater than 6 tends to be linked with faulty machines.

$$CF = \frac{Peak.value}{RMS_x} = \frac{\sup|x(n)|}{\sqrt{\frac{1}{N} \sum_{n=1}^N [x(n)]^2}} \quad (2.2)$$

where, $\sup|x(n)|$ is the maximum absolute value of the signal.

2.2.3 Kurtosis

Kurtosis is a statistical signal calculation, (as seen in Equation 2.3). It is a statistical measure for the number of peaks and their amplitudes in a signal. The sharper and more the peaks in a signal, the higher the kurtosis value [92]

Mathematically, the normalised fourth moment of the signal is known as kurtosis [93]. The use of the fourth power makes kurtosis sensitive to the peakedness.

$$kurtosis = \frac{\frac{1}{N} \sum_{n=1}^N \left(x(n) - \bar{x} \right)^4}{\left[\frac{1}{N} \sum_{i=1}^N \left(x(n) - \bar{x} \right)^2 \right]^2} \quad (2.3)$$

As gear fault commences, kurtosis increases which suggests that the vibration distribution is not Gaussian anymore. This can be attributed to mainly impulses (isolated high amplitude peaks) that are generated by the affected gears. Nonetheless, this parameter is of little use once the incipient of the defects becomes quite severe due to the fact at such conditions, the signal peakedness begins to decrease and the kurtosis also reduces down to a level that is normally found with gears of acceptable condition [93].

2.3 Frequency Domain Analysis

Frequency-domain analysis is a powerful and useful conservative technique used to analyse vibration and has proved to be a tool that is useful in detecting and diagnosing faults in a simple machinery that rotates [94, 95]. By using this technique, the time-domain vibration signal is converted into frequency domain. The signal spectral content being measured has been found to be more useful when compared to the time-domain to determine the gear condition. This is because, the signal which is quite complex in the time-domain can be divided into several components of frequency. It has therefore been made easy for researchers to focus more on these frequencies that are very useful in diagnosing faults [94], where the overall vibration can be determined by the vibration that is being produced over a set of broadband frequencies. The frequency spectrum can be determined by the vibrations occurrence over a large number of discrete contiguous narrow frequency bands. Therefore, the commonly used approach for vibration CM is the FFT (Fast Fourier Transform) which transforms the vibration signal to the frequency domain. Using this type of approach should have no issues if the signal being

measured does not vary over time in its spectral content (i.e. there is no variations in the machines rotational speed).

2.3.1 Power Spectrum Analysis

A discrete time signal $x(t)$, and its DFT (Discrete Fourier Transform) $X(f)$, is defined as [96]:

$$X(f) = DFT[x(t)] = \sum_{t=-\infty}^{\infty} x(t) e^{-2j\pi f t} \quad (2.4)$$

where *DFT* signifies to Discrete Fourier Transform

The second order power spectrum measure (*PS*) of $x(t)$, can be calculated by the formula

$$P(f) = EX(f) X^*(f) \quad (2.5)$$

where $X^*(f)$ is the complex conjugate of $X(f)$

and $E(\)$ is the expectation operator showing that a statistical averaging is necessary in the spectrum estimation process.

2.3.2 Diagnostic Features in the Frequency Domain

2.3.2.1 Meshing Frequency Characteristics

Every gear set produces a frequency components profile that is unique which depends highly on the participating gears speed of rotation [97]. The gear-mesh frequencies can appear as harmonics in the spectrum when the transmission is subjected to steady speed and also as transients, when the transmission is operating at an angular acceleration.

The gear-mesh essential frequency is the product of the gear teeth number and the gear speed of rotation. The frequency components gear-mesh amplitudes are a strong function of torque being transmitted by the participating gears, and any moderating effects on the gears [98].

2.3.2.2 Sideband Characteristics

Vibration spectra of machines have their energy being distributed in multiples of frequencies. In geared transmission systems, mesh-force modulation is a commonly observed phenomenon [99]. The processes of modulation transfer their energy to the sidebands from their actual frequency around both sides of their fundamental and harmonics frequencies of their gear mesh. In rotating systems, there are observations of multiple sidebands around each of the

harmonics which are spaced symmetrically and then exponentially decay as they further separate away from the gear-mesh frequency. The sidebands of the gear mesh does not need to be symmetric [100]. When this spectral information is analysed in detail, it provides information that is significant about the condition of the gear tooth as well as the drive systems fluctuations and the gearbox bearings condition [101].

Either frequency modulation or amplitude modulation can cause sidebands, or simply a combination of both modulations. The components that modulate most often, do not, manifest themselves as sidebands surrounding the gear-mesh harmonics. The structures of the sideband have been observed in the rotating machinery measured vibration signatures including that of the gearboxes. This spectral information is usually used for the diagnosis of faults in gears [99] [102].

2.4 Envelope Analysis

Envelope analysis, sometimes referred to as amplitude demodulation is a technique that is reliable and powerful for fault detection in bearing with rolling element. Envelope analysis has been in existence for hundreds of years with the “cat’s whisker” detectors which have been used since the earlier years of radio communication, making the basis for its mathematics very well recognised. In AM (Amplitude Modulated) transmission, the information carrying signal, is used in modulating the carrier wave amplitude transmitted by the antenna. For transmission using radio, the carrier wave, whose function is to carry only the information being transmitted from place to place, will be a wave of radio frequency while the wave being modulated will be at an audio frequency below 20 kHz [103].

AM can be simply seen as in terms of the signal at the time domain. For an easier understanding, analogue description is best used. If $y_c = A_c \cos(\omega t)$ represents the carrier wave and $y_i = p(t)$ represents the information carrying the modulating wave, then the wave being modulated becomes $y_{am}(t) = y_c y_i = p(t) A_c \cos(\omega t)$ [104], see Figure 2-1.

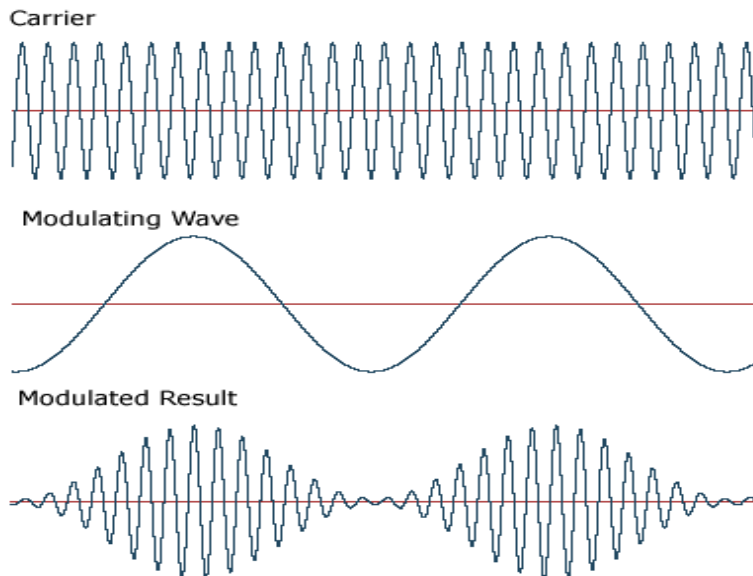


Figure 2-1 Simple example of carrier wave modulation in producing a modulated wave with the signals having an amplitude [104]

2.5 Time-Frequency Domain Analysis

Vibration signal analysis in frequency and time domains produce signal characteristics that provide information only in their respective domains. No spectral information is contained in the time-domain and when the signal is transformed to frequency-domain from time-domain, detailed information will be lost about the time-domain. This therefore limits both of the above methods. Furthermore, it must not be forgotten that limitations exist on the results obtained from the FT, they are only valid for signals that are stationary [105].

FT can be used in identifying what spectral components that is within the non-stationary signal exists. Nevertheless, the interval or time of the occurrence of these spectral components can never be pre-determined. If there is a requirement for time information, then analysis using FT would not be a suitable method. Lately, there has been much work carried out on CM signals analysis in time-frequency domain whilst also combining with analysis in frequency domain, in producing a full signal representation [87].

Analysis in time-frequency domain helps to provide information on the development of the signal spectral content with time, thereby enabling the investigation of transient features including impacts [106, 107]. Recently, combined time-frequency representations like the WT [87, 108, 109], STFT [105] and WVD [17, 110, 111] have grown in popularity to address the

omissions that might occur in either frequency or time domain analysis alone. Atlas, et al., [112] researched on combined time-frequency application to diagnose machine faults.

Wang and McFadden considered the gearbox vibration signal measured on the casing and investigated the use of such signals for fault detection, using different wavelets to analyse the signals [113]. Detection of clear symptoms for gear defects was greatly assisted if TSA was applied to the signal before the wavelets. This type of technique might fail in differentiating between faults if several faults within the gearbox simultaneously occur in multiple gears. A wide range of various techniques over the years have been explored in order to enhance TSA for extra sensitivity in detecting faults in their early stages [110].

2.5.1 Spectrograms

The STFT divides an entire signal or splits into segments of short duration and then applies to each segment, Fourier analysis. Time-frequency distribution can be attained by sliding the window successively along the time axis of the signal. The data is assumed to be piecewise stationary as it is used or applied based on the traditional Fourier analysis. For data that is non-stationary, allowance is not always made for this assumption. It is quite difficult in making sure that the adopted window size always coincides with the non-moving time scales. There are some limitations with Spectrograms in time-frequency resolution because of the signal segmentation [87]. The width of the window must be made narrow to be able to localise an event on time. Alternatively, the resolution of the frequency requires the time window to be long [114].

However, the STFT has a pre-set resolution constant for all frequencies because the same window length is used for the entire analysis of the signal. Hence, a good frequency resolution based on STFT analysis cannot be obtained when low-frequency wide window components is used for the analysis and good time resolution cannot be obtained when using a narrow window for high-frequency component analysis. Furthermore, orthogonal bases cannot be constituted in STFT during the window function translation. It therefore becomes difficult to find an algorithm that is effective and fast in order to calculate STFTs [87]. Spectrograms applications are therefore limited by these requirements because they can be applied to the signals that are non-stationary only when the signal changes slowly.

2.5.2 Wavelets

This technique is used widely for time-frequency domain analysis and has been proven to be a tool that is ideal for gears CM. Comparing to STFT, the WT is a time-scale signal representation which analyses the signal using narrow time with high frequency windows and wide time with low frequency windows with the time dilation meaning that more information can be extracted from the signal at time domain [115, 116]. This can be attributed as WT's main advantage as it produces at low frequency, resolution with high frequency and vice versa at high frequency. It is a method that is very effective for analysing non-stationary and transient signals and has also become very well established as a tool that is quite useful for applications that involves various signal processing [117]. Abnormal transients, for example those that are generated when the gear fault is at early stage, can be detected using continuous [118] and discrete [113] wavelet transformation.

WT has been applied successfully to analyse data for diagnosing gears [87, 108], bearings [119] and other faults in mechanical systems [120]. Baydar and Ball [121] used the WT in investigating the acoustic signal ability for local fault detection in gearboxes. It was later established that the "acoustic signals are very significant in detecting early faults and can provide a powerful tool also in indicating the various types of progressing faults in gearboxes".

Meneghetti and Rubini [119] researched on a method in processing signal in order to evaluate, using WT technique, the detection of rolling bearings faults. Comparing their results with those they obtained using spectral analysis and envelope in investigating the fault evolution effects. The WT method has been used in various applications that are related to fault diagnosis and CM in crack detection, structures and rotor systems etc. Peng and Chu [87] reviewed fault diagnosis and CM in machines by using wavelets. A summary was presented by them for WT application for diagnosing machine faults diagnostics in areas of feature extraction, time-frequency analysis, de-noising and weak signals extraction.

WT basics has some drawbacks [122]. First is the leakage the wavelet function generates which have limited length and leads to difficulties in quantitatively defining the time-frequency-energy distribution, this can then lead to wavelet interpretation being counter-intuitive. For instance, a high range of frequency should be investigated by the WT to define a change that is occurs locally, but for higher frequencies, the basic wavelet will be more localised. If only

in low frequency range a local event occurs, it will still, in high range of frequencies, be made to check for effects.

Secondly is the wavelet analysis non-adaptive nature which will affect the result of its analysis. This means that once the function of the wavelet has been selected, it must then be used for all the data analysis. Wavelet analysis performance relies mainly on wavelet functions selection [122]. Different functions of wavelet cause the analysed results to be different and the choice for the suitable wavelet function basically depends wholly on the signal and the reason for the analysis. In general, the characteristics of the signal being analysed changes over time and if a wavelet function already pre-determined is used for the analysis of the entire signal, some analysed signal features would not be accurately extracted.

It is seen that though discrete WT produces signal representation that is very efficient without any redundancies, the time-scale map resulting from this becomes limited and less useful. Lin et al. presented a linear WT, where the wavelet map, according to the signal amplitude was normalised instead of its energy [123]. Boulahbal et al. [124], simultaneously applied both WT phase and amplitude to study faults in chipped and cracked tooth and then proposed as a useful tool, a polar representation to pinpoint the damage location on the gear on WT maps.

2.6 Time Synchronous Averaging (TSA)

TSA is a technique for pre-processing of signals which is used commonly with analysis in the time domain in order to remove non-stationary noises from repetitive signals [125]. The important principle behind this technique is that the corresponding signal to a rotation of, lets say, the interested gear, is sampled making use of a tachometer so the signal sample starts at the same point in the gear cycle every time and then the ensemble average is computed over many periods. The synchronous signal average tends to cancel out the asynchronous vibration frequency components, leaving only the gear vibration signal currently under investigation and the signal's local variations become more observable. A huge amount of data is needed by TSA to guarantee the ensemble averages converge and aids greatly to detect early gear faults when the analysis requires a more refined signal processing to enhance the obtained information [17].

A common TSA application is in the analysis of the waveform of the vibration signals from gear drives composed of multiple gears, since each vibration signal is subject to noise from other elements in the system. In this case, the trigger to commence each set of readings is derived from tachometer which is a shaft encoder, providing one pulse per revolution. By

commencing the readings in this way, all of the time samples would be synchronized to begin at the same exact point in the gear's angular motion. For computational reliability and efficient implementation, in this research, a method based on a shaft encoder on the input shaft was used, this produced 100 pulses per revolution, which provided the reference signal angular position with sufficient gear accuracy for use with this project [126].

Since using TSA signals can be aligned according to any particular rotating shaft and any angular position, phase information can be provided which can then be used in eliminating the influences of random variations of speed. It has been found that TSA can be very effective in detecting signals subject to processes that vary with time, by the suppression of random noise and uncorrelated sources of noisy components, such as vibrations from components nearby [83].

The theoretical basis that is used in deriving the time signal, $x(t)$ synchronous average $y(t)$ using a trigger signal $c(t)$ with frequency f_t is equal to the convolution of $c(t)$ and $x(t)$ [37] [38] [83].

Which is

$$y(t) = c(t) * x(t) \quad (2.6)$$

where $c(t)$ is a N impulses train of amplitude $1/N$, spaced at intervals $T_t=1/f_t$ expressed as;

$$c(t) = \frac{1}{N} \sum_{n=0}^{N-1} \delta(t + nT_t) \quad (2.7)$$

This corresponds to Fourier transform, $x(f)$ multiplication of the signal by $c(f)$

$$y(f) = c(f) * x(f) \quad (2.8)$$

where $c(f)$ is a comb filter function of the form;

$$c(f) = \frac{1}{N} \frac{\text{Sin}(\pi NT_t f)}{\text{Sin}(\pi T_t f)} \quad (2.9)$$

When the number N is increased, the peak of the narrows and the side lobes amplitude between the peaks reduces. Therefore, large N values in synchronous averaging in the frequency domain is seen as removing completely, all components except for those occurring at multiples frequency integer f_t [127].

TSA does not remove only those unwanted acoustic and vibration waveform noises, but brings also into the angular domain, the signal which synchronises with the rotational motion of the rotors of interest.

2.6.1 Order Spectrum by Applying Fourier to TSA Signals

Stewart [128] revealed that with the use of TSA, the complex vibration signal in the time-domain from a transmission shaft, could be reduced to vibration estimates for individual shafts and their related gears. A synchronous average of the shaft is treated as if it were a vibration signal in the time domain for just one revolution of an isolated individual shaft with gears attached. TSA processing is fundamentally different from the typical spectrum averaging normally used in analysing FFT. While they have a comparable concept, TSA gives rise in a signal in the time domain having lower noise than the results from just one single sample. An FFT from the averaged signal can then be computed. The signal can then be sampled by using a synchronized trigger with the signal. Averaging process eliminates random noise as this is incoherent with that of the trigger. Only the trigger with coherent and synchronous signal in the averaged calculation will persist.

The traditional spectrum based on averaging records in the time domain, a data frame, then the FFT is computed and added to the already averaged spectrum. The process is repeated until the desired averaging number is reached. The result then becomes a spectrum with very low noise. However, if each recorded time used in computing the FFT spectra is examined, it will include the interested signal and random noise as the averaging will be in frequency domain and not in time domain [129].

2.7 Empirical Mode Decomposition (EMD)

EMD method is used in the time domain for signal processing which is also effective for analysing nonlinear or non-stationary data [122]. EMD breaks down signals into its corresponding IMFs (Intrinsic Mode Functions), which are well-defined as a class of functions used in indicating the analytical non-stationary local signal properties [122]. Each of the IMFs has its own characteristic frequency. The sum of each IMFs will identify the instantaneous frequencies that are contained in the signal.

As the nonlinear or non-stationary frequency data changes with time as the signal being measured may contain more than one oscillation mode; EMD can be used in decomposing the signal into components of IMF. An IMF has to satisfy two conditions [122]:

- 1) The number of zero crossing and extremes must differ or equal by one in the whole data set.
- 2) The mean envelope value is well-defined by the local maxima and at any point as the local minima is equal zero.

The properties of IMFs using the shifting process can be used to decompose a signal. Refer to Huang [122] for more of the algorithmic implementation details.

For signal decomposition into a finite IMFs sum, EMD can be used based on the energy that is associated with the various inherent time scales. As a result, EMD is suitable particularly for nonlinear and non-stationary signals processing and can also adaptively decompose a signal into different components, where each of the components has an instantaneous frequency that is meaningful, with the different components corresponding to the different scales of frequency. The obtained IMFs from the EMD provides physical insights that are very crucial in numerous applications in engineering [130].

There are also many techniques used for time-domain analysis in analysing data from waveforms for diagnosing fault of machinery. Jardine and Lin [131] reviewed methods of time domain that are used for data analyses in CM, such as pseudo-phase portrait, singular spectrum analysis, PCA (Principal Component Analysis) and models in time series which include the Autoregressive Moving Average (ARMA) and the autoregressive (AR) models. These are all used for modelling time series, diagnosing faults and extracting features. Lin and Jardine concluded [131] that “the application of either autoregressive moving average or autoregressive models is quite difficult due to their modelling complexities, especially their need in determining order in their respective model.”

2.8 Key Findings

As seen from this chapter, the theoretical basis for the conventional methods of diagnosing faults using vibro-acoustic signals from gear is in order to assist in the understanding of results. It was first discussed briefly the advanced techniques for data processing that are being used

commonly in areas of diagnosis and fault detection in gears including in frequency domain, time domain, TSA (time synchronous averaging) and a number of other domains. A brief background theory, each methods disadvantages and the advantages have also been discussed. Furthermore, an application overview of each of the method has also been discussed by citing the work of different researchers that have successfully implemented some of these techniques for their various applications. Analysing using MSB can also be used when analysing vibration data on complex machines like gearbox with two-stage, where this type of domain would provide an improved non-stationary signals results as the vibrations are being generated by the gear impacts.

Chapter 3 FUNDAMENTALS OF VIBRO- ACOUSTICS FROM A TWO STAGE HELICAL GEARBOX WITH TOOTH WEAR

This chapter details the fundamentals of vibro-acoustics of a two stage helical gear gearbox with tooth wears. It starts with developing a lumped parameter model for the vibration responses of the gearbox subject to the dynamic effects of tooth wear. Numerical solutions to the model were then obtained to examine the changes in both the waveforms and spectra in order to identify key features to indicate wear progressions in vibration response. The chapter also analyses the general characteristics of airborne sound radiated from the vibration of a gearbox housing and the influences of background noise on acoustic measurements.

3.1 Introduction

To carry out effective monitoring of gearbox with vibro-acoustic measurements, it is necessary to have sufficient understanding of behaviours of vibro-acoustics from gearboxes, especially, with fault conditions. In addition to previous general understandings gained from literature review, this chapter will focus on the dynamic modelling for gear vibrations, which enables a deeper understanding of the mechanisms generating vibration in gear transmission systems and assists in the characterisation of changes in the dynamic properties that arise due to various types of gear faults. This then sets a framework for the measurements made, data processing methods selected and diagnosis rule development [132].

This chapter develops a mathematical model of a two stage gearbox system using suitable stiffness functions in representing the forces acting between gear pairs. Damping and rotational stiffness and damping are used in simulating the shaft and gear angular motion. The model results showed that the vibration frequency spectrums take the form that was expected, with the peaks at the associated harmonics and meshing frequency. In addition, if the stiffness function between the first gear pair were modelled as containing a broken tooth with varying degrees of damage, the model outputs would have similar sideband to the signals produced in experiments. Varying model load and speed produce effects that corresponding to those seen in the experiments. These parallels demonstrate that the model, though simple, can explain the mechanisms at work in the real gearbox that has been used in the CM experiments.

3.2 Key Advancement in Modelling Gear Dynamics

There are numerous publication in gear modelling. Key progression made in modelling helical gear are overviewed in order to understand any predicted signatures due to gears with small defects such as light gear wear and hence to implement more accurate diagnostics.

Freudenstein and Dubowsky developed a theoretical model of elastic impacts in their paper: “The dynamic response of mechanical systems with clearance” [133, 134]. Based on their study, Crossley and Azar [135] explored the dynamic behaviour of engaged gearing systems with time-varying stiffness, damping and gear backlash of the gear teeth.

Nearly a decade later, Yang and Sun [136] published a dynamic model that is more realistic for spur gear systems with backlash. By including, in their model, involute tooth profile, they succeeded in accounting for energy dissipation, material compliance, damping and time-

varying mesh stiffness due to time varying teeth-pair contact during the gear engagement cycle. Initial work modelled either the meshing stiffness as a piecewise or an average linear variation but now it is generally accepted that to simulate accurately dynamic behaviour of gear, the gear mesh stiffness should at least, include two factors: tooth bending and local Hertzian deformation. Nevertheless, even though Yang and Sun [136] considered only Hertzian contact stiffness, their dynamic simulation of free vibration under sinusoidal excitation and constant load operation presented insightful results.

Two review papers that notably discussed the gear dynamics numerical modelling were published in 1988 by Özgüven and Houser [137] and in 2003 by Parey and Tandon [138]. Özgüven and Houser categorised gear models systems as; models with tooth compliance, dynamic factor models, models for gear dynamics for rotor dynamics, and for torsional vibration. They listed the goals for the different studies as stress, reliability, life, noise, vibratory motion and loading. Inquisitively, CM was not part of the list. Tandon and Parey's review mostly focussed on the defects modelling but includes extensive consideration of various lumped parameter models.

Dalpiaz, et al., [83] examined a pair of gear with a fatigue crack and assessed the sensitivity and effectiveness of TSA (Time-Synchronous Average) and cyclostationary analysis based on their experimental results. They also discussed quefrency as a possibly useful measure of harmonic amplitude in traditional cepstrum analysis.

Parey, et al., [139] developed a six DOF non-linear model on two shafts for a pair of spur gears. They calculated, for the tooth surface contact, the Hertzian stiffness and used EMD (empirical mode decomposition) as a method in simulating different crack widths. Other authors [140-143] have utilised various methods of time-varying stiffness estimation to get practically useful results of dynamic simulation. Meagher, et al., [144] showed three different modelling strategies dynamic system subsequently used by researchers in identifying gear health diagnostic indicators: a materials strength based lumped parameter model, a non-linear quasi-static finite element model, and a multi-body kinematic model with non-linear contact stiffness. The research contrasted all of these methods for modelling gear dynamics by the comparison their predicted stiffness cycle with its dynamic response effect.

3.3 Modelling Overview

With the increasing sophistication of modern industrial machines there is a growing utilisation of ever more complex gear trains, there is a corresponding increase in attention being given to modelling the dynamics of gear systems. Researchers are developing high-level models which include the importance of the dynamic factors present in gearboxes; including cyclic variation in tooth stiffness, excitations initiated by errors in gear transmission systems, the inter-coupling between lateral, rotational and torsional vibrations of shafts and gears [53, 145-147]. Other researchers have focused their attention on modelling tooth meshing because, typically, the major vibration forces source is the gear meshing in geared transmission [148-150]. The aim of this research programme is to investigate the interplay of non-linear effects including; gear backlash, the forces due to meshing friction and time-varying mesh stiffness.

Tooth breakage effect on the behaviour of the vibration of a two-stage helical gearbox has been studied via computer simulation. The modelling has been limited to variation in meshing stiffness as this is the fundamental source of vibration [131].

The main purpose of this exercise is the investigation of stresses in gear tooth within the gear system, determining important vibration characteristics such as signal amplitude, frequency components, natural/resonant frequencies of the system, airborne noise radiated from the surface of the gearbox, etc. The modelling of one and/or two-stage gear systems has been undertaken using mass-spring or mass-spring-damper SDOF (Single Degree Of Freedom) and MDOF (Multiple Degree Of Freedom) systems [151] .

Recent models combine lateral and torsional vibrations including gear mesh stiffness [145, 152] as a constant, as a rectangular waveform, as a simple sinusoid, as a linear function capable of being expressed as a Fourier series and as an approximate function all corresponding to a single and double-tooth pair mesh. In simpler SDOF cases, the resulting derived dynamic equations were solved using analytical methods and approximate analytical methods, the more complex equations derived for MDOF systems were solved using numerical methods. The numerical solutions were generally obtained using, Runge-Kutta method of integration, which are popular due to their shorter calculation time and relative accuracy.

3.4 Mathematical Model of a Multi-Stage Gearbox

The main aim of developing the mathematical model is to provide a useful tool to investigate gearbox vibration characteristics, in both frequency and time domains. Early studies limited consideration to single stage torsional vibrations [151], but more recently modelling of gear transmission systems has included both lateral and torsional vibrations [145], [146], [147], [53]. These latter models have provided understanding into the inner workings of gear systems and have established a basis for remote and local fault diagnostic methods.

“The model used in this research is a MDOF system with standard mass-spring-damper elements based on Bartelmus work [145] where the mesh stiffness proportional to the damping in order to represent, between gear pairs, the forces. K_1 and K_2 which are the mesh stiffness functions between gear pairs are based on the simplified piecewise linear analysis and tooth breakage faults as described earlier and can be easily introduced into the model”.

A model of a two stage system that allows for torsional vibrations of the drive shafts has been developed. This model also permits vertical vibration of the first gear pair, where the gears are attached to the casing which is divided into two parts, each of which can vibrate vertically with its own characteristics of mass/stiffness, allowing the vertical accelerations effect to be measured at two different points. Vibrations in the horizontal plane were discounted as it was presumed that these would die away due to the presence of damping [153]. A schematic diagram can be seen in Figure 3-1

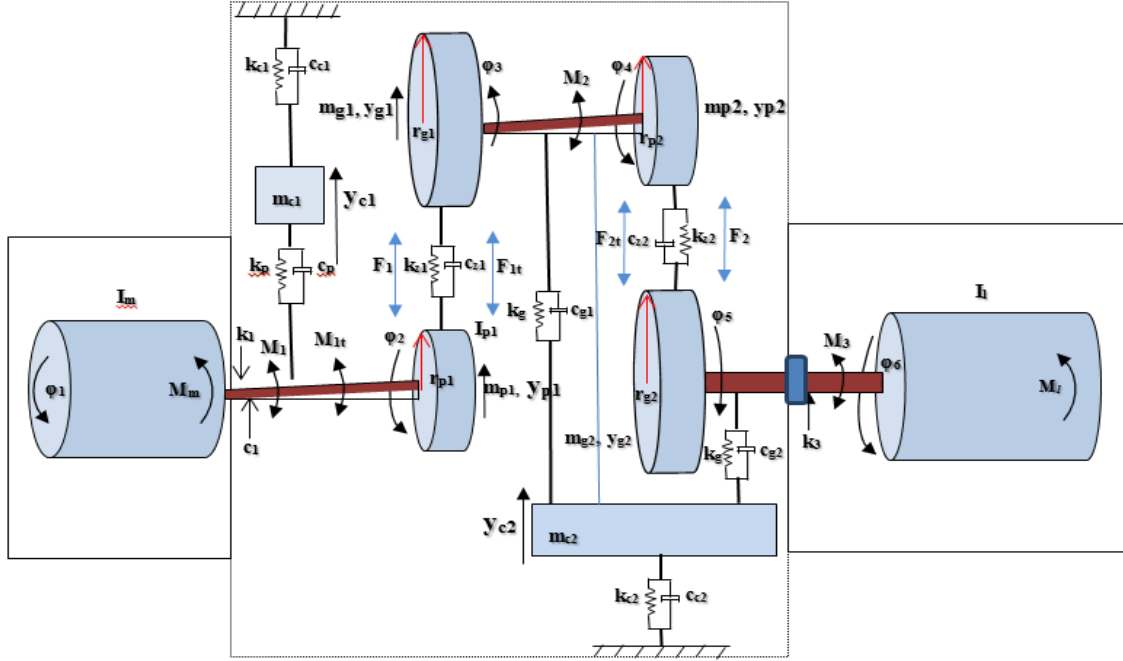


Figure 3-1 The dynamic model of motor-gearbox and load system

Based on the forces shown in above figure3.1, the governing equations due to the motor rotor rotational motion can be expressed as

$$I_m \ddot{\varphi}_1 + k_1 (\varphi_1 - \varphi_2) + c_1 \left(\dot{\varphi}_1 - \dot{\varphi}_2 \right) = M_m \quad (3.1)$$

The drive gear rotation (Z_1) in first stage is;

$$I_{p1} \ddot{\varphi}_2 - k_1 (\varphi_1 - \varphi_2) - c_1 \left(\dot{\varphi}_1 - \dot{\varphi}_2 \right) + r_{p1} k_{z1} (r_{p1} \varphi_2 - r_{g1} \varphi_3 - y_{p1} + y_{g1}) + r_{p1} c_{z1} \left(r_{p1} \dot{\varphi}_2 - r_{g1} \dot{\varphi}_3 - \dot{y}_{p1} + \dot{y}_{g1} \right) = 0 \quad (3.2)$$

The first stage driven gear rotation (Z_2) is given by:

$$I_{g1} \ddot{\varphi}_3 + k_2 (\varphi_3 - \varphi_4) + c_2 \left(\dot{\varphi}_3 - \dot{\varphi}_4 \right) - r_{g1} k_{z1} (r_{p1} \varphi_2 - r_{g1} \varphi_3 - y_{p1} + y_{g1}) - r_{g1} c_{z1} \left(r_{p1} \dot{\varphi}_2 - r_{g1} \dot{\varphi}_3 - \dot{y}_{p1} + \dot{y}_{g1} \right) = 0 \quad (3.3)$$

The second stage drive gear rotation (Z_3) is given by:

$$I_{p2} \ddot{\varphi}_4 - k_2 (\varphi_3 - \varphi_4) - c_2 \left(\dot{\varphi}_3 - \dot{\varphi}_4 \right) + r_{p2} k_{z2} (r_{p2} \varphi_4 - r_{g2} \varphi_5 - y_{p2} + y_{g2}) + r_{p2} c_{z2} \left(r_{p2} \dot{\varphi}_4 - r_{g2} \dot{\varphi}_5 - \dot{y}_{p2} + \dot{y}_{g2} \right) = 0 \quad (3.4)$$

The second stage driven gear rotation (Z_4) is given by:

$$I_{g2} \ddot{\varphi}_5 + k_3 (\varphi_5 - \varphi_6) + c_3 (\dot{\varphi}_5 - \dot{\varphi}_6) - r_{g2} k_{z2} (r_{p2} \varphi_4 - r_{g2} \varphi_5 - y_{p2} + y_{g2}) - r_{g2} c_{z2} (r_{p2} \dot{\varphi}_4 - r_{g2} \dot{\varphi}_5 - \dot{y}_{p2} + \dot{y}_{g2}) = 0 \quad (3.5)$$

The load rotation (output shaft) is given by:

$$I_l \ddot{\varphi}_6 - k_3 (\varphi_5 - \varphi_6) - c_3 (\dot{\varphi}_5 - \dot{\varphi}_4) = M_l \quad (3.6)$$

The equation that governs the drive gear translational motion (Z_1) in the first gear pair is given by:

$$m_{p1} \ddot{y}_{p1} + k_{p1} (y_{p1} - y_{c1}) + c_{p1} (\dot{y}_{p1} - \dot{y}_{c1}) - k_{z1} (r_{p1} \varphi_2 - r_{g1} \varphi_3 - y_{p1} + y_{g1}) - c_{z1} (r_{p1} \dot{\varphi}_2 - r_{g1} \dot{\varphi}_3 - \dot{y}_{p1} + \dot{y}_{g1}) = 0 \quad (3.7)$$

The first stage driven gear translational motion (Z_2) is given by:

$$m_{g1} \ddot{y}_{g1} + k_{g1} (y_{g1} - y_{c2}) + c_{g1} (\dot{y}_{g1} - \dot{y}_{c2}) - k_{z1} (r_{p1} \varphi_2 - r_{g1} \varphi_3 - y_{p1} + y_{g1}) - c_{z1} (r_{p1} \dot{\varphi}_2 - r_{g1} \dot{\varphi}_3 - \dot{y}_{p1} + \dot{y}_{g1}) = 0 \quad (3.8)$$

The second stage drive gear translational motion (Z_3) is given by:

$$m_{p1} \ddot{y}_{p2} + k_{p2} (y_{p2} - y_{c2}) + c_{p1} (\dot{y}_{p2} - \dot{y}_{c2}) - k_{z2} (r_{p2} \varphi_4 - r_{g2} \varphi_5 - y_{p2} + y_{g2}) - c_{z2} (r_{p2} \dot{\varphi}_4 - r_{g2} \dot{\varphi}_5 - \dot{y}_{p2} + \dot{y}_{g2}) = 0 \quad (3.9)$$

The second stage driven gear translational motion (Z_4) is given by:

$$m_{g2} \ddot{y}_{g2} + k_{g2} (y_{g2} - y_{c2}) + c_{g2} (\dot{y}_{g2} - \dot{y}_{c2}) - k_{z1} (r_{p2} \varphi_4 - r_{g2} \varphi_5 - y_{p2} + y_{g2}) - c_{z2} (r_{p2} \dot{\varphi}_4 - r_{g2} \dot{\varphi}_5 - \dot{y}_{p2} + \dot{y}_{g2}) = 0 \quad (3.10)$$

For the motion of case m_{c1} the governing equation is

$$m_{c1} \ddot{y}_{c1} + k_{c1} y_{c1} + c_{c1} \dot{y}_{c1} - k_{p1} (y_{p1} - y_{c1}) - c_{p1} (\dot{y}_{p1} - \dot{y}_{c1}) = 0 \quad (3.11)$$

For the motion of case m_{c2} the governing equation is:

$$m_{c2} \ddot{y}_{c2} + k_{c2} y_{c2} + c_{c2} \dot{y}_{c2} - k_{g1} (y_{g1} - y_{c2}) - c_{g2} (\dot{y}_{g2} - \dot{y}_{c2}) = 0 \quad (3.12)$$

Moments and forces can be obtained in the following forms:

$$M_1 = k_1 (\varphi_1 - \varphi_2) \quad (3.13)$$

$$M_{1t} = C_1 (\dot{\varphi}_1 - \dot{\varphi}_2) \quad (3.14)$$

$$M_2 = K_2 (\varphi_3 - \varphi_4) \quad (3.15)$$

$$M_{2t} = C_2 \left(\dot{\varphi}_3 - \dot{\varphi}_4 \right) \quad (3.16)$$

$$M_3 = K_3 (\varphi_5 - \varphi_6) \quad (3.17)$$

$$M_{3t} = C_3 \left(\dot{\varphi}_5 - \dot{\varphi}_6 \right) \quad (3.18)$$

$$F_1 = k_{z1} (r_{p1}\varphi_2 - r_{g1}\varphi_3 - y_{p1} + y_{g1}) \quad (3.19)$$

$$F_2 = k_{z2} (r_{p2}\varphi_4 - r_{g2}\varphi_5 - y_{p2} + y_{g2}) \quad (3.20)$$

$$F_{1t} = c_{z1} \left(r_{p1} \dot{\varphi}_2 - r_{g1} \dot{\varphi}_3 - \dot{y}_{p1} + \dot{y}_{g1} \right) \quad (3.21)$$

$$F_{2t} = c_{z2} \left(r_{p2} \dot{\varphi}_4 - r_{g2} \dot{\varphi}_5 - \dot{y}_{p2} + \dot{y}_{g2} \right) \quad (3.22)$$

Here

I_m = electric motor moment of inertia.

I_l = the load system moment of inertia.

I_{p1} = drive gear one (pinion one) moment of inertia in the first stage.

I_{g1} = driven gear moment of inertia in the first stage.

I_{p2} = drive gear moment of inertia (pinion two) in the second stage.

I_{g2} = driven gear moment of inertia in the second stage.

F_1, F_2 = gearing stiffness forces.

F_{1t}, F_{2t} = gearing damping forces.

M_m = motor torque at input.

M_1, M_{1t} = first shafts internal moments and coupling damping.

M_2, M_{2t} = second shaft internal moments and coupling damping.

M_3, M_{3t} = third shaft internal moments and coupling damping.

φ_1 = induction motor angular displacement.

φ_2, φ_3 = first stage drive gear angular displacement (Z_1) and driven gear angular displacement (Z_2).

φ_4, φ_5 = second stage gear one angular displacement (pinion) and gear two angular displacement.

φ_6 = load system angular displacement.

r_{p1}, r_{g1} = first stage base circle radius of the drive gear and driven gear respectively.

r_{p2}, r_{g2} = second stage drive gear and driven gear base circle radius.

y_p, y_g = first stage drive gear and the driven gear vertical displacement respectively.

y_{c1}, y_{c2} = upper and lower casings vertical displacement.

m_{p1}, m_{g1} = first stage drive and the driven gears mass.

m_{p2}, m_{g2} = second stage drive and the driven gears mass.

m_{c1}, m_{c2} = upper and lower casing mass.

c_p = pinion shaft damping at the first stage.

c_g = gear shaft damping at the first stage.

c_1 = damping at shaft one.

c_2 = damping at shaft two.

c_3 = damping at shaft three.

c_{z1} = gearing damping at the first stage.

c_{z2} = gearing damping at the Second stage.

c_{c1} = support damping of the upper casing.

c_{c2} = support damping of the lower casing.

k_p = pinion shaft stiffness at first stage.

k_g = gear shaft stiffness at first stage.

k_1 = stiffness (rotational stiffness) of shaft one.

k_2 = stiffness of shaft two.

k_3 = shaft three stiffness and coupling stiffness.

k_{z1} = gearing stiffness (meshing stiffness) at first stage.

k_{z2} = gearing stiffness (meshing stiffness) at second stage.

k_{c1} = support stiffness for upper casing.

k_{c2} = support stiffness for lower gearing [145].

3.5 Determination of Model Parameters

Based on the construction of the test rig and the design of gearbox, masses and moments of inertia can be calculated or measured relatively easily. The stiffness values for shafts can be also obtained based on the dimensions of gearbox drawings. However, the stiffness and damping factors for the coupling were determined by static deformation tests, in which it was found that the stiffness exhibits non-linearity for the range of operating loads used. Therefore, the stiffness values were set according to the system load applied. To highlight the resonance, effect the damping factor is set to be at 0.05 at low frequencies ($f < 500$ Hz). On the other hand, in all other cases the damping factors are set to be 0.9 for a fast convergence of the steady solution [219].

Gear tooth stiffness is a combination of tooth gross bending deflection and tooth local or Herzian contact deformation [123]. These deformations contribute to the major part of the mesh deflection under the load being transmitted. The compliance determination of these modes of deformation however is quite difficult as, over the entire loaded tooth, it is an integral function. Generally, a FE method is used to calculate tooth stiffness. However, the FE based prediction is just an estimation because it cannot take into the effect of friction moments, tooth errors, etc. [114].

Aimed at understanding the general characteristics of gear dynamic responses, this study took the stiffness estimates from the FE result [154] as the baseline references. The allow vibration responses to be obtained to consists of key vibration components such as mesh and sideband components and make comparison the responses between different conditions. This means that very accurate quantitative results is not very critical but the relative changes are the main focus. Nevertheless, the baseline stiffness was tuned carefully to suitable for the gears tested through a number of trial runs. The results from these runs were compared to the measured results so that tuned parameters can produce results close to the measured values in terms of RMS value values and spectrum patterns, which is outlined in Figure 3-2.

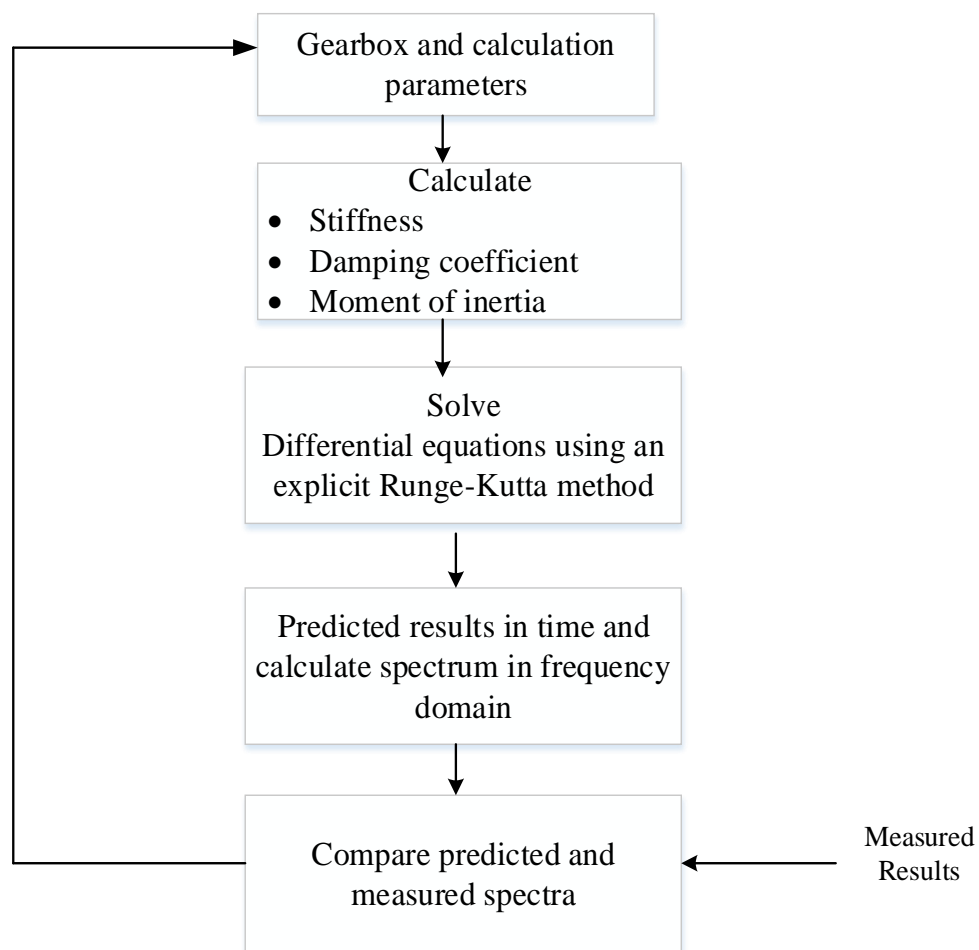


Figure 3-2 Main procedure for the analysis of gearbox dynamic responses [217]

Finally, model parameters for baseline conditions were determined as seen in Table 3-1.

Table 3-1 Key baseline parameters and specification for the test gearbox

Symbol	Description	Value	Unit
m_{s1}	Input shaft mass	1.42	kg
m_{s2}	Middle shaft mass	0.95	kg
m_{s3}	Output shaft mass	3.34	kg
m_{p1}	Drive gear (Z1) mass at 1st stage	0.23	kg
m_{g1}	Driven gear (Z2) mass at 1st stage	1.546	kg
m_{p2}	Drive gear (Z3) mass at 2nd stage	0.663	kg
m_{g2}	Driven gear (Z4) mass at 2nd stage	1.493	kg
ε_c	Contact ratio	1.45	[-]
ε_a	Overlap ratio	2.890	[-]
r_{s1}	Base radius of input shaft	0.015	m
r_{s2}	Base radius of middle shaft	0.0117	m
r_{s3}	Base radius of output shaft	0.0153	m
r_{p1}	Base radius of drive gear (Z1) at 1st stage	0.0217	m
r_{g1}	Base radius of driven gear (Z2) at 1st stage	0.0117	m
r_{p2}	Base radius of drive gear (Z3) at 2nd stage	0.01525	m
r_{g2}	Base radius of driven gear (Z4) at 2nd stage	0.0222	m
M_1	inertia moment of input shaft	0.0032	Kg.m ²
M_2	inertia moment of middle shaft	0.00013	Kg.m ²
M_3	inertia moment of output shaft	0.00078	Kg.m ²
I_{p1}	Drive gear inertia moment (Z1) at 1st stage	0.000042	Kg.m ²
I_{g1}	Drive gear inertia moment (Z2) at 1st stage	0.00073	Kg.m ²
I_{p2}	Drive gear inertia moment (Z3) at 2nd stage	0.000154	Kg.m ²
I_{g2}	Drive gear inertia moment (Z4) at 2nd stage	0.00074	Kg.m ²
ζ	Damping ratio	1.3	[]
c_{z1}	1st stage gearing damping	435.7295	N.s/m
c_{z2}	2nd stage gearing damping	831.1938	N.s/m
μ_1	1st stage gearing damping coefficient	4.357×10^{-5}	N.s/m
μ_2	2nd stage gearing damping coefficient	8.312×10^{-5}	N.s/m
I_m	Moment of motor	8.476×10^{-4}	Kg.m ²
I_l	Moment of load system	33.88×10^{-4}	Kg.m ²
k_p	Input shaft stiffness	1.0×10^6	N/m
k_g	Middle shaft stiffness	2.0×10^6	N/m
k_{z1}	tooth mesh stiffness amplitude for gear pair at 1st stage	2.0×10^6	N/m
k_{z2}	tooth mesh stiffness amplitude for gear pair at 2 nd stage	1.0×10^8	N/m

3.6 Wear Induced Changes in Tooth Stiffness

3.6.1 Changes in Tooth Profile

Based on the analysis FE results, this study models the tooth stiffness function for a pair of tooth as a trapezoid consisting three successive phases, as depicted in Figure (3-3) (a). As seen in Figure (3-3) (a), the normalised stiffness exhibits a gradual increase during mesh-in phase and decrease during the mesh-out phases due to larger bulk deflections, compared to the middle part of the teeth pair. This can be more realistic in simulating the observation in the gear mesh that the maximum dynamic loads take place both at the end and at the beginning of the engagement.

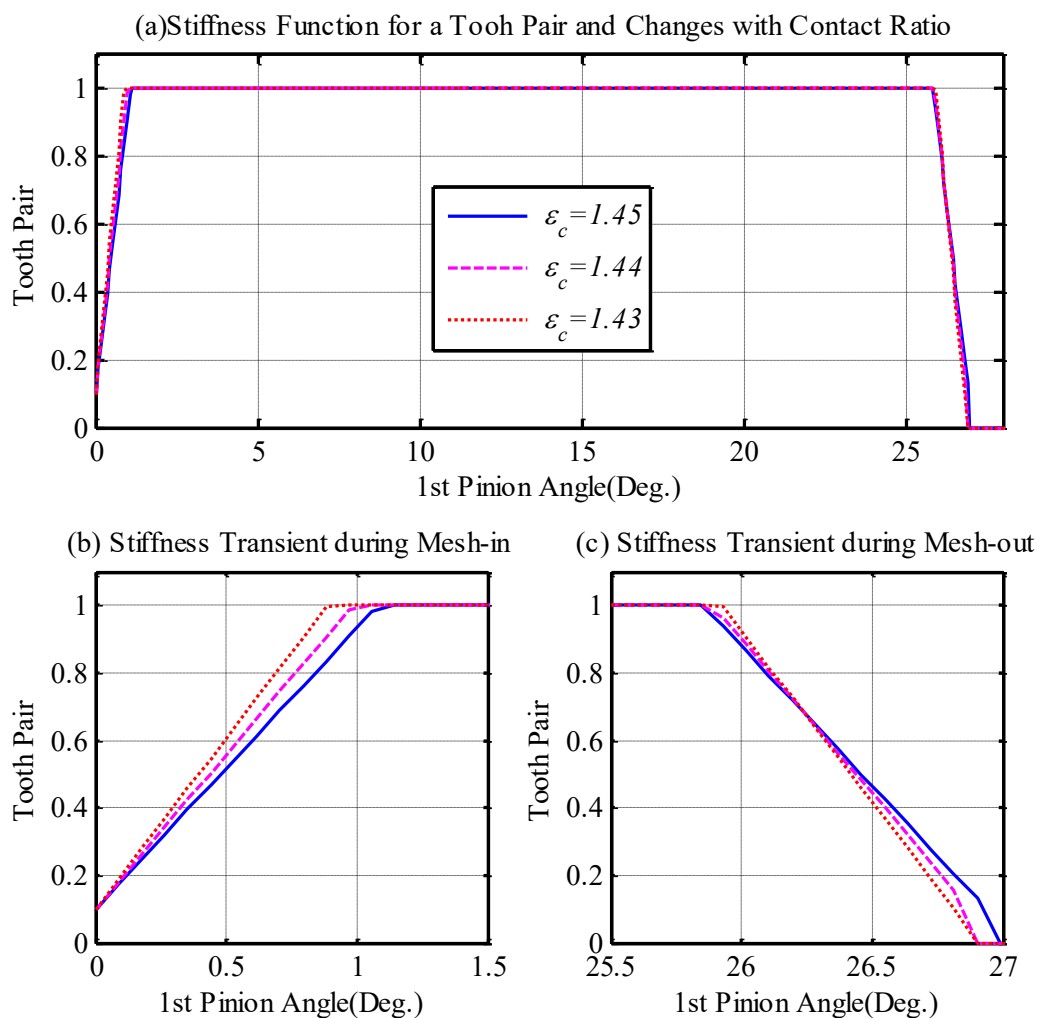


Figure 3-3 Models of tooth stiffness and the effects of tooth wear

Moreover, it models wear effects by increasing the transient slopes in the two transient phases to reflect the addition impacts induced by incorrect engagements of the tooth pair subject different degrees of wear. As shown in Figure (3-3) (b) and (c), the transverse ratio ε_c , which represents the overlap degrees for the tooth profile along the height direction, is reduced from its baseline values of 1.45 to 1.344 and 1.43 respectively to represents two successive increments of tooth wear.

To show the combined tooth wear effect, the stiffness function for multiple tooth pairs are superimposed according to the total overlap ratio of the gear pair for the higher speed transmission stage of the gearbox under study:

$$\varepsilon = \varepsilon_c + \varepsilon_a = 1.45 + 2.89 = 4.34 \quad (3.23)$$

Where ε_a is the overlap ratio representing the overlap degrees for the tooth profile along the tooth width or axial direction. The total overlaps yields the combined stiffness function $k_{z1}(t)$ as can be seen in Figure 3-4. It is seen that this helical gear pair can have five pairs of teeth under engagement for 34% of a mesh cycle, whereas the other portion of the cycle have four tooth pairs in contact.

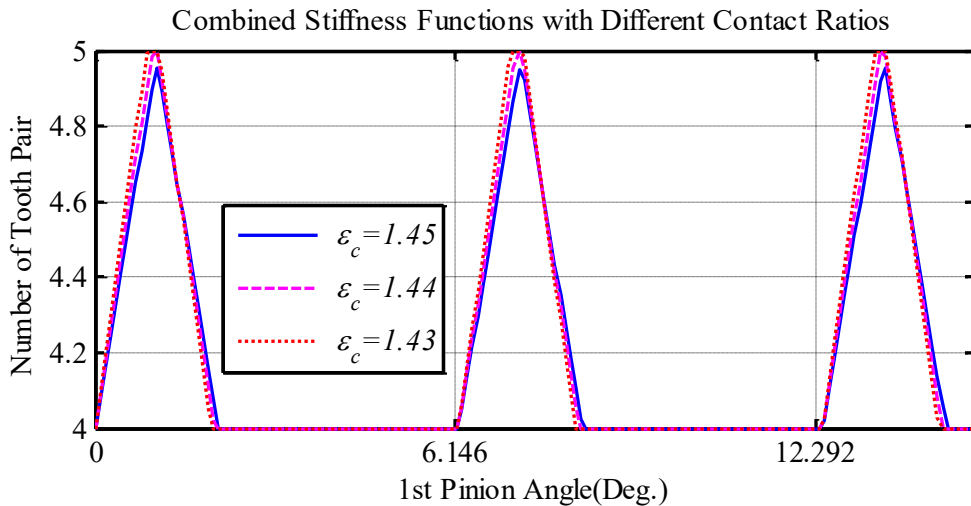


Figure 3-4 Tooth stiffness function superimposed by multiple tooth pair and the effect of gear wear

Moreover, the peak values for the stiffness function is seen to increase with the reduction of transverse ratio, thereby allowing more vibrations to be induced to reflect the effect of different degrees of tooth wear.

3.6.2 Influences of Gear Errors

Manufacturing errors such as misalignment affect the initial characteristics of tooth wear and wear progression. Gear eccentricity or misalignment will make the gear teeth undertake to greater contact forces and so produce greater wear. This characteristic was included in the model as a small addition to the error amplitudes. For a pair of gears Z_1 and Z_2 , the total error effects are

$$e_{12} = (\rho_1 + \rho_{w1})\sin(\varphi_1) + (\rho_2 + \rho_{w2})\sin(\varphi_2) \quad (3.24)$$

where ρ_1 and ρ_{w1} denote the eccentric and wear amplitudes for driving gear respectively. ρ_2 and ρ_{w2} denote the eccentric and wear amplitudes for driven gear respectively. Both of them are a periodic function of their rotational angular displacement and it will be included into the dynamic displacements respectively in Equations from (3.1) to (3.12).

3.7 Implementation of Numerical Studies of Gear Vibrations

As the mode consists of nonlinear stiffens terms, the second order differential equations of the dynamic model in Equation from (3.1) to (3.12) have been converted into equations of first order in solving them by the use of standard numerical algorithms. The most popular algorithm used is the Runge-Kutta formula for solving the model in the first instance [126]. However, for a single run, it took more than one hour to complete the simulation by applying standard Runge-Kutta method: ode45 in Matlab software.

“This confirmed the inefficiency of the Runge-Kutta method for solving these equations. Analysing further the equations showed the model as a stiff system. The equations that describes the angular motions of having a much slower time rate of variation when compared to those that describes the lateral motions. According to references and Mat lab instruction manual recommendations [127], the stiff solver: ode115s function must be selected in solving the equations. This has therefore reduced to less than 10 minutes of the run time and decided that the ode115s function is more efficient and used subsequently throughout this course of the simulation”.

In performing spectral analysis, each simulation is running for 15 turns of the input shaft or more than 4 turns of the output shaft. This size of the data is long enough in obtaining a resolution spectrum with high frequency allowing good differentiation between components of the different sideband.

3.7.1 Rotational Responses in the Time Domain

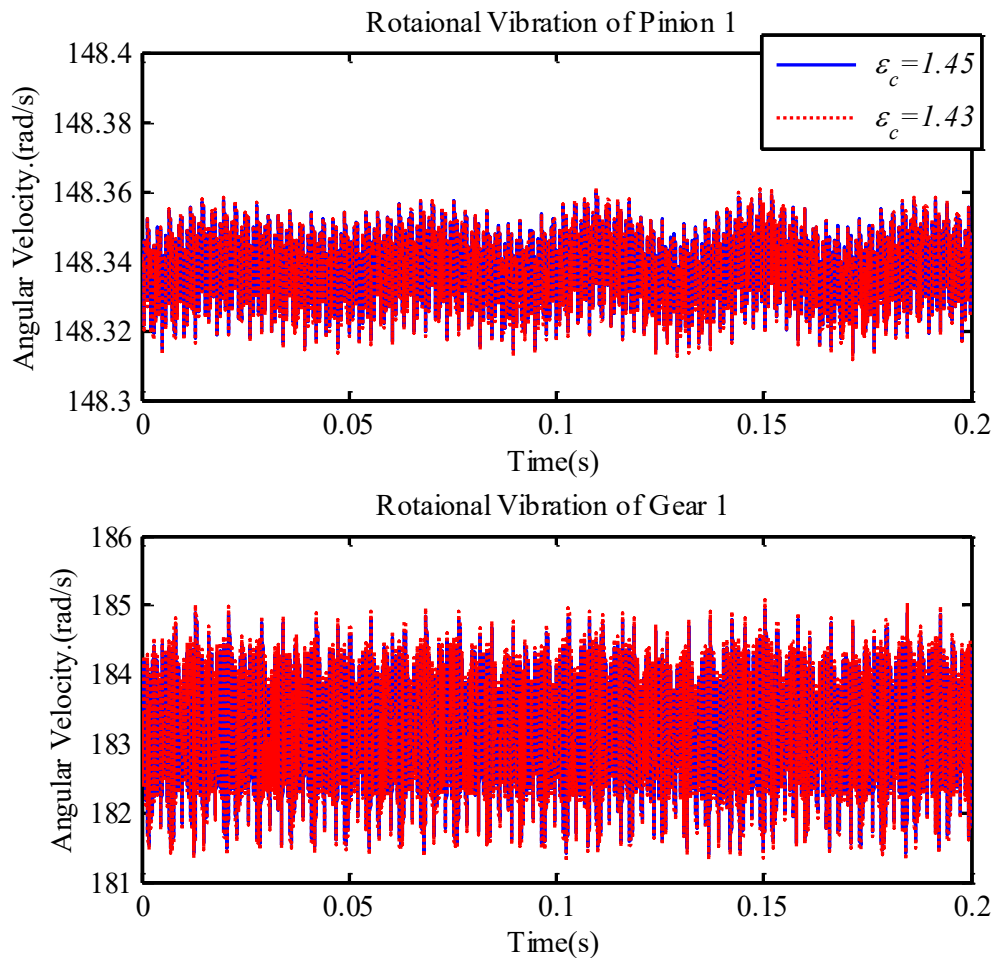


Figure 3-5 Angular speed of the first pinion and gear

Figure 3-5 depicts a standard solution for the first pinion and gear angular speed, which was obtained when the system was applied with a condition of 70Nm of full load at the AC motor speed of 1416 rpm (or 148.3rad/s). This operation condition corresponds to the highest operating condition of the test. It can be seen that both the pinion and gear exhibit clear oscillations due to the time-varying effect of the stiffness.

Moreover, the reduced transverse ratio $\varepsilon_c = 1.43$ causes higher oscillations compared to the baseline case of $\varepsilon_c = 1.45$.

It also shows at the beginning of the simulation process, a clear transient response, which may need to be removed for the extraction of spectral waveform and calculation. Nevertheless, the solution in the steady state, starting from 0.01s onward, is relatively stable. They show that the speed fluctuations of the input shaft are much smaller due to larger moments of inertia associated with driving motors. On the other hand, the middle shaft with smaller moments of inertia

exhibits a much higher fluctuation. These consistent results demonstrate that the ode115s solver and parameters used can produce for the model, reliable solutions.

3.7.2 Translational Response in the Time Domain

Correspondingly, both the pinion and the gear exhibit similar oscillations in the translational directions. As shown in Figure 3-6, in addition to the observation that the reduced transverse ratio $\varepsilon_c = 1.43$ shows a higher oscillations compared to the baseline case of $\varepsilon_c = 1.45$, the increase amplitude is more compared with that of the rotational directions, showing that the translational vibrations can more sensitively reflect the changes, which demonstrates that it is more suitable for vibration based monitoring.

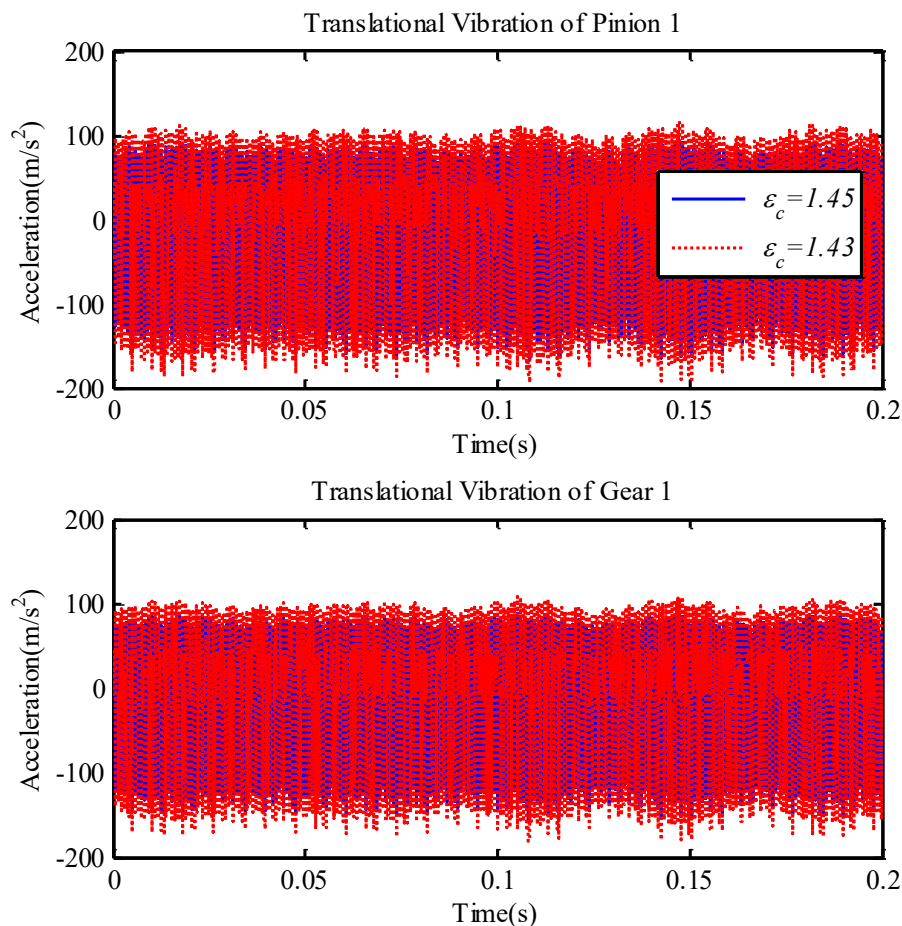


Figure 3-6 Vibration responses in the time domain of the first pinion and gear
However, these signals in the time domain provide less information in association with the gear dynamic characteristics of interest.

3.8 Spectral Characteristics

To understand the details of changes in vibration responses, the signals in time domain have been converted into the frequency domain by applying FFT to the signals.

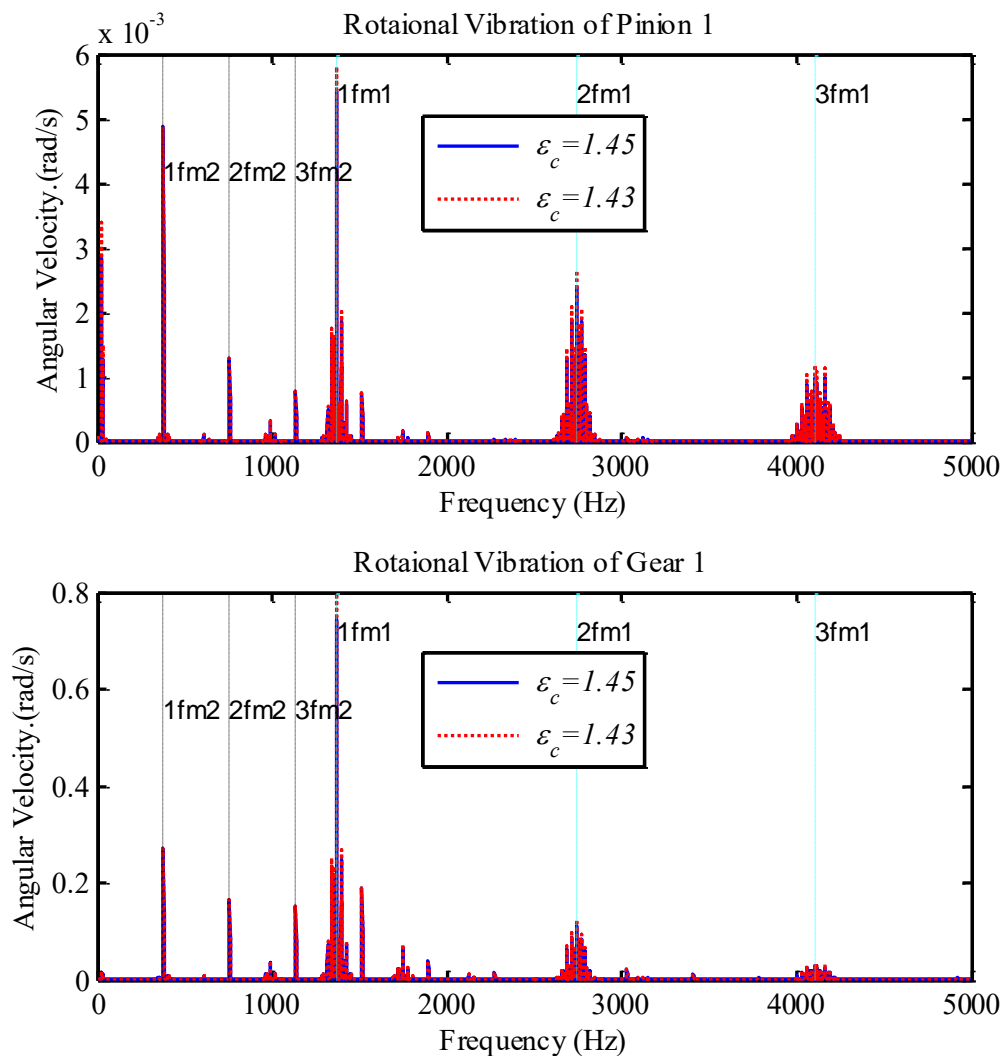


Figure 3-7 Spectral peaks of combined rotational responses of the first pinion and gear

3.8.1 Spectra of Rotational Responses

Figure 3-7 presents the spectrum comparison of the rotational responses between different degrees of reduction in contact ratios, and between different sensing positions. Clearly the spectra highlight that mesh frequency components at f_{m1} and f_{m2} , including their first three harmonics and associated sidebands are the dominated ones for both the higher and the lower speed transmission stages. This shows that the modelling and the simulation were carried out

adequately. Especially, the observable responses at f_{m2} shows that vibrations corresponding to different transmission stages and different gears are highly coupled as predicted by the model.

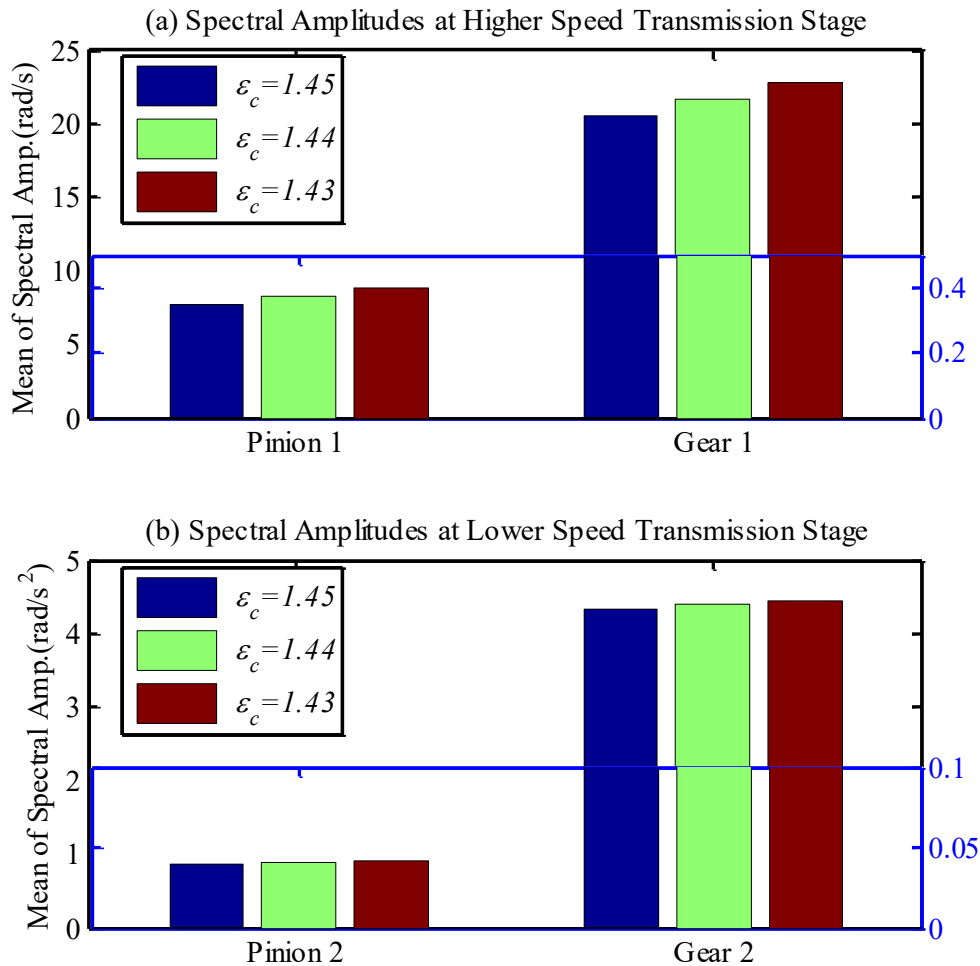


Figure 3-8 Increases of spectral amplitudes from rotational responses with wear severity.

Moreover, the spectral amplitudes for the wear case is higher across all mesh components. In particular, as shown in

Figure 3-8 (a), the spectral amplitudes calculated by averaging the components in the frequency range from 1200Hz to 4500Hz exhibit clear gradual increases with the decrease of the contact ratio, showing that they can be used to monitor the wear process happening on the higher speed stages.

In contrast, the spectral amplitudes calculated in the frequency range from 300Hz to 1200Hz, relating to lower speed transmission at f_{m2} also exhibit an increase because of the nonlinear coupling. However, as the increase is very slight, it will cause less influences on a corrective diagnosis of the wear is from the higher speed transmissions at f_{m1} .

Furthermore, components such as at 990Hz and 1750Hz are observable, which are not associated to any of the characteristic frequencies. Through, by a frequency transfer function (FTF), they are identified to be the effect of resonances from the two rotors. Because they magnify the responses in a nonlinear way, their amplitudes can have high fluctuations due to noise and load variations when used for fault severity diagnostics. However, they could be useful for early detections if an effective noise reduction can be applied.

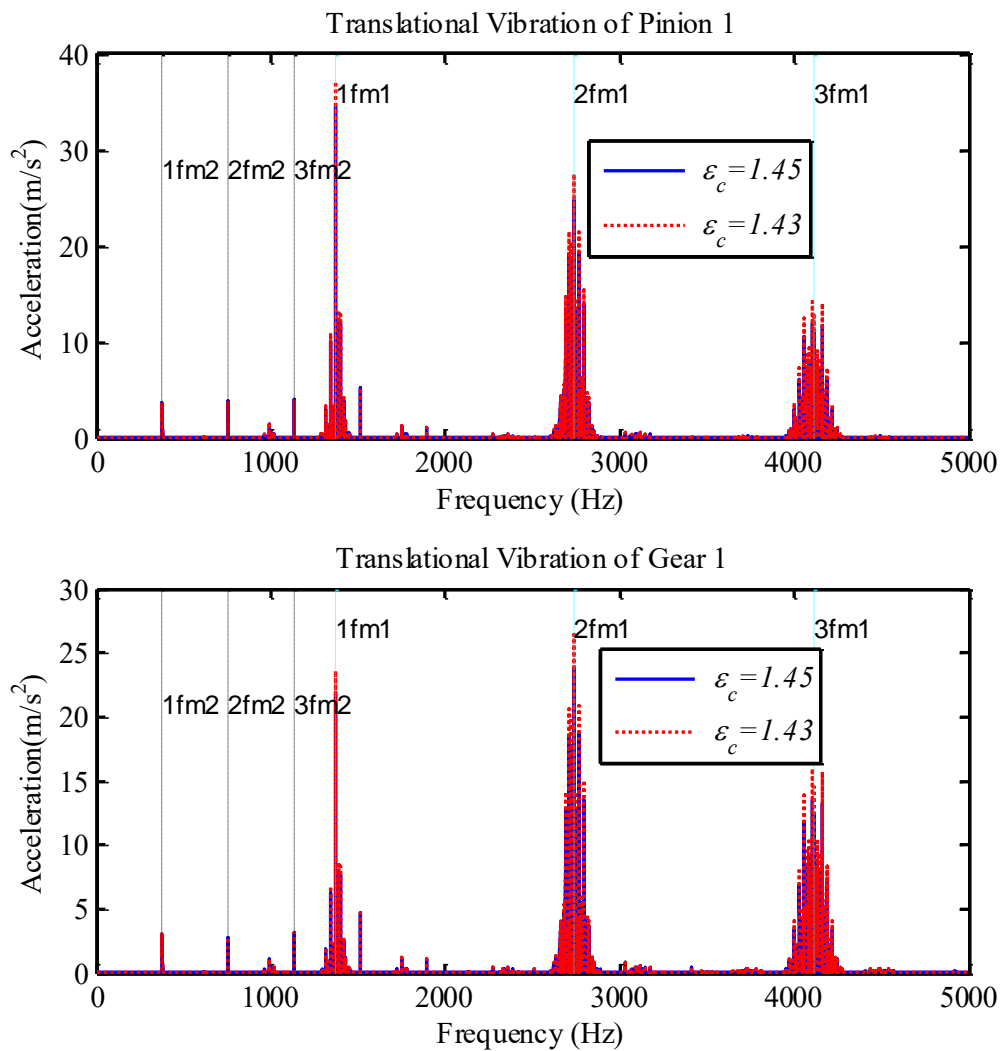


Figure 3-9 Spectral peaks of combined translational responses of the first pinion and gear

3.8.2 Spectra of Translational Responses

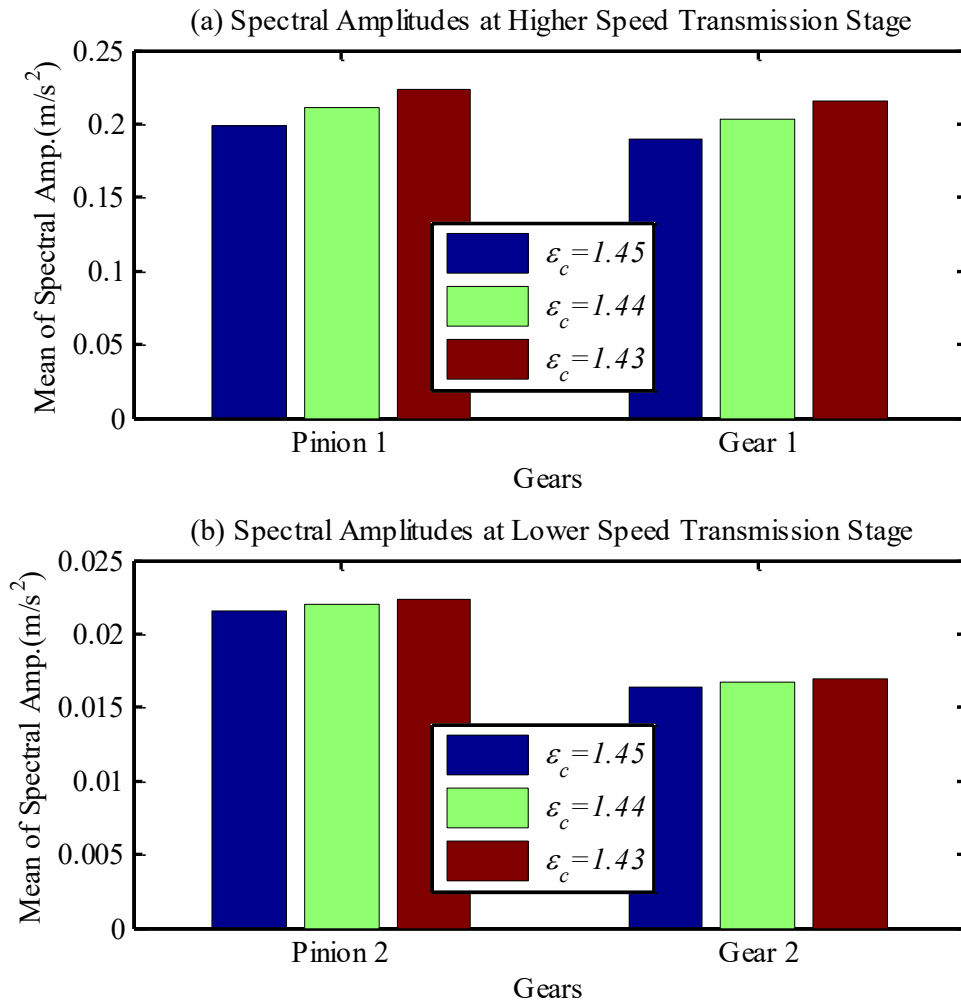


Figure 3-10 Average of spectral amplitudes for both transmission stages of the gearbox.

The spectra of translational responses in Figure 3-9 show very similar patterns with that of the rotational response. Spectral components at the mesh frequencies of both f_{m1} and f_{m2} , and their associated sidebands are major contents and exhibit with the decrease of the transfer ratio, which is detailed in Figure 3-10. These demonstrate further the effectiveness of the modelling and that it is feasible to tract the wear progression based on the characteristic components.

Moreover, the spectral amplitudes are of the similar orders for both responses at the pinion and the gear. This means that the translational responses is not so sensitive to the sensing positions. In other words, the signals perceived in any positions of a gearbox housing will allows the dynamic behaviours to be reflected equally well, therefore, measurement can be easily

implemented on for achieving better diagnostics. Comparatively, the large difference in amplitudes between the two rotational responses makes it difficult set measurement system in order to capture the responses accurately.

3.9 Acoustic Signals from Vibrating Structures

Surface vibrations can couple to surround fluid in the form of sound waves or airborne acoustics. This offers a merit that condition monitoring of machinery can be achieved by remote measurements of the sound waves, which provides significant conveniences to implement CM in industry and has received intensive research in last two decades in solving challenges in obtaining accurate and reliable diagnostic information from nosy measurements [155].

This section focus on understanding of the general properties of airborne acoustics in order to provide sufficient knowledge for acquiring high quality acoustic data and identifying effective signal analysis tools.

3.9.1 Mechanisms of Sound Radiation by Vibrating Surfaces

The sound generation mechanism by surface vibration, which is the fluid acceleration in contact with the surface, is common to all sources as the radiation mechanism effectiveness widely varies from source to source [156].

Sound radiation process by the vibration of the solid surfaces can be understood in terms of the fluid molecular nature in contact with those surfaces. Air, which is a gaseous fluid media, whose bulk mechanical properties are usually determined by the interaction between molecules that are ‘widely’ spaced on average, on their individual size scale. The gas molecule freely moves between ‘close encounters’ with others in space. The gas molecules can be pictured as moving in straight lines (in three dimensions), with mutually repulsive electrostatic forces between them causing changes in the molecular momentum and movement direction. The molecular motion is random, with a level of activity largely dependent on temperature, though from a macroscopic view point in a bulk gas flow, whether oscillatory or steady, a mean motion in the flow direction of flow must also obviously exists. The pressure acting on any plane elementary surface that lies within, or bounded by a gas is a manifestation of the components momentum average rate of change that is directed normal to the surface unit area experienced during the ‘collision’ process by the molecules. Gas pressure is directly proportional to the

kinetic energy *density* of the molecules translational motion [157]. The temperature of the gas is proportional to the average translational kinetic energy per molecule. In this lies the basis for the Ideal Gas Law: $\frac{P}{\rho} = RT$ (where ρ is density; p is pressure; R is ideal gas constant and T is temperature).

Given that local disturbances to the gas state can be propagated only at a limited speed through the molecular interaction process, it is not unexpected that the sound speed propagation in a gas state is close in any one direction, to that of the average molecular speed as expressed by the saying that ‘the molecule is the messenger’. Therefore, the response of the bulk-fluid to that of the imposed action because of the solid bounding surface vibration depends on frequency. As will be seen later that it also depends on the vibration spatial distribution [156].

Considering two small plane surface regions adjacent to one another undergoing normal displacements that are equal and opposite and then halts. It is ‘easier’ for the compressed regions molecules of the contiguous fluid to move in the direction of the rarefied region than moving toward the, as yet, unaffected fluid slight away from the surface. This bulk movement tends to equalise both the densities and pressures local to the surface, which produces a much weaker *propagating* disturbance on the surrounding fluid compared to when the two regions had in unison, displaced the fluid. This type of phenomenon is called the ‘radiation cancellation’, though it is never complete. If the displacements is reversed, the molecules then moves for equilibrium to be re-establish [158].

The more the distance between both regions, the more rapid the reversal will be and the less likely that the cancellation process will affect the molecules, with effectively radiated of more sound. The critical time for the reversal to occur is given by the distance that is between the region centres that is oppositely displaced, divided by the sound speed. Therefore, for any given two regions spatial separation, high frequency process will have radiated more effectively when compared to lower frequency process. Regarding spatially sinusoidal wave motion and harmonic vibration of a surface, the critical half period can be calculated by half the wavelength of the surface divided by the sound speed in the fluid. If the speed of the vibrational wave is less than that of fluid sound, cancellation of the radiation occurs [157].

3.9.2 Modelling of Sound Radiation

Based on above mechanisms, for a vibrating surface, the sound generated can be predicted based on vibration responses by

$$P = \sigma \rho c S \bar{v}^2 \quad (3.25)$$

where P is sound power, σ is the surface radiation ratio which depends on orientation, size and shape, ρc is the fluid specific acoustic impedance (ρ is the fluid local density while c is the fluid local sound velocity), S is the surface area radiating the sound, and \bar{v}^2 is the mean square surface-averaged velocity of that surface [159].

3.9.3 Source Addition

The acoustic source additive effects can be illustrated in Figure 3-11. In this figure, the sources are assumed to be point sources and the measurement is taken in the far field, i.e. $R \gg d$. This restriction is often true for the measurement of noise generated by helical gears when the microphones are placed in the far field away from the gear surfaces [160].

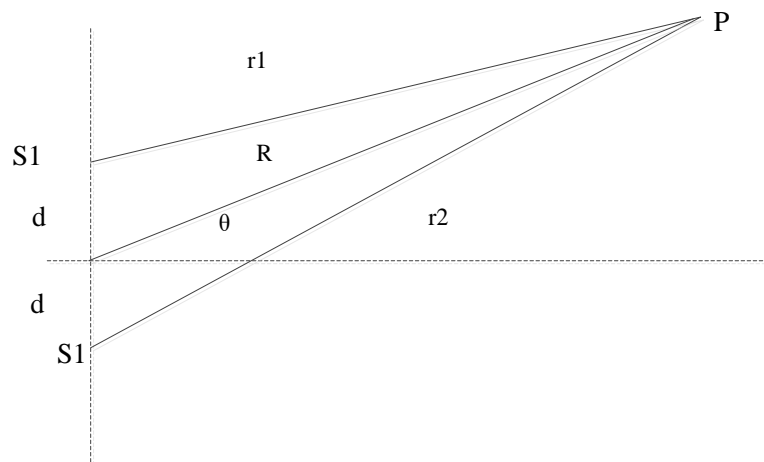


Figure 3-11 The additional effects from two point sound sources [160]

The sound pressures from the two point sources at the measuring point are denoted by P_1 and P_2 respectively and can be expressed as:

$$P_1(r_1, t) = \frac{zQ_1}{4\pi r_1} e^{-ikr_1} \quad (3.26)$$

$$P_2(r_2, t) = \frac{zQ_2}{4\pi r_2} e^{-ikr_2} \quad (3.27)$$

where Z is the characteristic acoustic impedance, $Z = \rho c$. $Q(t)$ is the source strength.

$K = 2\pi / \lambda$ is the interested sound wavelength.

The total pressure at the measurement point is simply additive as pressure is a scalar quantity, and may be expressed as;

$$P = P_1 + P_2 \quad (3.28)$$

Noting the geometric relationships in the above figure, where $R \gg d$,

$$\begin{aligned} r_1 &= R - d \sin \theta \\ r_2 &= R + d \sin \theta \end{aligned} \quad (3.29)$$

Furthermore, for the sake of simplicity, the distances from the sources to the measurement point can be regarded as $r_1 = r_2 = R$ in the case of $R \gg d$ as assumed above.

Therefore, the sound pressure from these two sources are

$$P(R, T) = \frac{Z e^{-ikr}}{4\pi r} \left(Q_1(t) e^{ikd \sin \theta} + Q_2(t) e^{-ikd \sin \theta} \right) \quad (3.30)$$

From the above equation, it can be seen that once the sources are fixed in terms of physical positions, the sound pressure at a particular surface is a function of the radius and polar angle. In gearing, there are a variety of acoustic sources. Each source radiates its power in an Omni-direction. The total power radiated to a particular surface, as shown in Figure 3-12, is normal to the surface.

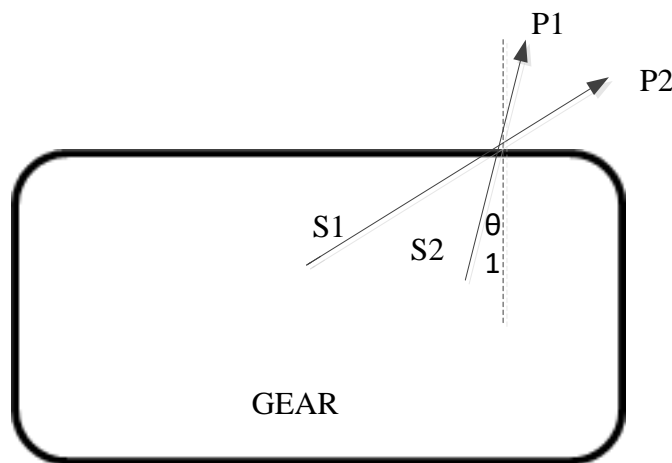


Figure 3-12 Diagram of the reverberation in an close space [160]

The total power can be calculated using equation:

$$W = \frac{1}{\rho C} \sum \int (p_{rms}^i)^2 \cos \theta_i ds \quad (3.31)$$

Obviously, if the vibrational forces moving the surface are band limited, then with the assumptions of linearity used here the frequency the radiated sound power will also be band limited [161]. The surface radiation impedance is determined by the pressure and velocity of the acoustic wave at the surface which is expressed as;

$$Z_r = \frac{P}{u} \text{ where } (p, u) \in s \quad (3.32)$$

3.9.4 Sound Wave Propagation in Rooms

The sound in air volumes enclosed by solid boundaries behaviour is of considerable significance here because the feature extraction may be hampered by the reverberant acoustic field. Hence, it is essential to study the sound field characteristics in a closed room to understand how it might affect the sound source basic acoustic characteristics [162].

Compared to the characteristic of the enclosed sound field, the characteristics of outdoor sound field are simple because the sound wave from the sound source spreads out freely without obstacle and only attenuates with distance. However, sound emitted in a closed room creates a more complicated sound field due to the multiple reflections from the walls, ceiling and floor [163]. The sound field in a room becomes more complicated the more intricate the room shape, with different surface finishes and peculiar phenomena such as echoes and flutter echoes which might be problematic.

Assume an omnidirectional sound source in a closed space, as shown in Figure 3-13 and that the sound waves can be considered as numerous plane waves with different propagation directions. The sound waves will undergo multiple reflections at the wall surfaces. In the diagram the ray shown is first reflected from wall A, then walls B, C and D, and so on. Similarly, all the waves from the source will be reflected many times in different directions generating a complex sound field within the closed space. This reverberant field will reach a steady level when the energy produced by the source is equal to the energy absorbed at the wall reflections. Of course, gear covers may well not be omnidirectional sources [218].

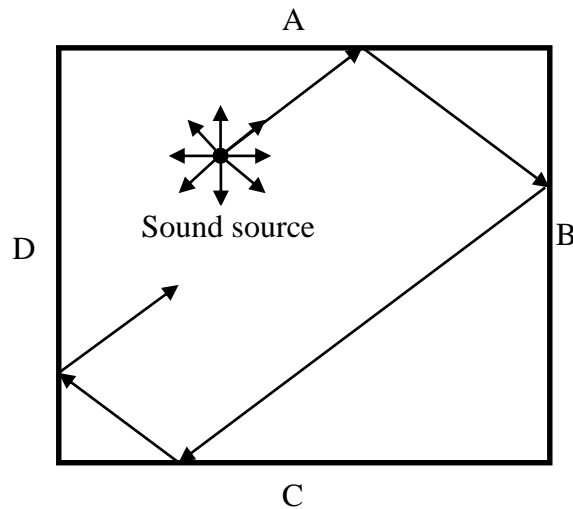


Figure 3-13 Diagram of the reverberation in a closed space [218]

3.9.5 Background Acoustics

Background noise is any undesired signals picked-up by sensors that is not significant to the monitored source. These can be from mechanical and/or electrical sources. Substantial progress has been made in the elimination of this interference since the early years of audio signal (AS) measurement. However, precautions should always be taken, including such obvious and simple measures as switching off the noise sources. In all gears the AS will certainly be generated by many sources, not only the interested source, and will be the complex sum of noise from gears, impacts and flow. These AS should be identified and/or removed in differentiating them from the interested generated gear signals [164].

To eliminate unwanted signals an appropriate frequency or range of interest must be determined for the particular application. Because of the rapid attenuation of high frequency signals, any signal reaching the measurement point from long distances will usually contain only frequencies of less than 20 kHz. This will have little effect on AE measurements which are concerned with frequencies above 20 kHz. Typically, 20 Hz to 20 kHz is a suitable range for the monitoring and study of gear generated AS noise. More work is needed in narrowing down the frequency range in improving the AS monitoring accuracy. Noise removal could be key to using successfully, AE for inspection online for industrial applications such as the precision welding monitoring, and fatigue crack initiation detection in flying aircraft [165, 166].

Electrical noise can be reduced or even eradicated by the use of differential sensors or appropriate threshold values, and substantially reduced using sensors with built-in preamplifiers.

3.10 Key Findings

Based numerical simulation studies, it has been understood that small gear wear can be simulated by changing the stiffness function. For current gear configuration, the reduction in overlap ratios will lead to clear increases of vibration responses in both two stages of the gearbox. However, the increase amplitudes are much more at the mesh components and their sidebands for the faulty transmission stage. So it can be based on to identify the faulty transmission stage.

The translational responses at any sensory positions show similar amplitudes and can be based on for easier implementation of diagnosis. However, the rotational responses vary largely with sensory positions, which can be difficult to collect high quality data for diagnostics.

In addition, based on the characteristics of sound radiation, propagation and background noise influences, the remote perception of gearbox dynamics can be more challenging in obtaining reliable diagnostic information.

Moreover, the deteriorations of gear mesh conditions such as the non-uniform wear induce principally as nonlinear modulations, presenting significant sidebands around mesh components in the frequency domain. This is a very key characteristic to be based on for selecting and improving signals processing tools for accurately extracting diagnostic information from noisy measurements.

Chapter 4 BISPECTRUM OF GEAR VIBRO- ACOUSTIC SIGNALS

Higher-order spectral (HOS) analysis and their relation to conventional second-order statistics to developing the mathematical basis of the modulation signal bispectrum (MSB) method for the effective analysis of vibro-acoustic signals from gearboxes are reviewed in this chapter. It proceeds to evaluate MSB performance in detecting incipient gear wear faults while still in an early stage of development under run-to-failure conditions.

The chapter starts by describing the concept of MSB and its implementation details to show its potential advantages over other conventional signal processing techniques, then explains its performance in deriving frequency and phase components in relation to fault detection in helical gears of multi stage gearboxes.

In extracting additional components of the signal caused by faults in helical gearbox, a new Modulated Signal Bispectrum - Sideband Estimator (MSB-SE) is applied to obtain a measure of the modulation that is more accurate. MSB-SE analysis is very effective as it takes into consideration, the phase information of the sideband and resulting in a more accurate sideband magnitudes estimation by the suppression of the influences of random noise from the operation of the motor and the processes of measurement.

4.1 Introduction

It is well-known that structural component faults of rotating machines such as bearing and gears can be sensed by the monitoring of the vibration they generate. Many techniques for signal processing such as Fourier transforms and related time-frequency analysis are widely used in diagnosing non-stationary frequency features which are the consequences of gear faults such as gear tooth breakage. In addition, with typical faults that are restricted spatially and have feature defect frequencies, there is the possibility of linking particular patterns of fault vibration with exact machine rotational frequencies [167].

The complexities in machine health diagnostics arise because of the necessity of searching through the massive number of frequencies that exist in a machine's vibration spectrum in order to extract features linked with the condition of a particular component. Unfortunately, the vibration signals in mechanical machines usually contain many thousands of combinations of frequencies that provides little or no relevant diagnostic information regarding the condition of the machine. Generally, vibration disturbances caused by localised faults in rotating machinery lead to a variety of cyclical impulses and the defect frequencies often arise around the carrier frequency (mains frequency) or its harmonics as sidebands - modulations. Furthermore, other effects may appear, such as when the imperfection of another component (e.g. a bearing) modulates the gear mesh fundamental. Until there is a dependable method of predicting which component should be monitored, a complete spectrum of frequencies has to be analysed and examined for defects. In addition, which component is dominant may depend on fault severity and a fault in its initial stages usually has a low SNR (Signal to Noise Ratio) resulting in it going unobserved [168].

Power spectrum methods (second-order technique) have been used extensively to investigate vibration signatures to extracting features relating to the faults of the component. Though there are serious disadvantages regarding this technique as it discards all information regarding the phase and practically makes it impossible to detect phase-coupled signal sets.

HOS and spectra provide a realistic and mathematically flexible approach to obtain information regarding the coupling of the phase. Particularly, cumulants with higher order and their related Fourier transforms, called polyspectra, exploit the information of the phase. This is not the case in second order statistics [169].

For completely Gaussian processes, higher order (i.e. third order) cumulants disappear; so HOS have the ability in increasing the SNR (Signal to Noise Ratio) in application regarding mechanical fault detection [168].

In addition, HOS have the ability to detect phase coupling between spectral components [167, 168]. The simplest type of this interaction between two frequency components is known as Quadratic Phase Coupling (QPC). It is characterised by the existence of additional frequencies at the difference and sum for the frequencies of the two component in the power spectrum. However, the existence of the difference and sum is a requirement for these frequencies but not a sufficient condition for QPC. It is obviously true that phase coupling is identified in cumulant sequences of the third order or in the frequency domain, but the bispectrum has the potential to detect and characterise non-linear coupling effects in mechanical machinery [167].

4.2 Bispectrum Background

This chapter studies higher order spectral techniques in terms of their application to signal analysis and use in gearbox CM, particularly at early stage fault detection.

The first HOS is usually considered to be the third order spectrum (Bispectrum). This produces information in cases where a random data distribution has been skewed [170].

In the previous chapter, it was assumed that the induction motor speed remained constant. However, a gearbox under test is subjected to varying gear tooth stiffness effects that lead to torque fluctuations and therefore to variations in the speed. These fluctuations in speed will produce variations in frequency in the time record, giving rise to non-stationary signal properties. However, traditional FFT (Fourier Transform Analysis) is based on signals that are stationary, so that a direct vibration signals FFT produces inexact results. This phenomenon is also present when a multistage gearbox is employed. Not only are many mesh frequency components produced when multistage gearboxes are used but also multiple modulations between shaft and mesh frequencies. As a result, the raw signals FFT cannot resolve accurately, the frequency content due to the high frequency density which, overall, can result in poor fault diagnosis [171].

Furthermore, gearbox vibration is invariably extremely contaminated by a variety of random noises which affect the measurement process, such as lubrication fluid turbulence. Because

traditional FFT signal analysis does not preserve the information of the phase being contained inside the original signal as it has limited success in reducing these noise effects.

Recently HOS methods have played an increasingly important role in many diverse fields, such as adaptive filtering, biomedicine and harmonic retrieval. HOS provides a signal processing tool with a number of unique features compared to ordinary spectra such as the traditional power spectral density, that only describe the different frequencies energy content and their magnitude in the signal. In contrast HOS:

- 1) Retain phase information
- 2) Eliminate Gaussian noise[172]
- 3) Provide non-linear system identification

To demonstrate these important diagnostic characteristics, bispectrum analysis was applied to the motor current signal in extracting and studying the non-linear features that are possible under different operation condition and faults, i.e. Gaussian noise received with a non-Gaussian signal can be suppressed by transformation to a higher order cumulant domain [173, 174].

The Bispectrum, a third-order statistic, can be used in identifying phase-related spectral components pairs that are helpful for fault detection [83, 167].

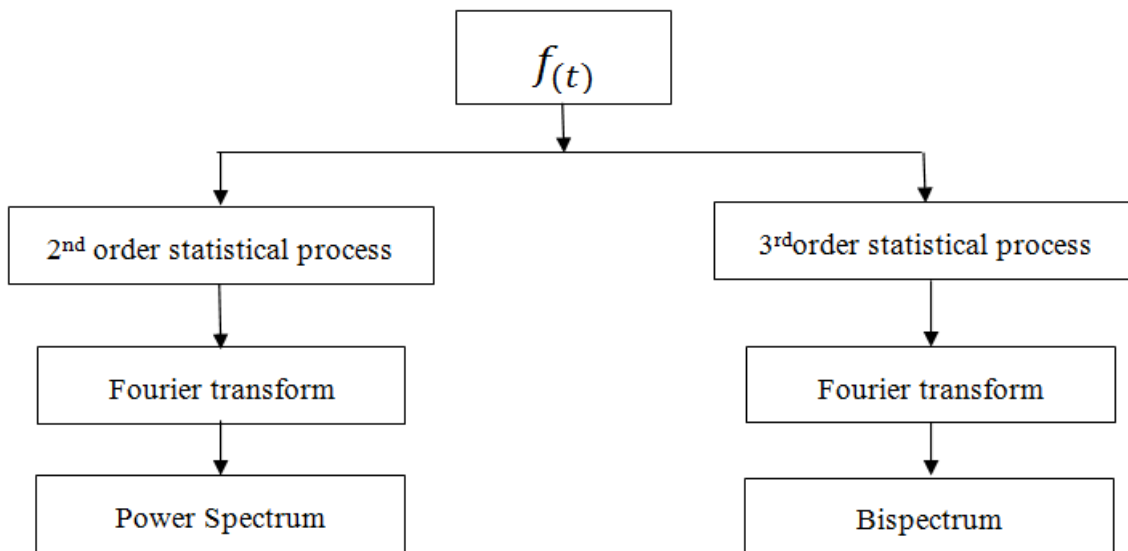


Figure 4-1 Classification of higher order spectra

Bispectrum is defined as the third order statistics Fourier Transform. Figure 4-1 shows the classification of HOS for a discrete time-domain signal. Several publications such as [175, 176] have reported the application of HOS techniques in machine CM where HOS cumulants, and

their related Fourier Transforms, have used phase information to provide a reliable means of extracting information about phase coupling.

The use of higher-order methods have the capability, in many applications where mechanical faults are detected, to enhance the SNR and it has been found that such measures can be used in a deterministic way to extract the vibration of induction motor HOS components in a manner sensitive to conditions of several faults [177]. Furthermore, it has been reported that HOS measures are fault conditions sensitive compared to normal spectral analysis and stator current for the induction motor analysis using the Bispectrum technique had significant benefits over the conventional second-order techniques [178].

In this chapter a third-order signal processing technique has been applied to investigate gearbox health for a high load and to determine whether the motor current frequency spectrum had the capability of both detecting the seeded faults magnitude and presence.

4.3 Quadratic Phase Coupling (QPC)

The frequencies that occur due to defects in rotating machinery applications occur around the 50Hz carrier frequency as sideband modulation components, but there are inter-component modulations also, including the fundamental Teeth Meshing Frequency (TMF) and its harmonics.

Spectral analysis has already provided reliable and satisfactory information about the health condition of the gearbox. However, that analysis was linear and the spectral components in the motor current signal were assumed to be uncorrelated and the phase relationship between the components of the frequency was ignored [111]. These limitations make it difficult in practice to identify sets of phase-coupled signals.

The information in the phase coupling relationship caused by the non-linearity between the components of the frequency is preserved by the HOS analysis. QPC is seen in the appearance of additional peaks in the power spectrum at the difference and sum of the frequencies of interacting components of a signal [178].

4.4 Review of Gearbox Fault Condition

It is common knowledge that the sidebands existence in induction motor current spectra can be due to load fluctuations, leading to motor air-gap eccentricities. This means that any

mechanical imbalance arising in the gearbox leads to the rotor experiencing an instantaneous transient radial vibration and the motor air-gap varies in a way described as a rotating eccentricity [179]. These variations in the air-gap produces stator current frequency components related to both the rotor shaft rotational speed and supply frequency by the expression:

$$f_{sb} = f_0 \pm mGf_{r1} \quad (4.1)$$

Where f_0 is the supply frequency, f_{sb} is the frequency of the sideband, $m = 1, 2, 3, \dots$, etc, G is the gear ratio and f_{r1} the rotor rotational speed in the stator reference given by:

$$f_{r1} = f_0(1 - S)/P \quad (4.2)$$

Where S is the per-unit slip and P the number of pole-pairs. Substituting the expression for f_{r1} from (4.2) into (4.1) gives an expression which directly relates f_{sb} to the supply frequency f_0

$$f_{sb} = f_0 \pm mG[f_0(1 - S)/P] \quad (4.3)$$

Where:

$$S = 0.023 \text{ and}$$

$$P = 2 \text{ (For the given induction motor)}$$

4.5 Conventional Bispectrum Calculation

For a current signal with discrete time $x[n]$, DFT, $X(f)$, is given as [180, 181]:

$$X(f) = \sum_{t=-\infty}^{\infty} x(t) e^{-2j\pi ft} \quad (4.4)$$

In the format of complex number, $X(f)$ in terms of magnitude $|X(f)|$ and phase ϕ_f can be rewritten as

$$X(f) = |X(f)| e^{j\phi(f)} \quad (4.5)$$

The power spectrum is a linear transform and a frequency function f . The power spectrum measure which a second-order measure of $x(t)$, can be calculated using the formula [180, 181]:

$$P(f) = E[X(f)X^*(f)] \quad (4.6)$$

where $X^*(f)$ the complex conjugate of $X(f)$ and $E[.]$ is the statistical expectation, showing that an average across a number of records will provide for more reliable results.

Equation (4.6) can be rewritten in the phase format as [173, 178]:

$$P(f) = E[X(f)X^*(f)] \quad (4.7)$$

where $X^*(f)$ the complex conjugate of $X(f)$ and $E[.]$ is the statistical expectation, showing that an average across a number of records for a reliable results.

Equation (4.6) can be rewritten in the phase format as:

$$P(f) = |X(f)|^2 e^{j\phi(f)}$$

Where, $\alpha(f) = \phi(f) + \phi(-f)$, and $\phi(f)$ is the phase of $X(f)$. For real signals $\phi(f) = -\phi(-f)$. Therefore $\alpha(f) = 0$.

Consequently, it is obvious that the power spectrum does not preserve the phase, which is necessary for signal reconstruction [182].

Extending the definition of power spectrum to third order measures results in the conventional Bispectrum $B(f_1, f_2)$ which is defined in the frequency domain as [173, 178]:

$$B(f_1, f_2) = E[X(f_1)X(f_2)X(f_1 + f_2)] \quad (4.8)$$

where f_1 , f_2 and $f_1 + f_2$ are individual components of the frequency gotten from the integral of the Fourier transform.

Note that there is difference between the second and third order measures as they are both complex quantities that contains both phase and magnitude information regarding the original time signal. Hence the Bispectrum detecting the QPC presence [183].

For example, if the components of the frequency at f_1 , f_2 and $f_1 + f_2$ in a signal are independent from each other as each frequency is characterised by independent random phases distributed statistically over $(-\pi, \pi)$. By carrying out averaging statistically, denoting expectation in Equations (4.6) and (4.7) by operator $E\langle \rangle$, the Bispectrum will then tend towards nil (0) due to the effects of random phase. The suppression of random noise can then in this

way, be suppressed. Alternatively, if the three spectral components: f_1, f_2 and $f_1 + f_2$ are to each other (even non-linearly) coupled, the combined components phases will not be random, though each individual phases may be random. The phases would have the type of relationship below[178]:

$$\varphi(f_2) + \varphi(f_1) + \varphi(f_2 + f_1) = 0 \quad (4.9)$$

Therefore, statistical averaging would then lead to a value in the Bispectrum that is non-zero. A peak in the Bispectrum at the bi-frequency indicates this non-linear coupling $B(f_1, f_2)$. In measuring, between coupled components, the degree of coupling, a normalised form of the bispectrum or bi-coherence is generally used which is defined as [173]:

$$b_{MS}^2(f_1, f_2) = \frac{|B_{MS}(f_1, f_2)|^2}{E|X(f_1)X(f_2)|^2 E|X(f_2 + f_1)|^2} \quad (4.10)$$

4.6 Difference between Bispectrum and Power Spectrum

This section discusses how the Bispectrum has the advantage of preserving phase information compared to the power spectrum.

Applying the same approach as used with the power spectrum to the Bispectrum, the latter can be written:

$$B(f_1, f_2) = |X(f_1)||X(f_2)||X(-f_1 - f_2)|e^{j(\varphi(f_1) + \varphi(f_2) - \varphi(f_1 + f_2))} \quad (4.11)$$

This equation clearly shows that the phase information is preserved using bispectrum which, as stated above, is important in the processing of speech signals [182, 184].

4.7 Modulation Signal Bispectrum Calculation (MSB)

According to MSB definition in the frequency domain, the meshing frequency component f_m and sideband at $X(f_r \pm f_m)$ in an vibro-acoustic signal can be correlated [178] as:

$$B_{MS}(f_r, f_m) = E[X(f_r - f_m)X(f_r + f_m)X^*(f_m)X^*(f_m)] \quad (4.12)$$

where $X^*(f)$ is the Fourier transform complex conjugate $X(f)$ of acoustic signal $x(t)$; and $E[]$ is the statistical expectation operator. And the power spectrum of $x(t)$ is

$$P_S(f_m) = E[X(f_m)X^*(f_m)] \quad (4.13)$$

Equation (4.13) illustrates that through the vector averaging frequency domain operation, MSB can extract at the meshing frequency, the higher sideband and the lower sideband of the components combination. Meanwhile, other components, which include the interfering components and random noise, which do not meet the phase relationship, is significantly suppressed. Say, this process, the effects of the modulation, can represent an acoustic signal more reliably and accurately.

In examining alone the modulating components, instead of combining with the components of the meshing, an MSB sideband estimator (MSB-SE) according to [182, 184] can be used:

$$B_{MS}^{SE}(f_r, f_m) = E\left[X(f_r + f_s)X(f_r - f_s)X^*(f_m)X^*(f_m) / |X(f_m)|^2 \right] \quad (4.14)$$

Because Equation (4.14) magnitude is normalised, the MSB-SE magnitude becomes only the products of the upper and upper sidebands, reflecting more the modulating faults component.

Furthermore, MSB coherence (MSBC) which has been given in Equation (4.14) can be used in estimating the random components influences [182, 184]:

$$b_{MS}^2(f_r, f_m) = \frac{|B_{MS}(f_r, f_m)|^2}{p_S(f_m)E[|X(f_m + f_r)(f_m - f_r)|^2]} \quad (4.15)$$

The coherence in MSB has boundary [0 1]. One (1) meaning that the magnitude of MSB is true from the modulation effects. On the other hand, a 0 (zero) value means that the magnitude of MSB is primarily from the influences of random noise. Therefore, other MSBC values will indicate the MSB peaks reliability. Furthermore, for any given environment where measurement is being carried, noise is relatively the same. The MSBC increase can be a modulation degree indicator that can be used to detect modulation presence.

4.7.1 Sideband Detection Using MSB

Mechanical faults gearbox system contains series of components of sideband (appearing mainly around the supply component). Bispectrum piece at the frequency of supply is sufficient in characterizing the sidebands for the detection of fault [178]. By putting the constant

frequency values such as at a mesh harmonics $f_m = z f_r$ into Equation (4.11) the supply frequency MSB can be given as [185]:

$$B_{MS}(f_r, f_m) = E[X(f_r + f_m)X(f_r - f_m)X^*(f_m)X^*(f_m)] \quad (4.16)$$

To extract the sidebands effect only, the supply component magnitude on the amplitudes of the resultant bispectrum can be eliminated by normalising the component of the supply by its magnitude $X_n(f_m) = X(f_m)/|X(f_m)|$ having unity amplitude but retains phase information that are useful. In this way Equation (4.15) becomes Equation (4.16) whose magnitude will be an estimate of sidebands strength only and denoted as MSB-SE:

$$B_{MS}^n(f_l, f_s) = E[X(f_s + f_l)X(f_s - f_l)X_n^*(f_s)X_n^*(f_s)] \quad (4.17)$$

and in magnitude-phase form, the MSB of the sideband is:

$$B_{MS}^n(f_l, f_s) = E|X(f_s + f_l)||X(f_s - f_l)|e^{j\varphi_{MS}(f_l+f_s)} \quad (4.18)$$

These equations however show that the carrier magnitude-normalized MSB magnitude is the product of the components of the two sideband only. Under the condition that the sideband amplitude is the same, Equation (4.16) or Equation (4.17) amplitude can be compared directly with the amplitudes of the sideband in the power spectrum from Equation (4.6).

Though, the Equation (4.18) amplitude can be calculated by the inclusion of the phase influences, in particular, the average is performed based on vector quantity. Any components with inconsistency in the phase will be suppressed including non-modulated components and random noise. Alternatively, the amplitudes of the sideband in Equation (4.6) include noise in the measured signal as the power spectrum is unable to use the information of the phase [186].

To check or quantify the influence of the random noise degree and hence, confirm MSB peaks existence, the corresponding bicoherence of the MSB for modulating signals (as in [173, 178]) can be simplified as:

$$b_{MS}^{2n}(f_r, f_m) = \frac{|B_{MS}^n(f_r, f_m)|^2}{E|X(f_m + f_r)X(f_m - f_r)|^2} \quad (4.19)$$

Likewise $b_{MS}^{2n}(f_r, f_m)$ will be close to unity if a bispectral peak is from modulation components. Otherwise a value close zero will indicate the peak is not a modulated component, and may possibly be due to noise.

4.7.2 Bispectrum Performance

As mentioned in Section 4.2, Bispectrum Analysis has a number of distinctive advantages when compared to the traditional power spectrum analysis. These include preservation of phase information, Gaussian noise elimination and non-linear component (modulation) recognition. Especially, the bispectrum can be very capable of detecting QPC that arises when two signals non-linearly interact with each other and produce a third signal with a phase and frequency equal to the difference and sum of the first two signals. As seen in the gear vibration model, the signal is produced due to a non-linear interaction only between the mesh frequency and shaft speed components. Thus, the bispectrum can provide a more precise vibration signal diagnosis for fault conditions [178].

4.8 Key Findings

Analysis of Higher-Order Spectra (HOS) and their relation to conventional statistics of the second-order has been reviewed in this chapter. Statistics of the first and second-order which include variance, mean, power spectrum and autocorrelation, which are signal-processing tools that are accepted and widely used for data analysis. Statistics of the second-order are suited particularly to describe linear and Gaussian processes. However, practically, there are several situations where practical processes deviate from linearity and Gaussian conditions, and then more advanced analysis techniques are required, these include the bispectrum.

Bispectrum has also been used in investigating vibro-acoustic signals in this chapter. Vibration and acoustic signals generated by faults from electrical and mechanical origin contains sideband components series that mainly appear around the supply frequency. A bispectrum piece at the frequency of supply will be sufficient enough in characterising these sidebands for detection and diagnosis of fault.

In extracting extra components caused by faults in helical gearbox on the vibro-acoustic signals, it has been seen that a new MSB-SE estimator can be a more accurate modulation measure. Analysis using MSB-SE is very effective as it considers the phase information of the sideband and the results gives a sideband magnitudes estimation that is more accurate by

suppressing the influences of the random noise from the motor operation and the process of measurement.

The CM mechanism involves a signal processing and sensors tools mix that ensures the provision of constant sensor signals that represents the system components condition based on acoustics, strain measurement, oil analysis, vibration analysis and thermography approaches, which make such approaches used for machines CM very important.

Analysis using Vibro-acoustic approach is very important in the industry for effective machine CM and helps in achieving and maintaining machines with better operating conditions and efficiency. Acoustic and vibration data have been presented in both frequency and time domain. Any of the data can be used in processing the vibro-acoustic signals for fault diagnosis and detection in gears. However, this thesis will investigate the MSB (modulation signal bispectrum) as an advanced technique for analysis in achieving better results.

Chapter 5 EXPERIMENTAL FACILITY FOR GEAR FATIGUE MONITORING TESTS

This chapter gives in details, the test facility and methodologies employed for the evaluation study of vibro-acoustic signals based monitoring. Commencing with explanations of the tested gearboxes and associated systems including diving AC motors, loading generators, control modules and data acquisition systems then an explanation of the test procedure, including load methods and monitoring schemes. The naturally resulted gear faults are later discussed.

5.1 Test System

In evaluating the CM techniques for the gearbox of interest, a run to failure test has been conducted on a gearbox test rig that has been developed at the University of Huddersfield. The gearbox test rig consists of two helical gearboxes in a back to back arrangement for effective loads and multiple compounds tests.

The operation of the rig and data acquisition is fully automated for any combination of load and speed, making each specified run completely controlled and repeatable in order to acquire high quality vibro-acoustic data.

In addition, the rig is one of 10 different rigs in a large laboratory. It means that its operation and data acquisition may be influenced by other rigs running simultaneously, which is very common scenario in industries and thus the data sets can be more realistic.

5.2 Test Rig Construction

As seen in Figure 5-1, the test rig of the gearbox comprises of AC motor as the driving power, two helical back-to-back gearboxes as the testing objects, and a DC generator as the load devices, which are linked by flexible couplings. In addition, both motors are associated with their electrical drives which are controlled through a PLC controller to operate the rig at various specified load and speeds automatically.

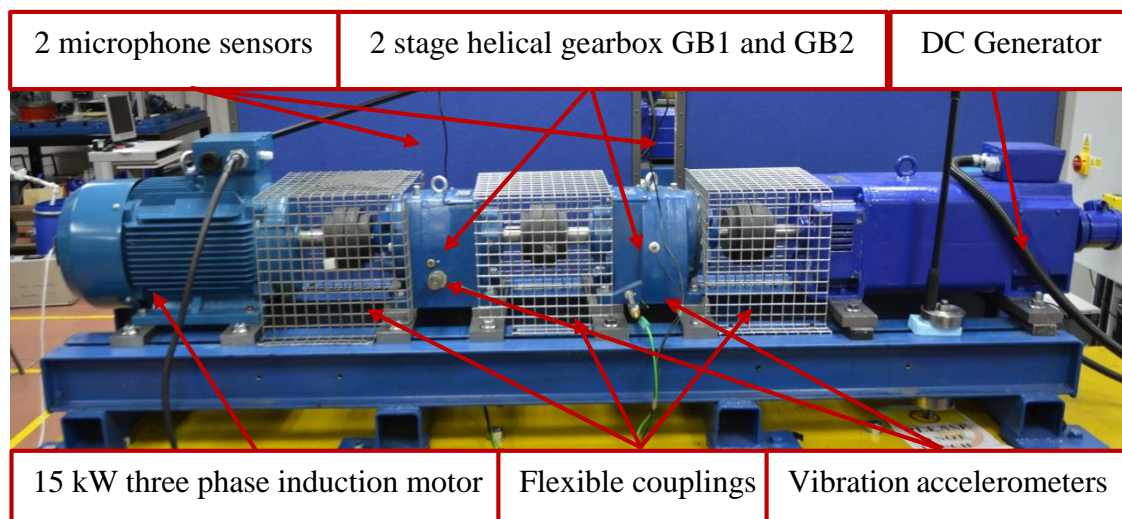


Figure 5-1 Mechanical/electromechanical test rig components.

The AC motor produces an output of 15 kW at rated speed of 1460 rpm, which is depicted in Table 5-1. This output is higher than that of the testing gearboxes in order to ensure the gearboxes operate at their rated load.

Table 5-1 Specification of AC induction motor [187] (Brook Crompton)

Type of Motor	Induction
Number of phase	3
Number of poles	2 pairs
Rated power	15 kW
Rated line voltage	415 V
Max. Current	22A @Full Load
Rated speed	1460 rpm @Full Load and 50Hz Supply
Winding	Y Star To Δ delta
Number of stator slots	48
Number of Rotor slots	40

The two gearboxes under tests, as illustrated Figure 5-2, are industrial gearboxes supplied from a major gearbox company. They are very commonly used as power transmissions in different industries such as oil refinery process, paper mills, etc., and are of the high speed layout of a typical wind turbine transmission system,

As both of them have identical constructions in terms of the centre distances between gears, bearings and housing, they have similar dynamic characteristics and their vibro-acoustics can be compared directly for any large discrepancies arising from installation errors.



Figure 5-2 Illustration of two stage helical gearbox under test

As shown in Table (5-2) and Table 5-3) , the two gearboxes are the same for transmission ratio $Z_{r3}/Z_{r4} = Z_{i3}/Z_{i4} = 13/59$ at the lower speed stages but they have a slight different gear parameter at the higher speed stages. Gearbox 1 (abbreviated to GB1 thereafter) operating as a

speed reducer has the gear ratio of $Z_{r1}/Z_{r2} = 49/55$ whereas gearbox 2 (abbreviated to GB2) operating as a speed increaser has the ratio of $Z_{i3}/Z_{i4} = 47/58$. These configurations make more than a 50% difference between the transmission ratios between the two gearboxes so that the DC generator can operate in high efficiency ranges and apply loads to the system efficiently over a wide range of speeds.

Table 5-2 Key specification of speed reduction two stage helical gearbox (GB1)

Description	1 st or higher speed transmission stage (GB1 input shaft 1)	2 nd or lower speed transmission stage (GB1 output shaft 3)
Number of gear teeth	$Z_{r1}/Z_{r2} = 49/55$	$Z_{r3}/Z_{r4} = 13/59$
Reduction ratio	1.224	4.5385
Centre Distance	74mm	74mm
Shaft diameter	24 mm	39.5 mm
Normal pitch	1.25mm	2.00 mm
Helix angle (°)	$\beta_1=13$	$\beta_2=27$
Pressure angle (°)	$\alpha=20$	$\alpha=20$
Module	$M_1=2.0\text{mm}$	$M_2=1.25\text{mm}$
Working face width	$b_1=25\text{mm}$	$b_2=26\text{mm}$
Contact ratio	$\epsilon_{a1}=1.521$	$\epsilon_{a2}=1.669$
Overlap ratio	$\epsilon_{b1}=1.289$	$\epsilon_{b2}=2.89$

Table 5-3 Key specification of two stage speed increase helical gearbox (GB2)

Description	1 st or lower speed transmission stage (GB2 Input Shaft 3)	2 nd or higher speed transmission stage (GB2 Shaft 5)
Number of teeth	$Z_{i1}/Z_{i2} = 59/13$	$Z_{i3}/Z_{i4} = 47/58$
Increase ratio	4.5385	0.8103
Centre Distance	74mm	74mm
Shaft diameter	39.5 mm	24 mm
Normal pitch	2.0mm	1.25mm
Helix angle (°)	$\beta_1=27$	$\beta_2=13$
Pressure angle (°)	$\alpha=20$	$\alpha=20$
Module	$M_1=2.0\text{mm}$	$M_2=1.25\text{mm}$
Working face width	$b_1=36\text{mm}$	$b_2=25\text{mm}$
Contact ratio	$\epsilon_{a1}=1.469$	$\epsilon_{a2}=1.45$
Overlap ratio	$\epsilon_{b1}=1.289$	$\epsilon_{b2}=2.89$

The DC generator/motor acts as the mechanical load for the system (test rig). At the maximum driving speed (1480 rpm, it produces an output of 17.5kW. This load is much higher than the rated power of the AC motor (15 kW) but the electric control module can automatically adjust the load to the demand and maintain it with at high accuracy.

Table 5-4 Specification of the DC generator [188, 189] (Brook Crompton)

Classification	DC (shunt)
Number of phases	3
Number of poles	2 pair
Rated power	17.5 kW
Voltage (excitation)	460 V
Current	44.5 A
Rated speed	1480 rpm

With this set up, the electric supply of the AC motor is from a control cabinet which adjusts the speed and power output of the motor. The AC motors transmits mechanical power directly to the gearbox via the gearbox input shaft and, hence, to the downstream components, see Figure 5-3.

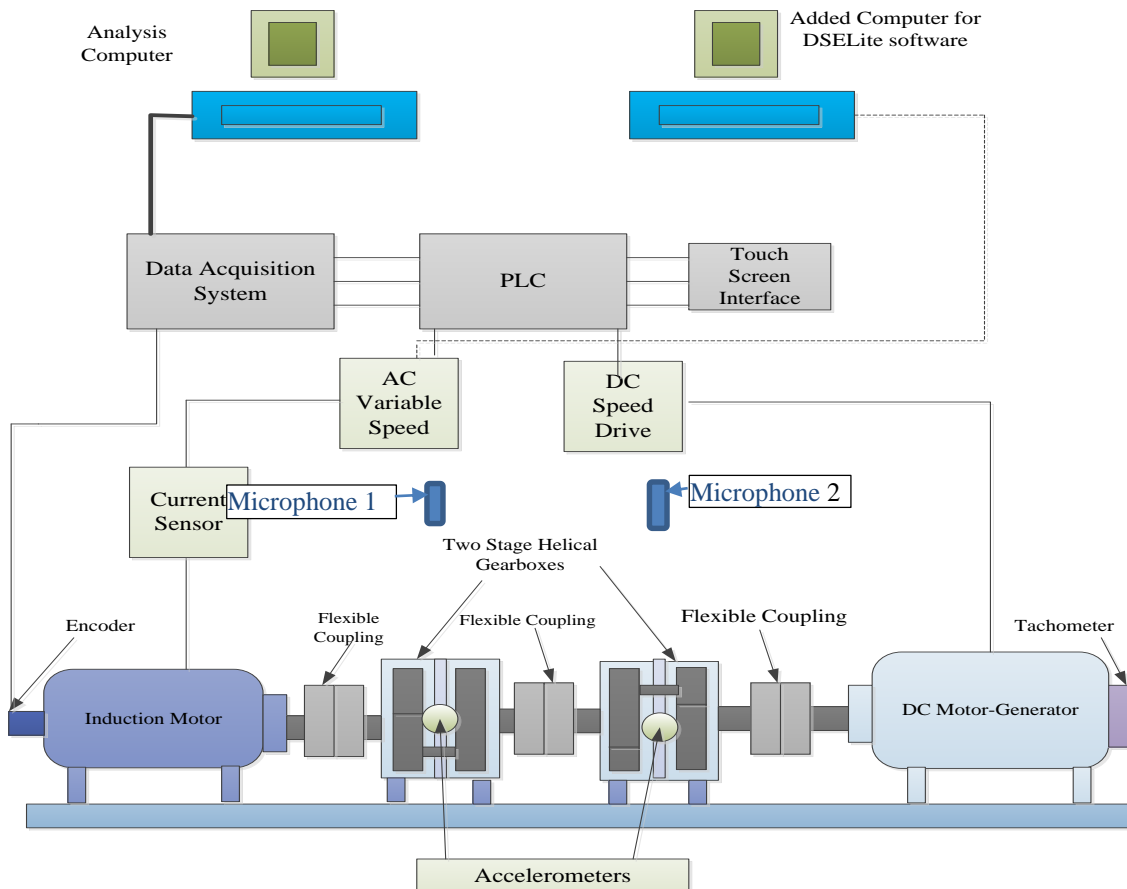


Figure 5-3 Test rig schematic diagram and placement of vibro-acoustic sensors

A third shaft supported by two bearing supports, couples the gearbox to the DC generator, which produces electricity that is dissipated as heat by a resistor bank. By varying the value of the resistance, different loads can be applied to the system.

5.2.1 Electrical Controls

A control system was used to maintain identical motor speed and load profiles automatically so that each test run was genuinely repeatable for accurate comparative studies [190]. It consists of an AC module, a DC module and a PLC controller.

The 3- ϕ (415 VAC) supply is connected to the AC module inverter which adjust the supply frequency according to the set point speed from PLC and generates new AC motor supply voltages. The AC motor is then driven by the voltage at the required speed and required load.

A DC motor control module adjusts the field supply to apply mechanical load to the desired value from the PLC. The armature outputs of the DC motor is fed back to the main supply grid through an inverter. Therefore, the energy generated is not wasted.

The PLC controller is mainly used for setting up desired load and speed for the test system

5.2.2 Sensors for Acquiring Vibration and Acoustics Signal

1- Accelerometers

The transducer that is commonly used the most for measuring vibration is the piezo-electric accelerometer. This type of transducer generally gives a strong signal over a wide range of frequency in capturing vibrations signals from many sources including at the rotations of the shaft with a low frequency of several Hz to several thousand Hz at gear mesh processes [191].

The piezo-electric accelerometer has a very high sensitivity also to measure signals with low amplitude, which are generated by faults inception. Also, this transducer have relatively small size, with good measurement linearity and stability and are highly durable [192].

The piezo-electric accelerometer has three main parts: the base, a seismic mass and piezo-electric crystal [192]. This piezo-electric crystal acts as a spring when placed between the accelerometer base and seismic mass. Both the seismic mass and accelerometer base vibrates with the same phase and magnitude. When the accelerometer is exposed to such vibration, the mounted seismic mass on the piezo-electric crystal exerts force on the element that is equal to

the product of acceleration and its mass ($F = ma$). This force then causes the piezo-electric crystal in generating a charge that is proportional to the level of acceleration. This charge can then have amplified for signal recording using either an internal or external charge amplifier. The ICP accelerometer, which is the internal charge amplifier accelerometer, allows for longer distance transfer of signal when compared with accelerometers with external amplifiers.

The transducer with ICP have been selected in this research have low output impedance, contains built-in IC circuit which convert the charge signal into a voltage signal, as given in Table 5-5. These type of transducers are used widely for measuring vibration as their mass have no significant effect on the surface movement. They also possess a frequency range that is wide enough, appropriate for gearbox vibration measurement (0.5 Hz to over 10 kHz). They are made to be very robust in withstanding harsh environmental conditions existing on gearboxes as they have adequate sensitivity. Also, they have an upper temperature limit of around 90°C because of their inbuilt microelectronics [193].



Figure 5-4 Vibration accelerometer CA-YD-1182A

Table 5-5 Technical specifications of accelerometer

Axial Sensitivity (20±5°C)	100mV/g
Measurement Range (peak)	50g
Transverse Sensitivity	≤5 %
Frequency Response	(0.5dB) 0.5to 10,000 Hz
Mounting Resonance Frequency	40,000 Hz
Temperature Response	Refer to the temp. curve
Polarity	Positive
Operating Temp. Range	-40 to +120 °C
Shock Limit (±peak)	3,000g
Operating Voltage (constant-current source)	+18 to +28 V (DC)
Operating Current	+2 to +10 mA (typical 4 mA)
Output Signal (peak)	≤6V
Noise (1 to 20kHz)	<0.5 mg

Base Strain Sensitivity	0.2mg/ $\mu\epsilon$
Magnetic Sensitivity	1.5g/T
Thermal Transient Sensitivity	10mg/ $^{\circ}\text{C}$
Output Impedance	<100 Ω
DC Offset Voltage	12 \pm 2 VDC/7 \pm 1 VDC
Weight	9g
Case Material	Stainless steel
Mounting Method	M5
Sensing Element	PZT-5
Structural Design	Loop shear
Output Type	L5 (side)

It is common for CM applications that sensors to be placed in close to the source of vibration in acquiring good response characteristics of the vibration. Two similar accelerometers have been used in measuring the vibration from the gearbox to monitoring the conditions of two gearboxes. One important considerations when accelerometers were being installed is that they should be easily accessed when they need to be removed, repaired or re-fitted. One accelerometer was mounted on the housing of gearbox 1 where the surface of the mounting is flat and where the sensor could be mounted relatively easily. The second accelerometer was installed on the casing of gearbox 2. The sensor placements are shown in Figure 5-3. In order to avoid undesirable signal distortion, the accelerometers have been attached rigidly to the surfaces through the brass stud that is screw-threaded and then glued with ceramic cement to the casing.

2 - Microphones

The acoustic signals were measured using a BAST omnidirectional microphone. It consists of an electret condenser microphone model CHZ-211 with YG-201 preamplifier. Figure 5.5 shows photos of both the microphone and the preamplifier. Table 5-6 and Table 5-7 presents the main specification of the microphone and its preamplifier, respectively. From Table 5-6 it can be seen that the frequency responses of the microphone and its preamplifier are determined by the electret microphone which has a range of up to 20 kHz. Higher frequencies can be measured and although the response does fluctuate slightly (within ± 1 dB) between 10 kHz and 20 kHz, it does not begin to drop away until frequencies above 20 kHz.



(a) Preamplifier



(b) Microphone

Figure 5-5 BAST's microphone system

Table 5-6 Specification of microphone CHZ-211

Items	Microphone CHZ-211
Sensitivity	-26±1.5dB (50mV/Pa)
Frequency response (Ref. 250Hz)	6.3Hz~20kHz (±2dB)
Sound field	Free sound field
Polarization voltage	0V
Safety limited	< 146dB
Background noise level	< 16dB
Operating temperature	-40°C~+80°C
Operating humidity	0~98 (RH, %)
Outer diameter	12.7mm

Table 5-7 Specification of preamplifier

Items	Preamplifier YG-201
Power supply	4mA current source
Frequency response (Ref. 250Hz)	10Hz~110kHz (±0.2dB)
Attenuation	0.3dB
Input impedance	5GΩ
Output impedance	< 100Ω
Maximum output voltages	5V
Operating temperature	-40°C~+80°C
Operating humidity	0~98 (RH, %)
Background noise level	< 7.0 uV
Length	70mm
Diameter	12.7mm

In the tests, two microphones were used to measure the generated acoustic signals from the gearbox at a position of about 350 cm away from the top of the gearbox body so that it can perceive directly from the respective gearbox with less influences from other sources for example the driving AC motor and the loading generator. In addition, such a distance also allows receive more globally the signals from vibration radiations of the full house of the gearbox.

3 Shaft Encoder

An incremental optical encoder which is manufactured by Hengstler; Type: RS-32-0/1024ER.11KB was fitted at the non-driving AC motor shaft end, as shown in Figure 5-6. This measures the shaft's angular displacement by calculating an angular increment reference signal. The output of optical encoder is connected to the DAQ system in parallel to the vibration and acoustic channels.

A square pulse output is generated from the encoder for each angular degree meaning that it is a 360-line encoder (for every complete revolution) and a short pulse per revolution. The latter is employed to fix the angular reference signal onto which the vibration and acoustic signals are decomposed. The decomposed vibration signals show high performances in detecting the location of the seeded fault (broken tooth) [194]. The 360 square pulse signals can also be used for the decomposition but may cause errors and computation complexity when used to produce a reference signal on other shafts.

It is worth noting that it is not so easy to mount the encoder on the shaft end with acceptable alignment and reliability. It is often found that the connecting devices can be damaged or malfunctioned due to poor alignments and high vibration. Couplings purchased from equipment suppliers and self-designed devices have been used to connect the encoder to the shaft on the test rig. Because of this inconvenience, encoder-free TSA has been investigated widely in recent years, but no reliable and robust method has yet been found.



Figure 5-6 Encoder mounted on the non-driving end of the AC motor

4 – Temperature Measurements

Two K-type thermocouple sensors were used to measure the oil temperatures in Gearboxes 1 and 2 respectively. This ensured the gearboxes operated within the specified temperature ranges, below 70°C. Their mean values were calculated by the acquisition software and displayed online.

5 –Voltage and Current Measurements

Three phase voltages and currents into the AC motor are also measured and their RMS values are calculated and displayed in the host PC online. This is to ensure the applied load of the system is correct. In addition, other researchers will also analyse such signals to evaluate if the MCSA (motor current signature analysis) can be also effective to monitor the gearbox systems.

5.2.3 Data Acquisition Hardware

Figure 5-7 shows the YE 6232B high performance data acquisition (DAQ) system that was used for acquiring vibro- acoustic signals. It consists of 16 channels capable of conditioning and acquiring data from ICP/IEPE accelerometers, microphones and normal voltage sensors at 24bit resolution and 96kHz. The DAQ system technical specifications is presented in Table 5-8. DAQ is connected to a host PC via USB port for controlling data acquisition process and storing collected data. The supporting software in the host PC is capable of analysing data in the time domain for basic waveform parameters including kurtosis and RMS, and spectrum in frequency domain via a FFT. Thus the gearbox conditions can be monitored by vibro-acoustics in real time based on the changes in the waveform parameters [195].

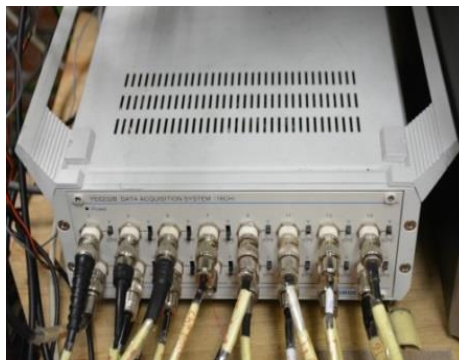


Figure 5-7 Global sensor technology YE6232B DAQ system for monitoring vibro-acoustic signals

Table 5-8 Technical specifications of the DAQ system

DAQ system manufacturer	Global Sensor Technology YE6232B
Number of Channels	16 (selectable)
A/D Conversion resolution	24 bit
Sampling rate (maximum)	96kHz per channel, Parallel sampling
Input range	±10 V
ICP or IEPE supply	24V
Gain	1, ×10, ×100
Filter	Anti-aliasing
Interface	USB 2.0

For more accurate monitoring, further signal processing jobs such as TSA and MSB analysis were carried out offline in another PC installed with MATLAB software. During the process of data acquisition, the sampling frequency and number of data points were set to 96 kHz and 1.92×10^6 points respectively, which allows sufficient averages to be implemented for reliable results. In the meantime, the high sampling rate ensures the encode pulse train to have good time resolution for estimating the rotational speed at high accuracy.

5.2.4 Data Acquisition Software System

To improve the real time monitoring capability, supporting software for the DAQ was done using National Instruments Lab Windows TM/CVI, a commercial engineering toolbox with a large run-time libraries set for data acquisition, for analysis and instrument control. The development environment of the Lab Windows offers features such as the generation of automatic code that allows measurements taking much easier when compared to traditional C or C++ environments. However C was the language in which the interface was written [196]. The software for data acquisition can control the process of data acquisition so that multiple dynamic data channels at different data lengths and rates can be acquired. Current, IAS, vibration, temperature and noise measurements can be acquired when using the software. The software package has a set-up panel for acquisition to enable the user make modifications to, for example, the sampling data length and frequency. The status indicator and control commands are displayed on the screen. This ensures optimal collection of data set for off-line analysis of data.

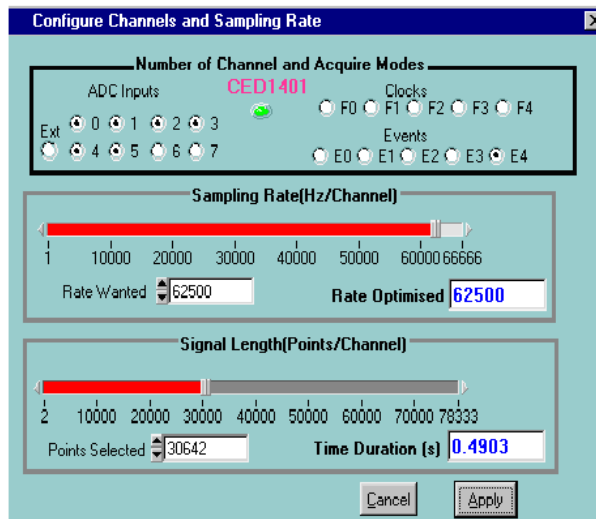


Figure 5-8 Set-up screen for data acquisition

Figure 5-8 Set-up screen for data acquisition. The sampling frequency is set at 96 kHz (this enables the high frequencies associated with transient events such as the pulse out of the encoder to be collected with sufficient accuracy for speed and angular calculation) and the length of the data is set at 30,642 samples. The data point collection time duration is equal to number of samples, divided by the sampling frequency. The exact sample time duration is therefore given as 0.3192 sec.

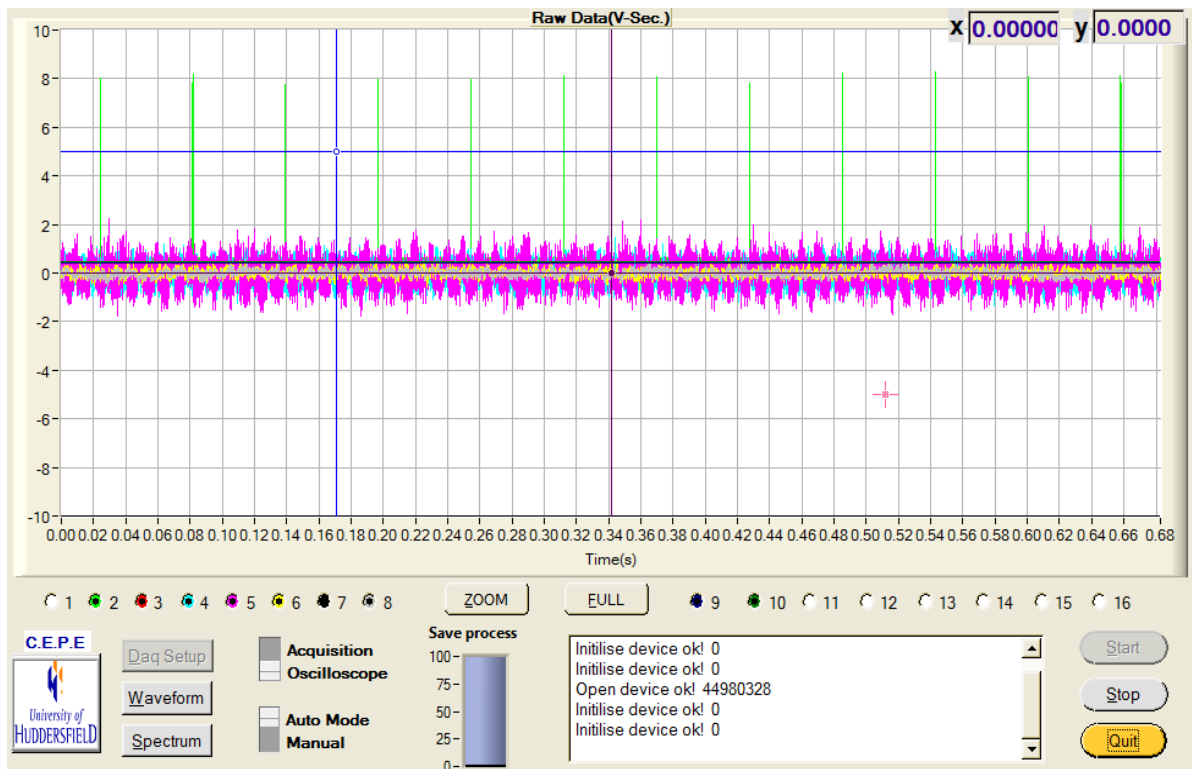


Figure 5-9 Screenshot of measured signals

The improved software can display the raw data in different ways, as illustrated Figure 5-9. Especially, it allows comparing data between different channels and checking if any inconsistencies caused by various problems such as loose wires and sensor mountings.

Moreover, the improved software also allows the display of both the operating conditions and the key monitoring parameters through a real-time ‘dashboard’, which is illustrated by Figure 5-10. This allows for an accurate online monitoring of rig operations.

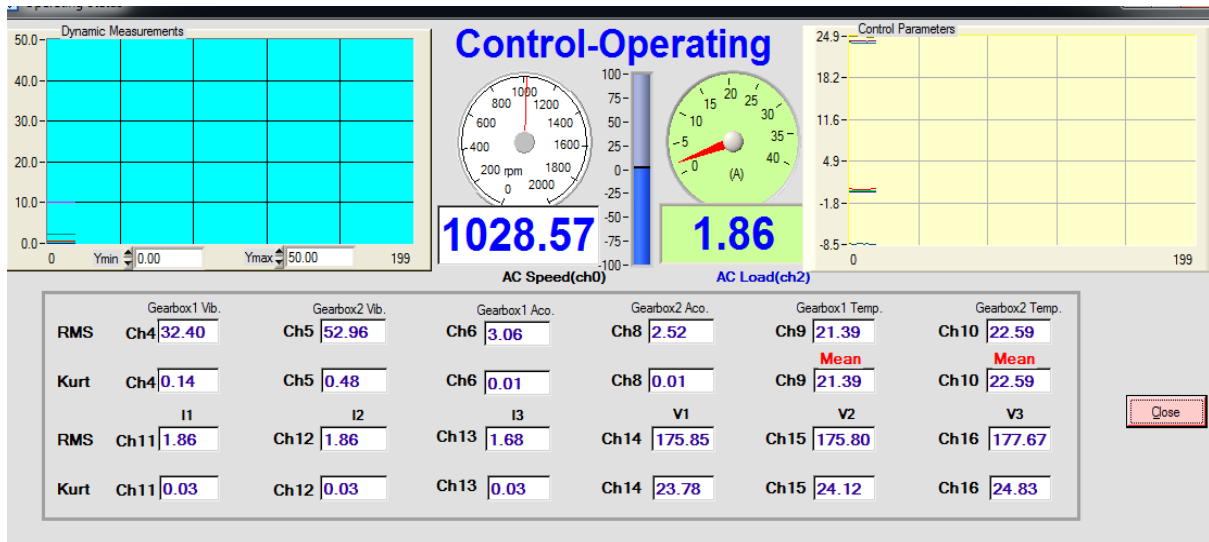


Figure 5-10 Screenshot of operating status and dynamic trend graphs.

Besides, the data acquisition system has been also validated by a number of trial operations and adjustments. Finally, vibro-acoustics signals can show the gear vibration features at characteristic frequencies very clear and overall signal strength shows good load and speed dependences.

5.3 Calculation of Gear Characteristic Frequencies

As discussed in Chapter 3 and the gear test system of Figure 5-1, there can be a number characteristic or fundamental frequencies appearing in the gearbox transmission system vibration. Based on the power flow and construction of these gearboxes, shown in Figure 5-11, these fundamental frequencies consists of 5 rotational frequencies and 4 mesh frequencies. For ease of discussion, the rotational requires are denoted as $f_{r1}, f_{r2}, f_{r3}, f_{r4}$ and f_{r5} , and the mesh frequencies are denoted as f_{m1}, f_{m2}, f_{m3} and f_{m4} , which are ordered based on the power flow from the speed reduction gearbox to the speed increase gearbox as illustrated in Figure 5-11.

For the analysis carried out the following chapters, these characteristic frequency values are calculated as follows according to the input speed (AC motor) at which the test was performed and the gear tooth numbers in As shown in Table (5-2) and Table 5-3), the two gearboxes are the same for transmission ratio $Z_{r3}/Z_{r4} = Z_{i3}/Z_{i4} = 13/59$ at the lower speed stages but they have a slight different gear parameter at the higher speed stages. Gearbox 1 (abbreviated to GB1 thereafter) operating as a speed reducer has the gear ratio of $Z_{r1}/Z_{r2} = 49/55$ whereas gearbox 2 (abbreviated to GB2) operating as a speed increaser has the ratio of $Z_{i3}/Z_{i4} = 47/58$. These configurations make more than a 50% difference between the trasmission ratios between the two gearboxes so that the DC generator can operate in high efficiency ranges and apply loads to the system efficiently over a wide range of speeds.

Table 5-2 and Table 5-3:

For Gearbox 1 (GB1)

$$f_{r1} = \frac{\text{Motor Speed}}{60} = \frac{1060\text{rpm}}{60} \approx 17.67\text{Hz} \quad (5.1)$$

$$f_{r2} = \left(\frac{Z_{r1}}{Z_{r2}} \right) f_{r1} = \left(\frac{49}{55} \right) \times 17.6 = 15.12\text{Hz} \quad (5.2)$$

$$f_{r3} = \left(\frac{Z_{r1}}{Z_{r2}} \right) \left(\frac{Z_{r3}}{Z_{r4}} \right) f_{r1} = \left(\frac{49}{55} \right) \left(\frac{13}{59} \right) \times 17.67 = 3.47\text{Hz} \quad (5.3)$$

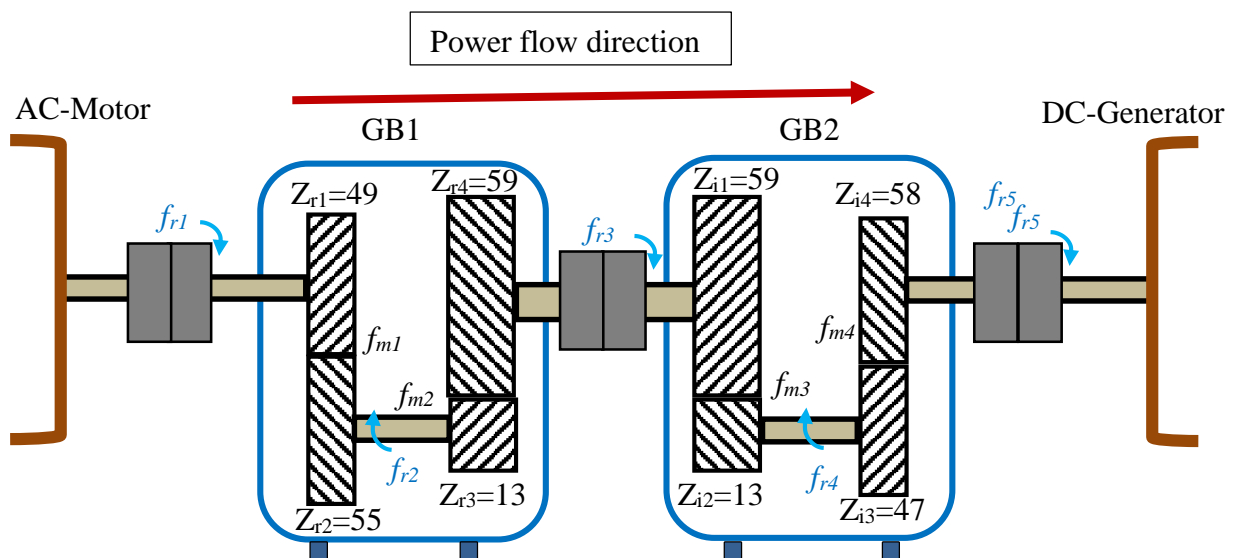


Figure 5-11 Schematic of the two gearbox transmission systems with key symbols used throughout the thesis

The mesh frequencies for the first and second stage transmissions of GB 1 are

$$f_{m1} = f_{r1}Z_{r1} = 17.67 \times 49 = 865.68Hz \quad (5.4)$$

$$f_{m2} = f_{r2}Z_{r3} = 15.7 \times 13 = 204.61Hz \quad (5.5)$$

Simultaneously the rotational frequencies of the shafts in the speed increaser of GB2 are

$$f_{r4} = f_{r3} \left(\frac{Z_{i1}}{Z_{i2}} \right) = 3.47 \times \frac{59}{13} = 15.75Hz$$

$$f_{r5} = f_{r4} \left(\frac{Z_{i3}}{Z_{i4}} \right) = 15.75 \times \frac{47}{58} = 12.75Hz$$

The mesh frequencies at the 1st and 2nd stages of gearbox 2 are

$$f_{m3} = f_{r3}Z_{i1} = 3.47 \times 59 = 204.61Hz \quad (5.6)$$

$$f_{m4} = f_{r4}Z_{i3} = 15.75 \times 47 = 739.75Hz \quad (5.7)$$

5.4 Test Procedure and Resulting Gear Faults

One of the challenges for the CM of gearboxes is to identify, at an early stage of the fault development developments. To develop a way of doing this, a run to failure tests was performed in making the gears to deteriorate under natural conditions on test rig that has been specially designed.

However, due to time and equipment restrictions in this PhD programme, the gear fault was created by operating the gear under a rough condition i.e. applying shock loads, oscillating loads and a range of constant loads at a wide range of speeds, which are more close to the scenarios of many gearbox applications like wind turbines and helicopters.

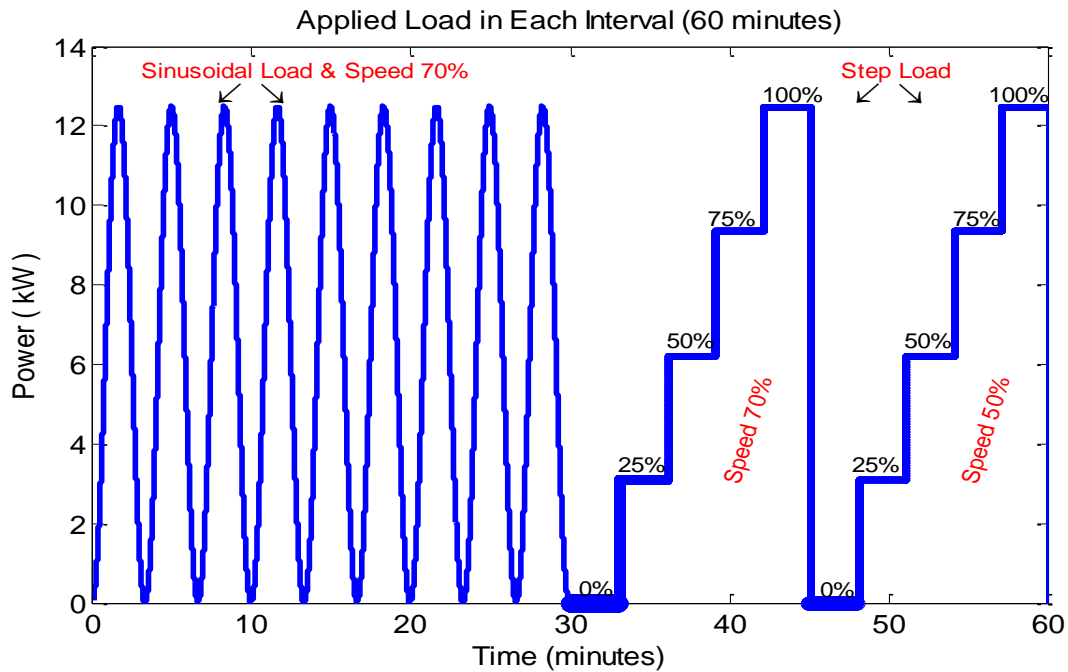


Figure 5-12 Test operation cycles

In addition, to make the gears deteriorate in a uniform way, a variable operation condition was designed to operate the test rig. Figure 5-12 shows the variable conditions for one operation cycle which was programmed in the PLC controller and repeated throughout the test course. These variable loads and speeds were expected to alternate the load levels and hence the elastic deformations of the tooth. In this way, the contact conditions of tooth surfaces are also alternated and result in more uniformly load distributions on the tooth surfaces, rather than just a localised part of the surface when applying a fixed load at a fixed speed. Therefore, the deteriorations can be more generic to represent the scenarios like wind turbines and helicopters, etc. which are usually operated under such conditions. In addition, these frequent transient operations can induce more severe load conditions to the gearboxes and thus the test can be completed in the short period of the PhD study programme.

Table 5- summaries the test cycle along with data acquisition detail. The acquisition was implemented automatically just before the end of each step. It has about two minutes for the system to be steady after each load transition. The transition of each step was also identified automatically by the improved acquisition software so that the data acquisition and corresponding load condition can be synchronised based on the PLC controller.

Table 5-9 Test operation cycle and data acquisition

Step No.	Duration	Speed	Time (min.)	Load (%)	Data record*
1 st Step	30 minutes	Variable load operation at 1022 rpm (70%)	30	100	30 sec at 26 th minute.
2 nd Step	30 minutes	1022 rpm (70%)	3	0	30 sec. at 2 nd minute
3 rd step			3	25	30 sec. at 2 nd minute
4 th Step			3	50	30 sec. at 2 nd minute
5 th Step			3	75	30 sec. at 2 nd minute
6 th Step			3	100	30 sec. at 2 nd minute
7 th Step			30 minutes	730 rpm (50%)	3
8 th Step	3	25			30 sec. at 2 nd minute
9 th Step	3	50			30 sec. at 2 nd minute
10 th Step	3	75			30 sec. at 2 nd minute
11 th Step	3	100			30 sec. at 2 nd minute
<p>*The 30 second data recorder was saved as a binary file, which is acquired at the second minute of each step with a sampling rate of 96kHz; The data file was named by the date and time instant with a prefix of 'Test' such as 'Test_2015-03-13-11-01-53.bin'.</p>					

In addition to monitoring the changes in online statistic parameters of the vibro-acoustics data, temperature data, and electrical supply data, offline trend graphs were also built up based on TSA and MSB analysis to show more accurate changes of these parameters, which are detailed in Chapter 6-9. Finally, the decision was made to stop the whole test when the offline vibro-acoustic signatures exhibited significant increases, about 3 times higher compared to the baseline values obtained at the beginning of the test.

Unfortunately, the online monitoring parameters including sound loudness and gearbox temperatures did not show any clear symptoms for the light wear observed in Figure 5-13
 Illustrative photos of the location

When the test was stopped, the gears at lower transmission stages were found by opening the gearboxes to have light wears. As illustrated location which are detailed with more magnified photos in Appendix B, clear fatigue wear marks can be seen on Z_{i1} because the higher number of operation cycles, whereas the only light adhesive wear happened on Z_{i2} because of lower operation cycles. In addition, nearly half of the teeth on a gear show such defects more than the rests, showing the effect of inevitable gear errors. However, there were little wear signs observed at high speed transmission stages. Therefore, it was understood that the less efficient hydraulic dynamic lubrication and high contact stress are the main causes of the defects on the lower speed transmission.

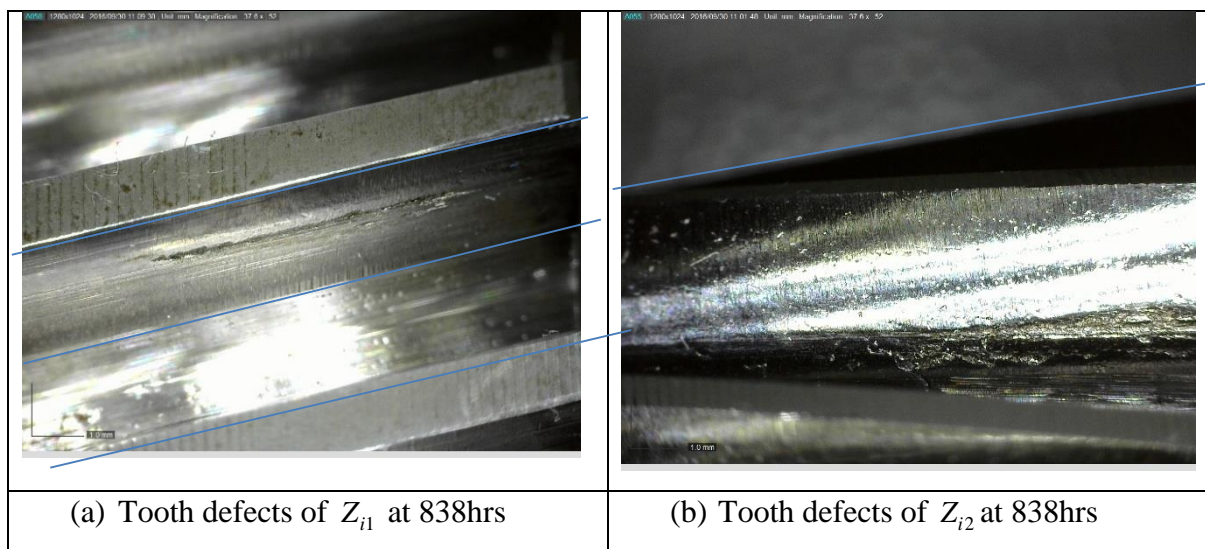


Figure 5-13 Illustrative photos of the location and severity of tooth wear and pitting on the surface of the gears at the lower speed stage of Gearbox 2

5.5 Key Findings

The test facility and methodologies have been elaborated for the evaluation study of vibro-acoustic signals based monitoring. Trial operations have demonstrated that the test system operated steadily and reliably. Moreover, the data acquisition system allows vibro-acoustics signals to be recorded sufficiently, showing the gear vibration features at characteristic frequencies very clear and the overall signal strength shows good load and speed dependences.

Especially, the run-to-failure test operated successfully. It resulted in slight gear wear on the lower speed transmission of tested gearboxes at 838 hours, while the other systems did not exhibit any clear faults. Moreover, this type of gear faults is one of common early fault modes

and provides very realistic and valuable database for evaluating various signal processing methods.

Chapter 6 MONITORING AND DIAGNOSIS OF GEARBOX DETERIORATION BASED ON THE TSA ANALYSIS OF THE SURFACE VIBRATION SIGNAL

As one of the most common processing signals used for analysing vibro-acoustic signals in CM, using TSA is used in analysing the two gearboxes the vibration signals for suppressing various noises and hence enhance the characteristic components relating to common gearbox faults. Based on the angular reference pulse train from the encoder at the non-driving end of the AC motor, TSA was implemented by reconstructing reference signals onto different shafts of the gearboxes, it then decomposes the vibrations onto the reconstructed references for obtaining order spectrum. The monitoring features are identified based on the primary characteristics of the TSA cleaned vibration signals in the order domain. Finally, monitoring trends were developed based on the identified feature parameters to show the variations of gear mesh conditions over the test operation period, which leads to an assessment of the health conditions of different gear sets.

6.1 Introduction

Analysis of vibration signal has been used traditionally for fault diagnostic in rotating machinery as such signals can carry important dynamic information relating to the machine's health. Several techniques in analysing vibration signal have been developed. They include analysis in frequency domain [90], time domain [95] and time-frequency domain analysis [118, 197], [198-201]. Unfortunately, vibration signal depends on the sensor location relative to the source and is often contaminated by structure borne noise from other sources. Therefore, in several cases, the vibration signal has a low SNR. To increase the SNR, researchers have successfully used IAS (Instantaneous Angular Speed) signal for suppressing noises and achieving accurate detection of faults rotating machines.

Here, the IAS reference signal is measured using an optical encoder, which is fairly cheap when compared to conventional accelerometers and it provides also, when compared to other measuring devices of IAS, high resolution. Based on the IAS signal, errors from gear transmission were detected by researchers a decade ago [202]. More recently, researchers have used signal processing with IAS as a technique in detecting fault using zero-crossing to measure the IAS signal and detect faults that are combustion related in diesel engines [203]. Researchers [202, 204] have applied also, technique of phase demodulation in processing the IAS signal from an encoder with the IAS signal being measured used in detecting an electric motor faulty rotor bar [204]. Li, et al., [205] presented a review in details from an encoder signal, for various IAS estimation techniques, in particular how the IAS signal varies in a helical gearbox, under both non-cyclic and cyclic load conditions Sasi, et al..

Nevertheless, the technique for IAS-based signal processing efficacy depends mainly on making a proper estimation of the IAS, and the detection of fault requires proper technique for signal processing in extracting in the signal, those hidden information. It has been established [206] that noise measurement can be relatively reduced by the use of an higher resolution encoder and an estimation algorithm for IAS has been developed in reducing the measurement noise effect. Using the signal from IAS, researchers/scientist have monitored rotor misalignment [206], a two stage reciprocating compressor [207], combustion related faults in a diesel engine [208], bearing faults [209] and faults in a multistage helical gearbox [210]. Recently, EEMD (ensemble empirical mode decomposition) technique has been applied to IAS signals in detecting a feed-axis gearbox fault [211].

FFT is the most commonly recognised technique for analysing signal, where the signal in time domain is converted to frequency domain. However, strictly, the FFT is applicable only to stationary signals, but the responses from a rotating machine captured by the sensors do not remain stationary. Faults in rotating machines change their dynamics. E.g., a defect in a helical gear tooth changes its dynamic parameters including torque, frictional force, etc. [210, 212]. Thus, the output shaft angular speed varies. Over the revolution of a shaft period, the IAS signal is represented as a non-periodic and periodic events combination. Therefore, the IAS signal is frequency modulated in addition to also being amplitude modulated. A signal processing technique known as Demodulation restores back the modulating signals' suppressed carrier frequency [210]. Since modulating frequencies are related to certain rotating machine faults, these modulating frequencies detection is necessary in order to detect a specific fault. However, the signal modulation characteristics vary with load and speed as the variation depends also the fault and its severity [213]. Beside the effect of modulation, structure-borne noise is contained the IAS signal. However, this non-stationary signal demodulation is unable to extract the signal true feature as contamination of noise smears the important frequencies amplitude.

Time Synchronous Averaging (TSA) [214, 215] is a significant technique in enhancing the periodic events by the suppression of non-periodic events. Furthermore, the FFT can be applied to signals that are synchronously averaged. Gelman and Combet, (2007) [215], suggested a new technique to obtain TSA without any sensor that detects speed. Guan, et al., (2009) [216] also applied EEMD and TSA to vibration signals in extracting the a two-stage helical gearbox features under different fault severity levels and load conditions. In their paper, they examined also signals from many locations in order to confirm how useful their method is. A different approach by Kar and Mohanty [199] used signal from motor current under different loading conditions and speeds in monitoring the a multistage helical gearbox condition, despite the current signal of the motor being dominated by the supply current frequency. Of recent, researchers/scientist [199] have used the technique of TSA together with IAS signal in detecting, in a multistage helical gearbox, the absence of one tooth.

The chapter aims to utilise TSA to suppress noise and interferences and hence achieve reliable fault detection of multiple and multistage helical gearboxes. The FFT is applied to the synchronously averaged TSA signals in obtaining order spectrum to allow for gear characteristic components to be enhanced. As a result, the interested monitoring content are selected conveniently to show reliable indication of gear mesh conditions. In addition, the

behaviour of TSA signals were also studied for varying gear fault conditions for different load conditions and speed.

6.2 Baseline Vibrations by Spectrum Analysis

The measured vibration signals exhibit very complicated behaviour and highly contamination by various noises including both the random background disturbances, measurement noises and vibrations from the AC driving motors and DC loading generators. They often present very little information in the time domain regarding to the mesh dynamics of the gear. Therefore, the time domain analysis is not performed often, apart from the online statistical parameter calculations. Instead, the popular frequency analysis has been used in exploring the measured signals basic characteristics and data quality.

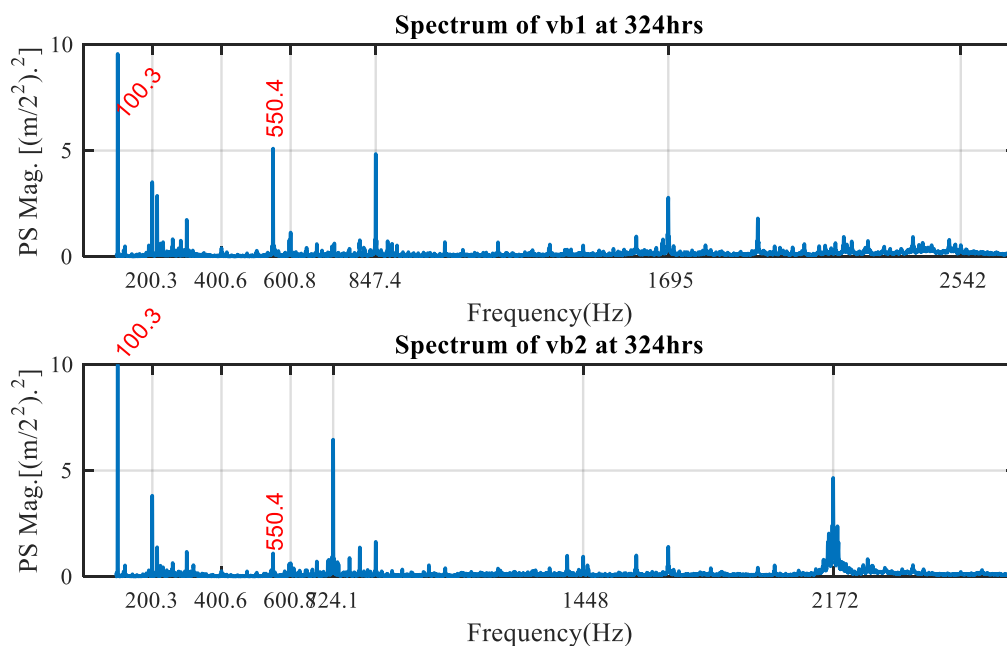


Figure 6-1 Power spectrum of vibration signal for the two stages of the helical gearbox at full load at 324 hours continuous running

The baseline vibration spectra are shown in Figure 6-1, which is the signal acquired at 324 hours when the data acquisition system was ensured to be reliable after fixing the problems with data loss and slips of the encoder coupling. They show that both gearboxes have distinctive components at the mesh frequencies of f_{m1} , f_{m2} , f_{m3} , and f_{m4} which are consistent with previous studies and also the prediction from the vibration model in Chapter 3. Moreover,

the main vibration components exhibit below 3,000 kHz. These show that the data and hence the measurement systems, are configured satisfactorily to acquire the dynamic behaviour of the gearboxes.

Based on spectrum results, it is possible to track the changes of the spectral amplitudes at the mesh frequencies for the purpose of CM. However, because of inevitable noises, spectral leakages, bearing and motor vibrations, such components obtained by this spectrum analysis usually results in poor and even inadequate results due to high oscillations of the spectral amplitudes.

In particular, there are also two very distinctive components appearing at 100Hz and 550 Hz respectively, highlighted in Figure 6-1. These two components are not relating to gear dynamics according to the preliminary analysis made in Chapter 3 for test system design and the model predictions obtained in Chapter 3. Instead, they are more likely from electric interferences arisen from the sensorless variable speed drive which is used in controlling the AC motor. Moreover, they have significant amplitudes which can significantly affect the statistic parameters such as RMS and kurtosis in reflecting the basic vibration characteristics. Therefore, further signal processing must be taken to avoid such interfering components including any random contents in the signals.

6.3 Implementation of TSA

As explored in Chapter 2 and further reviews in the introduction, TSA is the most popular method to suppress noise components for accurate characterisation of signals of interest. The vibration signal therefore is processed firstly with the TSA method.

There are a number of schemes available to realise TSA to the measured vibration and acoustic signals. However, as there is only one encoder signal available in current multiple rotor layout of gear transmissions, it is not possible to implement TSA for every shaft according to the original specification of TSA that an encoder is used for each rotating shaft. Obviously, it is costly and difficult to apply to industrial systems with more complicated rotor layouts. The TSA was implemented in this study by mapping the TSA reference signals to the middle shaft of each gearbox, provided that the fluctuation of angular speeds is negligible as speed controller can maintain a high accuracy of steady operations. In this way, the synchronous average operation only needs to be carried out two times, each for one gearbox, in enhancing the two transmissions mesh components simultaneously. Therefore, it is more efficient in computations

compared with applying TSA six times for the six shafts of the two gearbox. In addition, it can also be more reliable compared with the soft-encode based method in which one of main mesh components will be used to calculate a phasor signal and can be affected by noise and interferences.

As shown in Chapter 5, the mounted shaft encoder on the non-driving end in the driving AC motor can produce one pulse per each revolution of the AC motor. This pulse train can be based to create an angular increment reference signal for each shaft as its speed is confined by gear transmission/tooth ratio. As both the vibration and the pulse train signal are recorded simultaneously the vibration signal can be decomposed onto the decomposed reference signals and converted into angular domain , which is detailed in the flow chart of Figure 6-2.

Especially, the time domain signals are decomposed onto the angular reference signal associated with the shaft speed: f_{r2} . In this way, both mesh events of the two stages; the higher speed and the lower speed transmissions, with respect to each gearbox, can be obtained and monitored by just one implementation of the decomposition as they all be aligned with the middle shaft.

Through the proposed procedure, data samples per each revolution can be resampled uniformly into 1,000 points per revolution. As the length of original data records is 30 seconds, TSA decomposition onto the middle shaft results in nearly 460 short segments, each having 1,000 points, which allows for sufficient averages and obtains reliable results.

For the ease of discussion, this implementation of TSA based on the angular reference signal generated from the rotational movement of f_{r2} is abbreviated to TSA-fr2 thereafter. Likewise, TSA-fr1, TSA-fr3 and TSA-fr5 can be also implemented in the gearbox transmission systems under study based on the rotational movements of f_{r1} , f_{r3} and f_{r5} respectively.

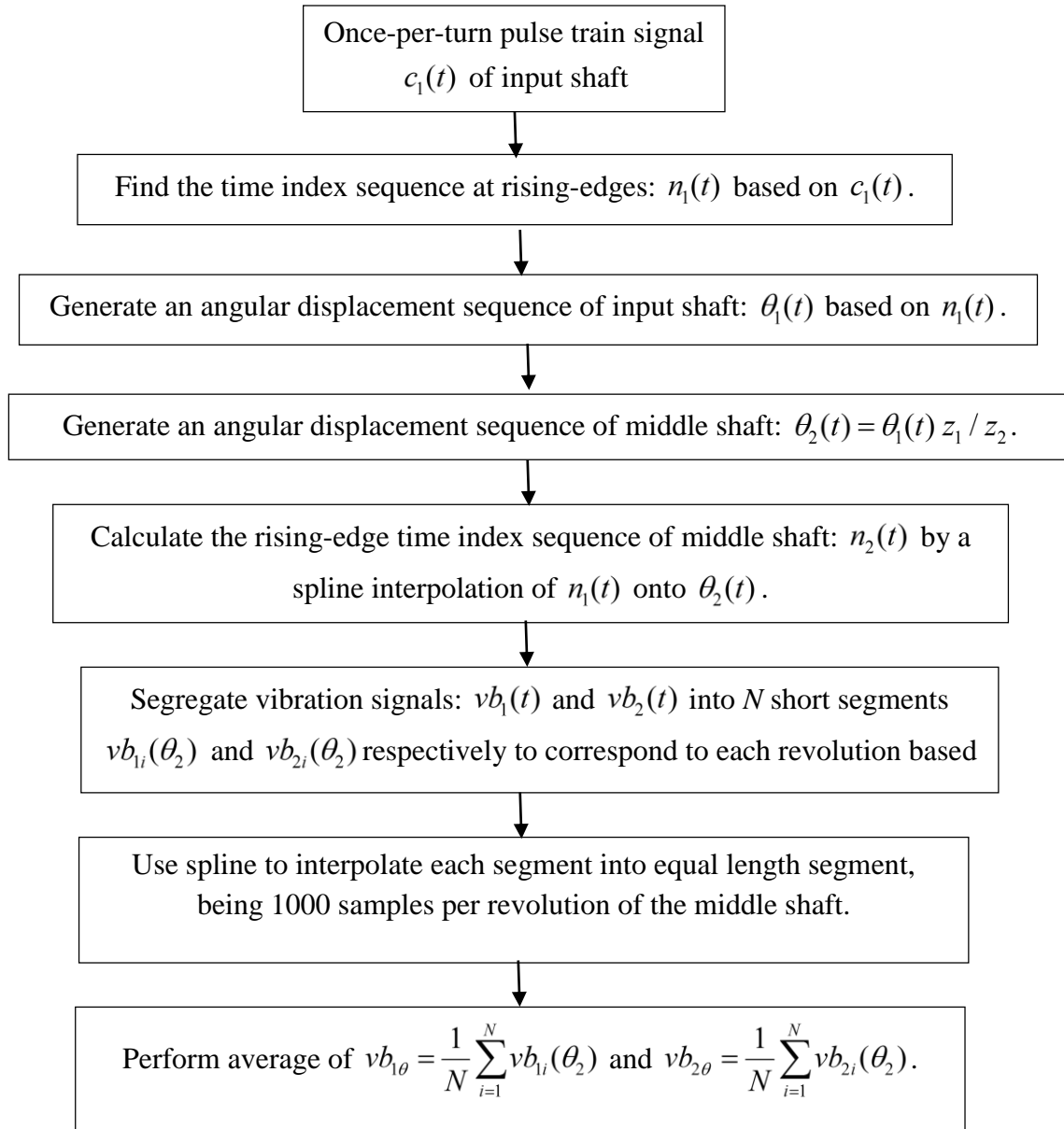


Figure 6-2 Implementation of TSA vibration signals based on the angular position of the middle shaft rotating at the speed of f_{r2}

➤ TSA signatures

Typical TSA-fr2 signals synchronised to Gear Zr2 on shaft 2 and Gear Zi2 on shaft 4 are shown respectively in Figure 6-3 (a) and (b) at early test operation phases. They consist of 5 periods of f_{r2} as a result from 92 averages based on the 460 short segments. From the waveform, it is clear that they both exhibit clear periodic waveforms synchronised to the gears or the shafts. This periodicity indicates that these gears and their associated shafts may have a certain degree of eccentricity errors such as gear run-out and misalignments. However, it is not possible to differentiate the details of the exact source between Zr2 gear, Zr3 gear and their mounted shafts

in GB1, or between Zi2 gear, Zi3 gear and their mounted shafts in GB2. In general, these raw TSA signals still cannot provide sufficient detail of gear mesh characteristics.

Surprisingly, the RMS values of the vibration in GB1 is 16.49, whereas GB2 is 21.5, which shows GB2 produces mesh vibrations about 30% higher than GB1. This is not anticipated as GB2 operates at a lower speed, the mesh frequency at the higher speed stage of GB1 being $f_{m1} = 847$ Hz and GB2 being $f_{m4} = 724$ Hz. In addition, the non-stationary or local oscillations of GB2 also looks higher. This may show that the dynamic performance of GB2 is poorer than that of GB1. However, this simple waveform analysis is unable to identify which gear accounts for the higher vibration amongst the four gears in the multistage gearbox system.

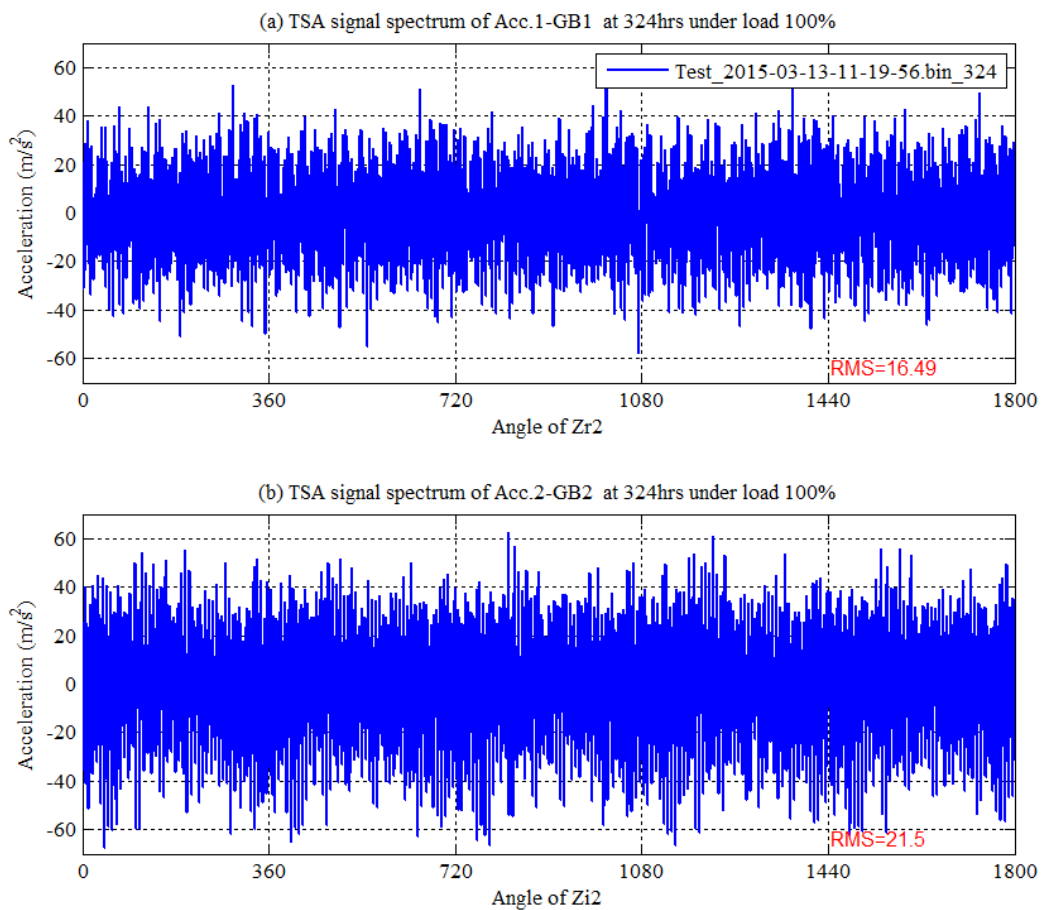


Figure 6-3 TSA-fr2 signals synchronised to Gear Zr2 or Gear Zi2 with respect to f_{r2}

➤ Order Spectrum

To attain more detail of the gear dynamics, these TSA-fr2 signals are converted into the frequency domain to the signals in Figure 6-3 by applying FFT, which results in two corresponding order spectra as seen in Figure 6-4 (a) and (b) respectively. By examining the two spectra it can be found that:

- The higher speed transmission stages produces higher vibrations at their mesh frequencies f_{m1} and f_{m4} and their harmonics up the 3rd order. However, the mesh components of GB2 show higher amplitudes. Especially, the 1st and the 3rd and 4th harmonics show nearly 30% higher than that of GB1. As the speed at this higher speed stage of GB2 is lower than that of GB1 ($f_{m4} = 724Hz < f_{m1} = 824Hz$), this higher mesh vibration may show that the dynamic loads at GB2 is relatively high which may be as result from higher tooth errors such as the high non-uniformity between tooth pitch.
- The lower speed transmission stages of the two gearbox show a different spectrum pattern from the higher speed. They all show much lower amplitudes at the mesh frequencies f_{m2} and f_{m3} note that ($f_{m2} = f_{m3}$), compared with the higher speed stages. In addition, the first three harmonics of the mesh components from GB1 show high amplitudes, compare with that of GB2, showing that mesh conditions of GB1 is lower or the dynamic load is higher.

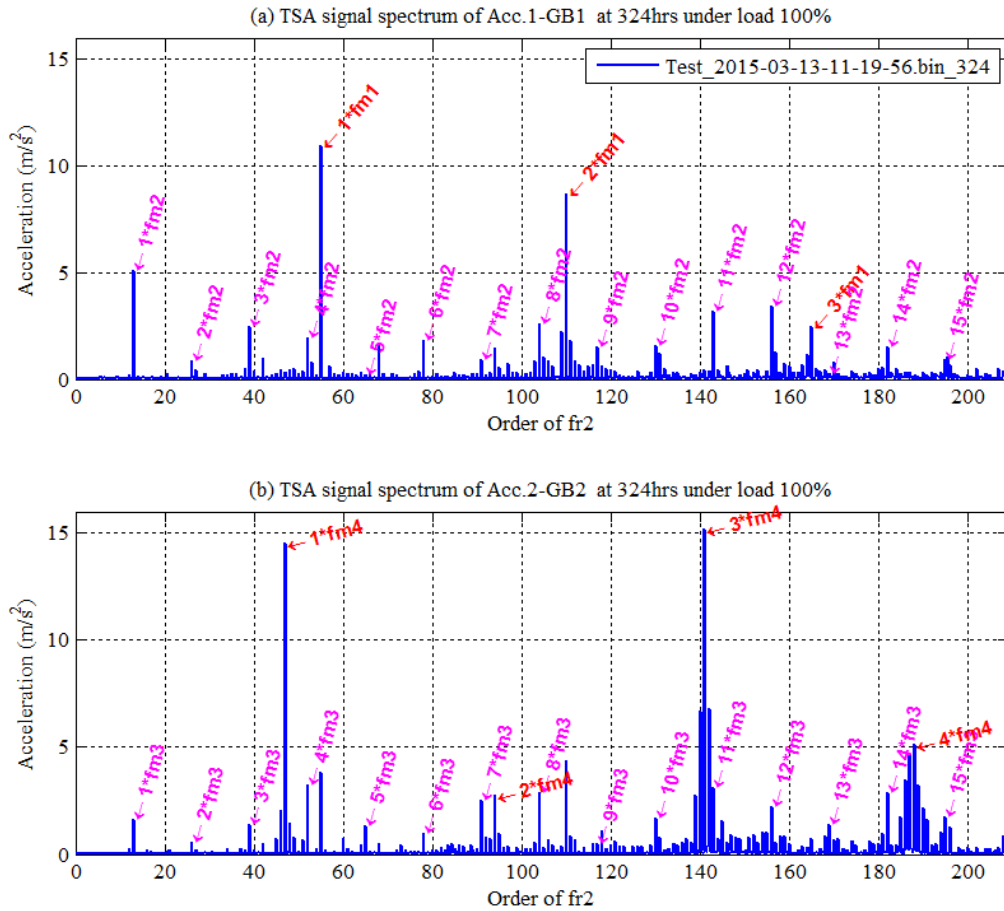


Figure 6-4 TSA-fr2 signal spectrum based on Order f_{r2}

In addition, the lower speed transmission stages also show significant amplitudes at a string of higher order harmonics, up to 15 orders. Notably some of them have higher amplitudes than the 1st order, which indicates the effect of structure resonances. These components can be sensitive to the small changes in the process of gear mesh, which can benefit for early fault detection. However, they may exhibit high fluctuations with the time-varying contact conditions such as slight changes in gear load, speed, temperature and the wear dynamic wear effects with operating time evolving. These fluctuations can lead to unstable detections at different time instants. Consequently, it can result in an unstable trend which is not useful for the indication of fault severity and the prognosis of gear conditions.

Furthermore, TSA spectra also show significant sidebands of f_{r2} associated with mesh components, which is linked to the manufacturing errors of Gear Zr2 or Zr3 of GB1, and of Gear Zi2 or Zi3 of GB2. Comparatively, sidebands are more significant around the mesh

components of $2 * f_{m1}$, $1 * f_{m3}$, $3 * f_{m3}$, and $4 * f_{m4}$ at which there may exist structure resonances. Such sidebands may also exhibit highly fluctuation with small changes in the contact conditions and hence cannot be relied on for tracking gear health conditions.

Although the order spectra show that the TSA signal is composed mainly from mesh components and their higher order harmonics, a significant peak found at 47th order presents in the spectrum of GB1. As this associates the gear with tooth number of $Z_{i2}=47$ in GB2, it means that vibration of GB1 can be interfered with GB2. Therefore, signal from TSA cannot be used directly in indicating the condition of GB1 even if it has been cleaned to a great degree. Instead, each spectral amplitude at the characteristic frequency, obtained by applying FFT to TSA signal, has to be used for performing more accurate diagnosis, otherwise; such cross influences will lead to misleading indication.

In addition, this TSA-fr2 scheme provides limited information regarding to diagnosing the healthy conditions of Gear Z_{r1} and Z_{r4} of GB1, and Gear Z_{i1} and Z_{i4} of GB2 which are mounted on shafts rotating at a speed other than f_{r2} . Nevertheless, they will alter their corresponding mesh components if they become faulty, which will be reflected at the orders of Z_{r2} , Z_{r3} , Z_{i2} and Z_{i3} respectively.

6.4 Monitoring and Diagnosis of Gear Deteriorations

As reviewed in Chapter 1, there are numerous feature parameters developed for monitoring gear conditions. However, the majority of them are developed for local gear faults such as individual tooth breakages and limited such parameters are effective for both local and distributed faults such as gear wear. Therefore, this study uses a set of parameters which correlates more directly with gear dynamics. They include components at mesh frequencies and sidebands around such frequencies as investigated in Chapter 3.

In addition to the findings that the mesh components show a direct connection to gear mesh conditions, a further study was also performed to investigate the dependence of the mesh components upon the gear loads. By accumulating the first few harmonics of the mesh components, it has been found that the sum of the first three harmonics allows a better representation the load dependence. As shown in Figure 6-5, the accumulative amplitudes show approximately that the amplitudes increase with loads, which is consistent with that of model prediction in Chapter 3. In addition, these amplitudes also show stable behaviour across the

four consecutive measurements. Therefore, these further demonstrate that the mesh components can be a steady and reliable indicator to show the progression of the gear mesh quality and health condition with operating time.

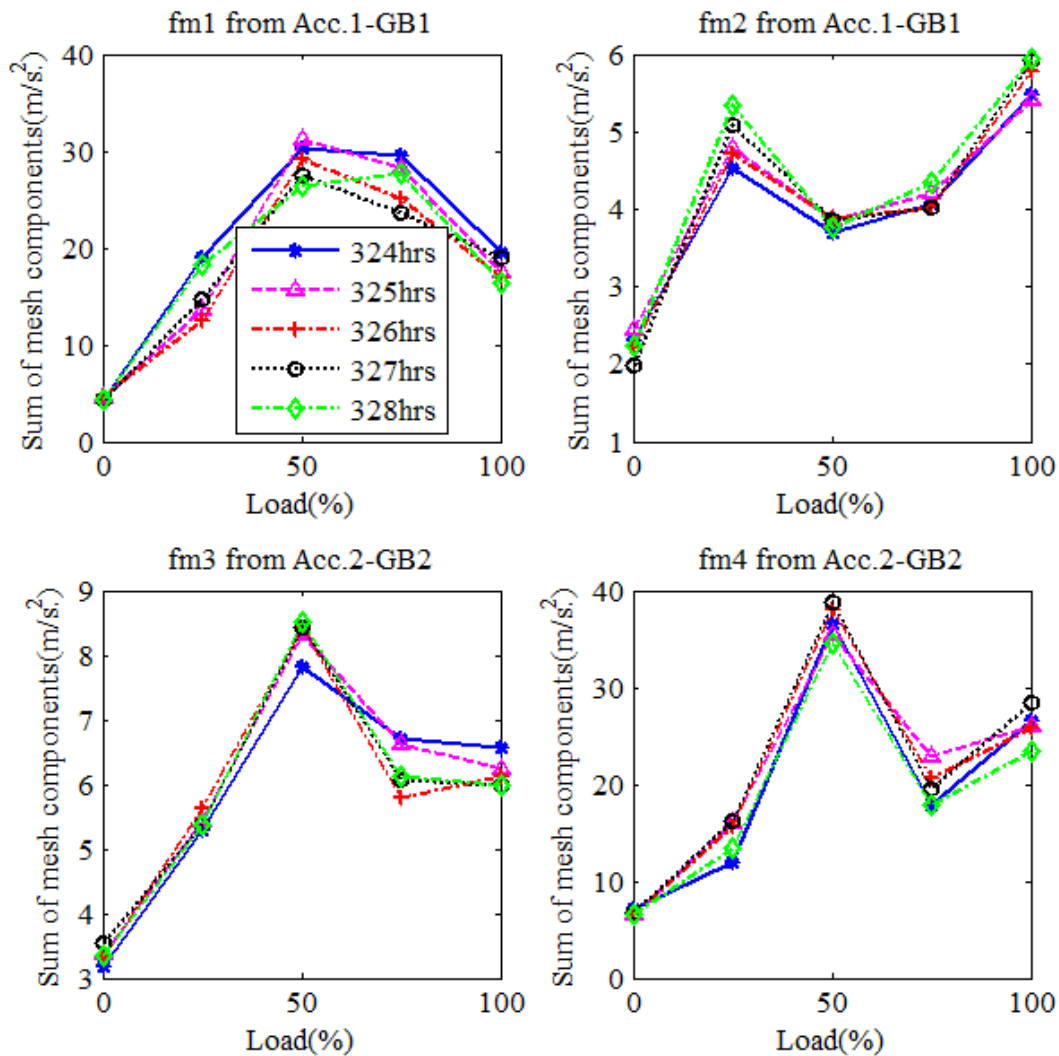


Figure 6-5 The correlation of mesh components with loads

To simplify the monitoring tasks, the following study only focused on the case of 100% load. This is based on the consideration that the highest magnitudes under the middle loads can be unstable as it can be the typical consequence of the nonlinearity of the load dependent mesh stiffness. Moreover, monitoring gear conditions under different loads is another key research subject that is also actively studied in the field of gear condition field but is not the focus of this study.

6.4.1 Monitoring of the Higher Speed Stage in Gearbox 1 based on Mesh Components and Sidebands

Figure 6-6 presents the evolution trends of mesh components and sidebands in GB1 associated with f_{m1} and their 2nd and 3rd order harmonics in the full test operation period. The trends are established starting at 24 hours when the data acquisition system performs relatively stable, and ending at 838 hours when the test was stopped because a significant change was found in several monitored feature parameters which will be depicted in following sections.

As illustrated in Figure 6-6 (a), all three mesh components from the higher speed transmission stage show little change throughout the test period. This can indicate that the mesh quality at the end of the period maintains roughly the same as that of the initial period, or the gear set of Zr1 and Zr2 that formulates the dynamics at the first stage of GB1 has little deterioration on their tooth profiles and engagement performances. Therefore, they are regarded as to be healthy and can be used further.

Simultaneously, the sidebands associated with f_{m1} also show little change. As shown in Figure 6-6 (b), the average sideband amplitudes even exhibits a slight decrease during the period of testing. This shows that the manufacturing errors of Gear Zr2 may become less due to the effect of self-modification on the tooth profiles which are formalised by light and gradual wear.

These little changes in both the mesh components and their sidebands indicate that the gears at the high speed transmission stage in GB1 remain healthy.

6.4.2 Monitoring of the Lower Speed Stage in Gearbox 1 based on Mesh Components and Sidebands

Although there are no clear changes in the vibration features associated with the higher speed in GB1, the vibration features associated the lower speed stage exhibit significant changes, which can be observed in Figure 6-7 (a). Firstly, the mesh component at $3*f_{m1}$ remains nearly level for the entire period of the test. There is a slight peak at about 300 hours, increases firstly at a higher rate from 323 hours to 400 hours, and then exhibits a very slight monotonic decrease until end of the test. Secondly, the mesh component at $2*f_{m1}$ shows a slight downward trend which increases after about 700 hours. The mesh component at $1*f_{m2}$ shows a very slight downward trend for the duration of the test.

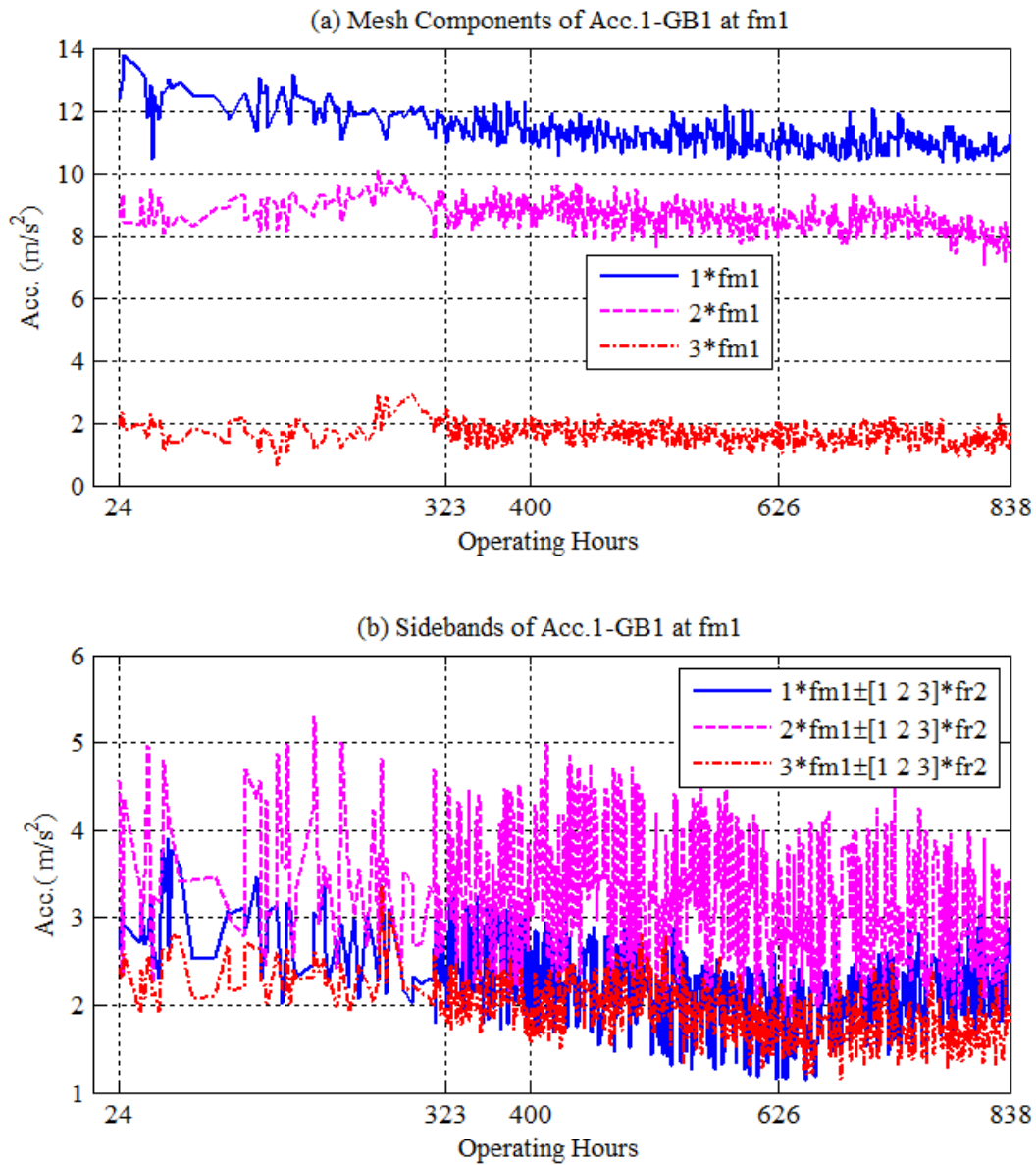


Figure 6-6 Mesh frequency components and sidebands of GB1 at f_{m1} and their harmonics as a function of operating time (f_{r1} cannot be seen as the TSA is based on f_{r2})

The changes in these two mesh components clearly indicate that the mesh process of the lower speed gears becomes worse at the late phases of the operation and thus they are regarded as faulty because the increased magnitudes represent there is an increase in the dynamic loads. This diagnostic result is made even though the amplitudes at 1^*f_{m2} minimally during the operation period. This is because that the component at 1^*f_{m2} may be distorted by the resonances as it exhibits high fluctuations which mask the basic trend largely.

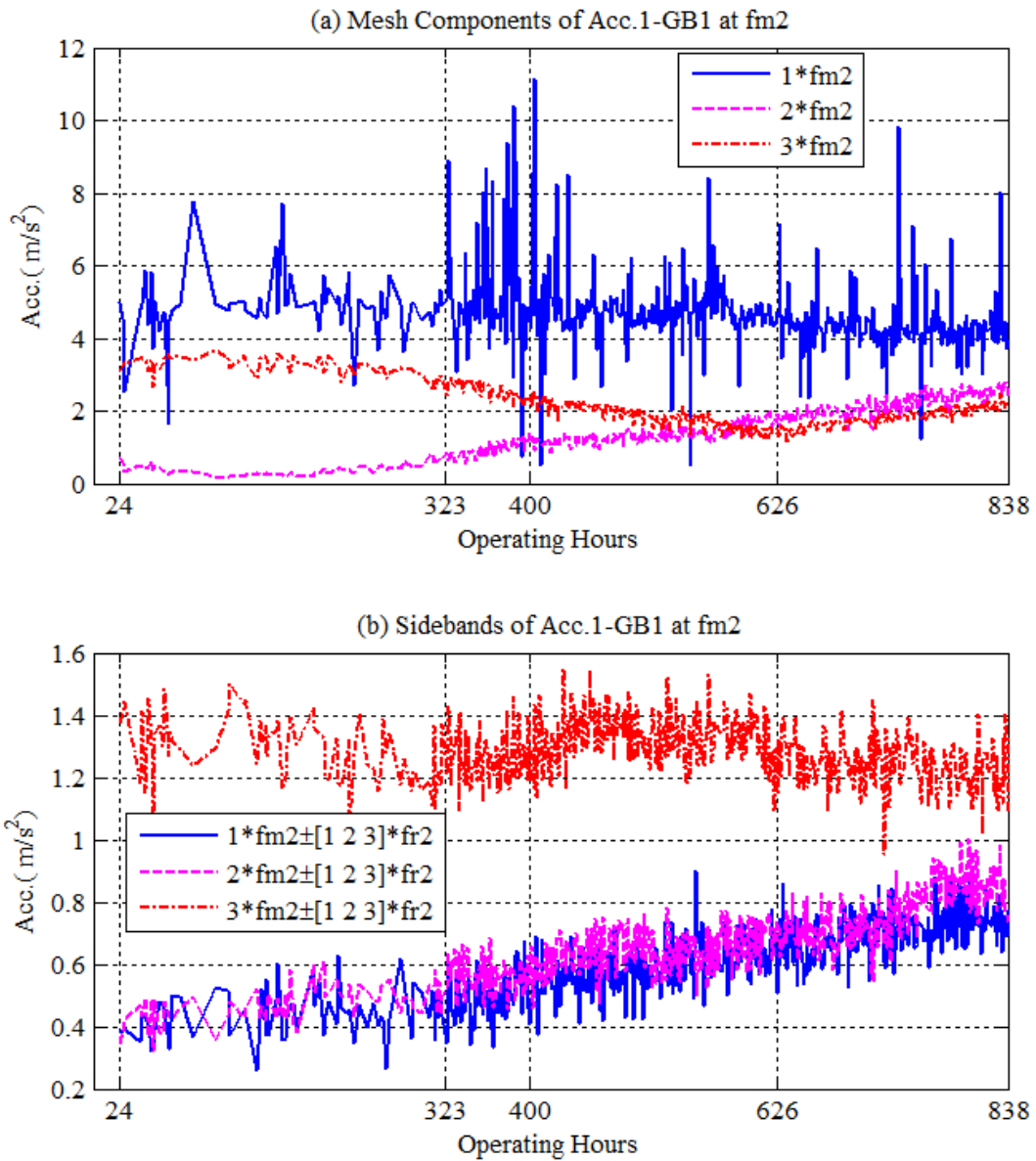


Figure 6-7 Mesh frequency components and sidebands of GB1 at f_{m2} and their harmonics as a function of operating time

Moreover, the diagnosis of the faulty lower speed transmission stage can be further confirmed by the sideband changes in Figure 6-7 (b). The sidebands associated with mesh components at both the $1*f_{m2}$ and $2*f_{m2}$ show a significant increase starting at the operation of 323 hours, which indicates that the gear gradually become more asymmetry in the period from 323 hours to the end of the test, when it is compared with its early operation phases.

Based on these gradual increasing changes with operation, it is concluded that the lower speed stage transmission of GB1 had severe wear, which may be caused by higher contact loads and poorer hydrodynamic lubrication conditions as the sliding velocity between tooth profiles is relatively lower, compared to that of the higher speed gears. This therefore is fully consistent with the wear markers presented in Chapter 5.

6.4.3 Monitoring of the Lower Speed Stage in GB2 based on Mesh Components and Sidebands

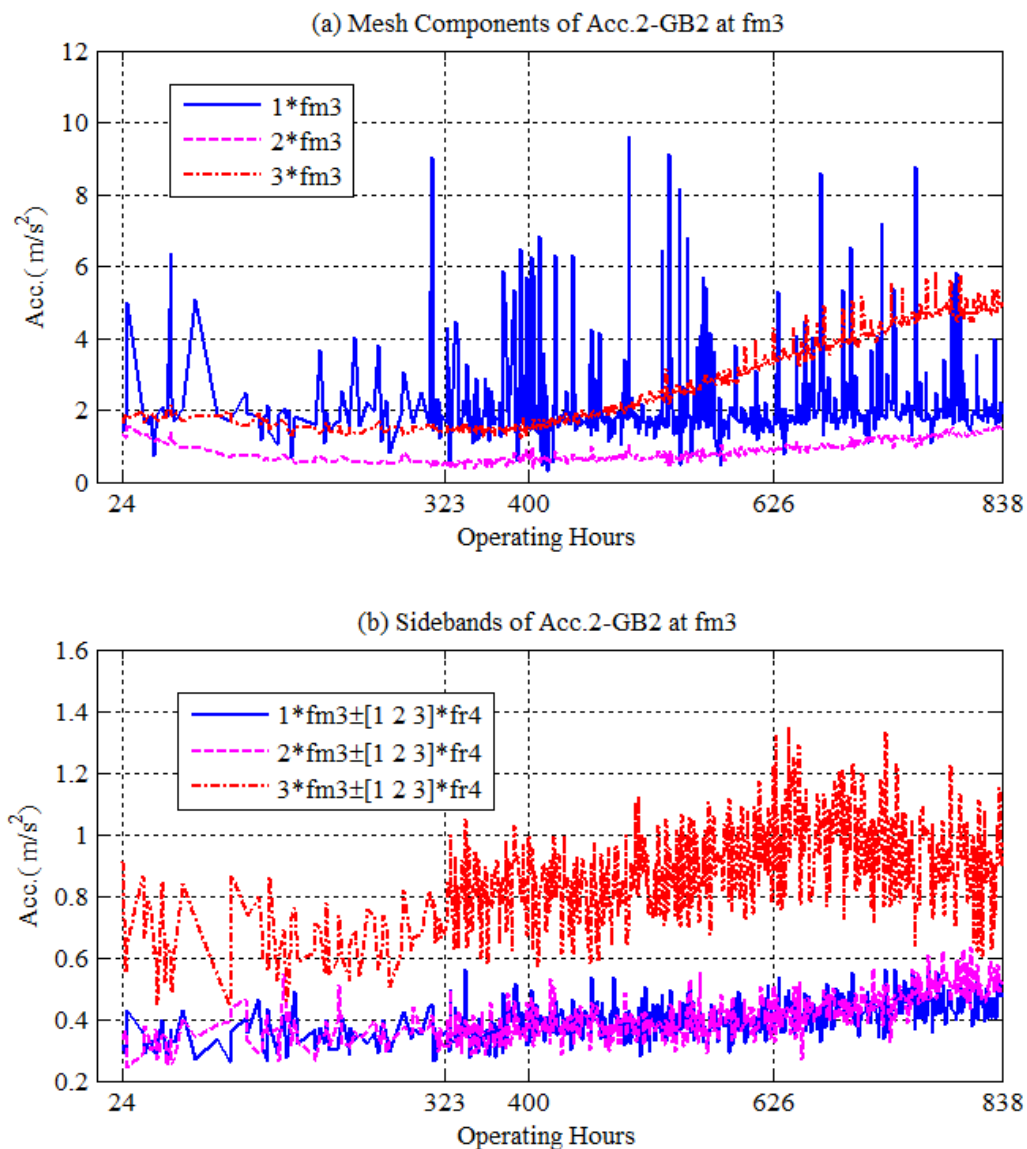


Figure 6-8 Mesh frequency components and sidebands of GB2 at f_{m3} and their harmonics as a function of operating time

Both the mesh components and sidebands in Figure 6-8 show that the vibrations of the lower speed transmission stage in GB2 also exhibit a gradual increase toward to the end of the test. Especially, the increase trends start at 424 hours and extend to considerable high amplitude at 838 hours. Therefore, it is also diagnosed that this stage has the similar fault with that of the GB1.

Normally, the test would be ended at 626 hours when the sideband associated with $3 * f_{m2}$ is about 150% higher than its baseline. However, as other components were not significantly increased, being only about <50%, the test was continued in order to show more severe results.

This stage could be diagnosed to be more severely worn or defected between the meshed teeth as most of the monitored parameters exhibit monotonic increases with operating time. However, a careful comparison of the relative changes in the late operation period (from 626 hours to 838hours) has found that the GB1 has a nearly 200% increase in the sidebands compared with its baseline whereas GB2 only has about 100% increase. Therefore, it is regarded that the lower speed stage of GB1 has a higher degree of wear or more defects on the tooth surfaces. This is also because a higher sideband always indicates poorer gear engagements.

6.4.4 Monitoring of the Higher Speed Stage in GB2 based on Mesh Components and Sidebands

Similar to the case of the higher speed stage transmission in GB1, the mesh components and sidebands in Figure 6-9 exhibit a clear tendency in amplitude decrease towards to the end of the test. This slight decrease is likely due to self-modification between mesh processes. As such a decrease usually indicates a reduced dynamic load between the meshing gear pairs, it is diagnosed that this set of gear is still healthy.

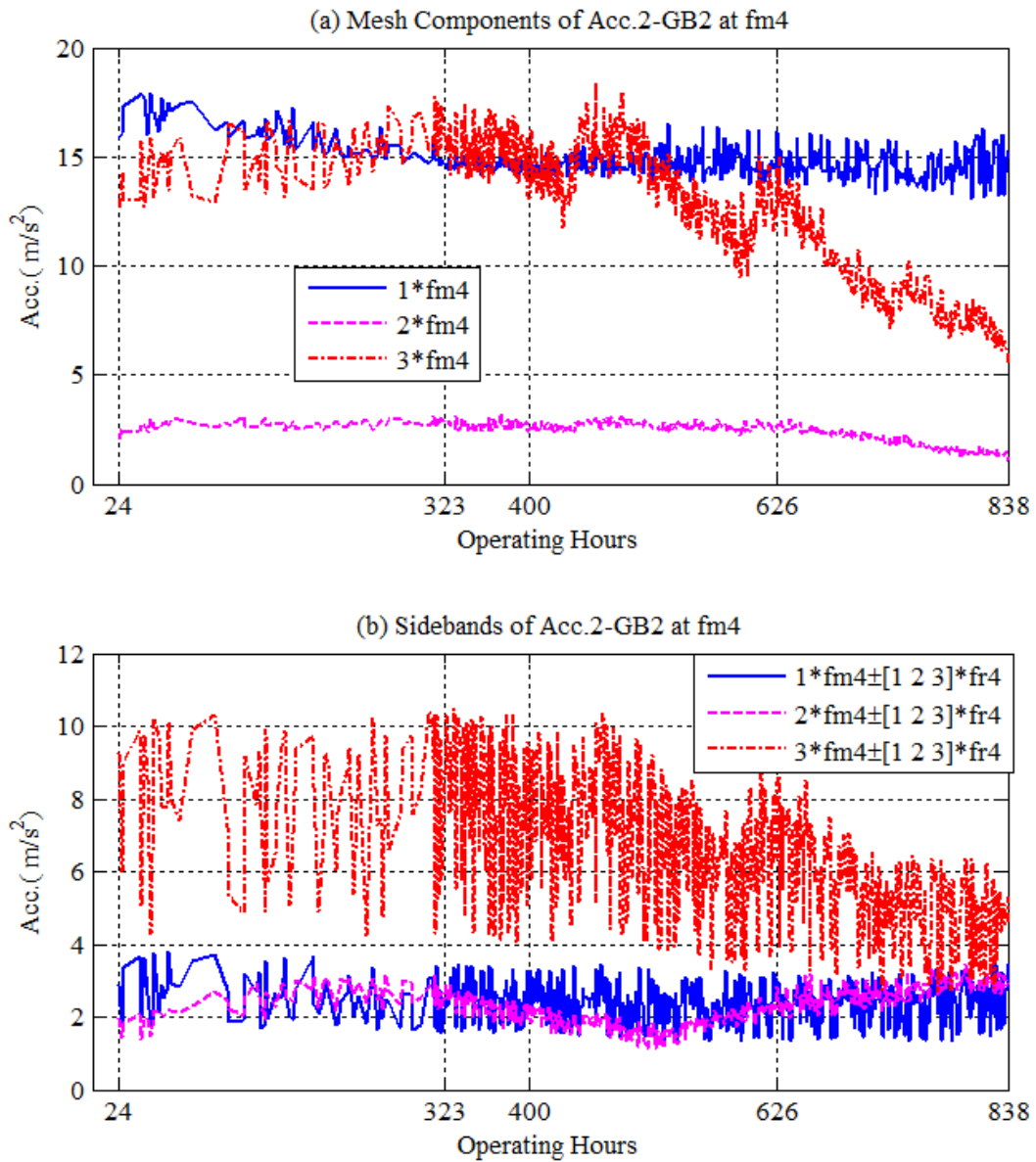


Figure 6-9 Mesh frequency components and sidebands of GB2 at f_{m4} and their harmonics as a function of operating time (f_{r5} cannot be seen as the TSA is based on $f_{r2} = f_{r4}$)

6.5 Key Findings from TSA Analysis of Vibrations

Based on the analysis in Section 6.4, it is shown that the vibration feature parameters from TSA-fr2 signatures, obtained through the computational efficiency scheme, needs only one implementation of the TSA procedure of reconstructing angular reference signals, based on a single encoder output and decomposing vibration signals onto the angular domain relating to

both stages of a gearbox and allows a detailed diagnosis and accurate monitoring of the gear deterioration process.

Specifically, the sidebands are more reliable to indicate the gear defects and more accurately show the defect severity in the lower speed stages of both gearboxes, compared with that of the mesh components.

If these findings are not fully consistent with that of the amplitude increase, which extends to the meshing frequency of the tooth and their harmonics, it is then likely to be a distributed fault like gear wear [113], as only some of the mesh components have been observed with increasing amplitudes for the lower speed transmission that is diagnosed to be faulty.

Despite the high performance of TSA analysis in diagnosing these gear faults, its implementation needs at least one additional channel to acquire rotation angular reference signal at a high sampling rate. Not only is it difficult to install a shaft encoder to the rotor system in practice, but also the additional channel means higher cost in the deployment and the implementation of this method. Moreover, TSA analysis is not capable of identifying a fault such as bearings and motor broken bars whose characteristic frequency are only fractions of the rotational frequency.

Chapter 7 MONITORING AND DIAGNOSIS OF GEARBOX DETERIORATION BASED ON THE TSA OF ACOUSTIC SIGNALS

Having evaluated the performance of using TSA with vibration signals, TSA is also applied to the acoustic signals measured remotely from the two testing gearboxes in order to explore if TSA is sufficiently effective to suppress the stronger noise and highlight the monitoring components in the gearboxes. As there is close correlation between acoustics and vibrations, the same monitoring features are extracted at gear characteristic frequencies in the order domain. Finally, monitoring trends are developed based on the identified feature parameters to show the variations of gear mesh conditions over the test period, based on the feature amplitudes, to obtain an assessment of the health conditions of different gear sets.

7.1 Introduction

To evaluate the performance of using acoustic signals perceived remotely for monitoring the two multi-stage gearboxes, this chapter uses the same signal processing techniques as that of vibration to suppress the noise signals which can contain more influences by the random background disturbances. Measurement of noises and vibrations from the AC driving motors and DC loading generators are acquired remotely using a general purpose omnidirectional microphone.

Subsequently, the similar feature parameters can be extracted from TSA-fr2 signals in monitoring the two tested gearboxes deterioration process.

In this way, a fair comment can be made on the performance of acoustics based monitoring in line with the vibration based monitoring.

7.2 Characteristics of Acoustic Signals

The time domain signal of acoustic measurements shows very random fluctuations, as illustrated in Figure 7-1. Similar to vibration signals, it gives little information on the dynamics of the gearbox and hence the health of the gear conditions. Therefore, effective signal process techniques need to be used to ascertain if the signal includes any information about gear transmission dynamics.

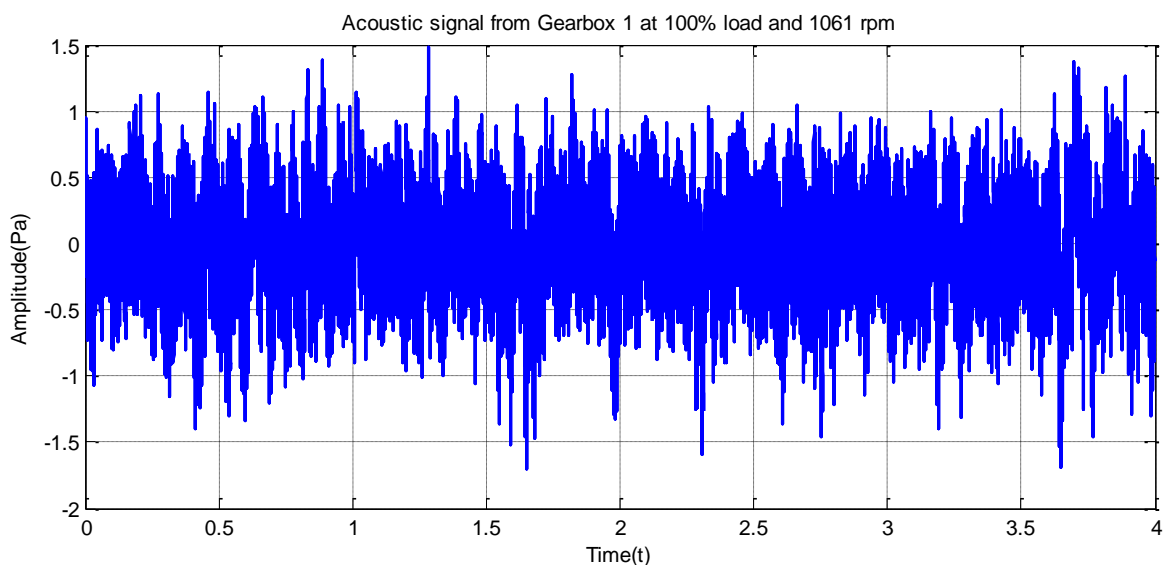


Figure 7-1 Raw acoustic signal of Mic.1-GB1 tested at full load and full speed

The baseline signal spectra are shown in Figure 7-2 for signals of GB1 and GB2, along with comparisons with vibration spectra acquired at the same time, instants of 324 hours, when the data acquisition system was ensured to be reliable after fixing the problems with data loss and slips of encoder joints. Clearly, acoustic spectra contain all the components relating to the gear transmission dynamics. Specifically, the spectral lines at f_{m1} , f_{m2} , f_{m3} , f_{m4} and their harmonics all show significant amplitudes, which is consistent with vibration analysis. Therefore, it is confirmed that the acoustic measurements are adequately configured for monitoring the gearboxes.

However, acoustic spectra also have distinctive differences from vibrations in the following aspects:

- 1) The high frequency mesh components appearing at f_{m1} and f_{m4} of the mesh process at the higher speed transmissions show lower amplitudes than that of vibration acceleration as the airborne acoustics is a function of vibration velocity.
- 2) The low frequency mesh components appearing at f_{m2} and f_{m3} of the mesh process at the lower speed stages are more significant than that of vibration acceleration as the airborne acoustics is a function of vibration velocity.
- 3) The acoustic signal shows fewer responses to the structure resonances appearing at $2 * f_{m1}$ and $3 * f_{m4}$ where vibration shows significantly high levels of amplitudes. This means acoustic levels can potentially reflect the dynamics of mesh process whereas the vibration may give an overestimate of the dynamic effect at such resonances.
- 4) More components are presented in the low frequency range as the microphones can perceive sounds from other sources such as AC motors and the DC generator.
- 5) The overall levels of background noise are higher.
- 6) There are also two very distinctive components appearing at 100Hz and 550Hz, which are due to the electric interferences arisen from the sensor less variable speed drive that can be used in controlling the motor of the AC.

This means that any statistical parameters in time domain including RMS, kurtosis, peak factors will give inadequate reflection of gear dynamics. Therefore, like the case of vibration signals, acoustic signals must be processed adequately in order to suppress the noise components and highlight the components relating to gear mesh processes for achieving the monitoring of gearboxes.

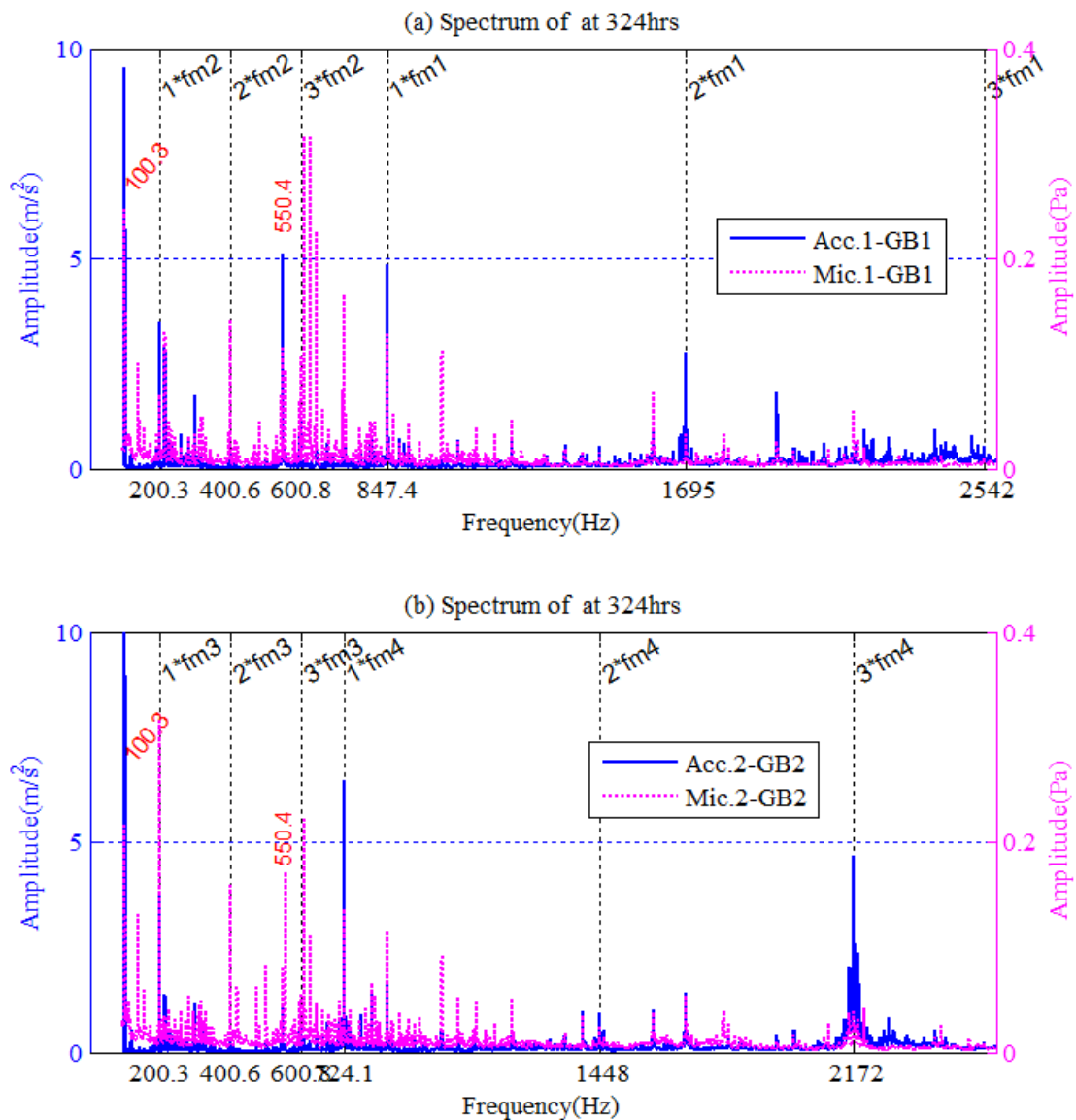


Figure 7-2 Acoustic power spectra of Mic.1-GB1 and Mic.2-GB2 at 324 hours

7.3 TSA-fr2 Acoustic Signals

Using the same procedure as that used to process vibration signals in Chapter 6, the TSA of acoustic signals was carried out according to the flow chart shown in Figure 7-3, in which the vibration signals are replaced by the acoustics signals acquired. In real implementation, both channels of vibration signals and the two channels of acoustic signals are simultaneously sampled based on one reference angular signal in one Matlab function.

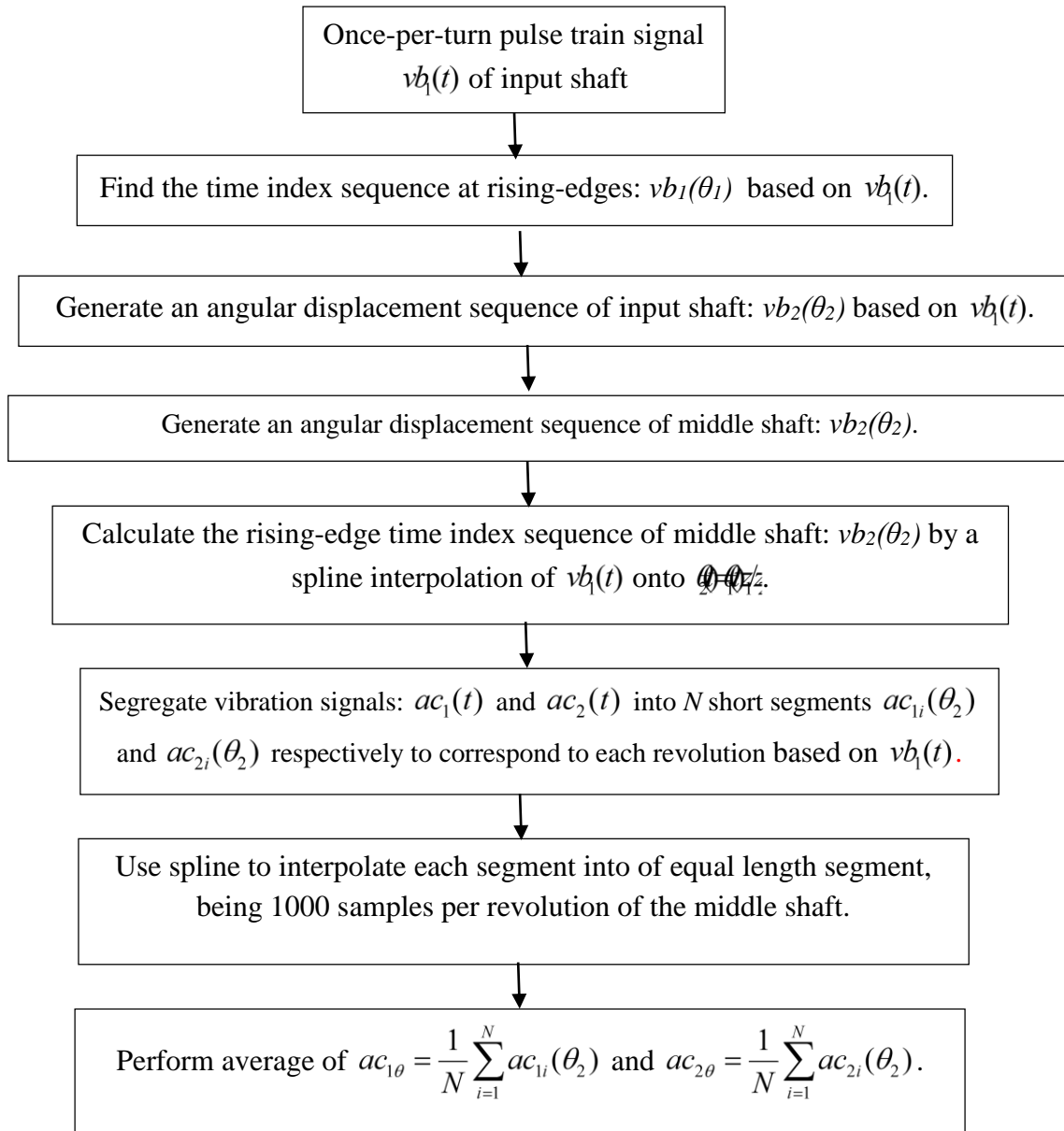


Figure 7-3 Implementation of TSA of acoustic signals based on the middle shaft angular position rotating at the speed of f_{r2}

Figure 7-4 presents acoustic signals obtained by the TSA-fr2 processing for Mic.1-GB1 and Mic.2-GB2. They show more stationary waveform, compared with the raw data in Figure 7-1. From these waveforms in the angular domain, it is noticed that both signals exhibit a visible periodic waveforms synchronized to their corresponding gears or the shafts, which shows that the noise components have been suppressed effectively. Similarly, this periodicity indicates that these gears and their associated shafts may have certain degree of eccentricity errors such as gear run-out and misalignments. However, the details of the exact source are not possible to be differentiated between Zr2 gear, Zr3 gear and their mounted shafts in GB1, or between Zi2

gear, Zi3 gear and their mounted shafts in GB2. In general, these TSA signals still cannot provide sufficient details of gear mesh characteristics.

Interestingly, the vibration intensity of GB2 is about 5% lower than GB1 when their RMS values are compared. This is very different from that of vibration of TSA-fr2.

However, as shown in Figure 7-4 (b), GB2 still exhibits a slightly higher local non-stationary within each rotation period. This shows that the dynamic performance of GB2 is poorer than that of GB1. However, this simple waveform analysis is not sufficient to identify which gear accounts for the higher vibration amongst the four gears in the gearbox.

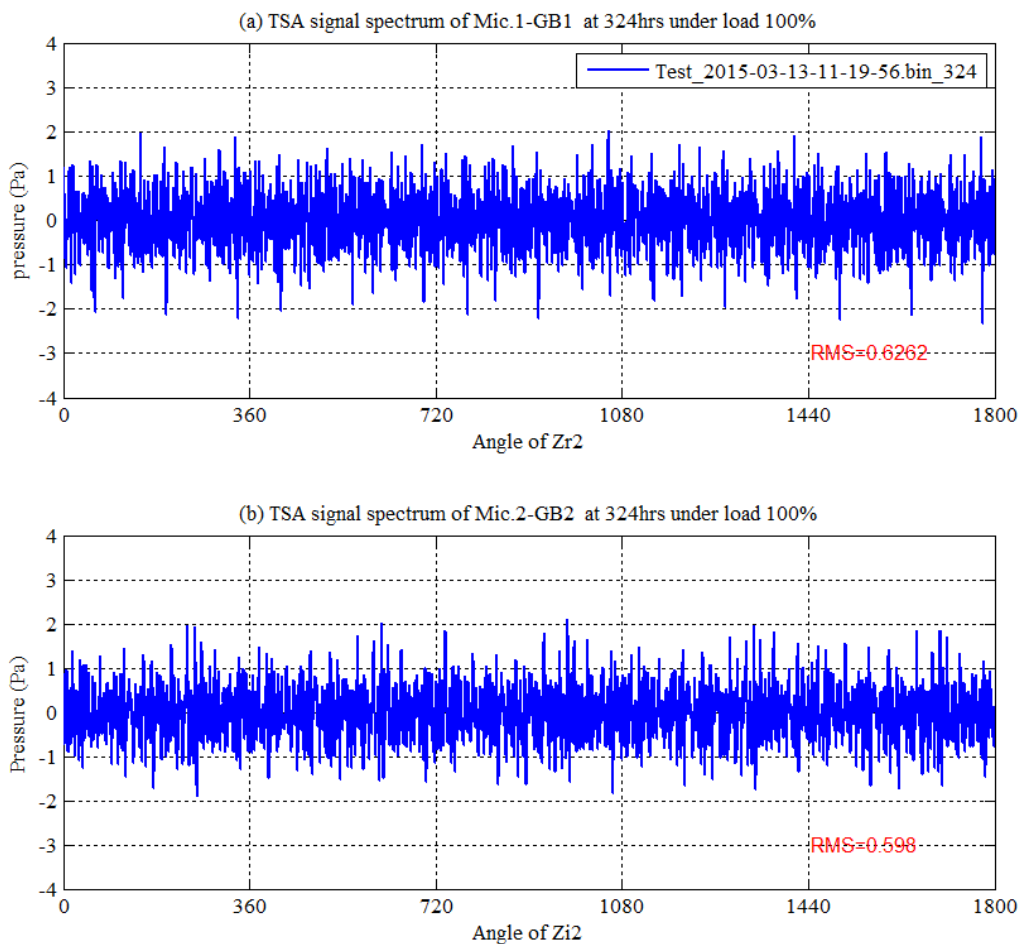


Figure 7-4 TSA-fr2 acoustic signals for Mic1 and Mic 2 plotted as a function of shaft angle. Further FFT processing of the TSA-fr2 signals results in the order spectra as shown in Figure 7-5. By a comparative study with the spectra from vibrations, it is noticed that in addition to the common corresponding vibration spectra features, the spectra are composed mainly from

mesh components and their higher order harmonics along with associated sidebands. The acoustics spectra have been found to have specific differences in the following aspects, which is also assisted by a direct spectra comparison between the vibration and acoustics shown in Figure 7-6:

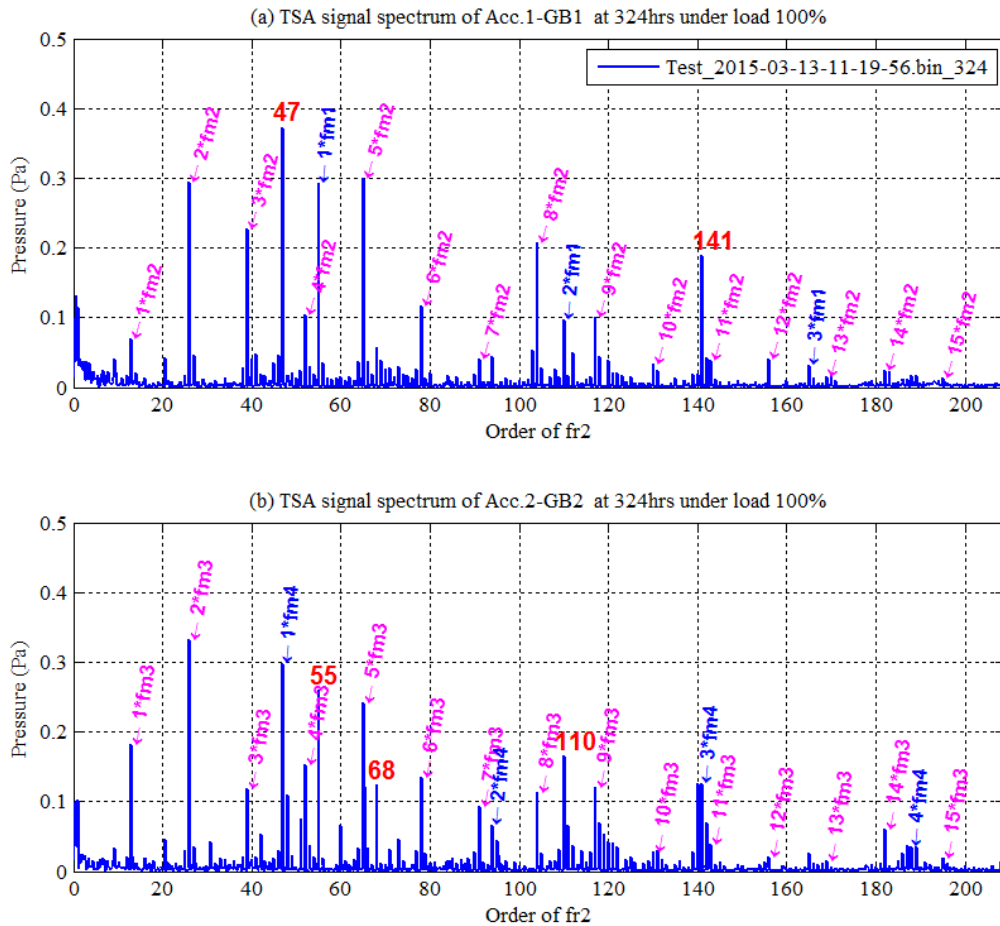


Figure 7-5 TSA-fr2 spectra of Mic.1-GB1 and Mic.2-GB2 at 324 hours

Comparison of the order spectra obtained from acoustic and vibration signals analysis are depicted in Figure 7-6. It is clear that in addition to common spectral features (both spectra are composed mainly from mesh components, their higher order harmonics and associated sidebands), the acoustic spectra have specific differences in following aspects:

- 1) Frequency contents relating to lower speed stages are relatively richer and stronger, showing that the microphone can perceive more signals which radiated more globally in this frequency range. In contrast, the accelerometer picks the vibrations more localised to the sensor point.

- 2) Spectral amplitudes at $1 * f_{m3}$, $3 * f_{m3}$, and $4 * f_{m4}$ in GB2 are not particularly high anymore, rather a reasonable decrease with the increase in orders which is predicted by the gearbox model. This also means that less distortion induced by the local resonances appearing in the vibration spectra.
- 3) The general pattern of two spectra of GB1 and GB2 is much similar. This reflects the fact that the two gearboxes are the same in construction, meaning similar sound radiation to the similar dynamic effect of the gear meshing processes.

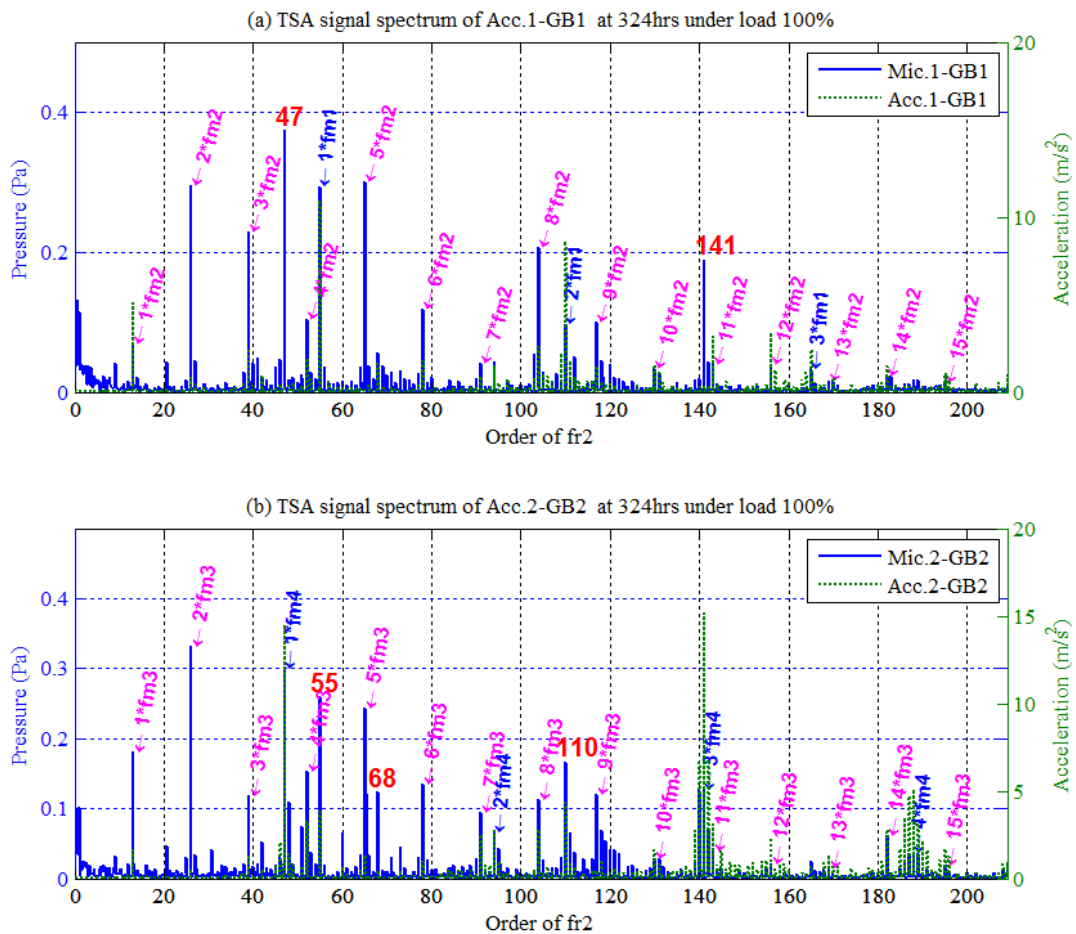


Figure 7-6 Comparison of spectra between acoustic signals and vibration signals

However, like the vibration spectra, the acoustic spectra show in figure 7.6 also have significant cross interferences, which appear at orders of 47 and $141=47 \times 3$ in Mic.1-GB1, being the tooth numbers or their combinations of GB2, and orders of 55, 110 and $68=55+13$ in Mic.2-GB2, being the tooth numbers or the combination of GB1. These show that the TSA signals still have

contamination and cannot be directly used, such as the use of any waveform parameters which include kurtosis, RMS, etc., to monitor the corresponding gearbox.

Therefore, to avoid such influences of the interferences on monitoring and diagnosis, individual mesh components and their associated sidebands have to be extracted in each spectrum and thereby are based to monitor the corresponding gearbox. Specifically, as the first a few harmonics are more significant, the monitoring is then implemented based on these significant components, which is the same as that adopted in vibration based monitoring.

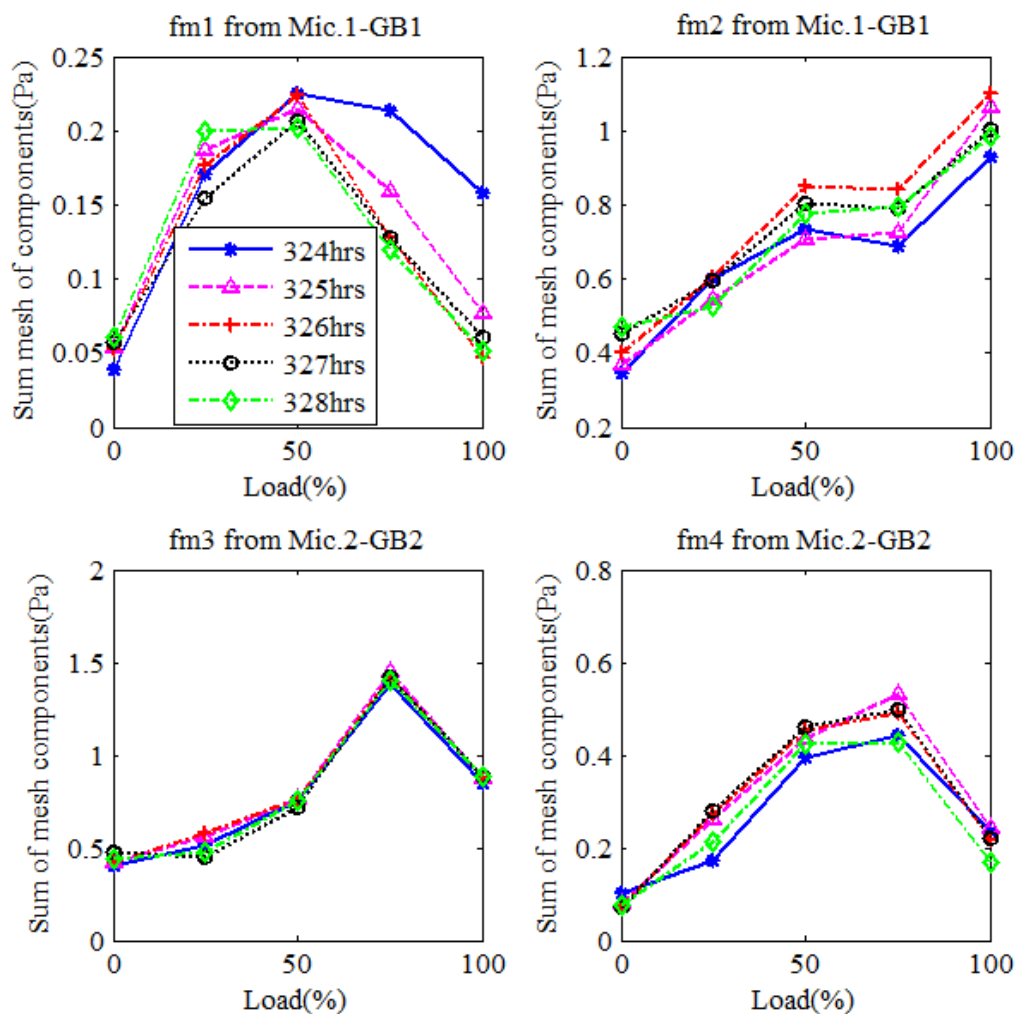


Figure 7-7 The dependency of mesh components upon loads

A further study was performed to confirm the dependency of the mesh components upon the gear loads tested. As shown in Figure 7-7, the accumulative amplitudes of acoustic TSA-fr2 signals also shows approximately that the amplitudes are higher at the higher loads, which is

consistent with that of model prediction in Chapter 3. In addition, these amplitudes also show stable behaviour across the four consecutive measurements. Therefore, the following acoustics based monitoring is performed by using these individual mesh components and their associated sidebands, which are all extracted from their corresponding order spectra.

7.4 Monitoring and Diagnosing Gear Deteriorations

To simplify the monitoring task, the monitoring performances of using acoustic signals is only focused on the case of 100% load. This is also based on a concern that the highest magnitudes under the middle loads, which is shown in Figure 7-7, may be unstable as a result of the load dependent nonlinearity mesh stiffness. Nevertheless, monitoring gear conditions under different loads is another subject challenge that is also actively studied in the field of gear CM by many researchers.

7.4.1 Monitoring of the Higher Speed Stage in GB1

The mesh components and their associated sidebands associated with f_{m1} , which is presented in Figure 7-8, exhibit no definitive trends during the period of the test. Like that of vibration, all the monitored parameters exhibit fluctuations but similar amplitudes to those of the initial operation remain at the end of this test.

Therefore, it is understood that similar to vibration, the mesh quality at the end of the period maintains roughly the same as that of the initial period, or the gear set of Zr1 and Zr2 that formulates the dynamics at the first stage of GB1 have little deterioration on their tooth profiles and hence engagement performance. Therefore, this stage transmission is regarded as healthy.

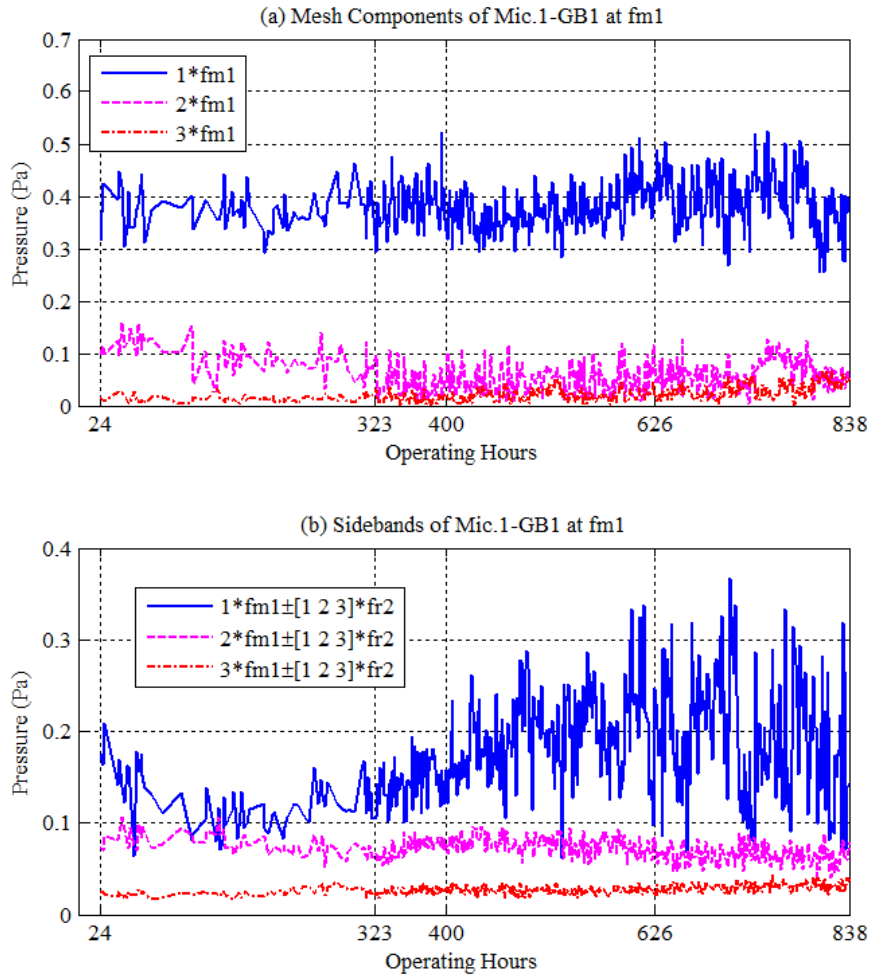


Figure 7-8 Acoustic amplitudes at meshing frequency f_{m1} harmonics and their sidebands for GB1 as a function of operating time

7.4.2 Monitoring of the Lower Speed Stage in GB1

Figure 7-9 presents the mesh components and their associated sidebands associated with f_{m2} for the lower speed stage in GB1. The increases at the mesh components at $2^* f_{m2}$ and $3^* f_{m2}$ together with that of sidebands at $1^* f_{m2} \pm [1 \ 2] f_{r2}$ and can indicate the gear has gradually deteriorated for the similar reasons to the vibrations associated with the gear contact dynamics. However, the mesh components provide more recommendation on the faults than the sidebands because of their significant amplitude in the spectra. This may be due to the sidebands having much lower values that could have been affected by the strong background noises.

Moreover, the deterioration can be indicated by the acoustics at very early stages i.e. at the onset of the test, which may be due to the capability that the microphone can observe in relation

to the vibrating responses from a wide range of the surfaces of a gearbox housing, whereas an accelerometer can only pick up the vibration at a particular point.

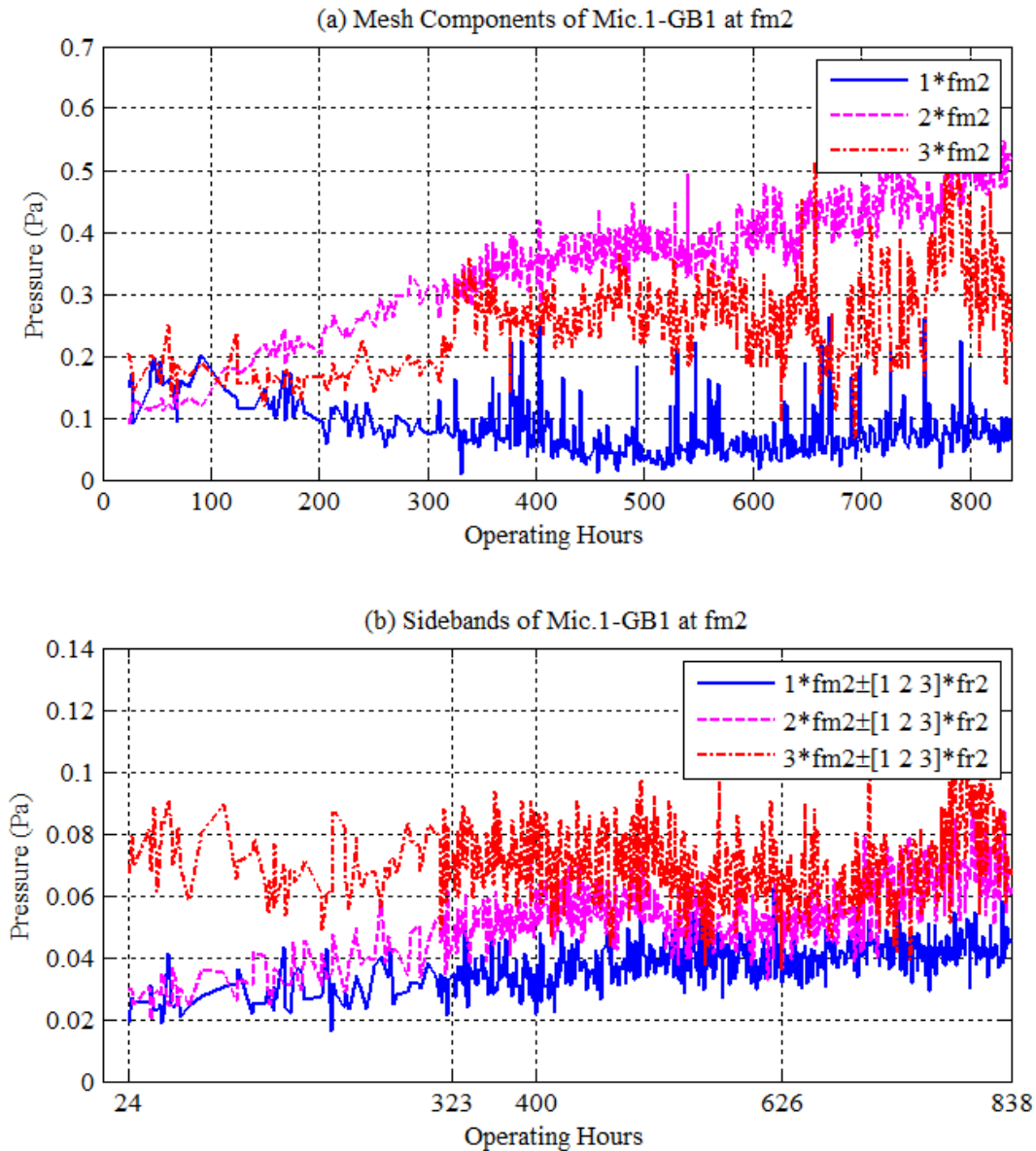


Figure 7-9 Acoustic amplitudes at meshing frequency f_{m2} harmonics and their sidebands for GB1 as a function of operating time

7.4.3 Monitoring of the Lower Speed Stage in GB2

Figure 7-10 presents the mesh components and their associated sidebands associated with f_{m3} for the lower speed stage in GB1. The increases at mesh components at $2 * f_{m3}$ together with

that of sidebands at $2 * f_{m3} \pm [1 \ 2] f_{r2}$ and $3 * f_{m3} \pm [1 \ 2] f_{r2}$ can indicate the gear is gradually deteriorated for the similar reasons to that of the vibrations associated with the gear contact dynamics.

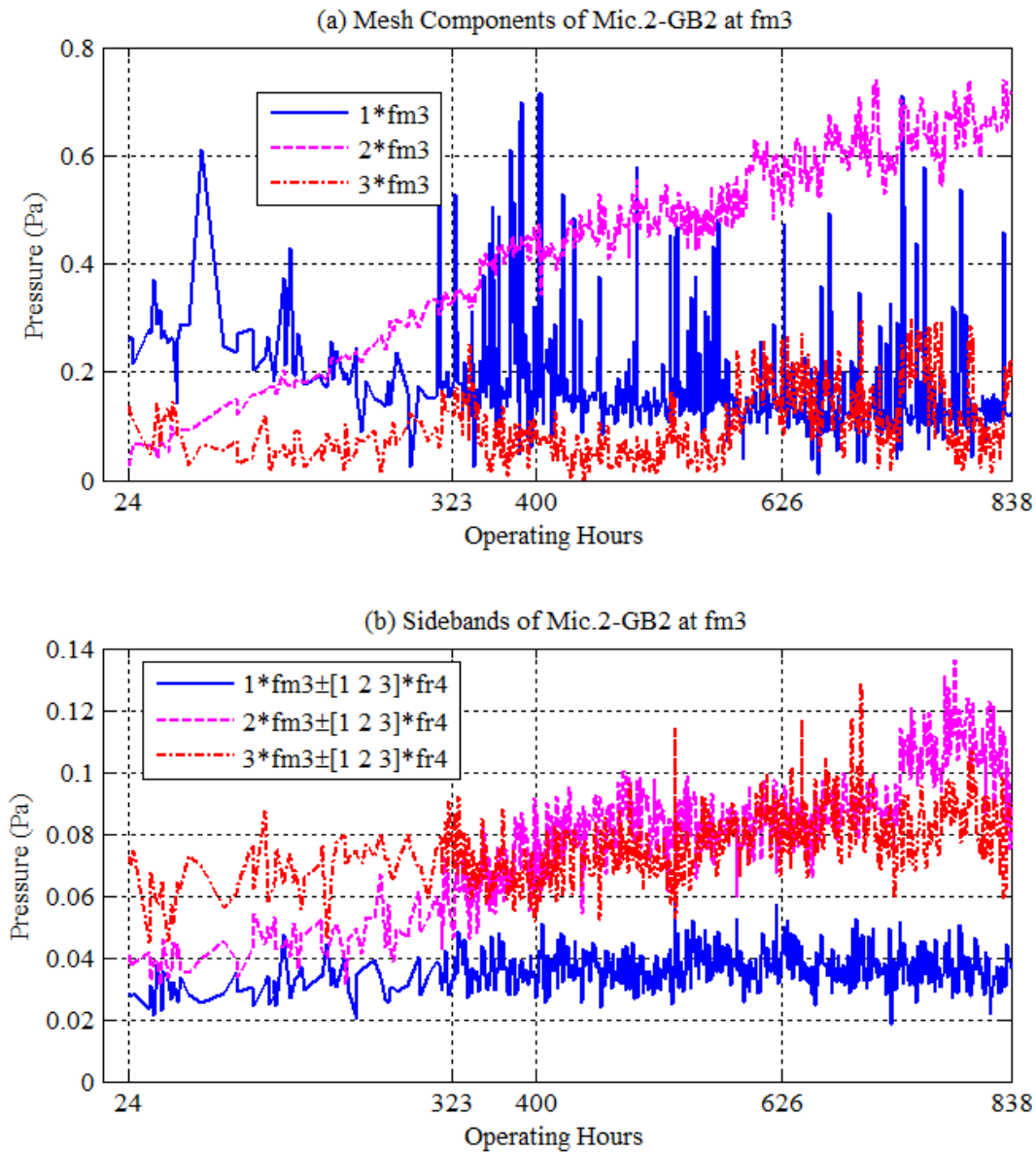


Figure 7-10 Acoustic amplitudes at meshing frequency f_{m3} harmonics and their sidebands for GB2 as a function of operating time

Once more, the mesh components at $2 * f_{m3}$ provides more recommendation on the faults than the sidebands because of its significant amplitude in the spectra. Also, the deterioration can be significantly indicated by the acoustics at the early stages due to the capability of the

microphone observing the vibrating responses from a wide range of the surfaces of a gearbox housing, compared with the local response an accelerometer received.

7.4.4 Monitoring of the Higher Speed Stage in GB2

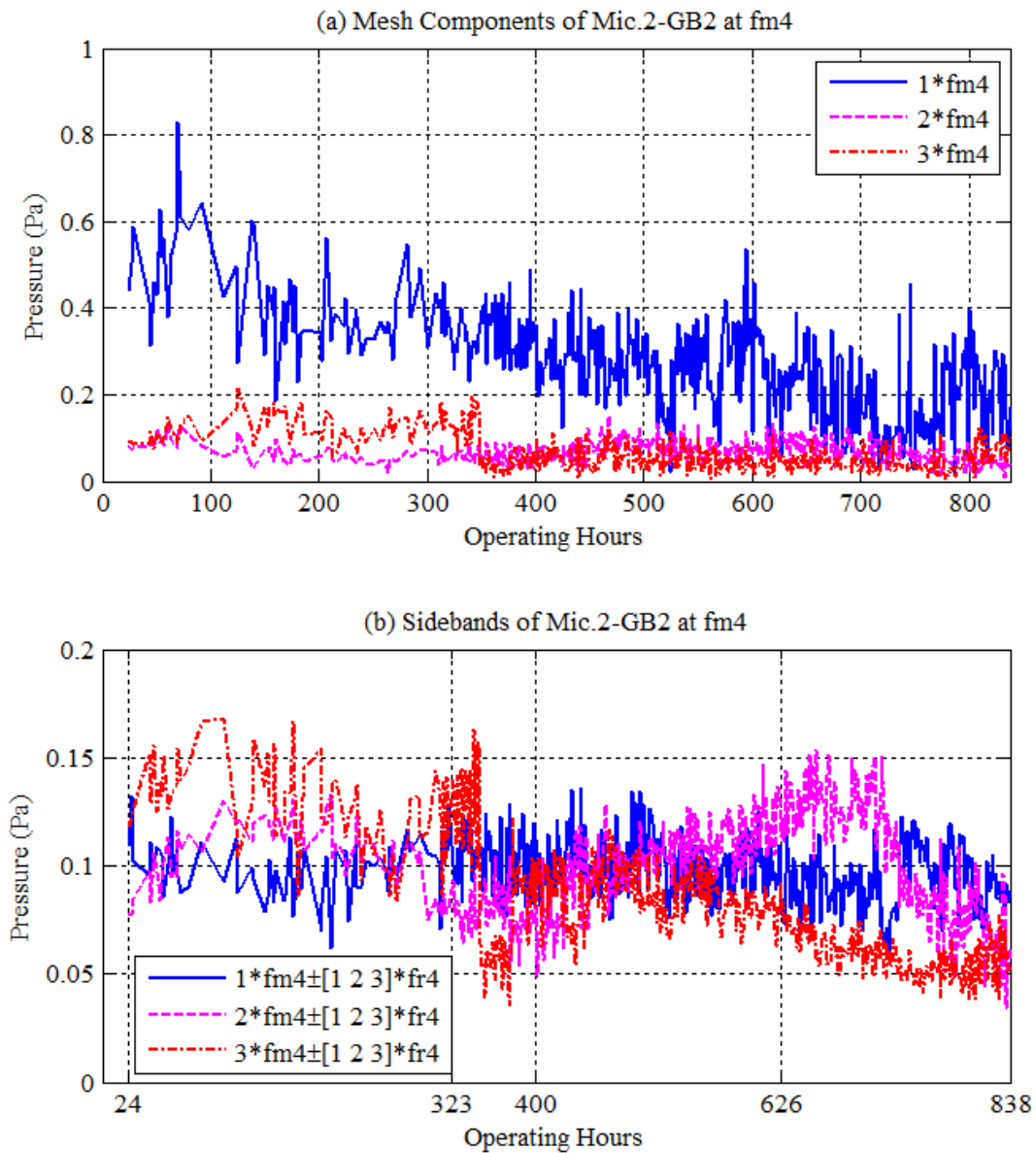


Figure 7-11 Acoustic amplitudes at meshing frequency f_{m4} harmonics and their sidebands for GB2 as an operating time function

Similar to the vibration cases of the higher speed stage transmission in GB1 and GB2, the mesh components and sidebands of GB2 from acoustic signals in Figure 7-11 also exhibit a small tendency to increase toward the end of the test. Instead, they all show a slight decrease due to

the self-modification between mesh processes. As such decreases usually indicate reduced dynamic loads between the meshing gear pairs, it is diagnosed that this set of gear is still in a healthy condition

7.5 Key Findings from TSA Analysis of Acoustic Signals

Regarding the results presented in this chapter, it can be established that the same TSA scheme used for processing the vibration signals is suppressing noise in acoustic signals. The acoustic feature parameters extracted from TSA-fr2 signals provide a diagnosis of a gear deterioration process at the lower speed transmission stages for both the GB1 and GB2.

However, it has been found that the mesh components in acoustic signals are more effective in characterising the deteriorations of the gearbox because the microphone signal contains more information gathered from a greater area of the gearbox surface than is picked up by an accelerometer. Different from the vibration spectra, the sidebands in the acoustic signal are a more reliable indication of gear defects, and more accurately present the defect severity. As a result, acoustic sensing allows deterioration of the lower speed stages to be identified at an earlier stage.

Likewise, these findings are not fully consistent as distributed faults cause an increase in both the meshing frequency of the tooth and their harmonics [113]. Instead, some of them may decrease or fluctuate with operating times because of gear mesh the self-modifications of tooth wear.

Similarly, the main deficiency of using TSA for de-noising the acoustic signals is the contact measurement of the rotation angular reference signal at a high sampling rate, which takes away the unique merit of remote monitoring using acoustics. Not only is it difficult to install a shaft encoder to the rotor system in practice, but also the additional channel means higher costs in the deployment and the implementation of this method. Moreover, TSA analysis is not capable of identifying a fault such as bearings and motor broken bars whose characteristic frequencies are only fractions of the rotational frequency.

Chapter 8 MONITORING AND DIAGNOSIS OF GEARBOX DETERIORATION BASED ON MSB ANALYSIS OF SURFACE VIBRATION SIGNALS

To overcome the deficiency of TSA analysis, this chapter evaluates the performance of monitoring and diagnosing gear deterioration process using an advanced MSB analysis applied to the surface vibration signals available. It starts with investigating the characteristic MSB magnitude peaks arisen from the modulation coupling between mesh components and their associated sidebands, which are also purified by the superb de-noising and modulation enhancement properties of MSB. Such MSB magnitude peaks that associate with both high and low MSB coherence values but with acceptable numbers or limited frequency bands are then taken as the monitoring features. Based on these features and their variations within the operational period of the assessment, gear deterioration progression is finally examined for fault diagnosis.

8.1 Introduction

To overcome the deficiency of TSA analysis, the updated MSB analysis is selected to pre-process vibration signals for detecting and diagnosing the gear faults. As overviewed in Chapter 4, MSB representations are able to suppress noises by utilising signal phase information and results in nonlinear features to characterise modulations in signals. In addition, it can make a concise representation of the complicated modulation spectrum and allow easy analysis and numerical manipulation of characteristic features.

To utilise these performances of MSB analysis for gear CM, this chapter examines the MSB analysis results of vibration signals of gearbox baseline conditions. It then monitors the evolution of critical features parameters that correlates with gear dynamics in order to detect and diagnostic any faults in the testing gear system.

8.2 Implementation of MSB for Vibration

MSB in Equation (4.11) is calculated based on the Welch scheme of estimating power spectrum. It has the following key steps:

- 1) Set FFT window length to be $nfft=2^{18}=262144$, allowing a frequency resolution of 0.3662Hz to be obtained as the sampling rate is 96kHz
- 2) Set an overlapping ratio to be 0.8, which leads to the overlapping points to be 20,9715 points
- 3) The original data segment of 2880000 points is split up into $L=50$ data segments of $nfft$ with the overlapping points.
- 4) The overlapping short segments are then weighted by a Hanning data window to reduce spectral leakages.
- 5) The time domain segments are applied with FFT to transform them into the frequency domain.
- 6) The multiple products of MSB are calculated for each FFT segment over the frequency ranges specified up to the highest mesh frequency 3rd harmonic and of the higher rotational speed the 3rd harmonic.

- 7) Average over 50 FFT segments to obtain MSB. The averages are confirmed is sufficient as the resulted coherence values are more stabilized when the average is at its late stages.

In addition, a trial calculation of MSB was carried out in ensuring the MSB de-noise performance and stability based on the data length available and the averaging number. The mean of MSB coherence values were checked for different average numbers. As shown in Figure 8-1, the mean value of MSB coherence exhibit a monotonic decrease with average numbers. The fast decrease for averages below 20 shows that MSB results are unstable or the random content is still significant. When the average number is about 40, the decrease is much smaller or the noise content is insignificant. Therefore, the average number of 50 is acceptable for stable results based on the data and calculation parameters.

Moreover, the decrease trends between the two vibration signals are very similar. It may indicate that the noise contamination is approximately the same for the two signals.

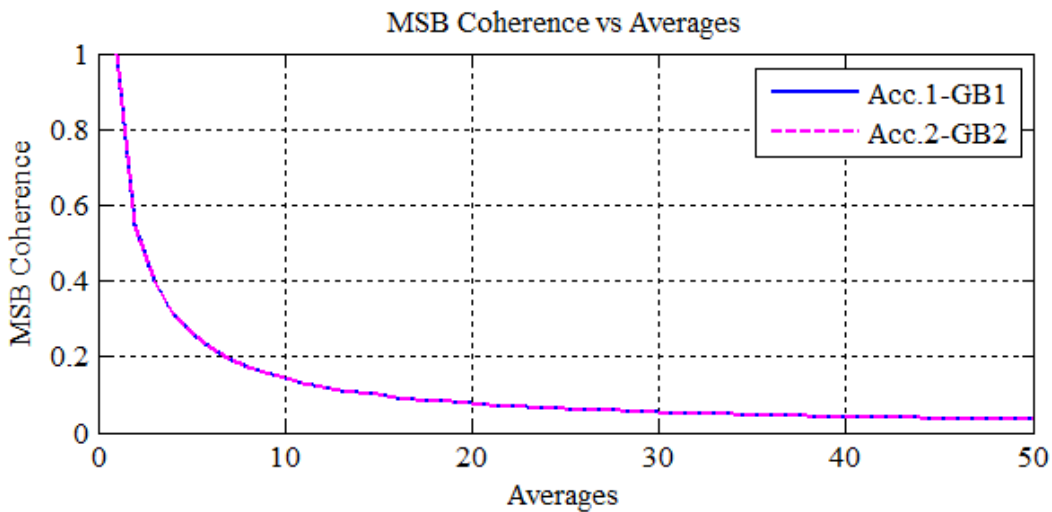


Figure 8-1 The stability of MSB estimation with averaging

8.3 MSB Characteristics of the Baseline Vibrations

Figure 8-2 presents the vibration MSB results of Acc.1-GB1 at operating hours of 324 hours when the signals are relatively stable. For clarity and further analysis, its bifrequency axis are labelled with only the characteristic frequencies of $f_{r1} = 17Hz$, $f_{r2} = 15Hz$, $f_{r3} = 3.4Hz$, $f_{m1} = 847.4Hz$, $f_{m2} = 200.3Hz$, and their first three harmonic frequency. In addition, MSB

magnitudes are root squared to match with the quantitative measure of a power spectrum and show up the small components.

The MSB magnitudes of the first three mesh harmonics at $1 * f_{m1} = 847Hz$ and $2 * f_{m1} = 1695Hz$ are significant, which are also confirmed by the sufficiently high amplitudes of MSB coherence at corresponding frequencies. The third harmonics of $3 * f_{m1} = 2542Hz$ is less significant. However, there are also observable peaks that associates with $f_{r2} = 15Hz$ at $3 * f_{m1} = 2542Hz$. This can be depicted by the slice of each the mesh component in Figure 8-3 (b) which is extracted by a simple search of the peak value around the corresponding mesh frequencies in the MSB magnitude result. It also shows in the Figure 8-2, it is much easier to identify gear associated components as the slices exhibit them into a harmonic pattern. Especially, the MSB coherences at these slices can be based to find all the relative components even if their MSB magnitudes are smaller such as those in the slice of $3 * f_{m1} = 2542Hz$.

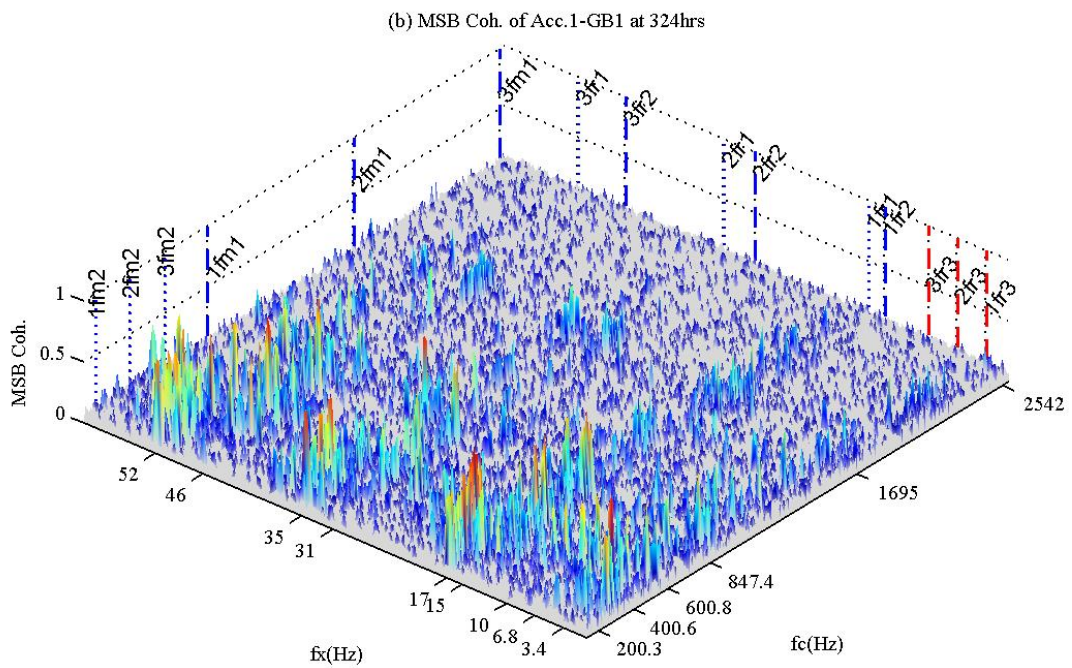
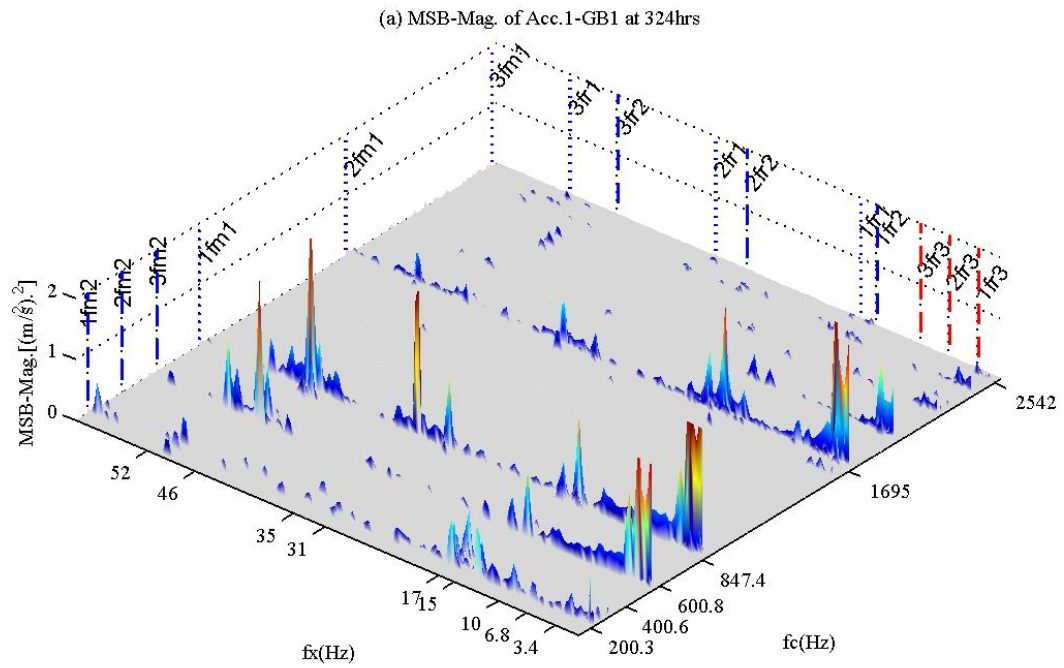


Figure 8-2 MSB results of Acc.1-GB1 vibration at 324 hours

The MSB magnitudes of the two mesh harmonics at $1 * f_{m2} = 200.3Hz$ and $3 * f_{m1} = 600.8Hz$ are significant, which can also be confirmed by the sufficiently high amplitudes of MSB coherence at corresponding frequencies. Similarly, the coherence results in Figure 8-4 indicate that there are potential MSB peaks that are associated with the gear rotation frequencies: $f_{r1} = 17Hz$, $f_{r2} = 15Hz$, $f_{r3} = 3.4Hz$, and their higher order harmonics although the 2nd harmonic is less significant.

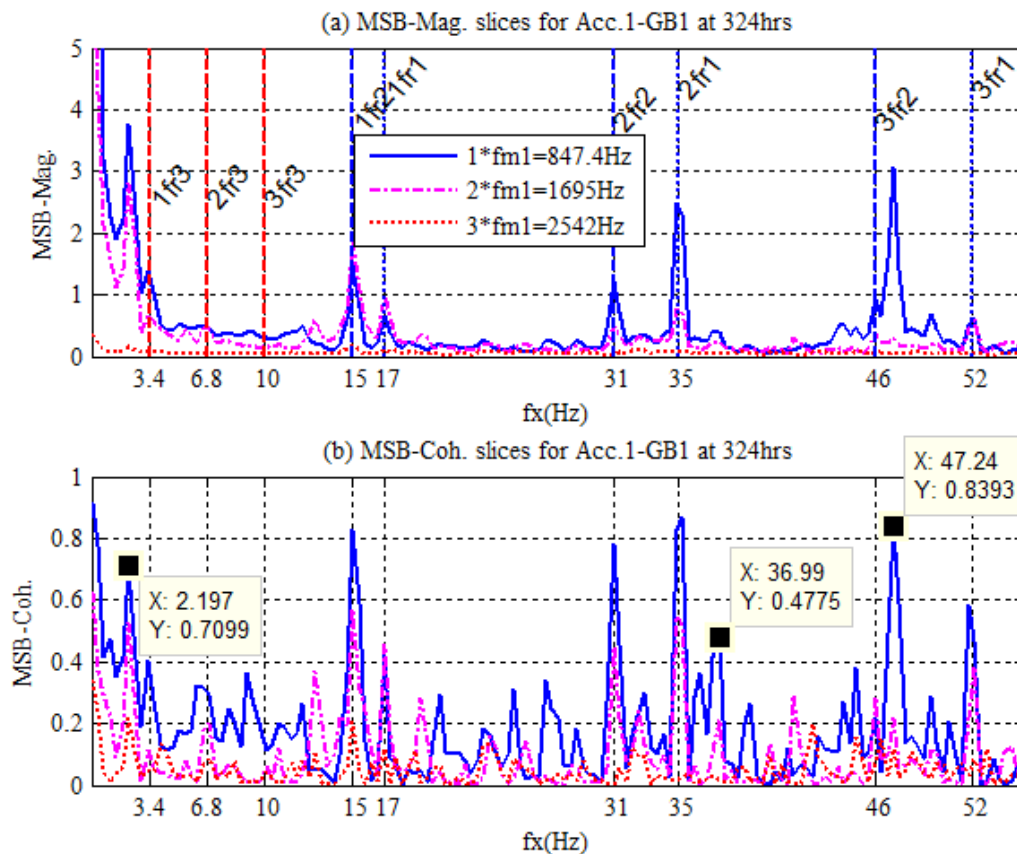


Figure 8-3 MSB slices at f_{m1} harmonics of Acc.1-GB1

In addition, there is a very significant peak at 2.197Hz. It has been identified to be the asymmetric rotor effect as this frequency value is just the broken bar or twice slip frequency $f_{bar} = 2sf_e$ (s motor slip rate and f_e electric frequency) which is the typical component due to the modulation of imperfection across rotor bars to the fundamental supply of induction motors which is detailed in Appendix C. Because of the presence of such a rotational excitation, several additional peaks such as those labeled in Figure 8-3 (b) due to its modulation to the gear rotation motions. Particularly, $2f_{r1} + f_{bar} = 2 \times 17.294 + 2.197 = 36.78Hz$ and $3f_{r1} - 2f_{bar} = 3 \times 17.294 -$

$2 \times 2.197 = 47.494\text{Hz}$, both of which are agreeable with the labelled one within frequency accuracy of 0.3662Hz)

Therefore, to concentrate the identification gear faults, only MSB peaks associated with gear rotation and mesh frequencies are extracted as the monitoring indicators. In this way, it avoids the influences of the asymmetric rotor components.

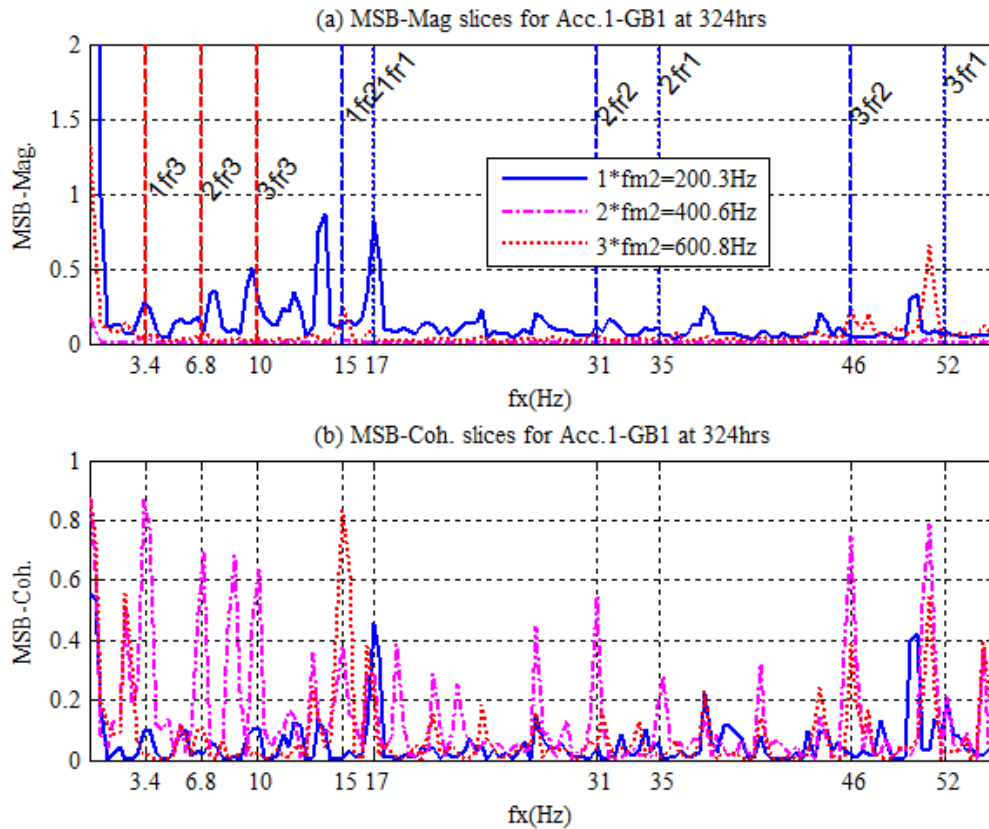


Figure 8-4 MSB slices at f_{m2} harmonics of Acc.1-GB1

For a further confirmation of MSB analysis, MSB results for Acc.2-GB2 are also shown in Figure 8-5 at the operating time of 324 hours. It exhibits similar behaviour to that of Acc.1-GB1. However, due to the enlargement of structure/mesh resonances the MSB magnitude at $3 * f_{m4} = 2172\text{Hz}$ of the higher speed stage is much higher. Particularly, this magnitude corresponds to just a smaller coherence value, shown by Figure 8-5 (b) because of instable dynamic behaviour at the resonances. Nevertheless, the observable amplitudes of MSB coherences shows that the MSB peaks at the rotation frequencies such as those of $f_{r3} = 3.4\text{Hz}$, $f_{r2} = 15\text{Hz}$, $f_{r5} = 12\text{Hz}$ and their higher order harmonics are significant or they exhibit higher SNR and can be based on for gear diagnostics.

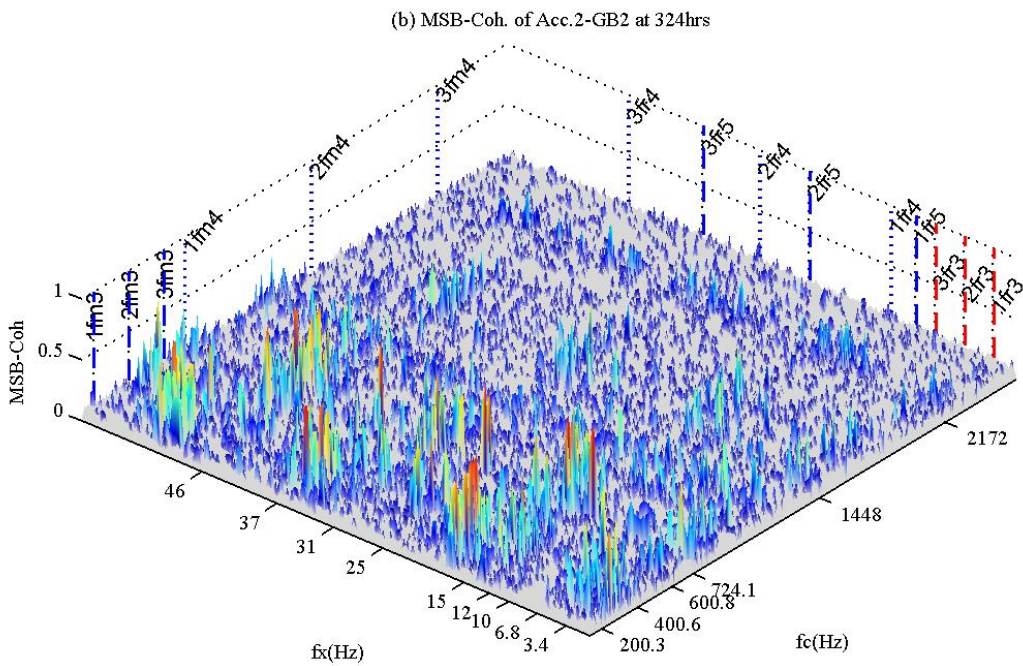
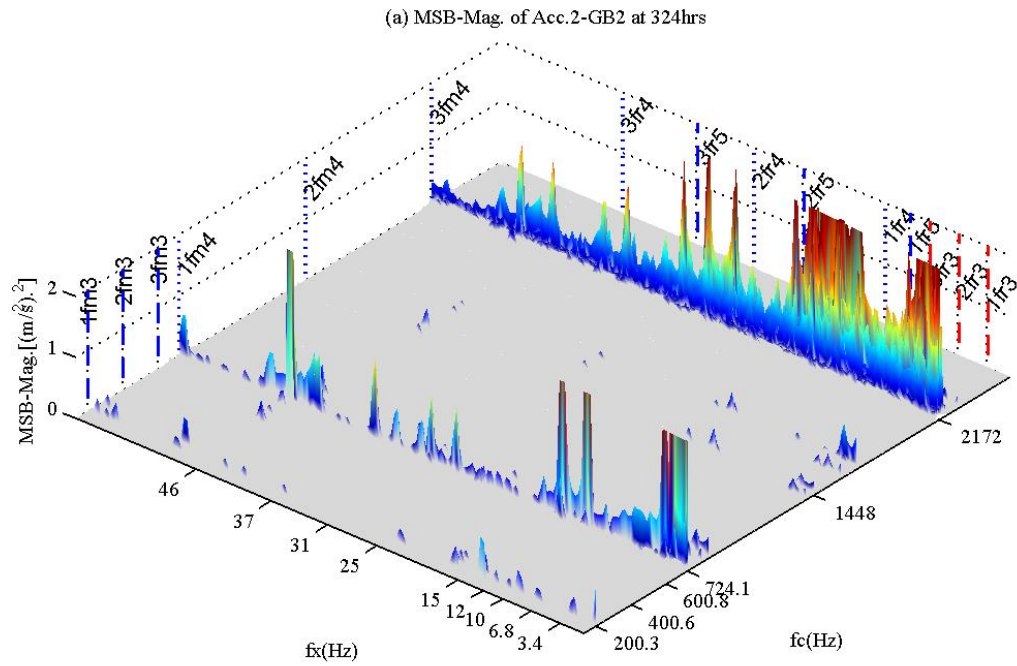


Figure 8-5 MSB results of Acc.2-GB2 at the operating time of 324 hours

8.4 Monitoring and Diagnosing Gear Deteriorations Based on MSB Vibration Signals Analysis

In exploring the MSB analysis monitoring performance, the MSB magnitude peaks at gear characteristic frequencies are extracted and averaged across corresponding rotational frequencies to obtain the monitoring feature:

$$A_j = \frac{\sum_{i=1}^3 |B_{MS}(f_{ri}, f_{mj})|^{0.5}}{3}, \quad j = 1, 2, 3 \quad (8.1)$$

where j represents the order of mesh frequencies and i represents the order of shaft frequencies. Because there are four transmission stages in the gear system, it will result in a features set of $4 \times 3 \times 3$ features, each 3×3 being designed to monitor one of four transmission stages. These high dimensional parameters are adopted in order to examine the changes within operating time, which can vary due to the dynamics of wear process and the differences of signal propagation behaviours in different frequency bands.

Once these parameters are extracted their evolution with operating time will be examined to gain insight into the gear deterioration dynamics and diagnose if any faults could happen in different components of the gearboxes.

8.4.1 Monitoring of the Higher Speed Stage of GB1

Figure 8-6 presents the evolution trends of the averaged MSB peaks at the slices of f_{m1} and their 2nd and 3rd order harmonics. Similarly, the trends were established starting at 24 hours when the data acquisition system is relatively stable and ending at 838 hours when the test was stopped because a significant change was found in several monitored feature parameters which will be depicted in the following sections.

As illustrated in Figure 8-6, all the MSB peaks associated with three mesh components from the higher speed stage transmission show little change throughout the test period. This then can indicate that the mesh quality at the end of the period maintains roughly the same as that of the initial period, or the gear set of Zr1 and Zr2 that formulates the dynamics at the first stage of GB1 have little deterioration on their tooth profiles and engagement performance. Therefore, they are regarded as being healthy.

Likewise, the MSB peak trends associated with f_{m1} also show a slight decrease. This also indicates that the manufacturing errors between Gear Zr1 and Zr2 may become less due to the effect of self-modification on the tooth profile which are formalised by the effect of gradual and dynamic wear. This dynamic wear can also be one of the reasons to account for the fluctuations of the trends.

Therefore, these little changes in both the mesh components and their sidebands indicate that the gears associated to the higher speed stage transmission in GB1 remain healthy.

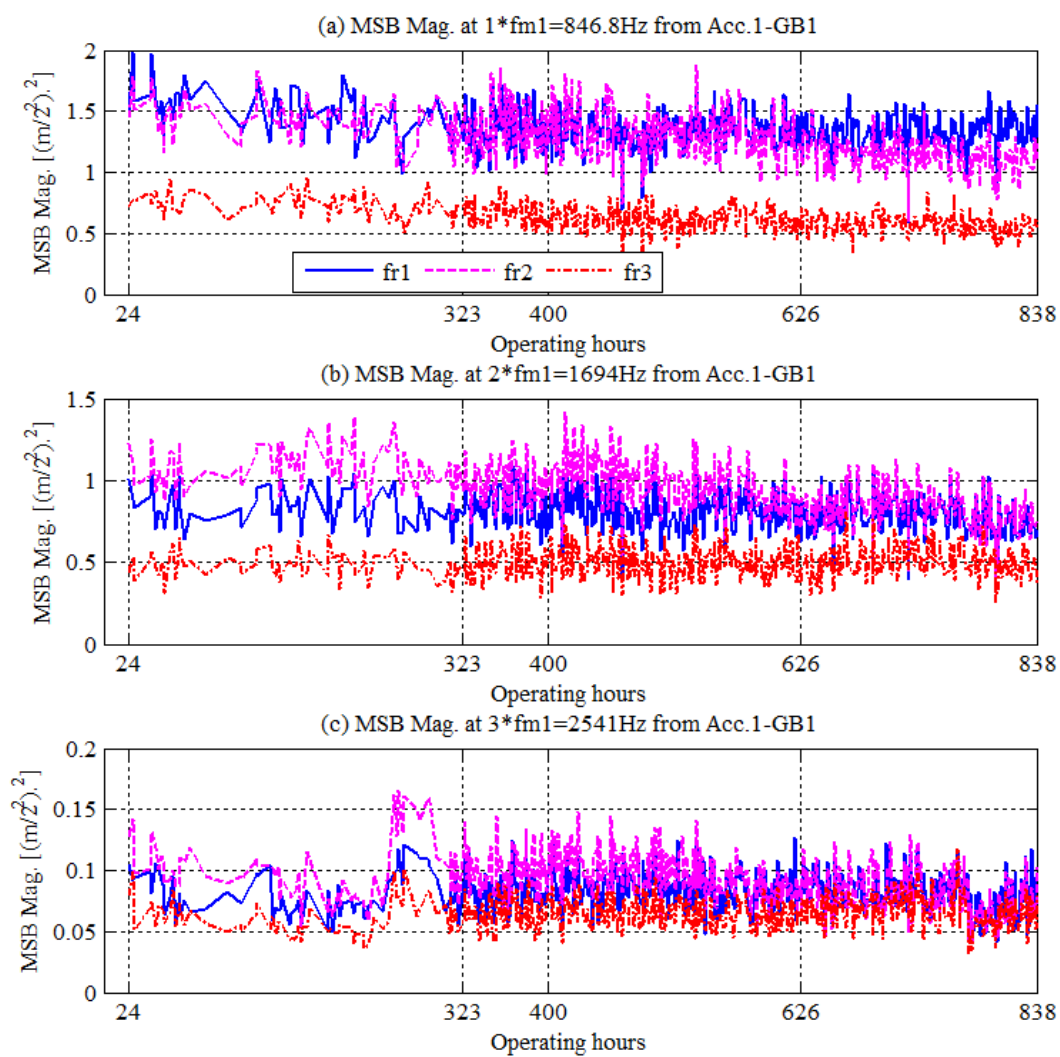


Figure 8-6 The evolution of MSB vibration peaks at rotational frequency of f_{r1} , f_{r2} and f_{r3} from f_{m1} slices for GB1

8.4.2 Monitoring of the Lower Speed Stage of GB1

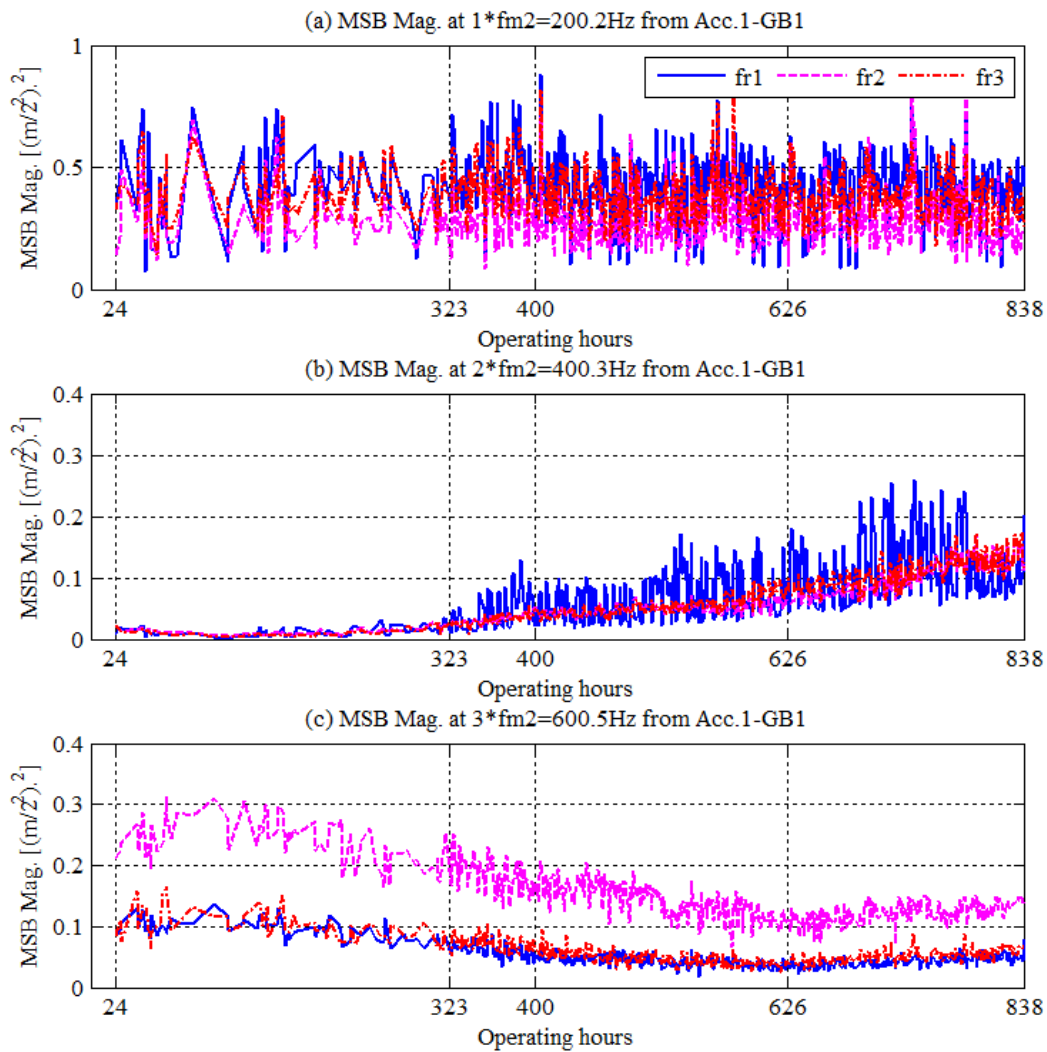


Figure 8-7 The evolution of MSB vibration peaks at rotational frequency of f_{r1} , f_{r2} and f_{r3}

from f_{m2} slices for GB1

Although there are not clear change profiles in the vibration features associated with the higher speed transmission in GB1, the MSB peak features relating to the lower speed transmission stage exhibit significant changes, which can be observed in Figure 8-7. The peaks at $2 \cdot f_{m2}$ and $3 \cdot f_{m2}$ remains similar in the period from 24 hours to 323 hours. Then, the peaks at $2 \cdot f_{m2}$ exhibit continuous increase until the end of the test, which can indicate that the dynamics of gear mesh process is becoming poor, and increasing even though the peaks at $3 \cdot f_{m2}$ exhibit

certain degrees of decreases in the period from 323 hours to 626 hours, being a result from the self-modulation. This continuous change trends at $2 * f_{m2}$ and $3 * f_{m2}$ can indicate there is considerable deterioration at the lower speed stage. In connection with the fact that the MSB peaks associated with f_{m1} slices in Figure 8-6 has little change, it can be diagnosed that the deterioration mainly happens in Gear Zr3 and Zr4 associating with f_{r2} and f_{r4} respectively.

8.4.3 Monitoring of the Lower Speed Stage of GB2

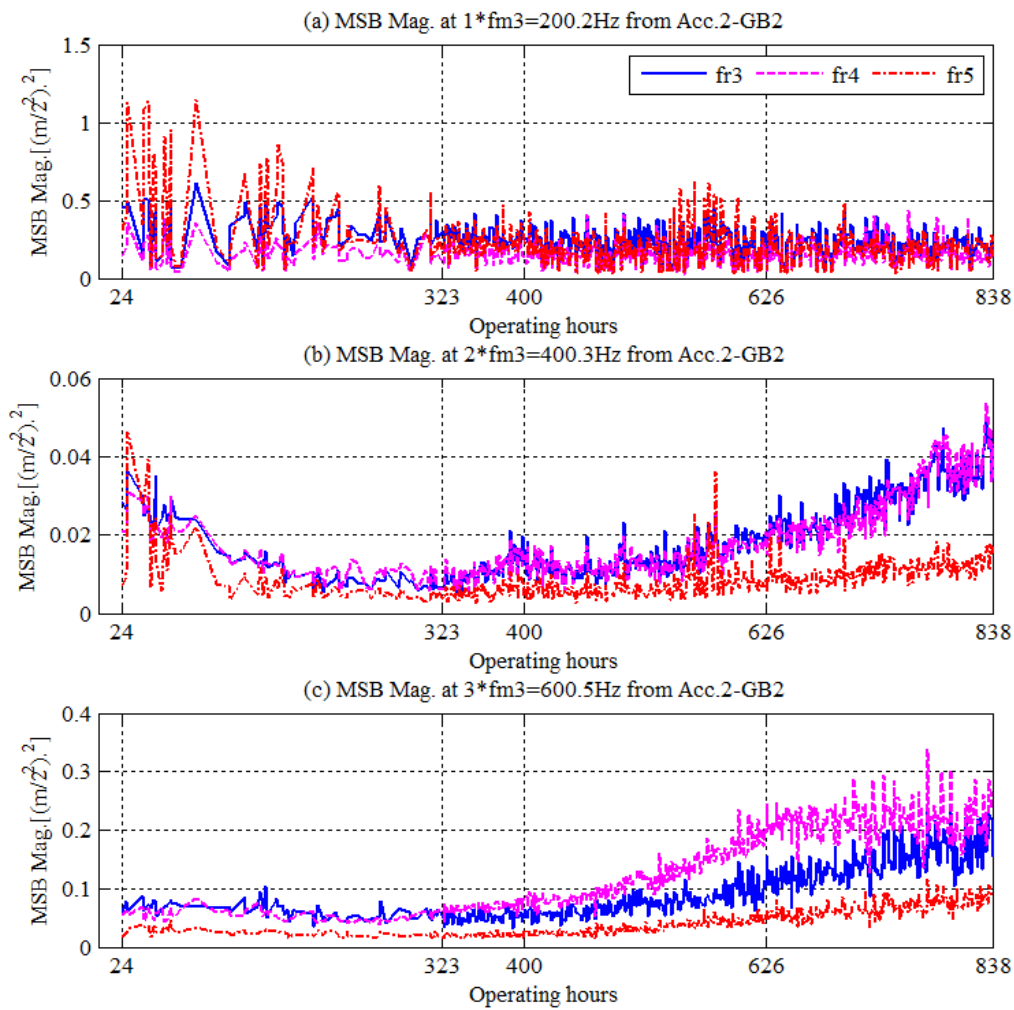


Figure 8-8 The evolution of vibration MSB peaks at rotational frequencies of f_{r3} , f_{r4} and f_{r5} from the f_{m3} slices for GB2

Figure 8-8 presents the MSB peak trends at the first three harmonics of f_{m3} for the vibration signal of GB2. Likewise, the MSB peaks at the first harmonic of mesh frequency f_{m3} do not show any definitive trends but approximately the similar amplitudes throughout the course of the test, showing that the component cannot be used for indicating the gear conditions.

However, MSB peaks at both the harmonics of $2 * f_{m3}$ and $3 * f_{m3}$ exhibit monotonic increases during the test course after the running-in process which is ended at about 323 hours. In addition, the peaks associated f_{r5} are much lower. Therefore, it can be diagnosed that there is a significant deterioration on the gear pair of Zi1 and Zi2.

Compared with the lower speed stage of GB1, this stage is considered to be slightly more severe as the peaks at both $2 * f_{m3}$ and $3 * f_{m3}$ all exhibit increases, whereas peaks only at $2 * f_{m2}$ increase with operations.

8.4.4 Monitoring of the Higher Speed Stage of GB2

Similar to the results from TSA analysis for the higher speed stage transmission in GB1 and GB2, most MSB peaks in Figure 8-9 also exhibit a slight decrease in the late test period from 626 to 838 hours. These show that the dynamic loads may become lower due to the effect of the self-modification between mesh tooth profiles.

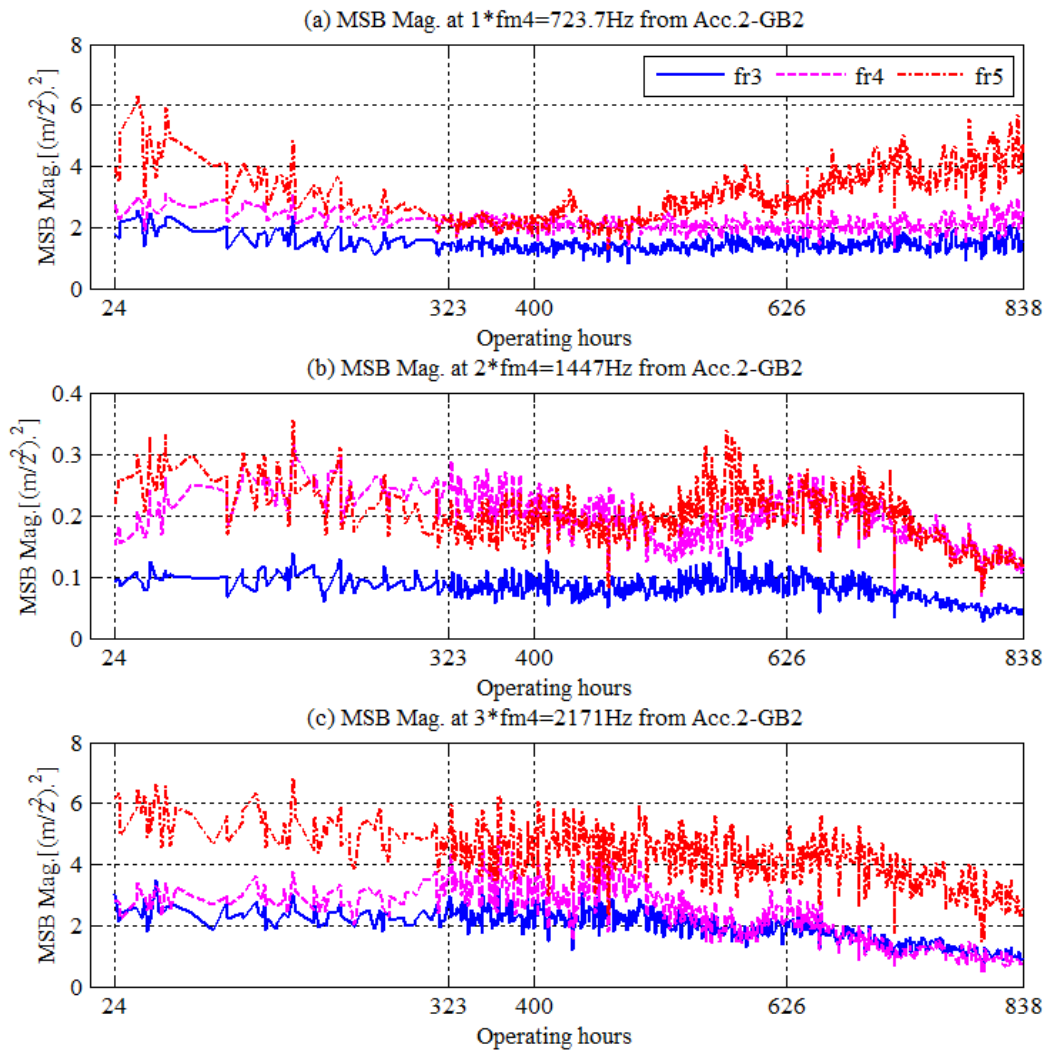


Figure 8-9 The evolution of vibration MSB peaks at f_{r3} , f_{r4} and f_{r5} from the f_{m4} slices for GB2

However, MSB peaks of f_{r5} at $1 * f_{m4}$ in Figure 8-9 (a) exhibit a clear increase in the period from 400 to 838 hours, showing that the dynamic load from f_{r5} may be higher and consequently there is also an occurrence of deterioration on the Gear Zi5 in the fifth shaft at the higher speed stage of GB2. This diagnostic result is made based on not only the significant increase in the feature values, but also the fact that the gear has certain deterioration after such a lengthy operation even if other features are reducing.

8.5 Key Findings from MSB Analysis of Vibration Signals

- The evaluation of MSB vibration analysis for monitoring multiple and multistage gearboxes has led to the following findings: The data available enabled the determination of a stable MSB result, in which noise is adequately suppressed. Higher order components which are not coupling with gear mesh dynamics are removed. As a result, the gear characteristic components can be enhanced at least as effectively as using TSA.
- The MSB peaks in the 1st three mesh components harmonics and sidebands are sufficient to reflect the progressive deterioration of the gearboxes. MSB coherence is very useful for identifying relatively small MSB magnitude peaks which are indicators of the gearbox condition and rejecting larger peaks which are not useful, but represent interference.
- The MSB peaks at different mesh slices behave differently with operating period. However, the monotonicity of increasing trends can be a reliable indicator by which to diagnose the deterioration of the gear. This occurred mainly at the lower speed transmission stages of both of the two gearboxes and on higher speed stage of the second gearbox.
- MSB analysis provides a more comprehensive diagnosis in that it allows the identification of the small defect on the rotor bars in the driving AC motor, which is not possible by using TSA as this twice slip frequency is not an integer times of the shaft rotations.

Chapter 9 MONITORING AND DIAGNOSIS OF GEARBOX DETERIORATION BASED ON THE MSB ANALYSIS OF ACOUSTIC SIGNALS

This chapter evaluates the monitoring and diagnosing of the gear deterioration performance process using an advanced MSB analysis applied to the acoustic signals available. It firstly investigates the characteristic MSB magnitude peaks found in the signals so that it correlates them with the effect of the modulation coupling between mesh components and their sidebands, which is expected to be purified sufficiently by the de-noising property of MSB. Such peaks associate with both high and low MSB coherence values but with acceptable numbers or limited frequency bands are taken as the monitoring features. Based on these features and their variations, adequate assessment of the gear deterioration progressions, within the operation period, can then be assessed.

9.1 Introduction

For the similar motivations in using MSB for analysing vibration signals, powerful MSB analysis is selected to pre-process acoustics signals for detecting and diagnosing the gear faults. As overviewed in Chapter 4, MSB representations are able to suppress noises by utilising signal phase information and results in nonlinear features to characterise modulations in signals. In addition, it can make a concise representation of the complicated modulation spectrum and allow easy analysis and numerical manipulation of characteristic features.

To utilise these superb performances of MSB analysis for gear CM, this chapter examines the MSB analysis results of acoustic signals of gearbox baseline conditions. It then examines the evolution of critical features parameters that correlates with gear dynamics in order for any fault to be detected and diagnosed in the testing gear system.

9.2 MSB Implementation for Acoustic Signals

The calculation of MSB for the two acoustic signals is the same as that of vibration signals. To ensure the results are stable when the calculation parameters and acoustic data amount available are used for MSB estimation, a comparison of the mean MSB coherences against averages, defined in Figure 8-1 of Chapter 8, are made between the vibration and the acoustic signals.

As shown in Figure 9-1 the mean values of MSB coherence exhibit a monotonic decrease with average numbers. The fast decrease for averages below 20 shows that MSB results are unstable or the random components of MSB are still significant. When the average number is about 40, the decrease is much smaller or the noise content is insignificant. Therefore, the average number of 50 can be acceptable in obtaining a stable result based on the data and calculation parameters.

Moreover, the decrease in trends for both acoustics and vibration signals are very similar. It may indicate that the noise contamination is approximately the same for the two types of signals. In another words, acoustic signals do not show every noise compared with vibrations. This can be a very interesting result to show that the acoustic signal is not as quiet as expected.

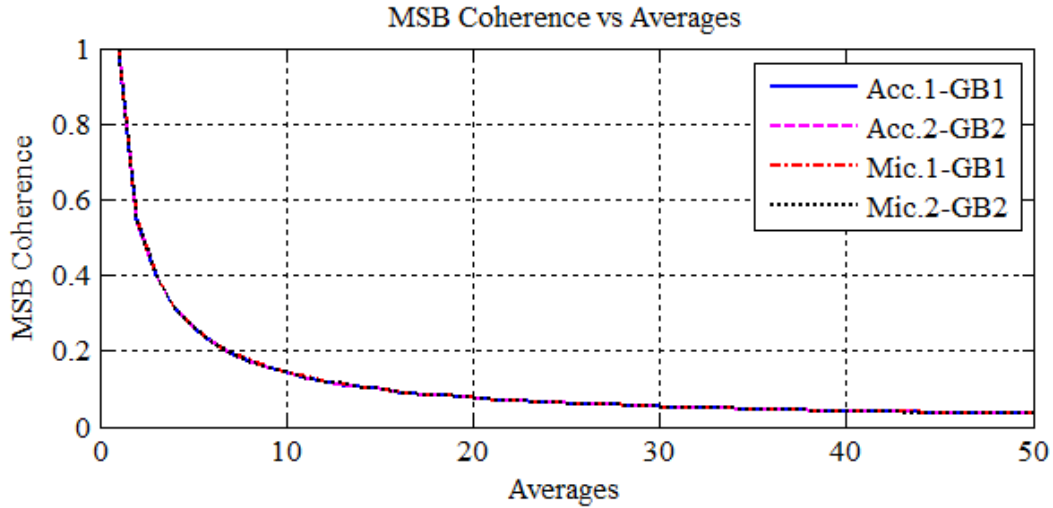


Figure 9-1 The stability of MSB estimation for acoustic and vibration signals

9.3 MSB Characteristics of Acoustic Signals

Figure 9-2 shows the MSB results of Mic.1-GB1 at operating hours of 324 hours when signal acquisition was relatively stable. For clearness and further analysis, MSB results are labelled with only the characteristic frequencies of $f_{r1} = 17Hz$, $f_{r2} = 15Hz$, $f_{r3} = 3.4Hz$, $f_{m1} = 847.4Hz$, $f_{m2} = 200.3Hz$, and their first three harmonic frequencies in the bifrequency plane, allowing the interesting peaks to be identified easily.

Although MSB magnitudes are dominant for the lower speed transmission in GB1 i.e. at $f_{m2} = 200.3Hz$ harmonics, there are still clearly significant amplitudes for the higher speed transmission i.e. $f_{m1} = 847.4Hz$. The MSB magnitudes of the first two mesh harmonics at $1 * f_{m1} = 847Hz$ and $2 * f_{m1} = 1695Hz$ are relatively significant, which are also confirmed by the high amplitudes of MSB coherence result at corresponding frequencies. The third harmonic $3 * f_{m1} = 2542Hz$ is less significant. However, there are also observable peaks that associate $f_{r2} = 15Hz$ at $3 * f_{m1} = 2542Hz$, which can be further depicted in Figure 9-4 (b) which presents three slices of the mesh components at f_{m1} . Particularly, the coherences of $3 * f_{m1} = 2542Hz$ slices show significant peaks at $f_{r2} = 15Hz$, $30Hz$ and $46Hz$.

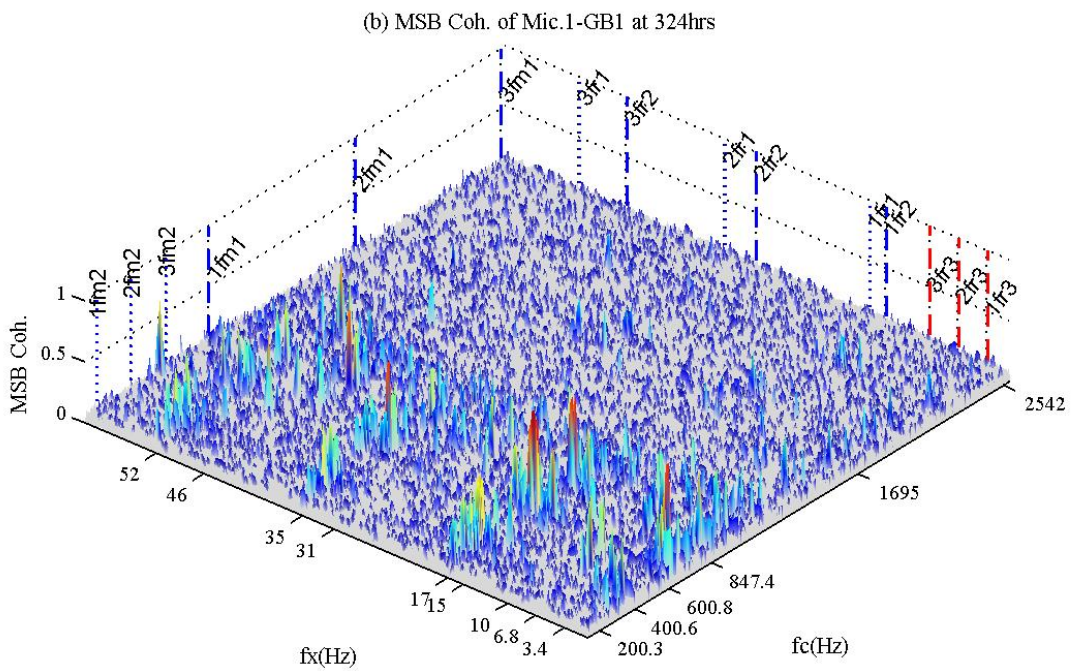
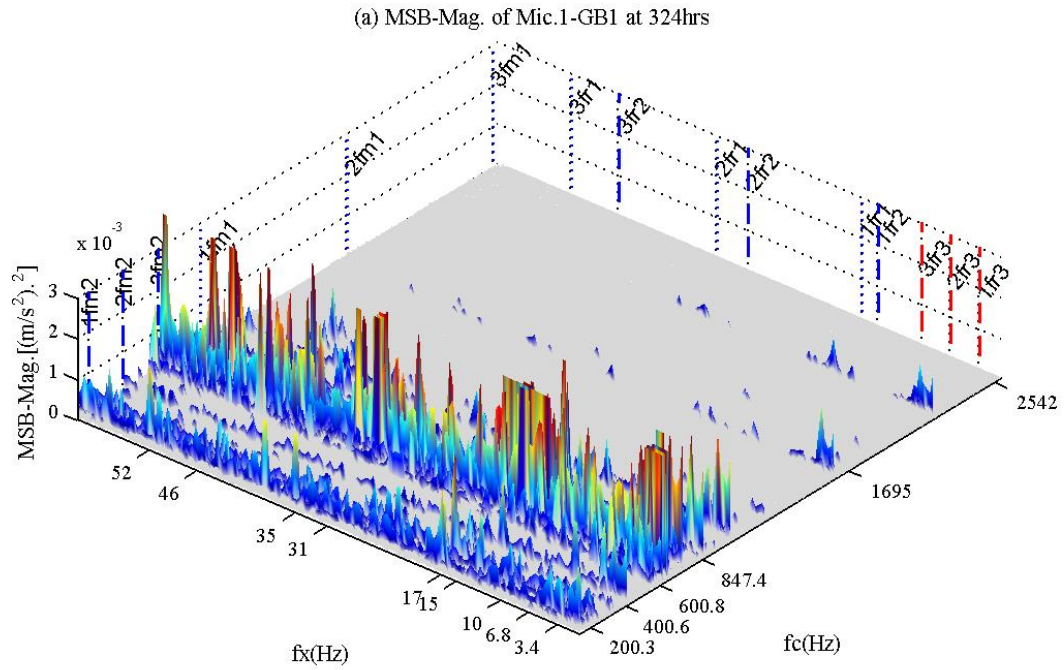


Figure 9-2 MSB magnitude and coherence results for acoustic signal from Mic.1-GB1 after an operating time of 324 hours

For the lower speed stage, the MSB magnitudes at $1 * f_{m2} = 200.3Hz$ · $3 * f_{m1} = 600.8Hz$ which looks more significant than $2 * f_{m2} = 400.6Hz$ in Figure 9-2 (a). However, when each slice was extracted, it has been found that MSB slices at $2 * f_{m2} = 400.6Hz$ and $3 * f_{m2} = 600.8Hz$ contains more components associated with three rotational frequencies of $f_{r1} = 17Hz$, $f_{r2} = 15Hz$, $f_{r3} = 3.4Hz$ and their higher order harmonics, as shown Figure 9-5. Particularly, they show clear amplitudes in both the magnitudes and coherences for the rotational frequency of $f_{r3} = 3.4Hz$, showing that these mesh components give more indication of the conditions of the lower speed gears. Conversely, the slice at $1 * f_{m2} = 200.3Hz$ contains little information relating to the rotational frequencies. This may be the reason that the sound radiation at this low frequency is very low and background interference is more, by stronger reflection of the low frequency sounds.

For GB-2, its MSB results exhibit a basic characteristic similar to GB-1. As shown in Figure 9-3, more MSB peaks present for the lower speed transmission in GB1 i.e. at $f_{m3} = 200.3Hz$ harmonics whereas the peaks are less significant for the higher speed transmission i.e. $f_{m4} = 724.1Hz$. The examination of these peaks has found they also exhibit high correlations with gear transmissions.

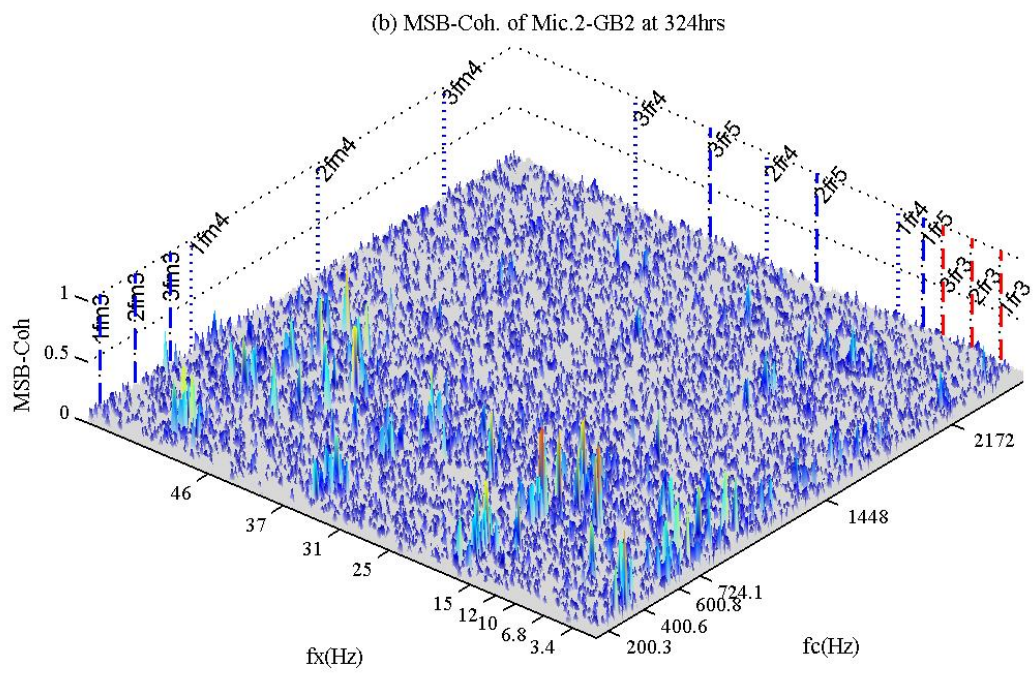
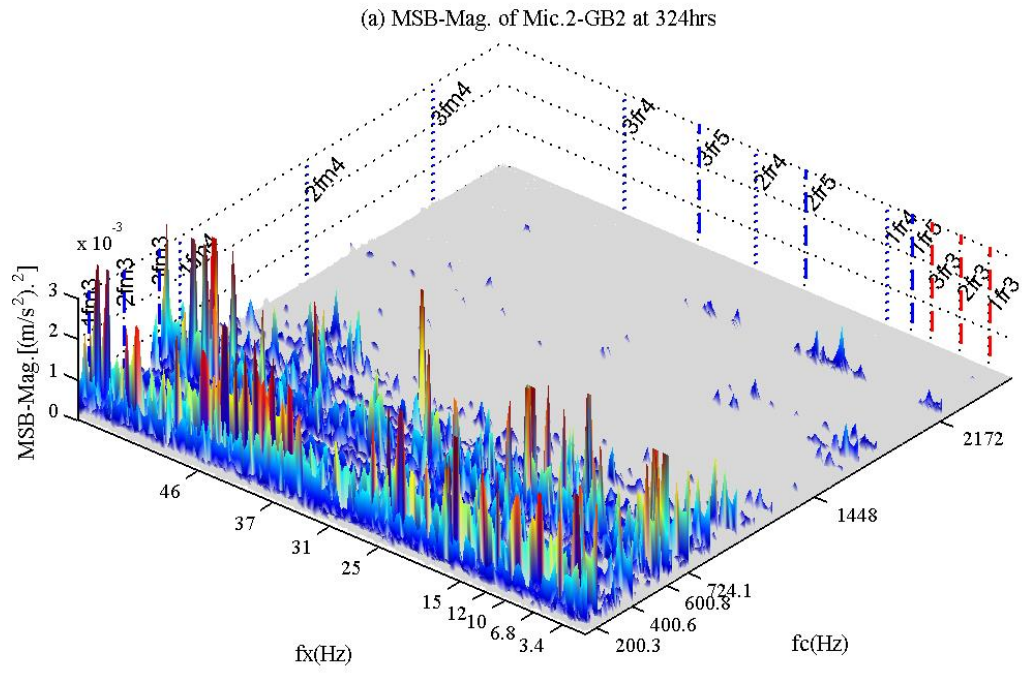


Figure 9-3 MSB results of acoustic signal from Mic.2-GB2 at the operating time of 324 hours

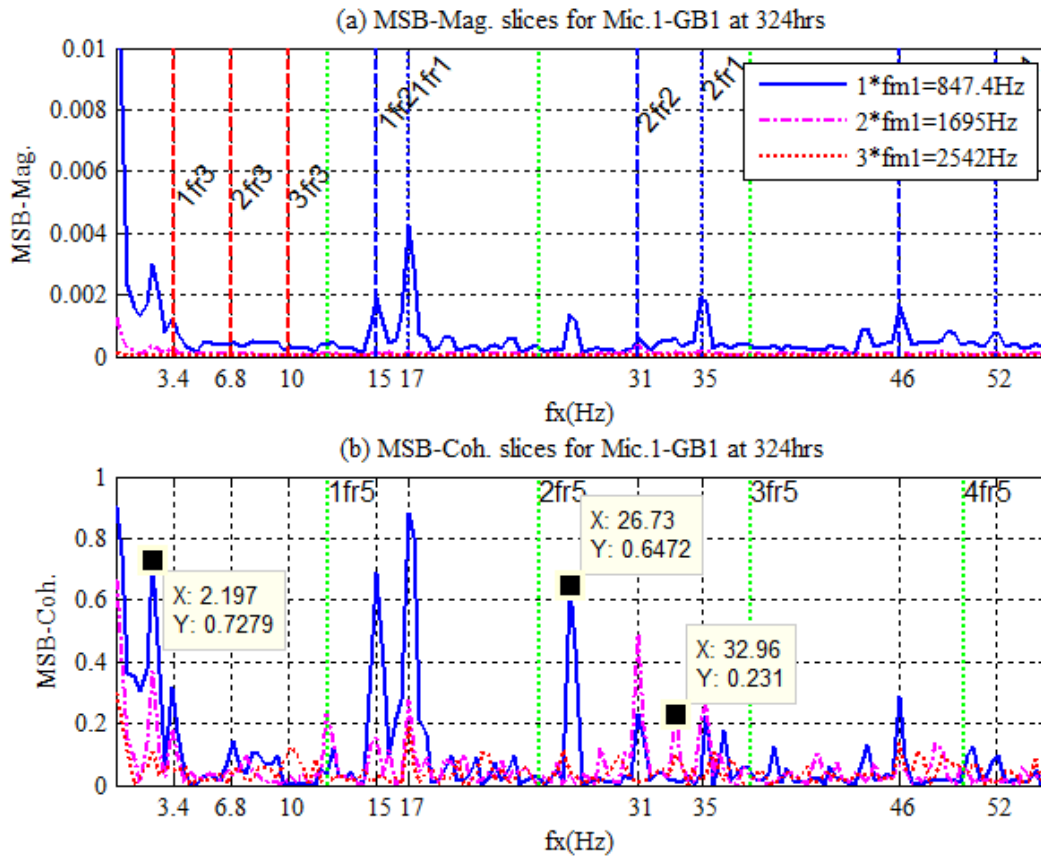


Figure 9-4 MSB slices at fm1 harmonics

In addition, the acoustic MSB results also have a very significant peak at 2.197Hz, as shown in Figure 9-4 and Figure 9-5. It has been identified to be the consequence of asymmetric rotor because this frequency value is just the twice slip frequency and decreases with a reduction in loads, which is the typical component responsible for the modulation of imperfect rotor bars to the fundamental electric supply to the induction motors [reference BRB papers]. Because of the presence of such a rotational excitation, several additional peaks such as those labelled in Figure 9-4, due to its modulation to the gear rotation motions. For example, the values of 26.73Hz results from the coupling of $2f_{r5} + 2.17Hz$.

In general, MSB results from acoustic signals contain sufficient information for monitoring the gearboxes. Considering that the insignificant peaks may emerge more with gear operations, they are also employed along with significant ones for monitoring the conditions of the gearboxes.

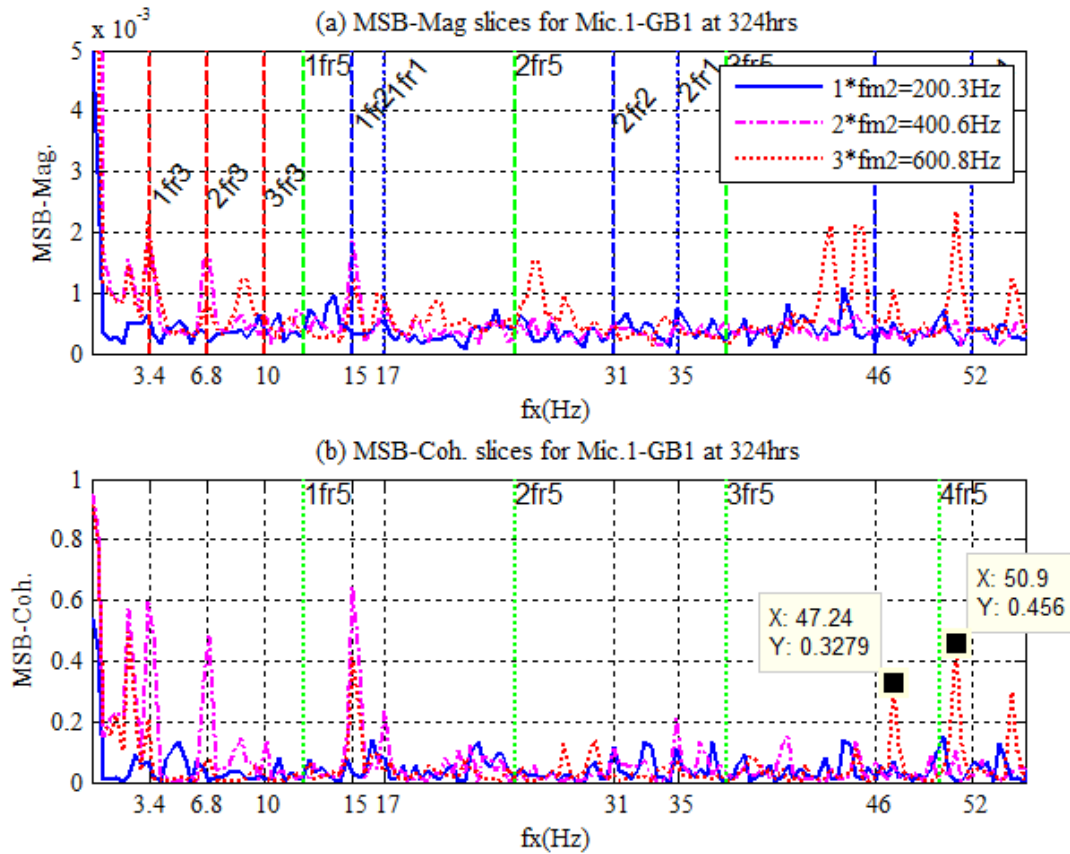


Figure 9-5 MSB slices at f_{m2} harmonics

9.4 Monitoring and Diagnosis of Gearbox Deteriorations Based on MSB Analysis of Acoustics Signals

To monitor and diagnose the health of gearboxes using MSB results from acoustic signals, the monitoring scheme adopted is the same as the vibration scheme which was addressed Chapter 8, this is because of the close connection between the vibration and acoustics. In addition, it also allows a direct comparison of monitoring performances between these two types of signals. The feature parameters are extracted from acoustic MSB results using Equation (7.1), which result in $4 \times 3 \times 3$ features, each 3×3 being constructed to monitor one of the four transmission stages.

Subsequently, a time evolution trend is built up to track the changes in these parameters in examining the gear mesh dynamic deteriorations conditions and thereby to detect whether there are any faults in the gearboxes and subsequently diagnose their locations and severities.

9.4.1 Monitoring of the Higher Speed Stage of GB1

The results presented in Figure 9-6 shows that for the higher speed transmission of GB1 MSB peaks at $3 * f_{m1} = 2541Hz$ shows a gentle increase for all three rotational frequencies. Based on this increased observation, it can be diagnosed that all the gears in GB1 may have deteriorations. However, as the overall increase in amplitudes are small, less than 50% compared with the baseline, the deteriorations are at their early stages, which takes into consideration that the monitoring features at the first two mesh components exhibit similar values throughout the operation course or even have a slight decrease at late operational phases.

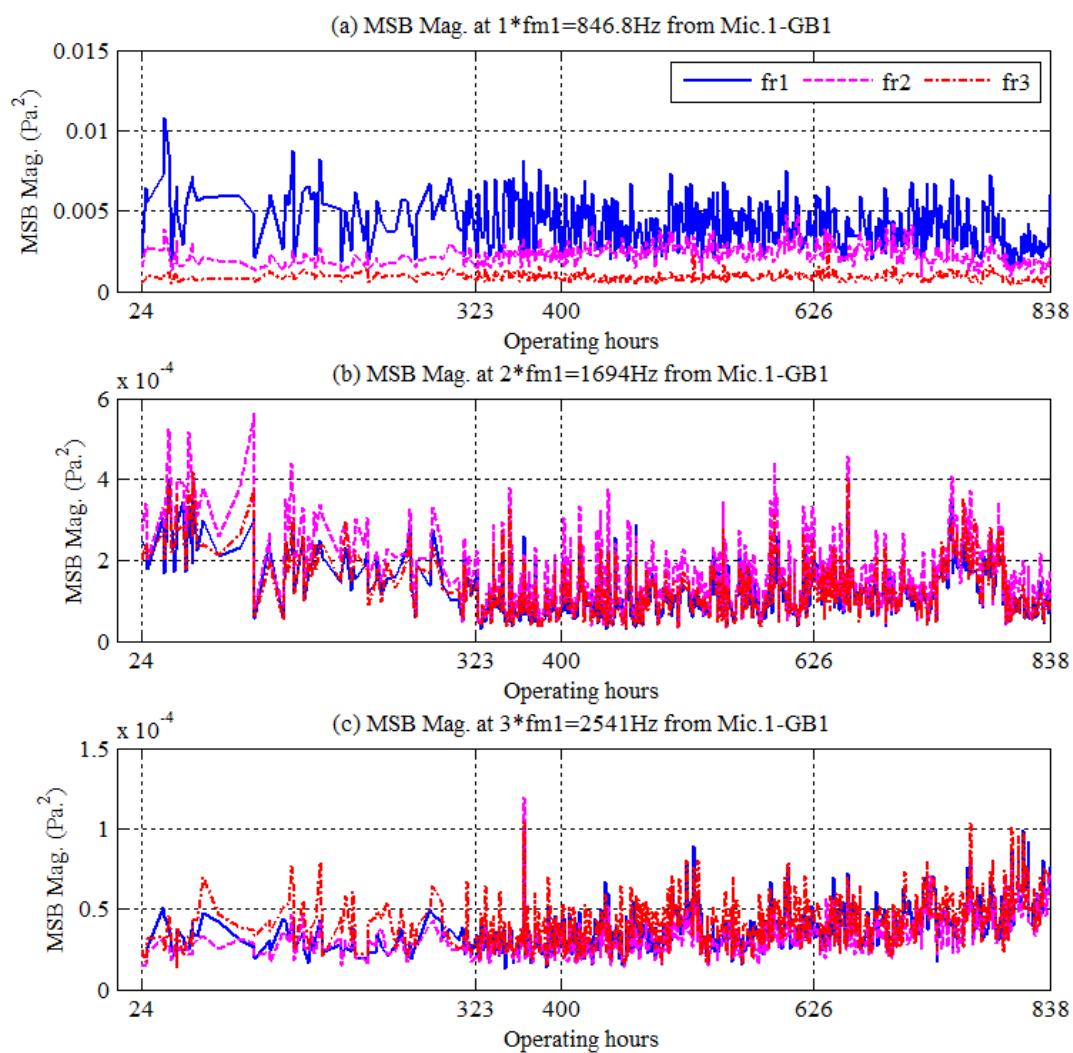


Figure 9-6 The evolution of acoustic MSB peaks at rotational frequencies of f_{r1} , f_{r2} and f_{r3}

from f_{m1} slices for GB1.

9.4.2 Monitoring of the Lower Speed Stage of GB1

Figure 9-7 presents MSB peak evolutions with time for the lower speed transmission of GB1. Similar to the changes in vibration monitoring trends, the monitoring features of mesh component of $2 * f_{m2} = 400.3Hz$ exhibit clear and monotonic increase during the whole operation periods.

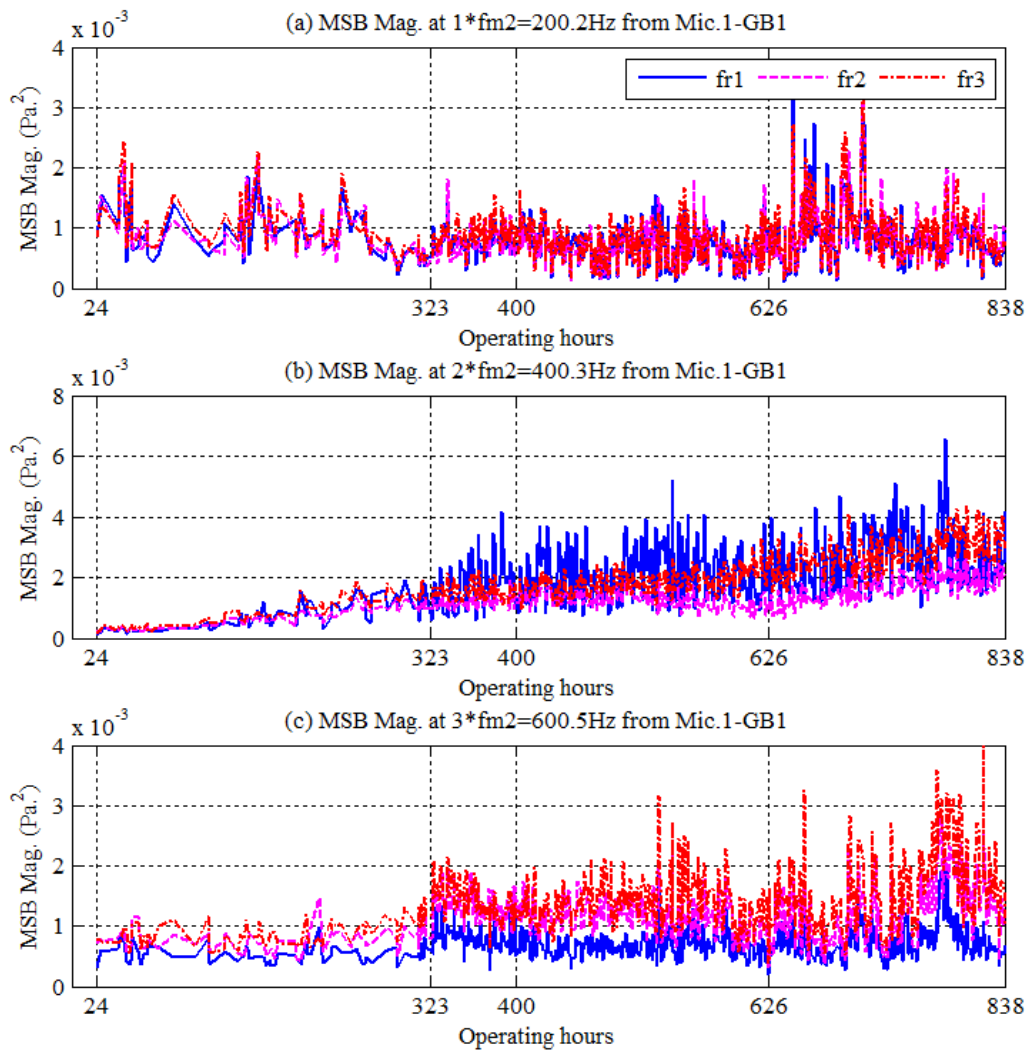


Figure 9-7 The evolution of acoustics MSB peaks at rotational frequencies of f_{r1} , f_{r2} and f_{r3} from f_{m2} slices for GB1

As the increase magnitudes are several times higher than their baselines, it is diagnosed that the gears are in GB1 all severely deteriorated. Especially gears Zr4 and Zr5 associated to

f_{r2} and f_{r3} can be faultier as the feature parameters at $3 * f_{m2} = 600.5Hz$ also exhibit largely an increase in trend. However, the gear Zr2 associated with f_{r1} only has a minor fault as the mated gear Zr1 is diagnosed to have a minor fault, as it is indicated by the smaller changes in Figure 9-6 (c) at $3 * f_{m1} = 2541Hz$.

Moreover, the deteriorations of gears Zr4 and Zr5 can be observed at the beginning of the operation. This may be due to the fact that microphones perceive more comprehensively sound signals across large regions of the gearbox housing, compared the localised signals picked up by the accelerometers.

9.4.3 Monitoring of the Lower Speed Transmission Stage of GB2

It can also be clearly observed in Figure 9-8 that three monitoring features at $2 * f_{m3} = 600.5Hz$ all exhibit a clear and monotonic increase. Based on this and the large amount of the increment, it can be diagnosed that gears Zi1 and Zi2 and associated with the lower speed transmission, a severe deterioration has been exposed.

However, gears Zi3 and Zi4 may have exhibited a very small deterioration as the increased amplitude of features at f_{r5} is relatively small. This can also be confirmed by the feature trends associated with f_{m4} in Figure 9-9 in which there has not been a definitive increase trend observed.

9.4.4 Monitoring of the Higher Speed Stage of GB2

For the higher speed transmission, all of the acoustics monitoring features in Figure 9-9 show little change. However, there is a noticeable increase in f_{r5} at $2 * f_{m3} = 600.5Hz$ observed starting at 790 hours to the end period of the test. This may indicate the consistent diagnosis that there is a small deterioration in gears Zi3 and Zi4 in section 9.4.4 and 8.4.4, which are not very significant in TSA analysis. Therefore, it shows that the acoustic signal along with MSB analysis is more sensitive to small deterioration in the gear transmission,

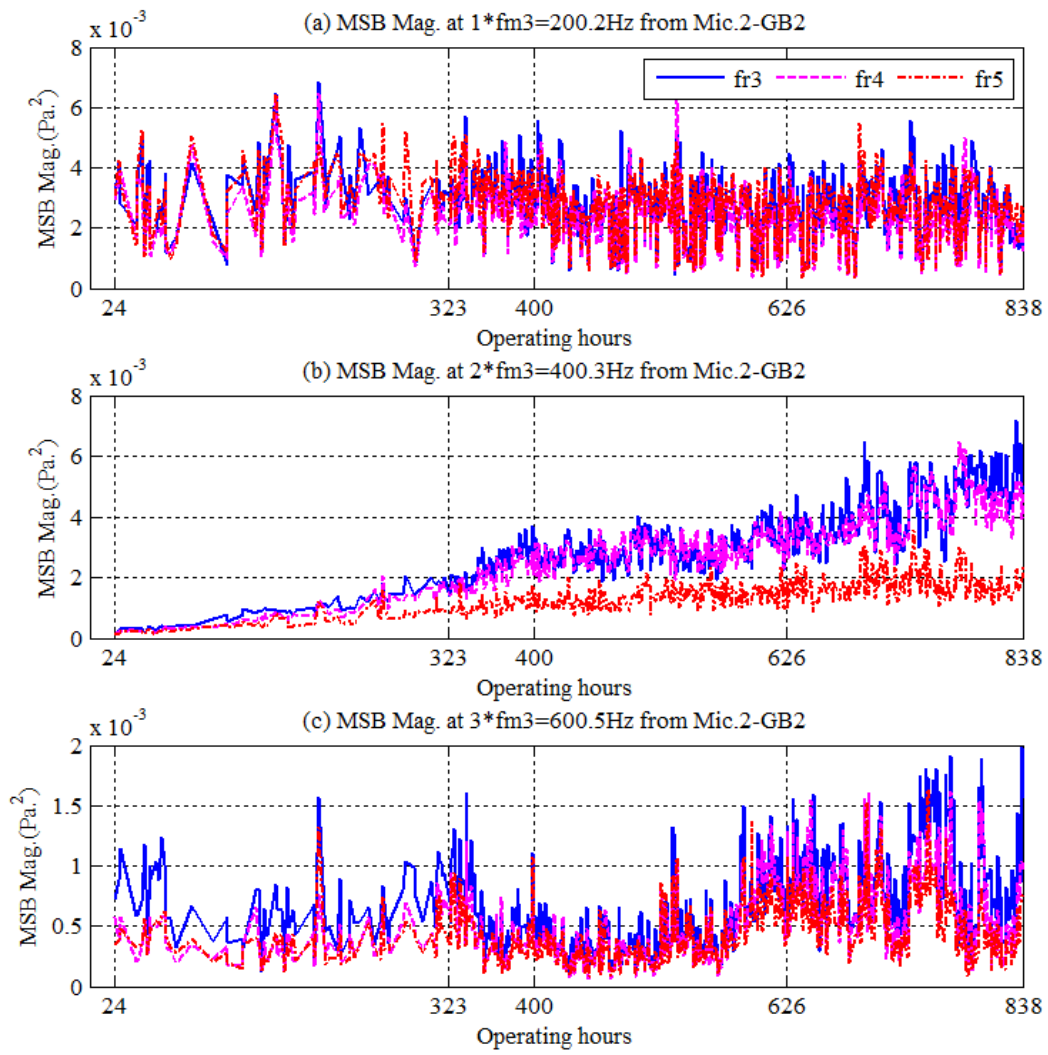


Figure 9-8 The evolution of acoustics MSB peaks at rotational frequencies of f_{r3} , f_{r4} and f_{r5} from the f_{m3} slices for GB2.

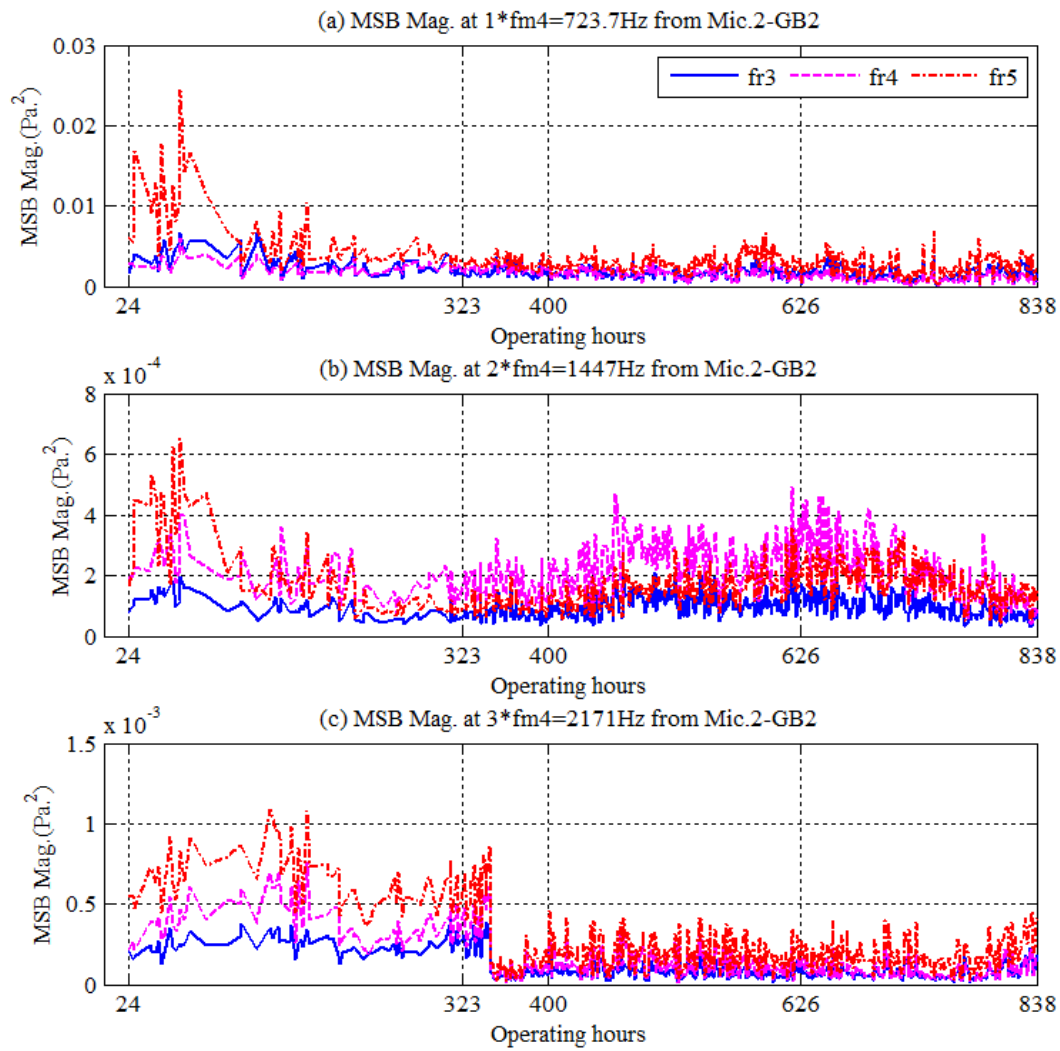


Figure 9-9 The evolution of acoustics MSB peaks at rotational frequencies of f_{r3} , f_{r4} and f_{r5} from the f_{m4} slices for GB2.

9.5 Key Findings from MSB Analysis of Acoustics Signals

The MSB analysis of acoustic signals for gearbox health monitoring has led to the following key findings:

- With the acoustic data available it is possible to obtain an MSB spectrum in which the various interfering noises are sufficiently suppressed to give accurate and stable estimates of the signal modulation due to inherent gear meshing components and fault induced sidebands. In particular, the high order electricity supply components which

are not coupling with gear mesh dynamics are excluded. As a result, the gear characteristic components are enhanced at least as as effective as when using TSA.

- The MSB peaks within first three harmonics of mesh components and sidebands are sufficient to reflect the progressive deterioration of the gearboxes. MSB coherence is important to identify small MSB magnitude peaks which truly reflect modulation effects and reject large peaks which are due not to modulation effects but noise interference with high amplitude.
- The MSB peaks at different mesh frequency slices behave differently depending on period of operation of the gearbox. However, the monotonicity of increasing trends is considered as a reference that is reliable with which to diagnose that gear deterioration has occurred. In this project this was mainly in the lower speed stages of both gearboxes and the higher speed stage of the second gearbox.
- The deteriorations that take place at the lower speeds can be also observed at the beginning of the test operation, which shows that the acoustics signal contains more comprehensive content regarding gear condition, because it is the sum of the sound radiated from a relatively large area of the gearbox housing. In contrast, the vibration may contain only the local dynamic responses of the gearbox housing.
- In addition, MSB results from acoustic signals also provide more comprehensive diagnostics in that it allows the identification of the small defect on the rotor bars in the driving AC motor, which is not possible by using TSA as this twice slip frequency is not an integer times of the shaft rotations.

Chapter 10 CONCLUSION AND FUTURE WORK

Conclusions for the entire research project and provides an explanation of how the objectives listed in Chapter 1 were achieved have been presented in this chapter. Also included are summaries of how this study has contributed to knowledge and this work novel aspects. The key results of the thesis on two stage helical gearbox CM using vibro-acoustic methods with the aid of TSA and MSB (a Higher Order Spectrum), and using numerical simulation, are drawn together. Finally, future work recommendations on the CM of gearbox transmission systems are given, that would, in the author's opinion, improve machine health monitoring and fault detection.

10.1 Review of the Objectives and Achievements

The contributions and achievements carried out during this research work have been described in this chapter. This study has emphasised the effectiveness of CM on a two-stage helical gear transmission system. Experimental studies together with theoretical analysis on gearbox acoustic and vibration signal characteristics have been conducted, and signal processing selection techniques and methods have been used in investigating the vibro-acoustic signals. The key achievements for this research have been presented in this thesis. They include:

Objective 1: To gain an in-depth understanding of gearbox CM using traditional detection and diagnostic techniques such as vibro-acoustic based spectrum analysis methods.

Achievement 1: With critical reviews made in Chapter 1 and 2, the author has gained sufficient understanding of vibro-acoustic based CM techniques. Moreover, the baseline vibration spectra of the healthy gearbox at low and high loads are examined in Chapter 6 with raw and TSA signatures. In addition, there is a detailed discussion relating to these figures. The author has successfully explored and identified all the observed frequency components that appeared in the gearbox vibration spectra indicating gear fatigue wear, and accurately linked them to their predicted sources. The author believes that this is a successful attempt to employ accurate vibration baseline spectra, including the influence of side effects such as high speeds and varied load conditions as well as manufacturing and installation errors, for fault monitoring and diagnosis in a multi-stage helical gearbox.

Objective 2: To further detail the deficiency of the traditional signal processing and methods of analysis in the frequency, time, time-frequency domains, order domains to identify the most potential techniques for analysing the noisy signals from gearboxes.

Achievement 2: With a general understanding of conventional signal analysis techniques in Chapter 2, it realised that most of these methods have deficiency in suppressing noises in measured signals, which is a decisive phase in obtaining a successful CM of gearboxes. The TSA technique is the most effective conventional way to de-noise. However, Chapter 2 highlighted that it needs additional measurement to construct the angular reference signals, which is costly and inaccurate for large power transmission system. This has been further explained in Chapters 6 and 7 when it was evaluated by the multiple gear transmission train tested. Moreover, Chapter 4 has explained how the state of art MSB can be the most potential methods to achieve simultaneous noise reduction and nonlinear feature enhancement.

Objective 3: To investigate the vibro-acoustic generation mechanisms and their characteristics of a multistage gearbox under common fault conditions.

Achievement 3: By modelling and simulation detailed in Chapters 3, the tooth wear, one of the common fault modes, cause a reduction of mesh stiffness but an increase of oscillations. Such changes often present asymmetrically across gear teeth and induce more dynamic loads and vibrations in terms of nonlinear modulations showing as sidebands in the spectrum. In addition, the vibration responses can be significantly different between measured points due to the influences of structure borne noises and transfer path resonances. In contrast, the sound field close to the gearbox but not the near field is more uniformly which reflects the overall vibration response. However, the sound fields can be affected easily by various background noises. Therefore, noise cancellation method must be applied to minimise their influences on the diagnostic information included in both the vibration and acoustics measurements.

Objective 4: To develop a realistic test scheme along with adequate test system to evaluate the vibro-acoustic based gear diagnostics proposed.

Achievement 4: The test rig facility and software for data acquisition have been developed as Chapter 5 describes. A helical reduction gearbox with two stage which, was manufactured by a company named David Brown Radicon Limited as Figure 5-1 shows, was chosen for this research study. This is because the environment where the experiment was carried out was made very similar to that of an industrial environment, close to a practical application of gearbox. Cost effective transducers: accelerometers and microphones with correct specification were used on the test rig to acquire the local and global monitoring information of the two multistage helical gearboxes. The test rig has been used in investigating the acoustic and vibration signals acquired from several locations which were used in providing experimental data to validate the derived two-stage model for the helical gearbox (Chapter 3). Moreover, a run-to-failure test programme was designed and operated successfully so that measured signals are closer to the practical applications. Finally, full gearbox test rig designs have also been provided for other research projects use.

Objective 5: To investigate the monitoring performances of using vibro-acoustics signals with conventional TSA analysis.

Based on TSA theory, Chapters 6 and 7 have suggested and evaluated an efficient implementation of TSA upon the measured vibration and acoustic signals. It allows effective

monitoring of the severer deteriorations of the lower speed transmissions in the two tested gearboxes using both the vibration and acoustics. However, it is unable to track the small fault of the higher speed transmission in the second gearbox because of large error of the constructed angular reference signal arisen from long transmission train.

Objective 6: To investigate the monitoring performances of using vibro-acoustics signals with the state of art efficient analysis such as Modulation Signal Bispectrum (MSB), which identified in Objective 2.

The state of art of MSB analysis performs outstandingly to track conditions of both the more severe deteriorations of the lower speed transmissions and smaller fault of the higher speed transmissions in the two tested gearboxes using both the vibration and acoustics. In additions, it shows that the acoustic can give an earlier indication of the deterioration progression because acoustics include wider range of dynamic responses of the gearbox housing.

Objective 7: To suggest and then recommended, for future research work activities, a guideline in this research area.

Achievement 7: The following Section 10.3 gives several useful suggestions for future research in the CM of helical gearbox using different modes of faults has been discussed and using the techniques developed in this research. In addition, preliminary work to extend the two-stage simulation model to multistage helical gear boxes has begun.

10.2 Conclusions Using Vibro-acoustics on the Gear Transmission CM

From the results and research work presented during the course of this thesis, the following conclusions have been provided:

10.2.1 Experimental System

The following have been concluded from investigating and analysing vibration signal data for the gear system:

1. The test rig, especially the two back-to-back industrial helical gearboxes, is a feasible design to operate the gearboxes under variable load and speed until they appear a natural fault.

2. The data acquisition system including the accelerometers, microphones high speed ADC used have good and reliable performances to allow for long period operation. Therefore, they can be recommended for industrial applications.
3. The time interval for collecting the dynamic data acquisition can be longer, such as four hours, which can be sufficient in capturing the slow gear deteriorations dynamic progression, rather than the one-hour interval, resulting in too many data. In the meantime, the data length could be 30% longer to increase more averages for more reliable TSA and MSB analysis.

10.2.2 Conclusions on CM Using TSA

TSA analysis of vibration signals and acoustics signals allows for accurate monitoring and diagnosis results of the deterioration in the lower speed transmission of both the tested gearboxes. However, it cannot give out the correct indication of the higher speed stages in the second gearbox, as there are errors in the reference angle signal due to the long transmission train. In addition, acoustic signals can indicate that there is a small determination in the higher speed transmission of the first gearbox.

10.2.3 Conclusions on CM Using MSB

The MSB analysis vibration signals and acoustics for more corrective monitoring and diagnosis results of the deterioration in the four stages of transmissions of the two tested gearboxes. Both of the two lower speed transmissions show monotonic increases with operation time and the increments are over at least three times higher than the baselines. So the deteriorations are regarded as severe. For the two higher speed transmissions, the MSB of vibration and acoustics is able to shows small of deteriorations in the late operating hours.

10.2.4 Conclusions on Modelling for Gearbox Vibro-acoustic Analysis

The lumped vibration model is sufficiently accurate to achieve an in-depth understanding of the interconnection between the internal mesh dynamic loads and the external vibro-acoustics. Particularly, it is adequate to model the wear effect with a modified tooth stiffness that results in more modulations and thereby sidebands in vibration and acoustics spectra.

10.3 Contribution to Knowledge and Novel Feature Summary

The research thesis has incorporated a number of significant features that are novel and has never been implemented previously in the subject of using vibro-acoustics for gearbox CM by any other practitioners or researchers. These novelty aspects have been summarised below.

- **First Novel Feature:** For this research, it is believed by the author that the way in which vibro-acoustic signals were acquired from the run-to-failure test of two multistage gearboxes is the first time adopted in gear CM research community. Especially, the variable load and speed applied to the gearbox are very close to practical applications and therefore, the signals are more reliable.
- **Second Novel Feature:** The proposed single encoder based TSA scheme used in this research for multiple stages of gear transmissions is novel and effective for more severe faults. No work describing any detail of both the advanced and traditional analysis of vibration has been found for different operation conditions of gear in the same way.
- **Third Novel Feature:** It is the first time for the use of vibration and acoustics to trace a full course of gearbox deteriorations which happen naturally.
- **Fourth Novel Feature:** The successful remote monitoring of gearbox deteriorations is novel by using acoustic airborne gearbox. No previous work describing the full deterioration process, though some feasibility studies reported has been found in the fields.
- **Fifth Novel Feature:** The use of MSB is novel in that it systemically is investigated to successfully monitor the full course of the deterioration.

10.4 The Contributions to Knowledge

- **The 1st Contribution:** The MSB peaks from the 1st three mesh components and sidebands harmonics are sufficient to indicate the gear deteriorations. Amongst them at least one of them can exhibit monotonic increases with operating time to indicate the deterioration evolution and predict the remaining life. Others may exhibit certain fluctuations because of the self-tooth modification of wear effect.
- **The 2nd Contribution:** A single encoder based TSA analysis can only be effective up to the gears close to the encoder. The detection performances can be significantly poor for the remote gears due to the accumulated effect of angular modulations of multiple transmission stages.

- **The 3rd Contribution:** Remotely acquired acoustics signals can include the sound radiated from a large area of vibrations and thereby are more sensitive to the faults at early stage, compared with the accelerations from a localised response that can be distorted by the structure noise and resonances.
- **The 4th Contribution:** The direct comparison of monitoring performance between vibration and acoustic measurements shows that both can be achieved by accurate monitoring of the gearbox. However, acoustics outperforms vibration, in that it included more compressive information which allows a comprehensive capture to reflect overall dynamic behaviours of the gearboxes.

10.5 Future Work Recommendations on the Gearboxes CM Using Vibro-acoustics:

The use of Time Synchronous Averaging and modulating signal bispectrum analysis for vibro-acoustic has been shown to be an appropriate technique in monitoring the health and in detecting a two stage helical gearbox faults and can be used as a reliable technique in obtaining adequate reference information regarding the condition of the gearbox. This research author has pointed to a number of recommendations for further improvement of vibro-acoustic using the MSB method in gearbox CM.

- **First Recommendation:** In furtherance to evaluating the reliability and sensitivity of the proposed method for detection on a simpler gearbox, (e.g. a gearbox with single stage), more experimental work would be needed to gain a more inclusive understanding on the path transmission effect on the acoustic and vibration signals.
- **Second Recommendation:** Since there is difference in characteristics of gear for the same size and type of gears, faults on same gear should be simulated for both faulty and healthy conditions. The spectrum identical gears characteristics should be examined in more detail as results have shown from this research that identical gears can apparently still produce different acoustic and vibration sound spectrums components.
- **Third Recommendation:** It is difficult in distinguishing the health conditions of the gear accurately when the vibration signal has a low SNR. In future work, higher features of dimension containing more information should be considered in achieving a more robust performance at varying conditions of operating.
- **Fourth Recommendation:** The proposed technique (vibro-acoustic using TSA and MSB) should be extended to include different gearbox types e.g. planetary, worm, bevel gear with different faults in gear and at their different severity levels.

- ***Fifth Recommendation:*** Future work should be conducted on simultaneous faults at the same stage and at different stages of the gearbox.

REFERENCES

1. Morris, R. and F. Pardue, *The Reliability Based Maintenance Strategy, A Vision for Improving Industrial Productivity*, Computational Systems Incorporated (CSI), in Knoxville Tennessee. 1994: USA.
2. Sondalini, M., *Plant and Equipment Wellness Rapid Success in Implementation and Sustaining Operational Excellence lifetime-reliability*. 2003.
3. Sondalini, M. *Equipment Maintenance Management Strategy 101* 2003 11 March]; Available from: Lifetime-reliability.com.
4. Sondalini, M., *Condition Based Maintenance Strategy*©. 2004, Copyright lifetime-reliability. com.
5. Fan, X. and J. Wang, *Improving Equipment Reliability in Non-operating State with an Integrated Prognostics Method: A Case Study of HLD-9C*. 2013.
6. Grall, A., C. Berenguer, and L. Dieulle, *A condition-based maintenance policy for stochastically deteriorating systems*. Reliability Engineering & System Safety, 2002. **76**(2): p. 167-180.
7. Ressler, K.J., S.L. Sullivan, and L.B. Buck, *Information coding in the olfactory system: evidence for a stereotyped and highly organized epitope map in the olfactory bulb*. Cell, 1994. **79**(7): p. 1245-1255.
8. Syuhaida, I. and M.Y. Aminah, *Benchmarking the performance of Malaysia's construction industry*. Management Research and Practice, 2009. **1**(1): p. 1-13.
9. Sondalini, M. *Plant and Equipment Wellness Rapid Success in Implementation and Sustaining Operational Excellence lifetime-reliability* 2003.
10. Bayder, N., *The Vibration-Acoustic Monitoring of Gearboxes*. 2000, University of Manchester: Manchester.
11. Hudachek, R. and V. Dodd. *Progress and Payout of a Machinery Surveillance and Diagnostic Program*. in *Mechanical Engineering*. 1977. Asme-Amer Soc Mechanical Eng 345 e 47th St, New York, 10017.
12. Wright, D., *Notes on design and analysis of machine elements*. 2001: Department of Mechanical and Materials Engineering, The University of Western Australia.
13. Shigley, J., C. Mischke, and R. Budynas, *6-4 Maximum-Shear-Stress Theory for Ductile Materials*. Mechanical Engineering Design, 2004: p. 259.
14. Engineers, U.S.A.C.o., *Engineering and Design - Lubricants and Hydraulic Fluids*. 1999, Army Corps of Engineers
15. Park, C. and J.M. Lee, *The load transmission and vibration characteristics of automobile gear*. 1993, SAE Technical Paper.
16. Regeai M N *Helical Gearbox Fault Detection Using Motor Current Signature Analysis*. 2007, The University of Manchester: Manchester.
17. Wang, W. and P. McFadden, *Decomposition of gear motion signals and its application to gearbox diagnostics*. Journal of vibration and Acoustics, 1995. **117**(3A): p. 363-369.

18. Tavakoli, M. and D. Houser, *Optimum profile modifications for the minimization of static transmission errors of spur gears*. Journal of Mechanical Design, 1986. **108**(1): p. 86-94.
19. Dudley, D.W. and D.P. Townsend, *Dudley's gear handbook*. 1991: Tata McGraw-Hill Education.
20. Ren, L., F. Da, and C. Zhaoyang, *Energy-saving & Control of Tunnel Illumination [J]*. Highway Engineering, 2007. **5**: p. 049.
21. Shigley, J.E., *Shigley's mechanical engineering design*. 2011: Tata McGraw-Hill Education.
22. Al-Arbi, S., *CM of gear systems using vibration analysis*. 2012, University of Huddersfield PDH 2012.
23. A. Bhatia, B.E., *Basic Fundamentals of Gear Drives*. PDHonline Course M229 (4 PDH), 2012.
24. Davis, J.R., *Gear materials, properties, and manufacture*. 2005: ASM International.
25. Errichello, R., R. Budny, and R. Eckert, *Investigations of bearing failures associated with white etching areas (WEAs) in wind turbine gearboxes*. Tribology Transactions, 2013. **56**(6): p. 1069-1076.
26. Barnes, M. *Precision Gear Lubrication Building a Foundation for Reliability - PART I*. iLearn Reliability [cited 2014 25-march]; Available from: http://reliabilityweb.com/index.php/print/precision_gear_lubrication_building_a_foundation_for_reliability.
27. Al Tubi, I., *Effects of Variable Load and Rotational Speed Conditions on Gear Micropitting in Wind Turbine Gearboxes*. 2014, University of Sheffield.
28. Ham, C.W., *Mechanics of machinery*. 1958: McGraw-Hill.
29. Smith, T., J. Willetts, and C. Mitchell, *An integrating framework for sustainable communities: exploring the possibilities and challenges*. 2007.
30. Bhushan, B. and O. Marti, *Scanning probe microscopy—principle of operation, instrumentation, and probes*. 2010: Springer.
31. Divakar, R., *Wear testing of advanced materials*. Vol. 1167. 1992: ASTM International.
32. Wulpi, D.J., *Understanding how components fail*. 2013: ASM international.
33. Izciler, M. and M. Tabur, *Abrasive wear behavior of different case depth gas carburized AISI 8620 gear steel*. Wear, 2006. **260**(1-2): p. 90-98.
34. Janakiraman, V., S. Li, and A. Kahraman, *An investigation of the impacts of contact parameters on wear coefficient*. Journal of Tribology, 2014. **136**(3): p. 031602.
35. Attia, M.H. and R.B. Waterhouse, *Standardization of fretting fatigue test methods and equipment*. 1992: ASTM International.
36. Gagg, C.R. and P.R. Lewis, *Wear as a product failure mechanism—overview and case studies*. Engineering Failure Analysis, 2007. **14**(8): p. 1618-1640.
37. Al-Tubi, I., et al., *Experimental and analytical study of gear micropitting initiation and propagation under varying loading conditions*. Wear, 2015. **328**: p. 8-16.
38. Yesilyurt, I., Gu, Fengshou, Ball, Andrew D., *Gear tooth stiffness reduction measurement using modal analysis and its use in wear fault severity assessment of spur gears*. NDT & E International, 2003. **36**(5): p. 357-372.

39. Winter, H. and T. Placzek, *Fundamentals of Gear Design by Raymond J. Drago* (Butterworths, Stoneham MA, USA, 1988) 576 pages, hardcover, £E54.00. *Journal of Synthetic Lubrication*, 1989. **6**(3): p. 256-256.
40. Hamzah, R.I.R., *xperimental Determination of Non Load Dependent Losses for A Dip Lubricated Worm Type Gear Unit: Gear Churning and Windage Losses*, in *School of Engineering*. 2004, Cranfield University: Cranfield
41. Oila, A. and S. Bull, *Assessment of the factors influencing micropitting in rolling/sliding contacts*. *Wear*, 2005. **258**(10): p. 1510-1524.
42. Lainé, E., et al., *The effect of a friction modifier additive on micropitting*. *Tribology Transactions*, 2009. **52**(4): p. 526-533.
43. Radzevich, S.P. and D.W. Dudley, *Handbook of practical gear design*. 1994: CRC press.
44. Troyer, D., *Contamination monitoring for maximum uptime*. 1996, The Machinery Publishing Co.
45. Ribrant, J. and L. Bertling. *Survey of failures in wind power systems with focus on Swedish wind power plants during 1997-2005*. in *Power Engineering Society General Meeting, 2007. IEEE*. 2007. IEEE.
46. Davies, A., *Handbook of CM: techniques and methodology*. 2012: Springer Science & Business Media.
47. Willetts, R., *Holistic CM*. 2002, University of Manchester: Manchester. p. 247.
48. Weidong, L., *A Study of Diesel Engine Acoustic Characteristics*, in *Department of Mechanical*. 2000, Manchester School of Engineering: Manchester.
49. Liang, B., *CM and Fault Diagnosis of Induction Motors*, in *Mechanical Engineering*. 2000, Manchester School of Engineering: Manchester UK.
50. Matthew, J., *Machine CM Using Vibration Analysis*, in *Acoustic Australia*. 1987: Australia. p. 7 13.
51. Kelly, A., *Maintenance strategy*. 1997: Elsevier.
52. Management., I.I.f.P. *Wear Debris Analysis*. Indian Institute for Production Management [cited 2014; Available from: <http://www.iipm.ac.com>
53. Huang, K. and T. Liu, *Dynamic analysis of a spur gear by the dynamic stiffness method*. *Journal of Sound and Vibration*, 2000. **234**(2): p. 311-329.
54. R Willetts 2002, H.c.m., PhD thesis, University of Manchester, number: M0174866MU, 247 p., *Holistic CM*. 2002, University of Manchester: Manchester. p. 247.
55. Doctor, C. *Corrosion Monitoring. Sponsored by MATCO associates*. Corrosion Doctor 1999 [cited 2014 21 March]; Available from: <http://www.corrosion-doctors.org/MonitorBasics/Introduction.htm>.
56. Dittmaier, S., Mariotti, C., Passarino, G., Tanaka, R., Alekhin, S., Alwall, J., ... & Chanon, N. (2012). Handbook of LHC Higgs cross sections: 2. Differential distributions. *arXiv preprint arXiv:1201.3084*.
57. Mobley, R.K., *An introduction to predictive maintenance*. 2002: Butterworth-Heinemann.

58. Ramroop, G., et al. *Airborne Acoustic CM of a Gearbox System*. in *2001 5th Annual Maintenance and Reliability Conference (MARCON 2001)*. 2001.
59. Runkel, J., et al., *CM of Industrial Machines, Institute of Nuclear Engineering and Non-destructive Testing*. 1996: Hannover Germany.
60. Li, Z., S. Akishita, and T. Kato, *Engine failure diagnosis with sound signal using wavelet transform*. 1997, SAE Technical Paper.
61. Li, W., et al., *A study of the noise from diesel engines using the independent component analysis*. *Mechanical Systems and Signal Processing*, 2001. **15**(6): p. 1165-1184.
62. Gu, F. and A. Ball, *Enhancement of the Fourier Spectrum of Acoustic Signals for Machinery CM*. 1998, Research Report, The University of Manchester.
63. Gu, F. and A. Ball, *Estimation of Noise Corrupted Diagnostic Components Using a Robust Kalman Filter*. 1998, Research Report, The University of Manchester.
64. Gu, F., et al., *The CM of diesel engines using acoustic measurements part 1: acoustic characteristics of the engine and representation of the acoustic signals*. 2000, SAE Technical Paper.
65. Ball, A., F. Gu, and W. Li, *The CM of diesel engines using acoustic measurements part 2: fault detection and diagnosis*. 2000, SAE Technical Paper.
66. Li, W., et al., *Acoustic based CM of a diesel engine using self-organising map networks*. *Applied acoustics*, 2002. **63**(7): p. 699-711.
67. Albarbar, A., et al., *Acoustic monitoring of engine fuel injection based on adaptive filtering techniques*. *Applied Acoustics*, 2010. **71**(12): p. 1132-1141.
68. Jiang, J., et al., *Monitoring of diesel engine combustions based on the acoustic source characterisation of the exhaust system*. *Mechanical Systems and Signal Processing*, 2008. **22**(6): p. 1465-1480.
69. Yih-Hsing, P., R.G. Ralph, and N.C. Ahmet, *Acoustic emission and transient waves in an elastic plate*. *The Journal of the Acoustical Society of America*, 1979. **65**(1): p. 96-105.
70. Al-Ghamd, A.M. and D. Mba, *A comparative experimental study on the use of acoustic emission and vibration analysis for bearing defect identification and estimation of defect size*. *Mechanical Systems and Signal Processing*, 2006. **20**(7): p. 1537-1571.
71. Qu, Y., et al. *Development of a new acoustic emission based fault diagnosis tool for gearbox*. in *Prognostics and Health Management (PHM), 2013 IEEE Conference on*. 2013. IEEE.
72. Tandon, N. and B. Nakra, *Defect detection in rolling element bearings by acoustic emission method*. *Journal of Acoustic Emission*, 1990. **9**(1): p. 25-28.
73. Tan, C., *Application of acoustic emission to the detection of bearing failures*. 1990.
74. Yan, D., T. El-Wardany, and M. Elbestawi, *A multi-sensor strategy for tool failure detection in milling*. *International Journal of Machine Tools and Manufacture*, 1995. **35**(3): p. 383-398.
75. Droge, M. *Recommended practice for acoustic emission testing of fiberglass reinforced plastic piping systems*. in *Proceedings of the 1st international symposium on Acoustic Emission from reinforced composites*. 1983.

76. Adams, C.H. *Recommended practice for acoustic emission testing of fiberglass tanks/vessels*. in *37th Annual Conference, Reinforced Plastics/Composites Institute*. 1982. the Society of the Plastics Industries, Inc.
77. Lee, J., D. Choi, and C. Chu, *Real-time tool breakage monitoring for NC turning and drilling*. *CIRP Annals-Manufacturing Technology*, 1994. **43**(1): p. 81-84.
78. Edwards, D.J., G.D. Holt, and F. Harris, *Predictive maintenance techniques and their relevance to construction plant*. *Journal of Quality in Maintenance Engineering*, 1998. **4**(1): p. 25-37.
79. Gu, F. and A. Ball, *Vibration Based Fault Diagnosis in Diesel Fuel Injection System*, in *IMEchE Seminar on Diesel Fuel Injection Systems*. 1995: London. p. 89-97.
80. Nandi, A., *Vibration Based Fault Detection Features Classifiers and Novelty Detection*, in *COMADEM*. 2002, Proc. CM and Diagnostic Engineering Management: Birmingham, UK. p. 23 - 36.
81. Troyer, D.D. and M. Williamson. *Effective integration of vibration analysis and oil analysis*. in *Proceedings of the International Conference on CM, University College of Swansea, Swansea, UK*. 1999.
82. Goldman, S., *Vibration spectrum analysis: a practical approach*. 1999: Industrial Press Inc.
83. Dalpiaz, G., A. Rivola, and R. Rubini, *Effectiveness and sensitivity of vibration processing techniques for local fault detection in gears*. *Mechanical systems and signal processing*, 2000. **14**(3): p. 387-412.
84. Meltzer, G. and N.P. Dien, *Some new advances in gear diagnostics by application of the wavelet transform*. *Strojnícky Časopis*, 2003. **54**(3): p. 129-148.
85. Jiang, J. and B. Zhang, *Rolling element bearing vibration modeling with applications to health monitoring*. *Journal of Vibration and Control*, 2012. **18**(12): p. 1768-1776.
86. Tavner, P., *Review of condition monitoring of rotating electrical machines*. *Electric Power Applications*, IET, 2008. **2**(4): p. 215-247.
87. Peng, Z. and F. Chu, *Application of the wavelet transform in machine CM and fault diagnostics: a review with bibliography*. *Mechanical Systems and Signal Processing*, 2004. **18**(2): p. 199-221.
88. Forrester, B.D., *Advanced vibration analysis techniques for fault detection and diagnosis in geared transmission systems*. 1996, Swinburne University of Technology Melbourne, VIC, Australia.
89. Tandon, N. and A. Choudhury, *A review of vibration and acoustic measurement methods for the detection of defects in rolling element bearings*. *Tribology international*, 1999. **32**(8): p. 469-480.
90. Lebold, M., et al. *Review of vibration analysis methods for gearbox diagnostics and prognostics*. in *Proceedings of the 54th Meeting of the Society for Machinery Failure Prevention Technology*. 2000.
91. Swansson, N., *Application of Vibration Signal Analysis Techniques to CM*. 1980.
92. Jayaswal, P. and A. Aherwar, *Fault Detection and Diagnosis of Gear Transmission System via Vibration Analysis*. 2012.
93. Stewart, R.M., *Application of signal processing techniques to machinery health monitoring*. 1980: Institute of Sound and Vibration Research.

94. Forrester, B.D., *Advanced vibration analysis techniques for fault detection and diagnosis in geared transmission systems*. 1996: Swinburne University of Technology.
95. Randall, R., *A new method of modeling gear faults*. *Journal of mechanical design*, 1982. **104**(2): p. 259-267.
96. Xinxin, L., et al. *Feature Extraction of Underwater Signals Based on Bispectrum Estimation*. in *Wireless Communications, Networking and Mobile Computing (WiCOM), 2011 7th International Conference on*. 2011. IEEE.
97. Tom, K.F., *Survey of Diagnostic Techniques for Dynamic Components*. 2010, DTIC Document.
98. McFadden, P. and J. Smith, *Vibration monitoring of rolling element bearings by the high-frequency resonance technique—a review*. *Tribology international*, 1984. **17**(1): p. 3-10.
99. Blankenship, G.W. and R. Singh, *Analytical solution for modulation sidebands associated with a class of mechanical oscillators*. *Journal of Sound and Vibration*, 1995. **179**(1): p. 13-36.
100. McFadden, P. and J. Smith, *An explanation for the asymmetry of the modulation sidebands about the tooth meshing frequency in epicyclic gear vibration*. *Proceedings of the Institution of Mechanical Engineers, Part C: Journal of Mechanical Engineering Science*, 1985. **199**(1): p. 65-70.
101. Nooli, P.K., *A versatile and computationally efficient condition indicator for AH-64 rotorcraft gearboxes*. 2011.
102. Lei, Y., et al., *CM and fault diagnosis of planetary gearboxes: A review*. *Measurement*, 2014. **48**: p. 292-305.
103. Patel, V., N. Tandon, and R. Pandey, *Defect detection in deep groove ball bearing in presence of external vibration using envelope analysis and Duffing oscillator*. *Measurement*, 2012. **45**(5): p. 960-970.
104. Sawalhi, N. and R. Randall. *Simulation of Vibrations Produced by Localised Faults in Rolling Elements of Bearings in Gearboxes*. in *Proceedings of the 5th Australasian Congress on Applied Mechanics*. 2007. Engineers Australia.
105. Wang, W. and P. McFadden, *Early detection of gear failure by vibration analysis i. calculation of the time-frequency distribution*. *Mechanical Systems and Signal Processing*, 1993. **7**(3): p. 193-203.
106. Suh, I.-S., *Application of time-frequency representation techniques to the impact-induced noise and vibration from engines*. 2002, SAE Technical Paper.
107. Yen, G.G. and W.F. Leong. *Fault classification on vibration data with wavelet based feature selection scheme*. in *Industrial Electronics Society, 2005. IECON 2005. 31st Annual Conference of IEEE*. 2005. IEEE.
108. Staszewski, W. and G. Tomlinson, *Application of the wavelet transform to fault detection in a spur gear*. *Mechanical Systems and Signal Processing*, 1994. **8**(3): p. 289-307.
109. Sung, C., H. Tai, and C. Chen, *Locating defects of a gear system by the technique of wavelet transform*. *Mechanism and machine theory*, 2000. **35**(8): p. 1169-1182.

110. McFadden, P., *Window functions for the calculation of the time domain averages of the vibration of the individual planet gears and sun gear in an epicyclic gearbox*. Journal of Vibration and Acoustics, 1994. **116**(2): p. 179-187.
111. Stander, C., P. Heyns, and W. Schoombie, *Using vibration monitoring for local fault detection on gears operating under fluctuating load conditions*. Mechanical Systems and Signal Processing, 2002. **16**(6): p. 1005-1024.
112. Atlas, L.E., G.D. Bernard, and S.B. Narayanan, *Applications of time-frequency analysis to signals from manufacturing and machine monitoring sensors*. Proceedings of the IEEE, 1996. **84**(9): p. 1319-1329.
113. Wang, W. and P. McFadden, *Application of wavelets to gearbox vibration signals for fault detection*. Journal of sound and vibration, 1996. **192**(5): p. 927-939.
114. Altes, R.A., *Detection, estimation, and classification with spectrograms*. The Journal of the Acoustical Society of America, 1980. **67**(4): p. 1232-1246.
115. Nguyen, T. and G. Strang, *Wavelets and filter banks*. Wellesley-Cambridge Press, Wellesley, 1996.
116. Yan, R., *Base wavelet selection criteria for non-stationary vibration analysis in bearing health diagnosis*. 2007: ProQuest.
117. Young, R.K., *Wavelet theory and its applications*. Vol. 189. 2012: Springer Science & Business Media.
118. Wang, W. and P. McFadden, *Application of orthogonal wavelets to early gear damage detection*. Mechanical Systems and Signal Processing, 1995. **9**(5): p. 497-507.
119. Rubini, R. and U. Meneghetti, *Application of the envelope and wavelet transform analyses for the diagnosis of incipient faults in ball bearings*. Mechanical systems and signal processing, 2001. **15**(2): p. 287-302.
120. Wu, J.-D. and P.-H. Chiang, *Application of Wigner–Ville distribution and probability neural network for scooter engine fault diagnosis*. Expert Systems with Applications, 2009. **36**(2): p. 2187-2199.
121. Baydar, N. and A. Ball, *Detection of gear failures via vibration and acoustic signals using wavelet transform*. Mechanical Systems and Signal Processing, 2003. **17**(4): p. 787-804.
122. Huang, N.E., et al. *The empirical mode decomposition and the Hilbert spectrum for nonlinear and non-stationary time series analysis*. in *Proceedings of the Royal Society of London A: Mathematical, Physical and Engineering Sciences*. 1998. The Royal Society.
123. Lin, J. and M. Zuo, *Gearbox fault diagnosis using adaptive wavelet filter*. Mechanical systems and signal processing, 2003. **17**(6): p. 1259-1269.
124. Boulahbal, D., M.F. Golnaraghi, and F. Ismail, *Amplitude and phase wavelet maps for the detection of cracks in geared systems*. Mechanical systems and signal processing, 1999. **13**(3): p. 423-436.
125. Zakrajsek, J.J., D.P. Townsend, and H.J. Decker, *An analysis of gear fault detection methods as applied to pitting fatigue failure data*. 1993, DTIC Document.
126. Zhen, D., et al., *Acoustic measurements for the combustion diagnosis of diesel engines fuelled with biodiesels*. Measurement Science and Technology, 2013. **24**(5): p. 055005.

127. McFadden, P. and M. Toozy, *Application of synchronous averaging to vibration monitoring of rolling element bearings*. Mechanical Systems and Signal Processing, 2000. **14**(6): p. 891-906.
128. Stewart, R., *Some useful data analysis techniques for gearbox diagnostics*. 1977: University of Southampton.
129. Combet, F. and L. Gelman, *Optimal filtering of gear signals for early damage detection based on the spectral kurtosis*. Mechanical Systems and Signal Processing, 2009. **23**(3): p. 652-668.
130. Xu, Y. and H. Zhang, *Recent mathematical developments on empirical mode decomposition*. Advances in Adaptive Data Analysis, 2009. **1**(04): p. 681-702.
131. Jardine, A.K., D. Lin, and D. Banjevic, *A review on machinery diagnostics and prognostics implementing condition-based maintenance*. Mechanical systems and signal processing, 2006. **20**(7): p. 1483-1510.
132. Andersson, A. and L. Vedmar, *A dynamic model to determine vibrations in involute helical gears*. Journal of Sound and Vibration, 2003. **260**(2): p. 195-212.
133. Dubowsky, S. and F. Freudenstein, *Dynamic Analysis of Mechanical Systems With Clearances—Part 1: Formation of Dynamic Model*. Journal of Manufacturing Science and Engineering, 1971. **93**(1): p. 305-309.
134. Dubowsky, S. and F. Freudenstein, *Dynamic Analysis of Mechanical Systems With Clearances—Part 2: Dynamic Response*. Journal of Manufacturing Science and Engineering, 1971. **93**(1): p. 310-316.
135. Azar, R. and F. Crossley, *Digital simulation of impact phenomenon in spur gear systems*. Journal of Manufacturing Science and Engineering, 1977. **99**(3): p. 792-798.
136. Yang, D. and Z. Sun, *A rotary model for spur gear dynamics*. Journal of Mechanical Design, 1985. **107**(4): p. 529-535.
137. Özgüven, H.N. and D.R. Houser, *Mathematical models used in gear dynamics—a review*. Journal of sound and vibration, 1988. **121**(3): p. 383-411.
138. Parey, A. and N. Tandon, *Spur gear dynamic models including defects: A review*. The Shock and Vibration Digest, 2003. **35**(6): p. 465-478.
139. Parey, A., et al., *Dynamic modelling of spur gear pair and application of empirical mode decomposition-based statistical analysis for early detection of localized tooth defect*. Journal of sound and vibration, 2006. **294**(3): p. 547-561.
140. Ebrahimi, S. and P. Eberhard, *Rigid-elastic modeling of meshing gear wheels in multibody systems*. Multibody System Dynamics, 2006. **16**(1): p. 55-71.
141. Fakhfakh, T., F. Chaari, and M. Haddar, *Numerical and experimental analysis of a gear system with teeth defects*. The International Journal of Advanced Manufacturing Technology, 2005. **25**(5-6): p. 542-550.
142. Cigliarič, I. and A. Kidrič, *Computer-aided derivation of the optimal mathematical models to study gear-pair dynamic by using genetic programming*. Structural and Multidisciplinary Optimization, 2006. **32**(2): p. 153-160.
143. Pimsarn, M. and K. Kazerounian, *Pseudo-interference stiffness estimation, a highly efficient numerical method for force evaluation in contact problems*. Engineering with Computers, 2003. **19**(2-3): p. 85-91.

144. Meagher, J., et al., *A comparison of gear mesh stiffness modeling strategies*, in *Structural Dynamics, Volume 3*. 2011, Springer. p. 255-263.
145. Bartelmus, W., *Mathematical modelling and computer simulations as an aid to gearbox diagnostics*. Mechanical Systems and Signal Processing, 2001. **15**(5): p. 855-871.
146. Howard, I., S. Jia, and J. Wang, *The dynamic modelling of a spur gear in mesh including friction and a crack*. Mechanical systems and signal processing, 2001. **15**(5): p. 831-853.
147. Vinayak, H. and R. Singh, *Multi-body dynamics and modal analysis of compliant gear bodies*. Journal of Sound and Vibration, 1998. **210**(2): p. 171-214.
148. Parker, R., S. Vijayakar, and T. Imajo, *Non-linear dynamic response of a spur gear pair: modelling and experimental comparisons*. Journal of sound and vibration, 2000. **237**(3): p. 435-455.
149. Theodossiades, S. and S. Natsiavas, *Non-linear dynamics of gear-pair systems with periodic stiffness and backlash*. Journal of Sound and vibration, 2000. **229**(2): p. 287-310.
150. Velex, P. and M. Maatar, *A mathematical model for analyzing the influence of shape deviations and mounting errors on gear dynamic behaviour*. Journal of Sound and Vibration, 1996. **191**(5): p. 629-660.
151. Sato, K. and S. Yamamoto, *Bifurcation sets and chaotic states of a gear system subjected to harmonic excitation*. Computational Mechanics, 1991. **7**(3): p. 173-182.
152. Kahraman, A., *Effect of axial vibrations on the dynamics of a helical gear pair*. Journal of Vibration and Acoustics, 1993. **115**(1): p. 33-39.
153. Amarnath, M., S. Chandramohan, and S. Seetharaman, *Experimental investigations of surface wear assessment of spur gear teeth*. Journal of Vibration and Control, 2012. **18**(7): p. 1009-1024.
154. Du, S., R. Randall, and D. Kelly, *Modelling of spur gear mesh stiffness and static transmission error*. Proceedings of the Institution of Mechanical Engineers, Part C: Journal of Mechanical Engineering Science, 1998. **212**(4): p. 287-297.
155. Sohn, H. and C.R. Farrar, *Damage diagnosis using time series analysis of vibration signals*. Smart materials and structures, 2001. **10**(3): p. 446.
156. Blake, W.K., *Mechanics of flow-induced sound and vibration, Volume 2: Complex flow-structure interactions*. 2017: Academic press.
157. Fahy, F.J. and P. Gardonio, *Sound and structural vibration: radiation, transmission and response*. 2007: Academic press.
158. Curle, N., *The influence of solid boundaries upon aerodynamic sound*. Proc. R. Soc. Lond. A, 1955. **231**(1187): p. 505-514.
159. Atalla, N., F. Sgard, and C.K. Amedin, *On the modeling of sound radiation from poroelastic materials*. The Journal of the Acoustical Society of America, 2006. **120**(4): p. 1990-1995.
160. Isaacs, S.H. and M. Henze, *Controlled carbon source addition to an alternating nitrification-denitrification wastewater treatment process including biological P removal*. Water Research, 1995. **29**(1): p. 77-89.
161. White, R.G. and J.G. Walker, *Noise and vibration*. 1982: Halsted Pr.

162. Beranek, L.L. and I.L. Ver, *Noise and vibration control engineering-principles and applications*. Noise and vibration control engineering-Principles and applications John Wiley & Sons, Inc., 814 p., 1992.
163. Jacobsen, F., et al., *Fundamentals of acoustics and noise control*. Technical University of Denmark, Department of Electrical Engineering, Note, 2011(31200).
164. Anderson, A.L. and L.D. Hampton, *Acoustics of gas-bearing sediments I. Background*. The Journal of the Acoustical Society of America, 1980. **67**(6): p. 1865-1889.
165. Tan, C.K., P. Irving, and D. Mba, *A comparative experimental study on the diagnostic and prognostic capabilities of acoustics emission, vibration and spectrometric oil analysis for spur gears*. Mechanical Systems and Signal Processing, 2007. **21**(1): p. 208-233.
166. Miller, R.K. and P. McIntire, *Acoustic emission testing*. 1987: American Society for Nondestructive Testing.
167. Eugene Parker JR, B., et al., *Fault diagnostics using statistical change detection in the bispectral domain*. Mechanical systems and signal processing, 2000. **14**(4): p. 561-570.
168. Crosby, M., R. Harwood, and D. Karnopp, *Vibration control using semi-active force generators*. Transactions of the ASME, Paper, 1974.
169. Nikias, C.L. and M.R. Raghuvver, *Bispectrum estimation: A digital signal processing framework*. Proceedings of the IEEE, 1987. **75**(7): p. 869-891.
170. Singh, P.K., et al. *Bispectrum and Arrhythmia Detection*. in *International Conference on Mathematical Biology*. 2004.
171. Johnson, P., *Emerging Challenges and Technologies in Signal Processing for Prognostics and Health Management in Wind Energy*.
172. Naid, A., et al. *Bispectrum Analysis of Motor Current Signals for Fault Diagnosis of Reciprocating Compressors*. in *Key Engineering Materials*. 2009. Trans Tech Publ.
173. Gu, F.S., et al., *Bispectrum Analysis of Motor Current Signals for Fault Diagnosis of Reciprocating Compressors*. Key Engineering Materials, 2009. **413**: p. 505-511.
174. Treetrong, J. *Fault detection and diagnosis of induction motors based on higher-order spectrum*. in *Proceedings of the International MultiConference of Engineers and Computer Scientists*. 2010.
175. Howard, I., *Higher-order spectral techniques for machine vibration CM*. Proceedings of the Institution of Mechanical Engineers, Part G: Journal of Aerospace Engineering, 1997. **211**(4): p. 211-219.
176. Arthur, N. and J. Penman, *Induction machine condition monitoring with higher order spectra*. Industrial Electronics, IEEE Transactions on, 2000. **47**(5): p. 1031-1041.
177. McLaughlin, S., A. Stogioglou, and J. Fackrell, *Introducing higher order statistics (HOS) for the detection of nonlinearities*. UK Nonlinear News, 1995. **15**.
178. Gu, F., et al., *Electrical motor current signal analysis using a modified bispectrum for fault diagnosis of downstream mechanical equipment*. Mechanical Systems and Signal Processing, 2011. **25**(1): p. 360-372.
179. Schoen, R.R., et al., *Motor bearing damage detection using stator current monitoring*. Industry Applications, IEEE Transactions on, 1995. **31**(6): p. 1274-1279.
180. Zhiyuan, Z.H.C.X.L., *Bispectrum Based Gear Fault Feature Extraction and Diagnosis [J]*. Journal of Vibration Engineering, 2002. **3**: p. 022.

181. Feng, F., A. Si, and P. Jiang, *Fault Diagnosis for Crankshaft Bearing in Diesel Engine Based on Bispectrum Analysis*. Chemical Engineering Transactions, 2013. **VOL. 33, 2013**: p. 1033-1038.
182. Seetharaman, S. and M. Jernigan. *Speech signal reconstruction based on higher order spectra*. in *Acoustics, Speech, and Signal Processing, 1988. ICASSP-88., 1988 International Conference on.* 1988. IEEE.
183. Fackrell, J.W., *Bispectral analysis of speech signals*. 1997.
184. Douglass, D.A., *Voice Analysis Using the Bispectrum*. 1994, DTIC Document.
185. Gu, F., et al. *Motor current signal analysis using a modified bispectrum for machine fault diagnosis*. in *ICCAS-SICE, 2009*. 2009. IEEE.
186. Ahmaida, A., et al., *Gear wear process monitoring using acoustic signals*. 2014.
187. Brook Crompton, *20 hp, 380-415 V Electric Motor*. Available from: <http://www.brookcrompton.com/products>.
188. Zhang, R., et al., *Gear wear process monitoring using a sideband estimator based on modulation signal bispectrum*. Applied Sciences, 2017. **7**(3): p. 274.
189. Crompton, I.B. and S. introduced by CEMEP, *Efficiency labelling scheme fully implemented*.
190. He, X., Gu, F., & Ball, A. (2012). Recent development in finite element analysis of self-piercing riveted joints. *The international journal of advanced manufacturing technology*, 58(5-8), 643-649..
191. Levinzon, F., *Piezoelectric Transducers Used for Piezoelectric Accelerometers with Integral Electronics*, in *Piezoelectric Accelerometers with Integral Electronics*. 2015, Springer. p. 43-57.
192. Serridge, M. and T. Licht, *Piezoelectric Accelerometer and Vibration Preamplifier Handbook*, Brüel & Kjær. Naerum, Denmark, 1987.
193. Lent, B., *Simple Steps to Selecting the Right Accelerometer*. Endevco Corp, 2009.
194. White and C.J, *Detection of gear failure*, in *Workshop in On-condition Maintenance*. 1972: ISVR Southampton.
195. Raharjo, P., et al. *A comparative study of the monitoring of a self aligning spherical journal using surface vibration, airborne sound and acoustic emission*. in *Journal of Physics: Conference Series*. 2012. IOP Publishing.
196. M, N.A.A., *Fault Detection and Diagnosis of Reciprocating Compressors using Motor Current Signature Analysis*, in *Diagnostic Engineering*. 2009, The University of Huddersfield: Huddersfield. p. 201.
197. Staszewski, W.J., K. Worden, and G.R. Tomlinson, *Time–frequency analysis in gearbox fault detection using the Wigner–Ville distribution and pattern recognition*. Mechanical systems and signal processing, 1997. **11**(5): p. 673-692.
198. Kar, C. and A. Mohanty, *Monitoring gear vibrations through motor current signature analysis and wavelet transform*. Mechanical systems and signal processing, 2006. **20**(1): p. 158-187.
199. Mohanty, A. and C. Kar, *Fault detection in a multistage gearbox by demodulation of motor current waveform*. Industrial Electronics, IEEE Transactions on, 2006. **53**(4): p. 1285-1297.

200. Öztürk, H., M. Sabuncu, and I. Yesilyurt, *Early detection of pitting damage in gears using mean frequency of scalogram*. Journal of Vibration and Control, 2008. **14**(4): p. 469-484.
201. Li, B., et al., *Gear fault detection using adaptive morphological gradient lifting wavelet*. Journal of Vibration and Control, 2012: p. 1077546312448502.
202. Sweeney, P. and R. Randall, *Gear transmission error measurement using phase demodulation*. Proceedings of the Institution of Mechanical Engineers, Part C: Journal of Mechanical Engineering Science, 1996. **210**(3): p. 201-213.
203. Yang, J., et al., *Fault detection in a diesel engine by analysing the instantaneous angular speed*. Mechanical systems and signal processing, 2001. **15**(3): p. 549-564.
204. Sasi, A.B., et al., *The Exploitation of Instantaneous an Gular Speed for CM of electric motors*. CM and Diagnostic Engineering Management, 2001: p. 311.
205. Stander, C. and P. Heyns, *Instantaneous angular speed monitoring of gearboxes under non-cyclic stationary load conditions*. Mechanical Systems and Signal Processing, 2005. **19**(4): p. 817-835.
206. Gu, F., et al., *An investigation of the effects of measurement noise in the use of instantaneous angular speed for machine diagnosis*. Mechanical Systems and Signal Processing, 2006. **20**(6): p. 1444-1460.
207. Elhaj, M., et al., *Numerical simulation and experimental study of a two-stage reciprocating compressor for CM*. Mechanical Systems and Signal Processing, 2008. **22**(2): p. 374-389.
208. Charles, P., et al., *Detecting the crankshaft torsional vibration of diesel engines for combustion related diagnosis*. Journal of Sound and Vibration, 2009. **321**(3): p. 1171-1185.
209. Renaudin, L., et al., *Natural roller bearing fault detection by angular measurement of true instantaneous angular speed*. Mechanical Systems and Signal Processing, 2010. **24**(7): p. 1998-2011.
210. Mohanty, A. and D. Agarwal. *Gear fault detection using instantaneous angular speed monitoring*. in *Proceedings of the 1st international workshop and congress on E-maintenance*. 2010.
211. Zhou, Y., et al., *Feed-axis gearbox CM using built-in position sensors and EEMD method*. Robotics and Computer-Integrated Manufacturing, 2011. **27**(4): p. 785-793.
212. Kar, C. and A. Mohanty, *An algorithm for determination of time-varying frictional force and torque in a helical gear system*. Mechanism and Machine Theory, 2007. **42**(4): p. 482-496.
213. Stander, C.J. and P.S. Heyns, *Instantaneous angular speed monitoring of gearboxes under non-cyclic stationary load conditions*. Mechanical Systems and Signal Processing, 2005. **19**(4): p. 817-835.
214. McFadden, P., *Examination of a technique for the early detection of failure in gears by signal processing of the time domain average of the meshing vibration*. Mechanical systems and signal processing, 1987. **1**(2): p. 173-183.
215. Combet, F. and L. Gelman, *An automated methodology for performing time synchronous averaging of a gearbox signal without speed sensor*. Mechanical systems and signal processing, 2007. **21**(6): p. 2590-2606.

216. Guan, L., et al. *Gearbox fault diagnosis under different operating conditions based on time synchronous average and ensemble empirical mode decomposition*. in *ICCAS-SICE, 2009*. 2009. IEEE.
217. Lei, Y., Lin, J., Zuo, M. J., & He, Z. (2014). CM and fault diagnosis of planetary gearboxes: A review. *Measurement*, 48, 292-305.
218. Beranek, L. L., & Ver, I. L. (1992). Noise and vibration control engineering-principles and applications. *Noise and vibration control engineering-Principles and applications John Wiley & Sons, Inc.*, 814 p.
219. Amarnath, M., Chandramohan, S., & Seetharaman, S. (2012). Experimental investigations of surface wear assessment of spur gear teeth. *Journal of Vibration and Control*, 18(7), 1009-1024.

Appendix A: Publications

1. Ahmaida Anwar, Zhen Dong, Gu, Fengshou and Ball, Andrew (2013) *Fatigue Prediction of a Gear Transmission System based on Vibro-Acoustic Measurements*. In: Proceedings of Computing and Engineering Annual Researchers' Conference 2013: CEARC'13. University of Huddersfield, Huddersfield, pp. 93-99. ISBN 9781862181212

Fatigue Prediction of a Gear Transmission System based on Vibro-Acoustic Measurements

Anwar Ahmaida, Dong Zhen, Fengshou Gu and Andrew Ball
University of Huddersfield, Queensgate, Huddersfield HD1 3DH, UK

ABSTRACT

Gearing components play a pivotal role in most power transmission mechanisms but their application in industry consistently results in significant disruption and losses due to gear failures. This emphasises the significance of condition monitoring and fault diagnostics techniques of gear transmission systems to enhance overall safety and operational reliability in order to minimise gearbox failure rates and their associated disruption and losses to industry. In a wide range of industrial contexts, vibration analysis is extensively used for machinery condition monitoring and diagnostics due to its good detection results. As vibration and acoustic noise have the same generation mechanism, acoustic noise can also be used for machinery condition monitoring combined with effective signal processing methods. In this paper, vibration and acoustic signals were both used to analyse the fatigue process of a gear transmission system based on synchronous vibro-acoustic measurements. In order to enhance the signal-to-noise ratio (SNR) of the measured signals, time synchronous average (TSA) technique was employed to pre-process the vibration and acoustic signals. The side band energy ratio (SER) is then extracted to predict the vibration and acoustic signals to indicate the fatigue process of the testing gearbox under different operating conditions. Further the fatigue process was detected through analysing the measured signals in the high frequency band as these are less contaminated by background reverberation interferences. The key results show that the gear transmission system can be monitored by vibration and acoustic analysis which show similar trend results for the gear fatigue process tested.

Keywords gearbox, vibration, acoustic, fatigue analysis

INTRODUCTION

Gears have long been used as a means of power transmission in many industrial applications such as terrestrial gearboxes and power generators [1]. Their function is to accomplish a change of speed which is usually rotational. Gearboxes essentially consist of a set, or sets, of gears

mounted on shafts and supported by bearings, with the entire system enclosed and supported within housing and lubricated. An electric motor power source drives the gearbox input shaft, normally at a relatively high speed. Internally the gears transmit a reduced speed to the output shaft resulting in an increase in output torque [2].

Vibration signals are the principle means of gearbox condition monitoring as they provide the easiest method to gather and reflect the basic excitation motion of the gearbox. Additionally, airborne acoustics or noise, being correlated closely to vibration but measured with more comprehensive information in a remote way, has also been actively investigated for condition monitoring and fault diagnosis of gearboxes in the last two decades. Nevertheless, both vibration and acoustic signals can be contaminated by different noises and careful analysis with more advanced tools should be carried out to obtain reliable features for fault diagnosis. Conventional methods of monitoring vibration are based on the assumption that the deterioration in the condition of a gearbox may be detected by changes in the measured structural response (vibration signal) [3]. Under constant load and speed, any change in the vibration signal may be attributed to the fault conditions. Nevertheless, this assumption may not be true for varying operating conditions and in most cases, the gearbox during service operates under varying or fluctuating conditions contributed by uncertain or unexpected sources [3]. Developing a robust technique for detecting gearbox deterioration when it is subjected to varying operation conditions becomes a serious issue. In addition, if the vibration signal is measured at different locations, these signals may be corrupted due to the effect from attenuation of transmission paths and interference from other sources.

Numerous analysis techniques have been fully developed and established over the years for processing vibration signals to obtain diagnostic information about progressively worsening gear faults. Earlier research on gear failure detection focused on the use of time-averaged vibration signal, spectrum, cepstrum, amplitudes and phase modulation techniques to detect different types of gear failures. Most of these conventional approaches work well to detect abnormalities and indicate faults without providing much information about them, such as location and severity of the faults (4-5).

Condition monitoring (CM) of gearboxes plays an important role in insuring the reliability and minimum cost operations of industrial facilities [6]. CM has the capability to detect early gear faults before unexpected breakdown occurs. The main task of the designer is to guarantee the reliability of the gearbox through using high quality gear material and manufacturing technology for the gearbox design. However, the reliability and stability of the gearbox will be decreased during its operation under a harsh working environment. Machines can be monitored during operation and repaired in a convenient time and CM can further help to achieve economical operations and reduce emissions. As the fatigue gearbox test is one of the common failure tests in a gearbox, this paper explores the performance of using Time Synchronous Average (TSA) analysis and Sideband Energy Ratio (SER) to diagnose fatigue faults based on a two stage helical gearbox. Vibration and acoustic signals for different conditions including baseline case are processed by TSA and SER for feature extraction and fault diagnostics. SER has been developed specifically to auto-detect and distinguish gear defect signatures within an overall vibration signal and provide an early warning of developing gear damage. The

following paper reviews the TSA technique in section 2 while section 3 details the test facility and section 4 presents and discusses the results of using TSA and SER analysis. The conclusion forms the final section [6].

SIGNAL ANALYSIS TECHNIQUES

Time domain techniques typically employ statistical analysis such as RMS, Kurtosis, peak value and a time synchronous signal averaging method [7]. Time domain approaches are suitable in situations where periodic vibration is observed and faults produce wideband vibration due to periodic impulses.

Time Synchronous Average (TSA)

TSA is a pre-processing technique used to isolate the vibration produced by each gear in the gearbox due to its significant suppression of random noise components. The vibration signal corresponding to one revolution of the gear of interest is sampled with the help of a tachometer and the ensemble average over the period is calculated. The synchronous averaged signal tends to eliminate the noise components that are not synchronous with the rotation of gear, leaving only the vibration signal of the gear under study during one revolution [8-9]. Therefore, detection and identification of the local defects of the gear become much simpler and effective. This technique is very applicable to investigate a gearbox composed of multiple gears since it attenuates the vibration signals from other system components. However, by simply applying this technique the early detection of gear faults is often difficult and requires more sophisticated signal processing techniques to enhance the information from the synchronous averaged signal.

Sideband Energy Ratio (SER)

In general, the Sideband Energy Ratio (SER) [10] is calculated from high resolution spectrum data. Each spectrum is created from time-based waveform data generated by an accelerometer sensor and collected by the monitoring system. Several accelerometer sensors were mounted in strategic locations on the gearbox to monitor each gear mesh. The waveforms from each sensor were synchronously sampled so that the sampling frequency tracks changes in speed. This technique produces narrow spectral lines of speed-dependent frequencies, like gear mesh frequencies and associated sidebands, for variable speed machines. They are essential to accurately calculate SER. Once the spectrum is generated the SER algorithm sums the amplitudes of the first six sideband peaks on each side of the centre mesh frequency and divides by the amplitude of the centre mesh frequency.

$$SER = \frac{\sum_{i=1}^6 \text{sideband amplitude } i}{\text{Centre mesh frequency amplitude}} \dots\dots\dots (1)$$

SER is sensitive to the sideband amplitudes relative to the centre mesh frequency. In a healthy gear mesh, any sidebands have small amplitude compared to the centre mesh frequency, or they may be missing altogether resulting in a low SER. SER is typically less than one for a healthy gear mesh. As damage develops on a gear tooth that passes through the gear mesh, the sidebands increase in amplitude.

TEST FACILITIES AND FAULT SIMULATION

The test rig shown in Fig. 1 consists of a reduction gearbox with two stages of helical gears manufactured by David Brown Radian Limited; a three phase induction motor (11kW, 1465rpm and four poles) produced by the Electro-Drive Company, and a load system consisting of two flexible couplings, DC generator and resister bank. The induction motor is flanged in a cantilever type arrangement to the gearbox while the input shaft is driven by an AC motor. The motor speed and load is controlled by a variable speed drive for studying condition monitoring performance. Table 1 presents the details of the two sets of gears. The fault was fatigue tested under different operating conditions.

In the experiment, a speed signal is measured with a rotary encoder attached to the motor shaft. The vibration signal from the gear was measured using a 50 kHz sampling rate by 2 accelerometers mounted at two different locations: gearbox casing one and two in the two respective locations. To measure the sound signals an integrated BAST microphone system was used. A reference signal obtained from an optical pick-up was then utilised to synchronise the time-domain averaging of both the vibration and acoustic signals. To investigate the effect of the operating conditions (different rotating frequencies of the shaft and different loads) on the vibration and acoustic signals, the signals were recorded at 0%, 40% 60% 80% and 90% of the full load. In the following sections, we explore if fault diagnosis can be implemented effectively based on vibration and acoustic signals recorded for a gear casing at a remote location.

Table 1 Performance Specification of Two-Stage Helical Gearbox

Gear Parameters	1 st Stage	2 nd Stage
Number of teeth	58/47	13/59
Shaft speed	24.42Hz	6.64Hz
Meshing frequency	1416.36Hz	391.76Hz
Contact ratio	1.45	1.469
Transmission ratio	0.8103	4.5385

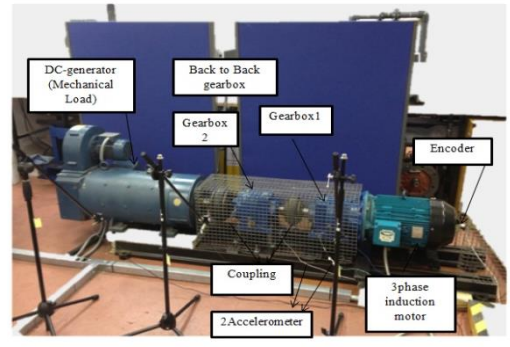


Fig1 Gearbox Test Set up

The two accelerometers connected to the gearbox can detect the vibration signal. The accelerometers have been taken from the PCB Type 336C04, attached to bases and firmly screwed in two different positions. The first was situated on the gearbox casing and the other positioned on the opposite side in the separate locations. The acoustic signals are measured by using BAST’s microphone system composed of an electrets microphone CHZ-211 and a preamplifier YG-201. The tables below show the specification for the accelerometers and microphone:

Table 2 ICP-type Accelerometer Specifications and Microphone Specification CHZ-211

Model and Serial Number	PCB Model No 338C04 accelerometer	Microphone Specification CHZ-21	Microphone CHZ-211
Frequency range	0.5Hz to 10 kHz ($\pm 5\%$)	Frequency response (Ref. 250Hz)	6.3Hz~20kHz ($\pm 2\text{dB}$)
Sensitivity	100mV/g ($\pm 10\%$)	Sensitivity	-26 \pm 1.5dB (50mV/Pa)
Temperature Range	-53 to 93°C	Temperature Range	-40°C~+80°C

A gear fatigue test was conducted by machining out a half width on input pinion. This reduction of gear loading profile increases local stress and leads to rapid and early failure. The data was collected in 1hour interval under 5different loads, and data was also collected after 20 minutes due the operation conditions. Use of Fast Fourier Transform FFT to get spectrum frequency analysis can be shown in the fig3. To investigate the effect of the operation condition (different rotating frequencies of the shaft and different loads) on the vibration signals, the signals were recorded at 0%, 40%, 60, 80 and 90% of full shaft speed and full load.

In the following sections, we would explore if fault diagnosis can be implemented effectively based on vibration and acoustic signals recorded at a remote location.

RESULTS and DISCUSSION

TSA Vibration Analysis

TSA is an effective technique in the time domain to remove noise in a repetitive signal and is widely used in vibration monitoring and fault diagnosis [11]. The SNR of a vibration signal can be improved significantly by suppressing the components which are asynchronous with those of interest. TSA is applied based on the knowledge of the revolution specifications of the rotating part. Traditionally, this requirement is met by using an external trigger signal provided by a shaft encoder, and the revolution period of rotating machinery can be obtained. Then, the vibration signal is divided into small segments according to the revolution period of the rotating part, and all the segments are summed up together so that no coherent components and asynchronous components are cancelled out. Normally, vibration signals from rotating machinery are a combination of periodic signals with random noise. Assuming a signal $x(t)$ consists of a periodic signal $x_T(t)$ and a noisy component $n(t)$, the period of $x_T(t)$ is T_0 whose corresponding frequency is f_0 , thus the signal can be expressed [11]

$$x(t) = x_T(t) + n(t) \dots \dots \dots (2)$$

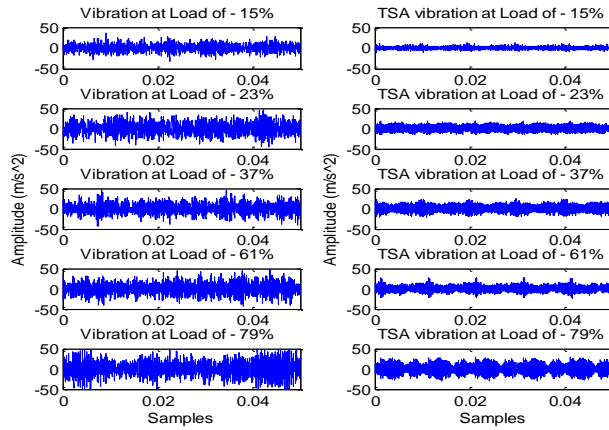


Fig 2 TSA vibration waveform from gearbox casing faulty case (Fatigue test)

Figure 2 shows the averaged vibration signal using TSA for three revolutions of the input shaft with the gearbox operating under different loads and different operating hours. The baseline is the faulty case. The findings demonstrate that the amplitude of the vibration signals increases with additional loads, and the impulse components of the vibration signals are highlighted for all the test conditions.

Vibration Spectrum Analysis

The spectrum of the vibration signal from the faulty gearbox is shown in Fig 3. Only the frequency range from 0Hz to 6000Hz is illustrated as this range is more effective for revealing gear vibration characteristics than the higher frequency range where the more sensor resonant are induced. Further Figure 3 shows that the amplitude peaks corresponding to the first and second meshing frequency 1450 Hz and 401Hz for the first, second, third and fourth harmonics are consistently the largest feature of the spectrum, dominating the signals due to the fatigue fault, and common to the two measurement positions. Thus this feature could be used to reliably detect gear faults.

Fig 4 shows the gear relationship between amplitude and different operation hours with the faulty case (fatigue test), at full load for the frequency range 5000-5500Hz. The analysis reveals that under the faulty conditions higher amplitudes of the SER components of the gear rotational speed exist.

The amplitudes of these components are very high in the faulty case, especially for the high loads. It is believed that their appearance is caused by the fatigue tests under different conditions such as load. Therefore, they can be used for the detection of such a fault. Moreover, the amplitude shows additional higher order frequency components at high frequency range. In general, the test results show that the presence of a fault in a gear is revealed by the introduction of higher amplitudes of sidebands already present, correlating with the drive shaft frequency. In addition, the fault also creates more sidebands relating to higher amplitudes of the shaft frequency

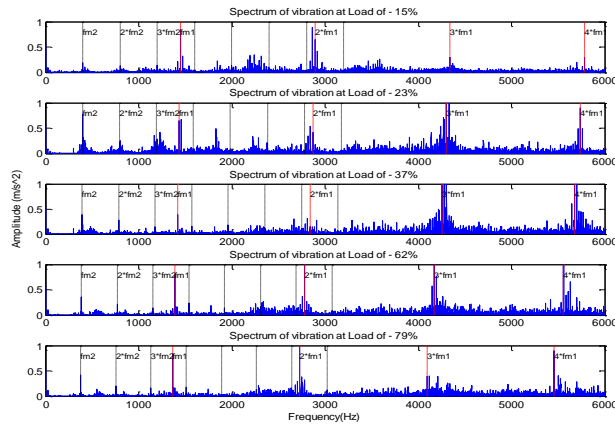


Fig3 Spectrum of vibration signal from faulty gearbox

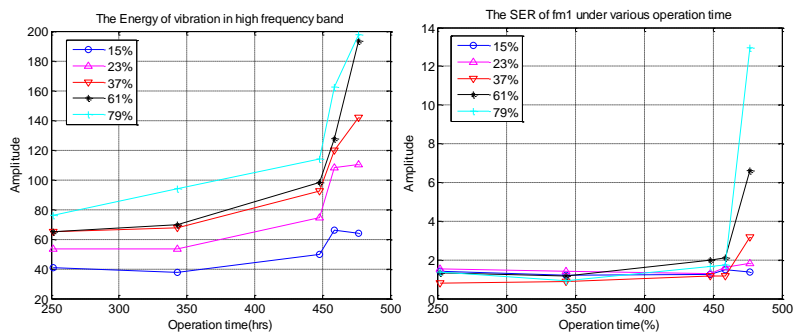


Fig4 SER of 1st meshing frequency (fm1) under various loads and energy of vibration in high frequency band

Acoustic Results (RMS and Energy of Acoustic)

Using a similar method, the Root Mean Square (RMS) statistical parameter and acoustic energy have been calculated for more accurate study of the waveforms. Fig 5 shows both the RMS value of the gearbox acoustic signals for faulty gears and acoustic energy in the high frequency band under different load and operating conditions that the value patterns of the RMS and acoustic energy for the gearbox are similar for the faulty condition, mainly at small load. A slight difference in the RMS amplitude value appears as the load increases, however this difference is sufficiently significant to be considered as a fault indicator.

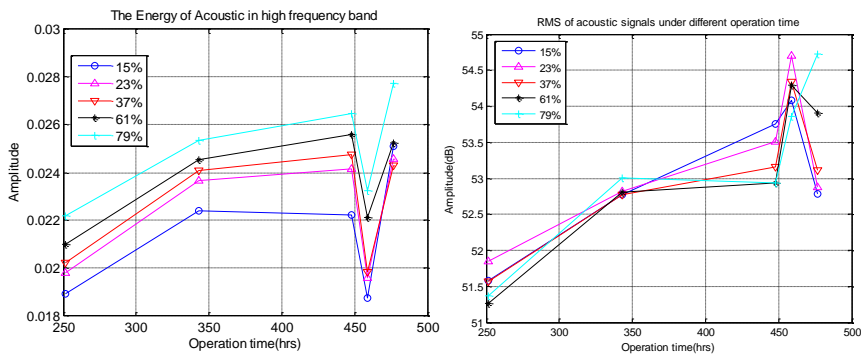


Fig 5 RMS of acoustic signals and acoustic energy in high frequency band

The findings illustrated in Fig5 show that the average amplitude has changed at low rotational speeds. More importantly, the results appear to show an increase in the average amplitude value for most of the applied loads as fault is introduced, especially on high loads. Given these results, the average amplitude data can be used effectively to indicate gear faults in all operating conditions.

The results demonstrate that the performance of the conventional frequency domain degrades due to the fluctuation of the operating conditions. Therefore, the average amplitude signal derived from the acoustic signal may be effective for detection of fatigue faults induced in the gear system under certain specific operating conditions. With different gear operation and the same location as seen in Figure 5, the average sideband amplitude (new feature) of the acoustic signals increases with higher load. Further these RMS values appear to increase in amplitude with the introduction of fault. The results of the special analysis described above illustrate that vibration and acoustic analysis based on TSA signals can achieve the same results from a remote position, though the amplitude of the SER is attenuated. Therefore, fault diagnosis from a remote position is certainly available with special analysis techniques.

CONCLUSIONS

Surface vibration and airborne acoustic monitoring both have distinct capabilities, advantages and disadvantages. The longstanding usefulness of conventional surface vibration consists in localised information obtainable from the rotating components, energy released by increasing friction or impacting throughout the components which allows vibration to be detectable. Similarly, the energy emitted by these components is detectable by an acoustic sensor that is mounted non-intrusively. It is remote and obtains information globally from other noise sources.

The study investigated the vibration and acoustic signals measured from the gearbox and under different operating conditions and different gear life times, and which were analysed in the time domain using TSA signals and SER. The key findings indicate that the performance of traditional signal processing techniques degrades due to the fluctuation of the operating conditions. However, the new feature from the SER is effective in detecting the fatigue fault induced to the gear system under most conditions. Moreover, it can achieve the same fault detection results from a remote positioned microphone; although it's acoustic signals are distorted significantly by background- interferences. However, it does not perform well under certain conditions. In future research, more advanced analysis methods should be adopted to obtain more robust features.

REFERENCES

- [1] Tasso, C. (1998). An Introduction to Artificial Intelligence and to the Development of Knowledge-Based Systems. In *Development of Knowledge-Based Systems for Engineering* (pp. 11-26). Springer, Vienna.
- [2] Wright, D. (2001). *Notes on design and analysis of machine elements*. Department of Mechanical and Materials Engineering, The University of Western Australia.

- [3] Stander, C. J., Heyns, P. S., & Schoombie, W. (2002). Using vibration monitoring for local fault detection on gears operating under fluctuating load conditions. *Mechanical Systems and Signal Processing*, 16(6), 1005-1024.
- [4] Jackson, J. E. (2005). *A user's guide to principal components* (Vol. 587). John Wiley & Sons.
- [5] Forrester, B. D. (1990, April). Analysis of gear vibration in the time-frequency domain. In *Proc. Of the 44th Meeting of the Mechanical Failure Prevention Group* (pp. 225-234).
- [6] Morris, R. and Pardue, F. 1994. *The Reliability Based Maintenance Strategy, A Vision for Improving Industrial Productivity*, Computational Systems Incorporated (CSI), Knoxville, Tennessee, USA.
- [7] Stevens, P. W., Hall, D., & Smith, E. (1996, June). A multidisciplinary research approach to rotorcraft health and usage monitoring. In *Proc. Annual Forum, American Helicopter Society* (Vol. 2, pp. 1732-1751).
- [8] Combet, F., & Gelman, L. (2007). An automated methodology for performing time synchronous averaging of a gearbox signal without speed sensor. *Mechanical systems and signal processing*, 21(6), 2590-2606.
- [9] Randall, R. B. (1982). A new method of modelling gear faults. *Journal of Mechanical Design*, 104(2), 259-267.
- [10] Hanna, J., Hatch, C., Kalb, M., Weiss, A., & Luo, H. (2011). Detection of wind turbine gear tooth defects using sideband energy ratioTM. *China Wind Power 2011; October, 19-21, 2011, Beijing, China*.
- [11] Zakrajsek, J. J., Townsend, D. P., & Decker, H. J. (1993). *An analysis of gear fault detection methods as applied to pitting fatigue failure data* (No. NASA-E-7470). National Aeronautics and Space Administration Cleveland OH Lewis Research Centre.

2. Ahmaida Anwar, Zhen Dong, Gu, Fengshou and Ball, Andrew (2014) Gear Wear Process Monitoring Using Acoustic Signals. The 21st International Congress on Sound and Vibration 13-17 July, 2014, Beijing/China.

GEAR WEAR PROCESS MONITORING USING ACOUSTIC SIGNALS

Anwar Ahmaida, Dong Zhen, Fengshou Gu and Andrew Ball

Centre for Efficiency and Performance Engineering, University of Huddersfield, UK

e-mail: F.gu@hud.ac.uk

Abstract

Airborne acoustic signals contain valuable information from machines and can be detected remotely for condition monitoring. However, the signal is often seriously contaminated by various noises from the environment as well as nearby machines. This paper presents an acoustic based method of monitoring a two stage helical gearbox, a common power transmission system used in various industries. A single microphone is employed to measure the acoustics of the gearbox undergoing a run-to-failure test. To suppress the background noise and interferences from nearby machines a modulation signal bispectrum (MSB) analysis is applied to the signal. It is shown that the analysis allows the meshing frequency components and the associated shaft modulating components to be captured more accurately to set up a clear monitoring trend to indicate the tooth wear of the gears under test. The results demonstrate that acoustic signals in conjunction with efficient signal processing methods provide an effective monitoring of the gear transmission process.

Keywords: Acoustic signals, Modulation signal bispectrum, Gear Transmission, Condition monitoring

1 Introduction

Gears have long been used as a means of power transmission in many industrial applications such as terrestrial gearboxes and power generators ^[12]. Significant evidence from industry shows that gear failure rates frequently result in major disruption and losses. To improve operational and safety effectiveness, condition monitoring and fault identification are common practices in modern industries.

Vibration based method is the mainstream techniques of CM. However, it is often difficult to locate an appreciate place for installing accelerometers. On the other hand, as the response of structural vibration, airborne sound can be picked up by microphones distant from the objects, which makes it much easier to be implemented in situ. Moreover, microphones generally have wider frequency response, ranging from 20Hz to 20 kHz, which can include a great deal and

detailed information in this bandwidth. Acoustic signals from one microphone can include information from different components of a machine. It means that only a couple of sensors are required to monitoring the whole system, whereas many accelerometers are needed monitoring different components [13, 14]

However, airborne acoustic signals may need to be pre-processed more intensively to suppress background noise and remove interferences for improving the signal to noise ratio (SNR) of interesting sources and extracting the characteristics of the sound sources from the noise signals for fault diagnosis. It has shown that wavelet transforms [1], independent component analysis (ICA) [2], and adaptive filtering techniques [3] are effective to process the non-stationary acoustic signals in monitoring engine problems with combustion, abnormal valves and fuel injectors of diesel engines.

Compared with diesel engines, the acoustic signals from a gear transmission may be more stationary and have more distinctive modulation. In the general review paper, many different signal processing techniques are investigated for processing such vibration data [4] in the time domain, frequency domain and time-frequency domain for monitoring gearbox. Among them novel methods such as cyclo-stationary analysis [5] and empirical mode decomposition method (EMD) [6] are of particular interesting as they focus on characterising the modulation nature in the vibration data which is the critical feature of the vibration.

On the other hand, higher order spectra (HOS) are useful signal processing tools due to its unique properties nonlinear system identification, phase information retention and Gaussian noise elimination. The application of HOS techniques in condition monitoring has been reported in [7]. Recently, Gu et al [8] examined the performance of a modulation signal bispectrum (MSB), an extension of conventional bispectrum, and showed that it is more efficient in characterising the weak modulation of electrical signals from compressors and gearboxes for diagnosing different common faults. As the vibro-acoustic signals has the modulation effects, this study will examine the use of MSB to extract the modulation from acoustic signals of gearbox for developing more accurate approaches to monitoring gearbox conditions.

2 Gearbox Vibro-Acoustics

2.1 Acoustic signal contamination

The vibration source will firstly show as the structural vibration response of the gearbox case through the effect of the transfer function derived from shafts and bearings. Usually, there are a number of resonances in the frequency range of interest due to both the transfer paths and the case dynamic characteristics. These resonances cause the vibration responses and their associated acoustics to have nonlinear connections to the faults. The resonance effect produces good signal to noise ratio data but it needs to be carefully analysed in using the signal amplitudes to explain the fault severity. It may give higher amplitudes in some frequency ranges compared with those in which there are no resonances.

Airborne sound is a sequence of pressure waves that propagate through a compressible media, and during its propagation the sound waves are reflected, as well as refracted and attenuated. Acoustics in typical industrial machinery undergo many thousands of reflections before eventual decaying below limits of detectability [11]. As such, the effect of room reflection on the sound power levels in the vicinity of a small machine situated in a relatively large room would be expected to be small. In a workshop, testing is done in a natural environment of a large room, with reflecting surfaces. However, if the sound sources are located in an enclosed space, the reflection caused by the boundary of the enclosed space will affect the basic characteristics of the sound source, and increase the difficulties for fault diagnosis by analysing airborne sound signals.

Although the resonance modes of the room were not considered as a reverberant chamber, the sound waves used, especially in the low frequency range, may be inaccurate and misleading. Great care has to be taken in interpreting the information content [15]. Also interference is generated by other signals (in other circuits or, more likely, in the same circuit), so it may give rise to artificial effects not related to the noise source under investigation.

2.2 Vibro-acoustic Sources of Gear Transmission

For a healthy gear set, ignoring manufacturing errors but including tooth deformation due to loads, the vibro-acoustic sources $x_h(t)$ will be dominated by the meshing frequency components and can be approximated in the following form [9, 10]:

$$x_h(t) = \sum_{k=0}^K A_k \cos(2\pi k f_m t + \varphi_k) + w(t) \quad (1)$$

where $f_m = z f_r$ is the meshing frequency which is the multiplication of tooth number z and the shaft rotating frequency f_r , A_k and φ_k are the amplitude and respectively phase of the k^{th} harmonic, K is the number of meshing frequency harmonics of interest, and $w(t)$ is the noise which is assumed to have a normal distribution.

However, there are inevitable manufacturing errors such as errors in tooth spacing, tooth profile, alignment, as well as gear faults including tooth wear, cracks and damages which all alter the meshing stiffness and cause variations in both amplitude and phase of the tooth meshing vibrations[16]. The variation in the amplitude and can be approximated by modulating functions $a_k(t)$ and $\varphi_k(t)$ respectively which are also periodic with the shaft frequency and can be written as:

$$a(t) = \sum_{k=0}^{\infty} A_k \cos(2\pi k f_r t + \alpha_k) \quad (2)$$

$$\varphi(t) = \sum_{k=0}^{\infty} B_k \cos(2\pi k f_r t + \beta_k) \quad (3)$$

Substituting these modulating components into Equation (1) yields the overall vibro-acoustic source expression:

$$x(t) = \sum_{k=0}^K A_k [1 + a_k(t)] \cos(2\pi k f_m t + \varphi_k + \varphi_k(t)) + w(t) \quad (4)$$

The form of equation (4) emphasises that the source contains a complicated modulation process due to the presence of errors in the gear system. Obviously gear faults such as tooth breakage

and wear will alter the characteristics of modulation further. Therefore, it is critical to characterise the modulation appropriately in order to differentiate faults from the manufacturing errors and noise.

3 Modulation Signal Bispectrum

According to the definition of MSB in the frequency domain, the meshing frequency f_m and sideband f_r in an acoustic signal can be correlated [8] as

$$B_{MS}(f_r, f_m) = E[X(f_r + f_s)X(f_r - f_s)X^*(f_m)X^*(f_m)] \quad (5)$$

where $X^*(f)$ is the complex conjugate of the Fourier transform $X(f)$ of acoustic signal $x(t)$; and $E[]$ is the statistical expectation operator. And the power spectrum of $x(t)$ is

$$PS(f_m) = E[X(f_m)X^*(f_m)]$$

Equation (5) shows that through the operation of vector average in the frequency domain, MSB can extract the combination of components at the meshing frequency, the lower sideband and the higher sideband. In the meantime, other components including random noise and interfering components that are not meet the phase relationship will be suppressed significantly. In this way the modulation effects in acoustic signal can be represented more accurately and reliably.

To examine the modulating components along, rather than that of the combination with the meshing component, a MSB sideband estimator (MSB-SE) can be used according to (6)

$$B_{MS}^{SE}(f_r, f_m) = E[X(f_r + f_s)X(f_r - f_s)X^*(f_m)X^*(f_m)/|X(f_m)|^2] \quad (6)$$

Because of the magnitude in equation (6) is normalised the magnitude of the MSB-SE is only the products of the lower and upper sideband, which reflects more the modulating component from faults.

In addition, MSB coherence (MSBC) defined in Equation (7) can be based on to estimate the influences of random components

$$b^2_{MS}(f_r, f_m) = \frac{|B_{MS}(f_r, f_m)|^2}{PS(f_m)E[|X(f_m + f_r)X(f_m - f_r)|^2]} \quad (7)$$

MSB coherence has boundary [0 1]. 1 means that MSB magnitude from true modulation effects. On other hand a zero value means that the MSB magnitude is mainly from random noise influences. Thus other values of MSBC will indicate the reliability of MSB peaks. In addition, for a given measurement environment, the noise is relative the same. The increase of MSBC can be an indicator of modulation degree and used for detecting the presence of modulation

4 Experiment Facilities and Procedure

Fig. 1 shows the gearbox test rig of the test facility employed to examine gearbox faults through acoustic measurements. The system consists of a 3-phase induction motor, a two-stage helical gearbox, flexible couplings and a DC motor which acts as a mechanical load. The induction

motor is rated at 11kW at 1470 rpm and controlled through a variable speed drive to operate under different operating conditions. The gearbox under test is also rated at 11kW at 1470 rpm. The technical specification of the helical gearbox is detailed in Table 1. In general, the rig is sufficiently large to represent many industrial applications for evaluating the performance of acoustic signal based condition monitoring.

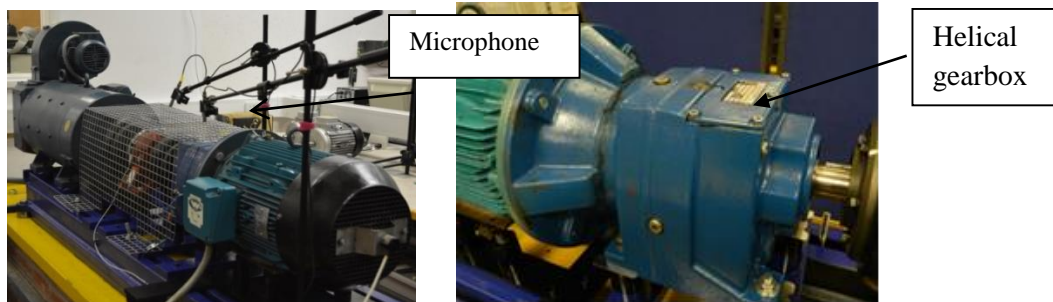


Fig 1. Photograph of the experimental test rig

Fig 2. Photo of Helical gearbox

Table 1. Specification of Two-Stage Helical Gearbox

Gear Parameters	1 st Stage	2 nd Stage
Number of teeth	58/47	13/59
Shaft speed	fr1=24.5Hz	fr2=30.23 and fr3=6.66
Meshing frequency	fm1=1416.36Hz	fm2=391.76Hz

Acoustic signals are measured by using a microphone system consisting of an electrets microphone, a preamplifier and a four channel portable ADC device. Table2 shows the specification for the system. During the test, a data length of 30 second is recorded for the speed channel and acoustic channel.

Table 2. Microphone Specification

Model	Preamplifier YG201	Microphone CHZ-211	USB Data Acquisition
Frequency rang	10Hz~110kHz (±0.2dB)	6.3Hz~20kHz (±2dB)	96kHz sampling rate
Sensitivity or gain	1	26±1.5dB (50mV/Pa)	24bit sensitivity
Temperature range	-40°C~+85°C	-40°C~+80°C	4 channel

To show the capability of acoustic signal based monitoring, a run-to-failure test was performed based on the helical gearbox. To speed up failure, the tooth width of pinion at the input shaft induced is removed to increase local stress for an early failure. However, as the high overlap ratio the gear can still maintain operates with notable reduction of performance. While the gearbox operates continuously during the test the gearbox was being monitored on-line by vibration, angular speed and instantaneous annular speed measurements. The test was terminated at the time instant when the sideband of instantaneous current signals shows a significant increase. During the course of the test, acoustic data was also collected at an interval of about 50 minutes, depending on the availability of the measurement system, and processed off line to identify an effective signal processing method to match the monitoring capability of other measurements.

5 Results and Discussion

The recorded acoustic data is processed using MSB and power spectrum methods. Both of them are calculated with 80 times of average and frequency resolution of xx.

5.1 Characteristics of Gearbox Acoustics under Different Loads

Fig 3 shows MSB and its corresponding MSBC results under different loads at an initial operation phases of 65.8hours for the first two meshing frequencies. In the graph, f_2 is for the carrier frequencies such as meshing frequency while f_1 is for the modulating components such as that of shaft rotating frequencies including: fr_1 , fr_2 and fr_3 . It can be seen that MSB magnitudes at fr_1 is the predominant components on both the 1st and the 2nd meshing frequencies. In the meantime, the magnitude at fr_2 and fr_3 are also visible, showing that MSB magnitude provides detailed information about the modulation effect of gear transmission due to the inherent manufacture errors. In addition, all these characteristic peaks are fully supported by MSBC peaks, showing Fig.3 (b1) and (b2).

Moreover, it is observed that MSB magnitudes at fr_1 and fr_2 on the second harmonics increase with the load, which is consistent with that the modulation amplitude increases with loads due to more deformation of tooth profile at higher loads. On the other hand, the MSB amplitudes on the 1st meshing frequency show an adverse connection to the load. This may be because of nonlinear effects of the vibro-acoustic transmission paths and more interfering influences from other low frequency sources. In addition, MSB amplitudes at fr_3 also show more distinctive peaks on the 1st meshing frequency, which may cause influences on the diagnosis accuracy of the fault from the gear set at fr_1 and fr_2 .

Therefore, the MSB results on the 2nd harmonic component of the meshing frequency is based on to characterise the dynamics of gear transmission and hence to develop more reliable features for monitoring any changes caused by abnormal gear transmission.

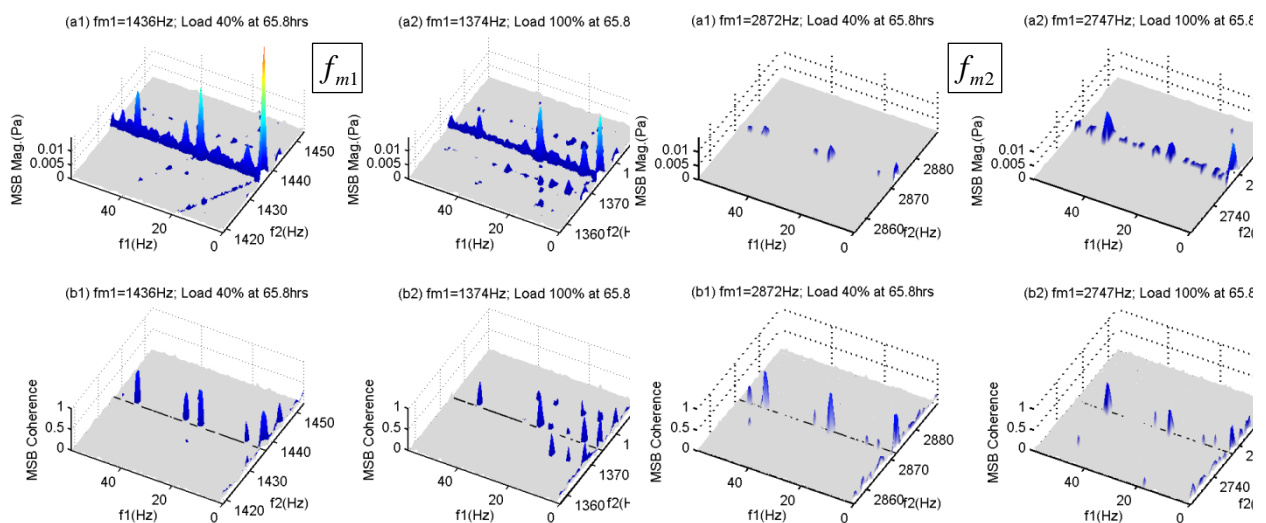


Fig 3. MSB and MSBC around different meshing frequencies and under different loads

5.2 MSB based Detection and Diagnosis

To confirm the detection and diagnosis performance of the selected carrier frequency band around f_{m2} , MSB results are examined at different time instants. Fig. 3 shows MSB and MSBC results around f_{m2} for 5 different advance time instants. Both MSB and MSBC exhibits two general features:

- The magnitudes are increasing with time advances; and
- The number of distinctive magnitudes is becoming higher with time advances.

These two critical features demonstrate that the modulation effects increase as the gear condition is becoming deterioration. As operating time advances, the gear tooth profile will be damaged gradually. This will lead to more vibrations and hence acoustics at frequencies relating to the gearing meshing process. In fact, when the gear is inspected after the test it has found that the tooth surfaces on both the pinion and gear show clear markers. Therefore, it has shown that acoustic data associated with MSB analysis is effective to detect and diagnose the gear condition.

In addition, it can be seen that MSB results at time instant of 406 hours is slightly deviated from the general features. It has less amplitude in the carrier frequency range between 2700Hz and 2750Hz. This may show that the acoustic signals may be interrupted by background noise such as communications of the test operators or other unknown factors. Nevertheless, the main features of modulation effect are still distinctively shown in the results.

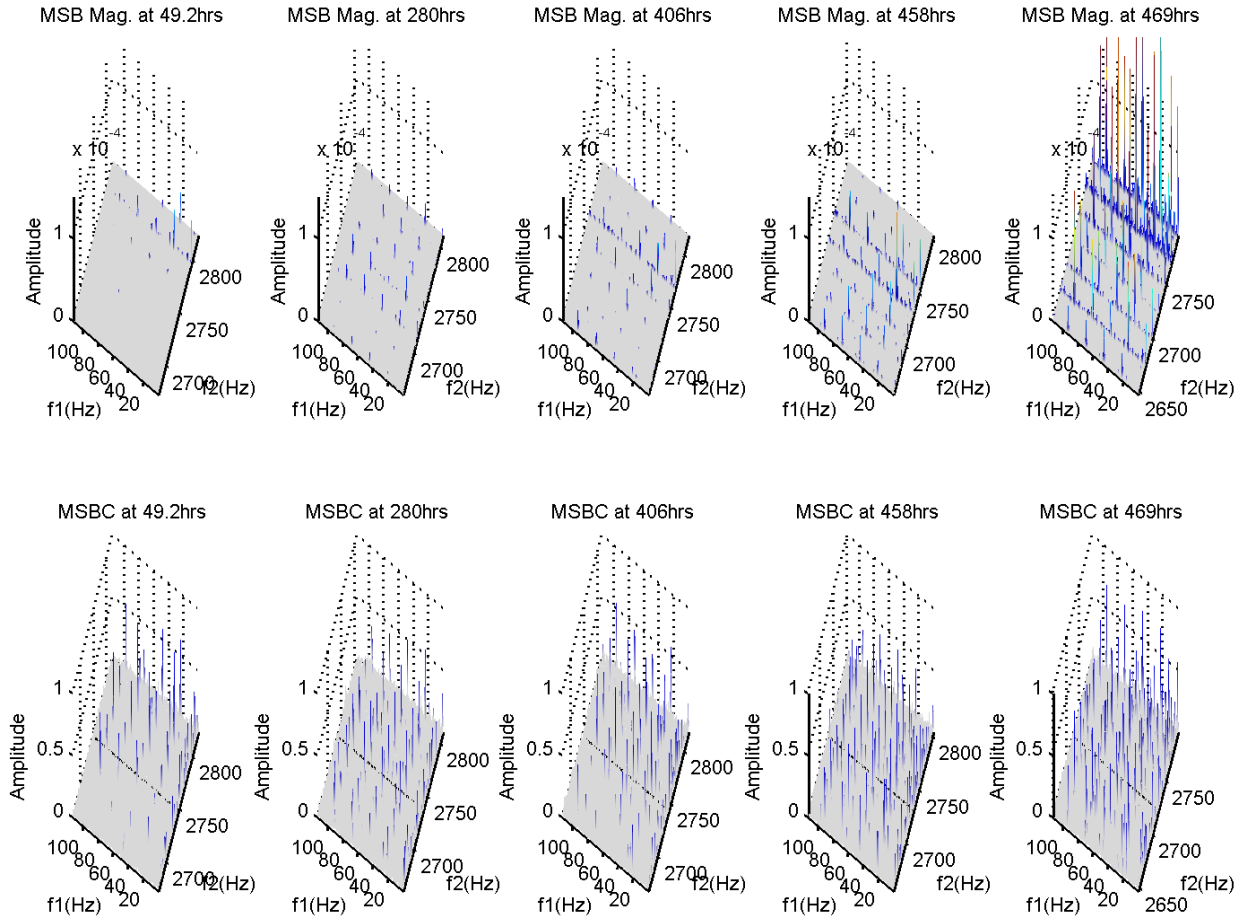


Fig4. MSB and MSBC for gearbox deterioration in successive time instants under high load

5.3 Monitoring Trend

To evaluate the performance of MSB analysis based acoustic monitoring, three MSB trends are developed based on features observed in the frequency range. The first one is the entropy of MSBC for describing the increase of coherence peaks. The second one is the average magnitude of MSB and the third is the average magnitude of MSB-SE. In addition, the average amplitude of power spectrum is also calculated for performance comparison. Fig. 4 shows the trend variation over the testing period. In general, they all show an increase trend with the operating time. However, the trend of power spectrum and entropy exhibit large variance because they contain the influences of random noise. On the other hand, although the trend of MSB-SE has less variance, it exhibits little change in the middle period of the operating. It shows that the sideband changes of MSB-SE show little indication of the deterioration of gear conditions in the period.

However, MSB trend, which is a combination of both the sidebands and the meshing frequency components, exhibits less variance and early indication. Thus it can be used for monitoring and predicting the fault advances more accurately. This proves that the MSB analysis is effective in extracting modulation characteristics of gear deterioration and excluding the noise influences on acoustic signals.

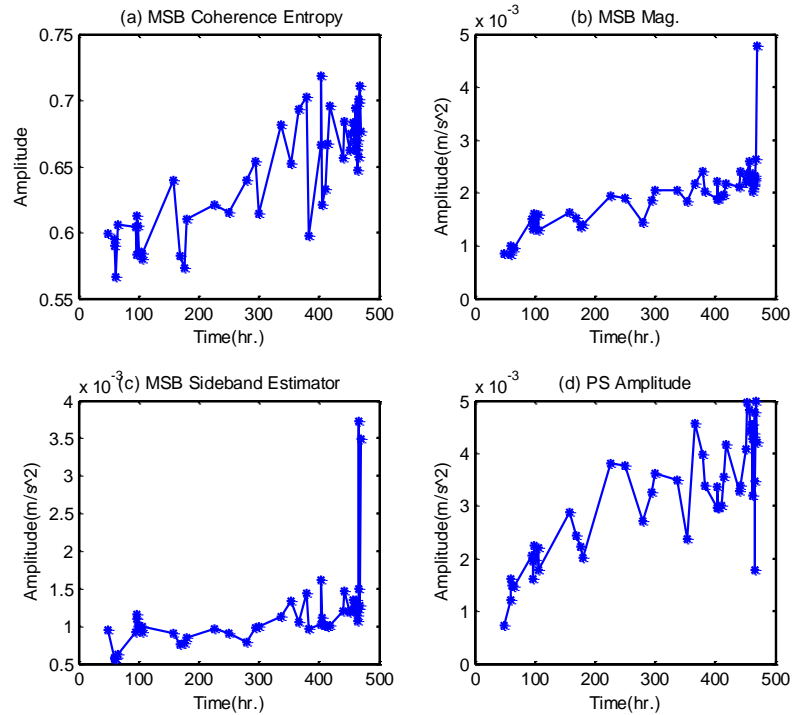


Fig5 Monitoring trends of MSBC, MSB, MSB-SE and PS for gearbox deterioration

6 Conclusion

This study shows that the acoustic signals contain the information of gearbox deterioration process. However, as the signals can be distorted by various factors including background random noise and interferences from nearby acoustic sources, MSB analysis is one of effective methods which are highly selective to the modulation characteristics of gearbox deterioration by suppressing such noise influences.

The results of gearbox deterioration monitoring shows that the monitoring feature need to be developed based on the frequency range around the 2nd harmonic components of the meshing frequency. Moreover, MSB magnitude which includes the magnitude changes at both the sidebands and meshing frequency has to be used to monitor the process.

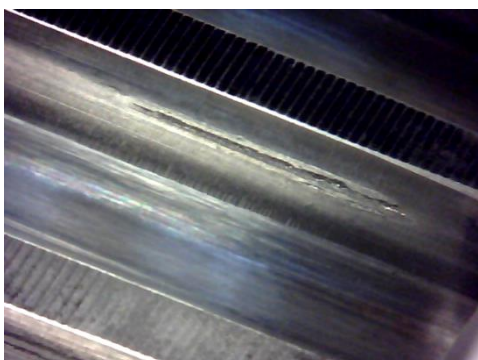
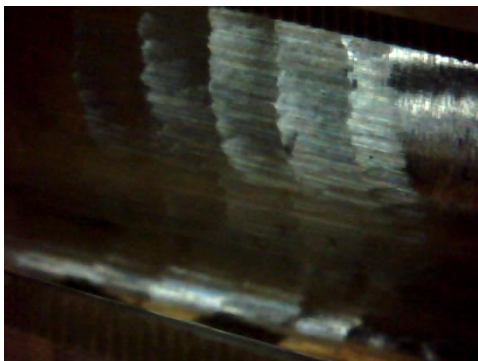
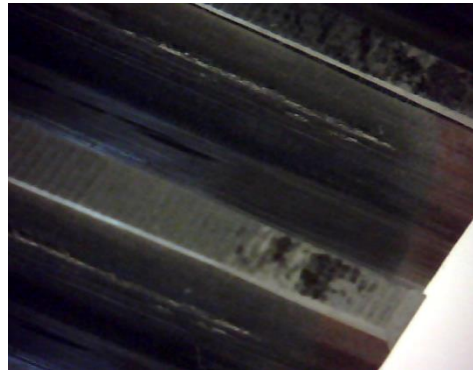
References

1. Gu, F., Ball, A. and Li, W. (2000) "The Condition Monitoring of Diesel Engines Using Acoustic Measurements-Part 1: Acoustic Characteristics of the Engine and Representation of the Acoustic Signals", SAE Technical Papers, ISSN 0148-7191.
2. Li, W., Gu, F., Ball, A., Leung, A.Y. T., Phipps, C.E, "A Study of the Noise from Diesel Engines Using Independent Component Analysis", Mechanical Systems and Signal Processing, Vol.15, No. 6, pp.1165-1184, 2001.
3. Albarbar, A., Gu, F., Ball A.D., Starr, A. "Acoustic monitoring of engine fuel injection based on adaptive filtering techniques". Applied Acoustics, 71(12), pp. 1132-1141, 2010.

4. Y. Lei, J. Lin, M. J. Zuo, Z. He, Condition monitoring and fault diagnosis of planetary gearboxes: A review, *Measurement* 48 (2014) 292–305.
5. R. Zimroz, W. Bartelmus, Gearbox condition estimation using cyclostationary properties of vibration signal, *Key Engineering Materials* 413–414 (2009) 471–478.
6. B Liu, S. Riemenschneider, Y. Xu Gearbox fault diagnosis using empirical mode decomposition and Hilbert spectrum, *Mechanical Systems and Signal Processing*, Volume 20, Issue 3, April 2006, Pages 718–734.
7. Stack, R., Hartley G. and Habetler, G. 2004, An amplitude modulation detector for fault diagnosis in rolling element bearings. *IEEE Trans Ind. Electro* Vol 51 No 5 pp 1097-1102.
8. Gu, F., Hu, Y., N Naid A and Ball A, Electrical motor current signal analysis using a modified bispectrum for fault diagnosis of downstream mechanical equipment, *Mechanical Systems and Signal Processing*, Vol. 25, no. 1, ISSN 0888-3270, 2011.
9. Blankenship G. W. and Singh R., "Analytical Solution for Modulation Sidebands Associated with a Class of Mechanical Oscillators," *Journal of Sound and Vibration*, vol. 179, no. 1, pp. 13-36, 1995.
10. McFadden P. D. and Smith J. D., An explanation for the asymmetry of the modulation sidebands about the tooth meshing frequency in epicyclical gearbox vibration, in *Proceedings of the Institution of Mechanical Engineers* 199, pp. 65-70, 1985.
11. Smith, J. D. - *Gear Noise and Vibration*, Marcel Dekker, NY, 1999. 7.
12. D. N. Chorafas 1990 *Knowledge Engineering*. Van Nostrand Reinhold, first editioned.
13. W. Li, *A Study of Diesel Engine Acoustic Characteristics*. PhD thesis, chapter 1, 2000
14. J. Benesty, J. Chen, and Y. Huang, *Microphone Array Signal Processing*. Springer, 2008
15. Gu, F., Li, W., Ball, A.D., Leung, A.Y.T., *The Condition Monitoring of Diesel Engines Using Acoustic Measurements Part 1: Acoustic Characteristics of the Engine and Representation of the Acoustic Signals*. SAE Technical Paper Series 2000-01-0730.
16. Li, C.J and Yoo, J.- *Prognosis of Gear Tooth Crack Growth*. Proc. 52th Meeting of the Society of mechanical failures Prevention Technology, Virginia Beach, VA, p 419-428, 1998.

Appendix B: Gear Tooth Wear Photos

More images are provided to detail the deteriorations of the tested gears.



Appendix C: The Diagnosis of the Asymmetric Rotor in the Induction Motor

The fault of asymmetric rotor in AC motors is further diagnosed by a higher resolution spectrum analysis. The method is conventionally used for detecting the problem. As shown in the spectrum below the sidebands at the twice slip frequency is distinctive.

